University of Modena and Reggio Emilia, Doctorate School in Earth System Sciences: Environment, Resources and Cultural Heritage

PHD Thesis

MULTI-SCALE ANALYSIS OF GROUND DEFORMATION BY POST-PROCESSING INSAR DATASETS:

LANDSLIDES AND MAN-INDUCED SUBSIDENCE

Author: Dr. Jean Pascal Iannacone

Tutor: Dr. Alessandro Corsini

Co-Tutor: Dr. Christian Iasio

April 2014

To my sweet grandmother Clelia,

I will never forget you

and your love for us,

Thank you!

Abstract

In the last decade, the use of Persistant Scatterers Interferometry (PSI) increased exponentially. While the use of PSI dataset "as it is" is well-documented, few studies have been carried on advanced post-processing applications that can enhance the analysis of ground deformation phenomena and the interpretation of driving processes. The PhD research has dealt with the co-development, testing and application of innovative post-processing routines which are meant to permit the dynamics characterization of ground deformations, time series analysis and mapping. Such routines have been tested at different scales of analysis to fully characterize the ground deformation due to landslides or by man-induced subsidence and, thus, analyse cause-effects relationships. The first routine is Geo-PSIC (Geomorphic-based Persistent Scatterers Coupling), a tool for the decomposition of velocities' vectors. The novelty of Geo-PSIC consists in the introduction of geomorphic criteria when coupling complementary PSs leading to a more accurate characterization of slopes dynamics. The second routine is PS-Time (Berti et al., 2013) a statistically-based software for automatic classification of PSI time series which allows ground deformations to be classified into six possible distinctive deformation trends. The Hotspot and Cluster Analysis routine (Lu et al., 2012) was also tested. As regards landslides, routines were applied in two different morphological and geological environments (South Tyrol and northern Apennines) and at regional as well as site specific scale. Geo-PSIC proved to be particularly valuable at slope scale in alpine contexts where, due to the abrupt change in slope, the local geomorphology cannot be neglected, while PS-Time

proved to be beneficial at all scale of analysis. For regional landslide mapping it enhanced radar interpretation by introducing a further factor to consider in the identification of active phenomena. At slope scale, time series analysis allowed assessing the date of activation, acceleration or a deceleration of a number of specific landslide sites, supporting the analysis of relationships between slope movements and triggering factors. As regards man-induced subsidence, routines were applied to excavation problems related to mining and tunnelling: the Metropolitan Mine (New South Wales, Australia) and the twin tunnel of the Seymour-Capilano water filtration plant (North Vancouver, Canada). In both case studies, PS-Time analysis allowed assessing a strong correlation between underground excavation and the different trend of ground subsidence (acceleration, linear and deceleration). On such basis it was possible to automatically discretize the time series in before and after the events, define the dates of the events, determine the velocity before and after the event, map the extent of the subsidence phenomena. Moreover at Metropolitan Mine, where rapid movements occurred in some portions of the analysed area, a combination of SqueeSAR™ and DInSAR data was carried out in order to fully characterize subsidence evolution in space and time. Such combination allowed the dynamics of the subsidence bowl (front and centre), the angle of draw and thus the area of influence to be defined. The angle of draw evaluated using the InSAR was used to calibrate SDPS (Surface Deformation Prediction Systems), a mathematical model widely used in long wall mining applications, based on empirical or site-specific regional parameters. The results of the simulation were thus compared with the SqueeSAR™ results, providing evidence of a much better agreement between measured and expected subsidence extent. PSI post-processing routines can significantly enhance

the interpretation of deformations allowing an integrated analysis in the spatial and time domain. Furthermore, when dealing with non-linear deformations (i.e. landslides reactivation, underground mining, tunnelling, etc.) time series analysis are encouraged.

Acknowledgments

I am grateful to several people which all in different way made possible the development of this research. First of all I would like to thank my tutor Alessandro Corsini and my co-tutor Christian Iasio, for their precious suggestions and contribution. During this three years I had the chance to learn from them how to approach and solve problems related to the research. I also feel to highlight how much I enjoyed the time working together. This work has been possible thanks to external collaborations such as the "Institute for Applied Remote Sensing" of the European Academy of Bozen (EURAC); the Earth Science Department of the University of Bologna; Telerilevamento Europa (T.R.E.) and T.R.E. Canada Inc. I am very grateful to Christian Iasio for the support I received during the year spent at EURAC, for the development of Geo-PSIC and for his patient to listen and "absorb" my brain-teaser on SAR geometries. I am also very grateful to Matteo Berti who shared his knowledge and for the implementation of PS-Time. How can I forget the "button" to listen the music played by each PS? After each meeting on the time series analysis with all the working group, I was more and more excited about the research I was working on. I am very grateful to Alessandro Ferretti, who gave me to chance collaborate with T.R.E. and for the datasets TRE made available for my PhD research. I also want to thank Giacomo Falorni who encouraged me working on InSAR for mining application and for making feeling me home during my stay in Vancouver. Thanks to Jacopo Allievi, Sara Del Conte and all the others colleagues from T.R.E. Special thanks goes to my girlfriend Vanessa and to my family for being close and supporting me

.

Table of Contents

1 Introduction

Precise and continuous monitoring of ground displacements over large areas is an important resource for the analysis of both natural and man-induced hazards. To this respect, the scientific community has embraced the InSAR with great interest since the pioneer application to the Landers earthquake (Massonnet et al. 1993). From then, an increasing interest toward this technique has pushed the InSAR community to develop different algorithms for extracting surface deformation from SAR images.

Simultaneously, earth science experts have applied InSAR techniques to different fields of application, such as landslides hazard (Fruneau et al., 1996, Colesanti et Wasowski, 2004, Strozzi et al., 2005; Corsini et al., 2006, Farina et al. 2006, Herrera et al. 2009), mining subsidence (Carnec and Delacourt, 2000, Raucoules et al. 2007, Jung et al. 2007), open pit mine (Woo et al. 2012), volcanoes (Jonsson et al., 1999, Berardino et al. 2007, Peltier et al. 2010, Manzo et al. 2012, Brunori et al. 2013), gas storage (Teatini et al. 2011), ground water pumping (Sneed et al., 2001) and water level changes (Alsdorf et al., 2000).

InSAR growth has been also supported by the expansion and continuity of SAR satellite missions (Figure 1), offering a diversity of radar products characterized by different wavelengths (i.e. X-band= ~3 cm, C-band= ~6 cm, L-band = ~24 cm). Therefore, nowadays the availability of InSAR datasets has increased for the end-users such as researchers, professionals, decision makers, civil protection, etc. As an example, the Italian Department for the Environment has financed a C-band PSI historical analysis at national scale. This project, named “Piano Straordinario per il Telerilevamento Ambientale (PST-A)”, is free of

charge for the public administration sector and represents an important source of data for any working professional in the field of geo-conservation.

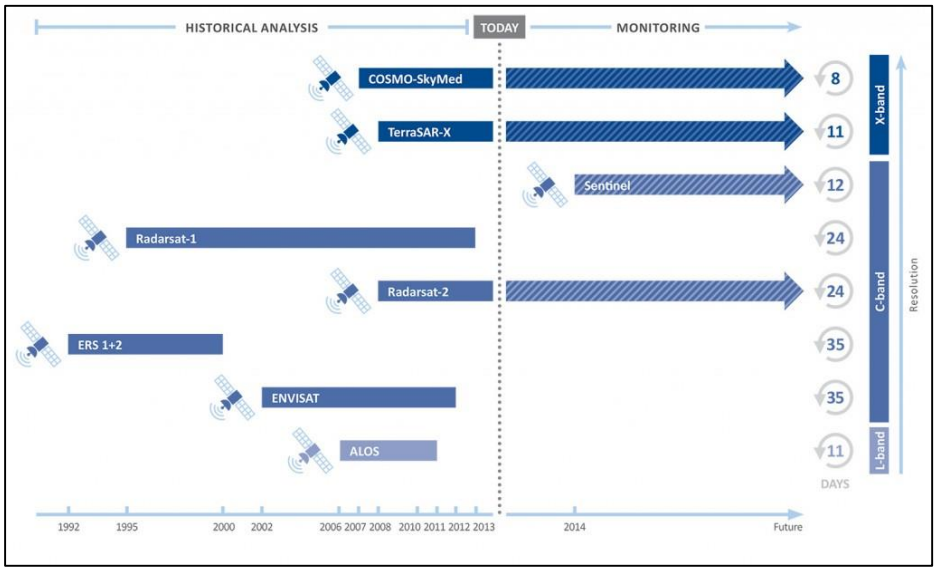

Figure 1. SAR Satellite constellation (source: treuropa.com)

Now that the InSAR processing is well consolidated within the SAR community and that data are easily accessible, the new challenge is to extract valuable information from the standardly available InSAR datasets. Correct interpretation is crucial, and geotechnical significance of mono-dimensional surface deformations is challenging, especially where ground truths are lacking. In these cases, it is necessary to characterize the local deformation in both space and time domains, identify "brotherhood" areas and investigate its geomorphic and geotechnical significance. To this end, it is necessary to characterize the components of deformation within different geomorphic units and to analyze time series of deformation in order to highlight linear and non-linear deformation trends and to highlight a critical phase of deformation (i.e. sudden acceleration).

This work focus on post-processing routines applicable at different scale level to provide added values to most of the InSAR application's fields. These routines have been presented and tested, where applicable, with reference to different type of ground movements (landslides and man induced subsidence due to underground mining, urban tunneling), at different scale of analysis, (regional and site specific-scale) and different geological and geomorphic contexts (Alpine, Apennine, Southern Coalfields in New South Wales and the Seymour glacial Valley from the Coast Mountains, in British Columbia).

This document is divided into seven Chapters, including this introduction and the conclusions. In Chapter 2 the technical InSAR background are reviewed, for an easier comprehension of this work. In Chapter 3, the post-processing routines presented and tested are discussed. In particular, the chapter addresses the novelty of two software developed. The first is GEO-PSIC (Geomorphic-based Persistent Scatterers Coupling), a tool for the decomposition of velocities' vectors. The second is PS-Time (Berti et al., 2013) a statistically-based software for automatic classification of PSI time series which allows ground deformations to be classified into six possible distinctive deformation trends. Chapter 4 focuses on landslides application and testing of the post-processing tools proposed. Analysis have been carried out at regional scale and slope-scale, and different geomorphic environment, such as Alpine and Apennine. In addition we tested the application of the Hot Spot Analysis (Lu et al., 2012) for automatic landslides detection at regional scale from large datasets. Chapter 5 discusses InSAR application to man-induced subsidence. The chapter is divided in two main sections: longwall mining and tunnelling. The longwall mining section present a combined use of traditional DInSAR with advanced SqueeSAR™. This double technique

integration has been carried out to identify the angle of draw, which defines the limit of the stable/unstable area. Based on the results, numerical modelling for mining subsidence have been carried out using the values of angle of draw estimated using InSAR and compared with numerical modelling using literature parameters. The second section of this chapter discuss the application to tunnelling induced subsidence, in urban area. In particular, time series analysis has been carried out due to the non-linear deformation affecting this area caused by the tunnels excavation. General discussions are addressed in Chapter 6 while summary and conclusion are drawn in Chapter 7.

2 Principles of InSAR and PSI analysis

2.1 Introduction to SAR

Satellites sensors can be grouped into active and passive types depending if the electromagnetic wave is emitted by the sensor or by the sun respectively. Most of active systems are radar (RAdio Detection And Ranging) systems operating in the microwave region of the electromagnetic spectrum (Figure 2).

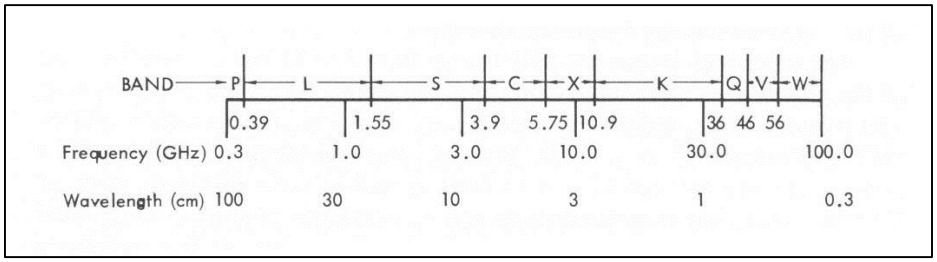

Figure 2. Microwave spectrum (Ulaby et. al., Microwave Remote Sensing, 1981)

RADAR systems allow the detection of objects by measuring the delay time of backscattered electromagnetic signals, retrieving information about the sensor-to-target distance (Ranging). In fact, a RADAR system has three primary functions: 1) transmits microwave (radio) signals towards a scene, 2) It receives the portion of the transmitted energy backscattered from the scene, 3) It observes the strength (detection) and the time delay (ranging) of the return signals. The potential ambiguity of left/right object (equi-distant) from the sensor is solved using side-looking RADAR with respect to the flight track.

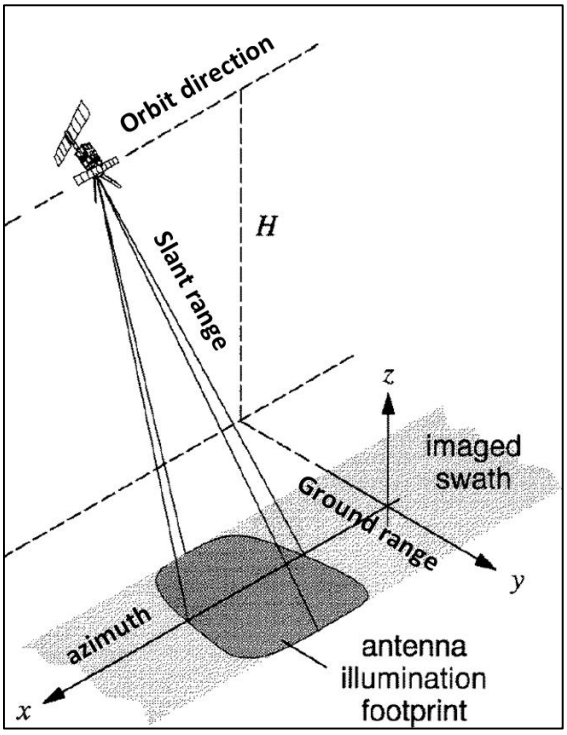

Figure 3. Imaging geometry (modified after Bamler and Hartl, 1998).

As a consequence, the electromagnetic wave emitted is not vertical and is geometrically defined by azimuth, the slant range and the look angle (Figure 3). Azimuth is the direction parallel to orbit path of the satellite. Slant range represents the distance measured along a line between the radar antenna and the target. Image direction as measured along the sequence of line-of-sight rays from the radar to each and every reflecting point in the illuminated scene. Since a SAR looks down and to the side, the slant range to ground range transformation has an inherent geometric scale which changes across the image swath.

The roughness of the ground also play an important role on the backscattering signal and is linked to the wavelength. In fact, flat areas do not produce backscattering and in general the longer the wavelength

the more surface areas behave as smooth surface. In particular, according to the Rayleigh criterion, a surface is considered smooth if:

$$h < \frac{\lambda}{8cos\delta} \quad (1)$$

While can be considered rough if:

$$h > \frac{\lambda}{8cos\delta} \quad (2)$$

Where h is the mean height surface variation, λ is the wavelength and δ is the look angle.

2.2 SAR Image resolution

Range resolution is the ability of a radar system to distinguish between two or more targets at different ranges. The degree of range resolution depends on the width of the transmitted pulse, the types and sizes of targets, and the efficiency of the receiver. Pulse length τ is the primary factor in range resolution. Additionally, Figure 4 shows the look angle δ, the spacecraft height H.

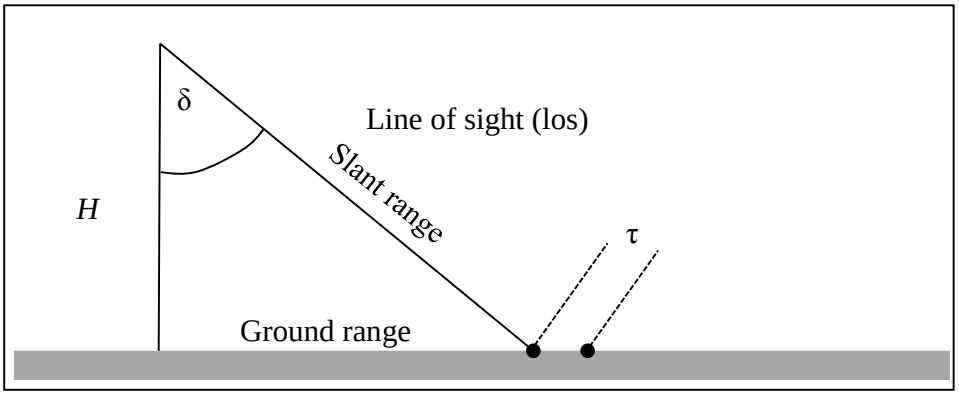

Figure 4. Slant range and ground range geometries.

The theoretical range resolution cell Δr of a radar system can be calculated from (3):

$$\Delta r = \frac{C\tau}{2} \quad (3)$$

Where *C* is the speed of light.

Furthermore, the ground range resolution R_r can be determined by (4):

$$R_r = \frac{C\tau}{2} \times \frac{1}{sen\delta} \quad (4)$$

Applying the (4) to an ERS-1 SAR image that has a range resolution of about 8 meters, and an average look angle of 23°, it is possible to estimate a ground resolution of about 20m. Equation (4) suggests that range resolution is infinite for vertical look angle and improves as look angle is increased.

Azimuth resolution of a radar, describes the ability to separate two objects in the direction parallel to the motion of the sensor. The azimuth

resolution is dependent on the bandwidth. Figure 5 shows the parameters involved in the azimuth resolution, expressed from (5)

$$R_a = \rho sin\theta_r = \frac{\rho\lambda}{L} \quad (5)$$

Where $sin\theta_r$ is the diffraction resolution and ρ is the slant range

$$\rho = \frac{H}{cos\delta} \quad (6)$$

For the case of a synthetic aperture radar, (strip-mode) where the length is 2Ra, the improved resolution is:

$$R_a = \frac{\rho\lambda}{2R_a} = \frac{L}{2} \quad (7)$$

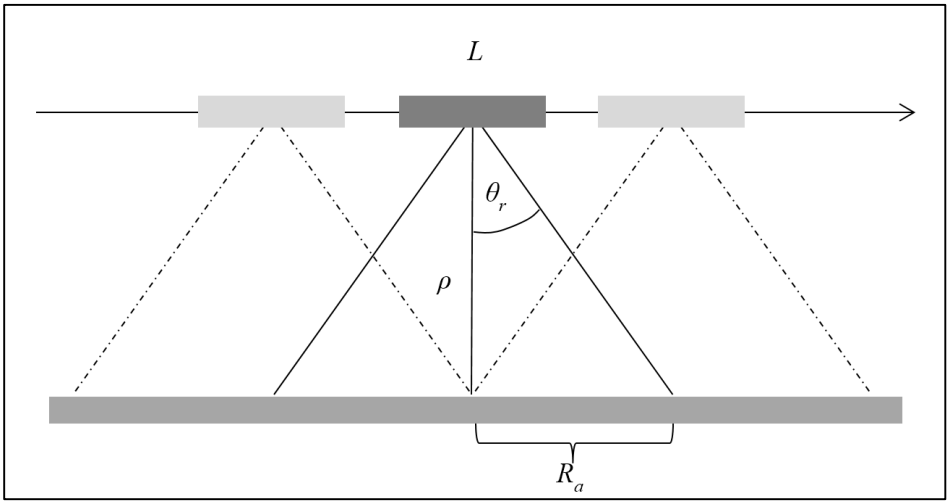

Figure 5. Azimuth resolution Ra.

In order to have metric azimuth resolution, a kilometric antenna is required. To overcome the spatial resolution limitation of real radar

antennas, Synthetic Aperture Radar (SAR) sensors are used to simulate longer antennas. Synthetic Aperture Radar take advantage from the fact that the same object is sensed from different position along track of the antenna. Therefore, a punctual object is recorded as a curve on the image in azimuth (Figure 6a) which is later compressed in the focusing phase while generating the SAR image. Each SAR image is composed by both amplitude and phase components and can be thus represented by complex numbers.

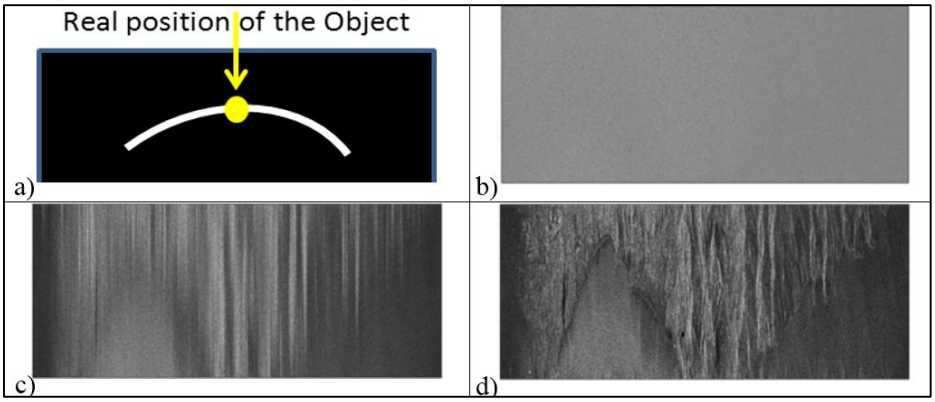

Figure 6. SAR focusing. a) punctual object recorded from different positions of the antenna; b) Raw image; c) range compressed image; d) Azimuth compressed image. (b, c, d, after Akliouat et al. 2007).

In particular, they are represented by an equivalent pair of numbers, the real in-phase component (I) and the imaginary quadrature component (Q). In particular, the phase component is the angle indicated in Figure 7.

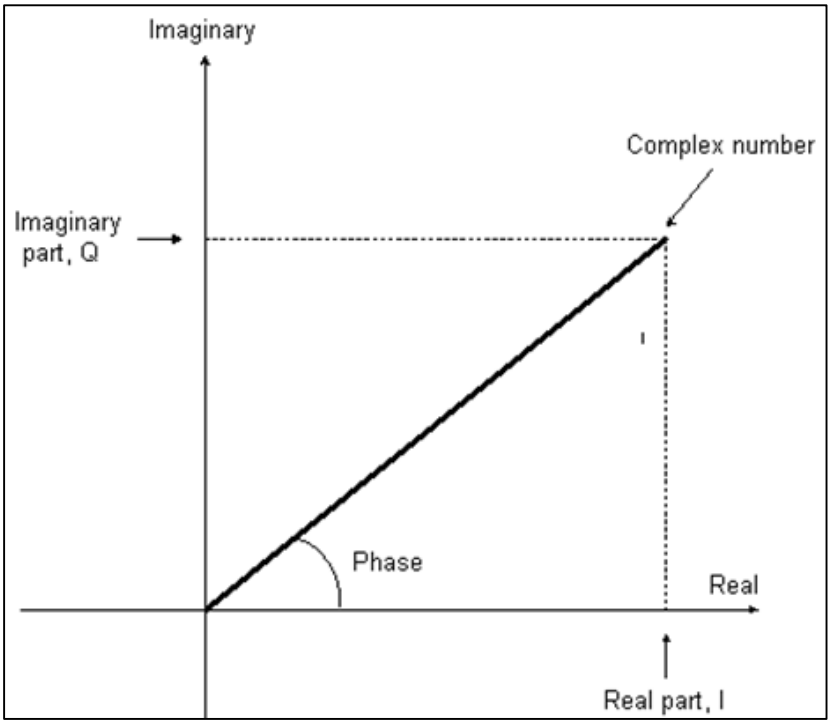

Figure 7. Complex number. (Source ESA: https://earth.esa.int/handbooks/asar/CNTR5-2.htm)

Once the SAR image have been focused in range and azimuth, they need to be visualized. It is accepted to represent the azimuth on the upper side and the range on the left side of the image. The "zero" is set to the upper left corner so that values on the image increase along the axes (azimuth and range sides). Figure 8 represents schematically how ascending and descending SAR image representation relates with the geographic coordinates. In particular, increasing values on the SAR images indicates the direction of satellite acquisition (lower values have been acquired earlier). For example, a descending satellite will acquire in azimuth direction, the North first and South later, while in range direction, objects in the near range (East) are acquired first then objects in the far range (West). Opposite representation is found for ascending SAR image. Use

of SAR images, in azimuth and range coordinates, is limited by these geometric distortions intrinsic to the range imaging mode.

As stated by (4), if the illuminated area is planar, a constant resolution (slant range) does not correspond to a similar constant resolution (ground range).

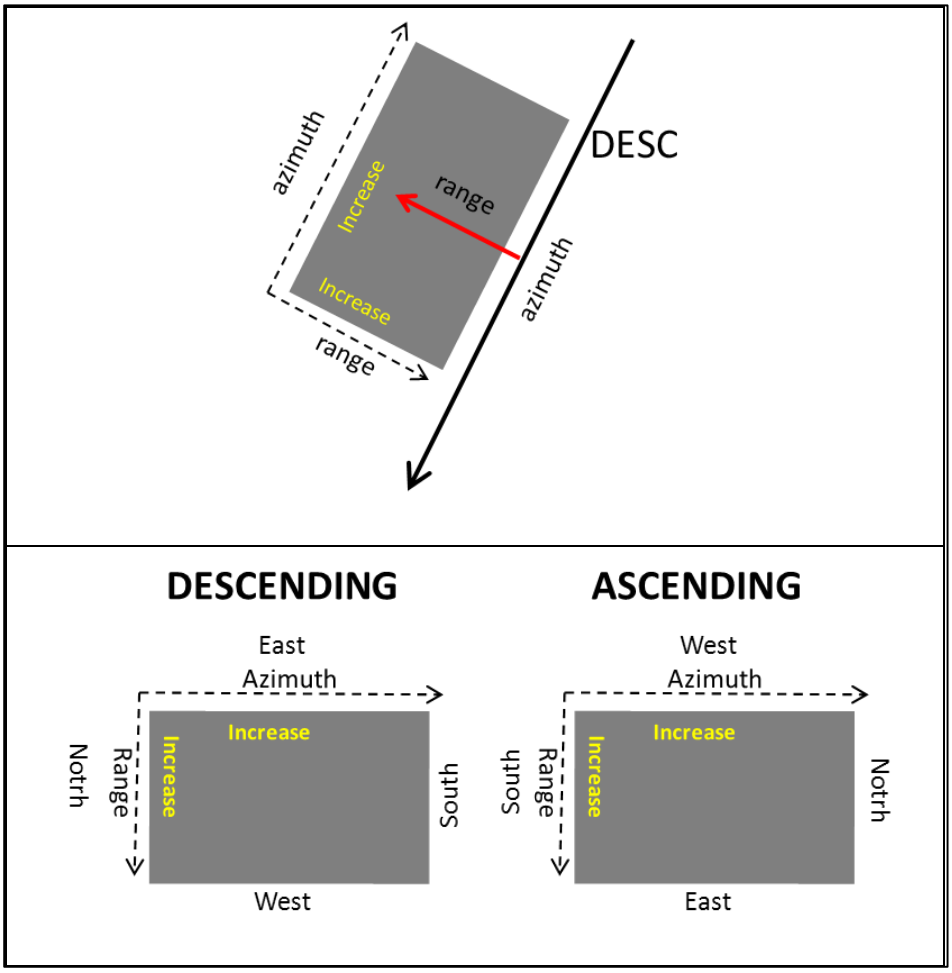

Figure 8. SAR image and geometries standard representation.

2.3 Geometric distortions in SAR images

Geometric distortion of SAR images are the consequence of the slant geometry and how object are detected. In fact, the Radar signal phase is related to the sensor-target distance. In other hand, SAR image (position of objects and intensity) is the combination of topographic effect and antenna orientation. The only topographic condition, when the ground cell is equal to the slant range cell, is when the slope is parallel to the LOS. In fact, for a given incident angle, can be defined three geometric distortion types: foreshortening, layover and shadowing. Foreshortening is the compression of slopes facing the radar antenna and with a slope angle lower than the look angle. Foreshortening appear bright on the SAR image and is maximum for slopes perpendicular to the Radar beam.

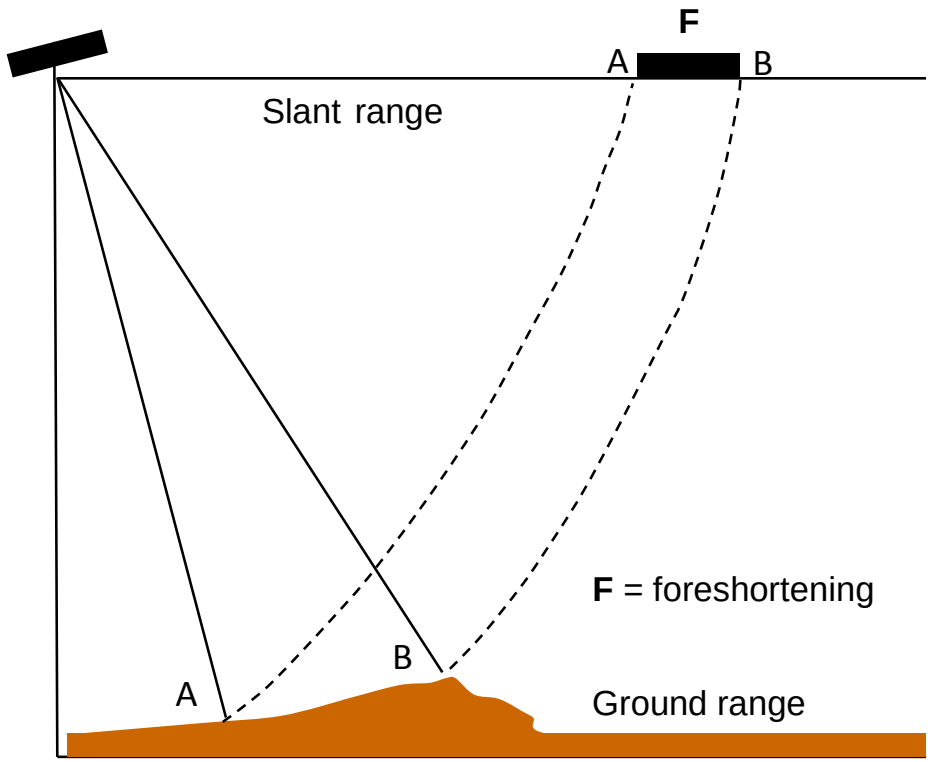

Figure 9. Geometric distortion: foreshortening.

In this extreme condition, the top of the hill is imaged at the same time of the toe of the hill, so that they cannot be distinguished. Figure 9 shows the compression of the slope **AB** in the Slant Range geometry. However, areas in foreshortening can still be used in SAR application.

Layover take place when a point is imaged before its real position on the ground. This is the case for example of mountain crests, where due to the topography, the crest reflects before then the base of the slope (Figure 10). This type of geometric distortion take place when slopes facing the antenna are steeper than the look angle (Figure 10).

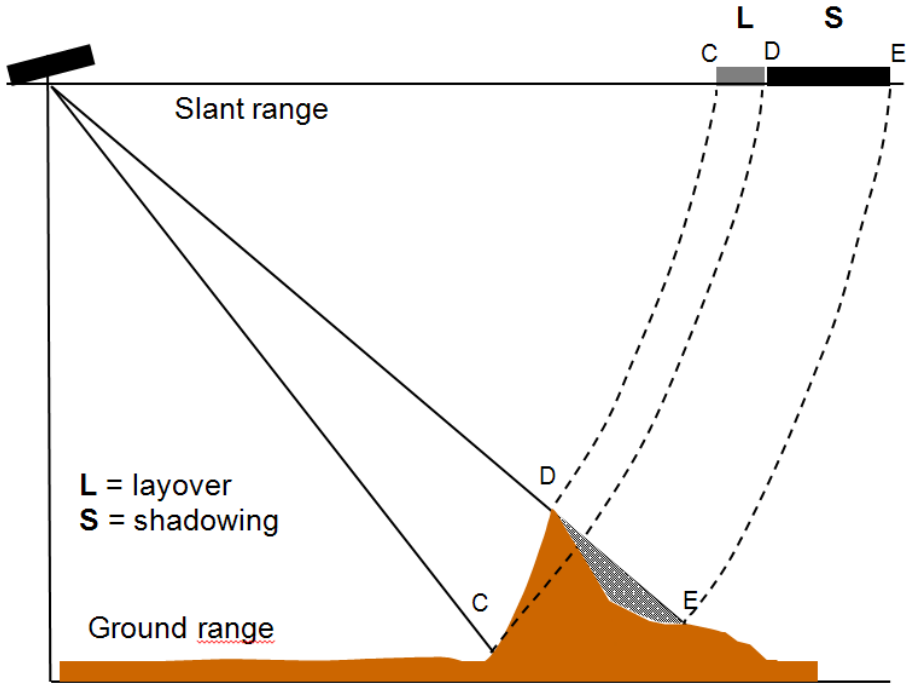

Figure 10. Geometric distortion: shadowing and layover.

The shadowing (Figure 11) is a distortion type affecting slope parallel to the slant range and steeper than 90-δ, where δ is the look angle. Since

these areas are not illuminated by the Radar, they will appear dark on the SAR image.

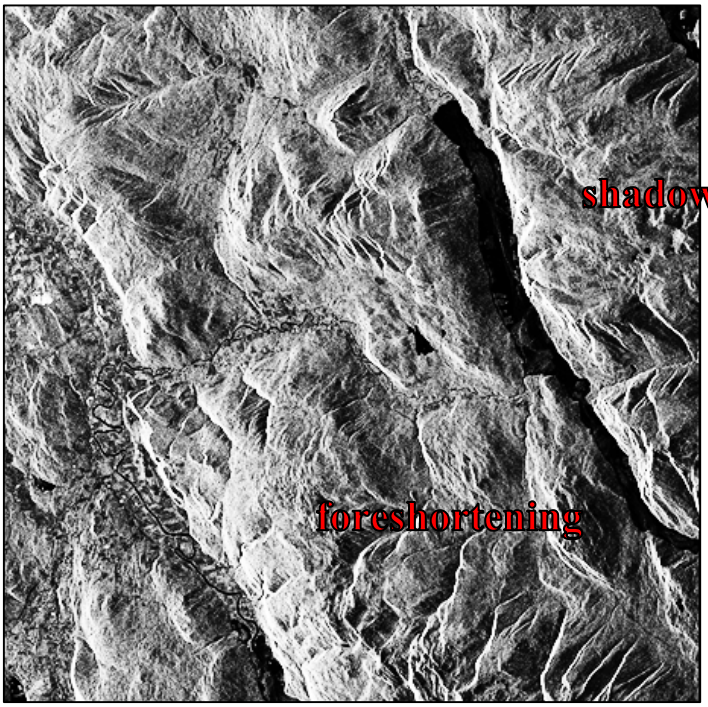

Figure 11. ERS-1 SAR image illustrating the foreshortening and shadowing geometric distortions (source: ESA).

2.4 Differential Interferometry (DInSAR)

As previously stated, a SAR image is made of two components: amplitude and phase. The phase is dependent on the distance-to-target and appears on a single SAR image a "salt and pepper" effect and is not intelligible. Considering an ideal case, where two SAR images are acquired at different time but with constant external condition (topography, atmosphere, no-displacement), we expect the phase term to be the same. Therefore, if an object or an area on the ground slightly

changes its relative position during the two SAR acquisitions, an additive phase term will appears (Figure 12).

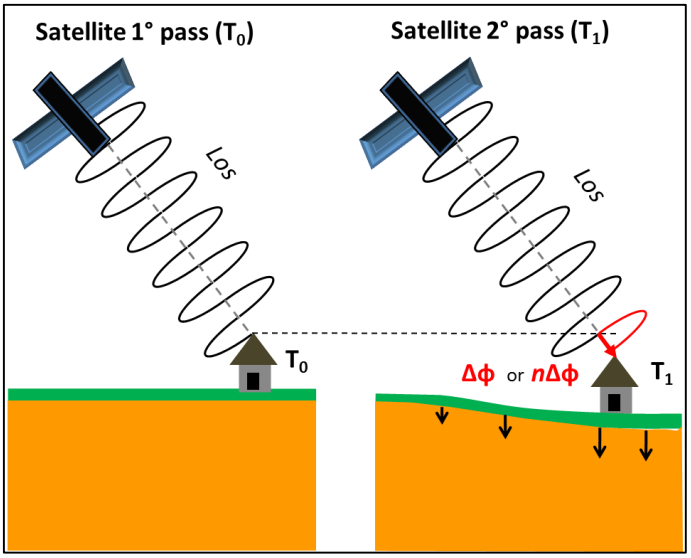

Figure 12 Interferometric phase shift due to object's movement at the time of the second SAR aquisition.

Taking advantage from this additive phase term, Differential Interferometry SAR (DInSAR) exploits the phase difference (interferogram) between two complex SAR images, achieved by processing the data acquired by two different antennas based on the (8).

$$\Delta\phi = \frac{4\pi}{\lambda} r_2 - r_1 = \frac{4\pi}{\lambda} \Delta r \qquad (8)$$

Where $\Delta\phi$ is the phase difference and Δr the displacement along the line of sight. DInSAR can only measure fractions of phase shift and is insensible to the total distance from the antenna. We can evaluate, for a given satellite, and thus a given wavelength λ, the maximum detectable displacement (9).

$$\Delta\phi = 2\pi \Rightarrow \Delta r = \frac{\lambda}{2} \quad (9)$$

As a result, an interferogram is the representation of a series of colored fringes where the deformation varies cyclically (wrapped) between 0 and 2π radians. In order to obtain displacement maps, it is necessary to unwrap the interferometric phase, that means to remove the 2π jumps present in the interferogram, by adding the adequate multiple of 2π where necessary. In the unwrapped interferogram, the deformation is not restricted (wrapped) to the interval 0 and 2π, but varies between $-\infty$ and $+\infty$.

In the real case, the differential phase do not depend solely from the ground motion but also from the contribute of flat earth, the topography, the atmosphere and the residual noise.

$$\Delta\phi = \Delta\phi_{flat} + \Delta\phi_{topo} + \Delta\phi_{def} + \Delta\phi_{noise} \quad (10)$$

The flat earth contribute is because targets located at the same elevation but with different look angle δ, have different interferometric phase which can be easily removed. Using a Digital Elevation Model (DEM) it is also possible to account for and for the topographic contribute$\Delta\phi_{topo}$. Once $\Delta\phi_{flat}$ and $\Delta\phi_{topo}$ have been removed, the phase $\Delta\phi$ depends only on the deformation and the atmospheric contribute, that for small and nearly flat area can be considered negligible. However, the main limitation in DInSAR analysis is related to the impossibility to estimate the atmospheric contribute, which generates a source of error and thus influencing the overall accuracy of the interferogram, which is typically

of centimeter. The signal to noise ratio (SNR) is affected also from the normal baseline (Bn) and the temporal baseline (Bt) which are respectively the normal distance between the orbits at the time of image acquisition and the time interval between the two images used for the interferogram. In general, the higher the Bt and Bn, the higher the decorrelation. In particular, spatial decorrelation appears when the difference in incidence angle due to the Bt, alters the coherent sum of wavelets from the many small scattering elements within a resolution cell, so that measurements do not repeat exactly (Zebker and Villasenor , 1992). On the other hand surface conditions variation, (i.e vegetation, snow coverage, etc.,) affect the scattering properties, leading in coherence loss. This phenomena is known as temporal decorrelation (Li and Goldstein, 1990; Zebker and Villasenor, 1992).

The first DInSAR application date at 1993, when Massonnet et coauthors mapped the ground displacements of the Landers earthquake. Figure 13 shows an example of an interferogram using Radarsat C-band and a perpendicular baseline=68 m at “la Réunion island”, in the Indian Ocean (Delacourt et al, 2009). The master and slave images were acquired in 15/05/2001 and 23/11/2001 respectively, leading into a Bt of 192 days.

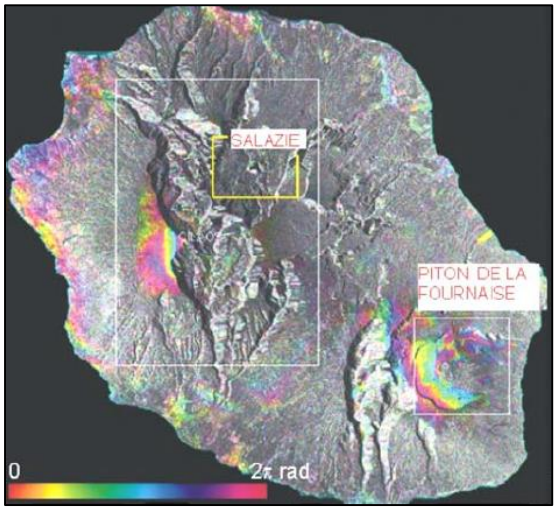

Figure 13. Wrapped interferogram at la Réunion island, in the Indian Ocean. Radarsat C-band; Bn=68 m; Bt=192 days, (Delacourt et al, 2009).

Information from interferograms can only be extracted in good quality areas, which are reflective areas where electromagnetic characteristics are substantially preserved with time.

The interferogram quality can represented trough the interferogram coherence that is mathematically defined as the amplitude of the complex correlation coefficient of the two signals (Bamler and Hartl, 1998, Duro 2010):

$$\gamma = \frac{E[u_1 u_2^*]}{\sqrt{E[|u_1|^2]E[|u_2|^2]}} \quad (11)$$

Where E[] are the expected values or mean operator, while u_1 and u_2 are the complex pixels of the SAR image. The coherence varie between 0 (no-coherence) to 1 (max-coherence). Noise renders the two images to be not fully correlated ($|\gamma| < 1$). Exhaustive information on InSAR, that are beyond the scope of this work, can be found in Henderson and Lewis,

(1998); Franceschetti and Lanari, (1999); Hanssen, (2001), Massonnet and Feigl, (1998); Rosen et al., (2000).

2.5 Persistent Scatterer-InSAR (PSI)

Often interferograms include large areas where the signals decorrelate and no measurement is possible. Atmospheric phase delay is generally correlated in time on the scale of hours to days. As the time between satellite passes is of order of 15-30 days, the atmospheric signal is effectively decorrelated in time. A common method for reducing atmospheric signal is, therefore, to stack multiple interferograms acquired over time. Using large SAR image datastack it is possible to identify pixels with a reduced level of noise and by means of spatio-temporal statistical analysis of phase information, several parameters of the scatterers can be estimated. These parameters typically include 1) elevation 2) displacements, 3) atmospheric noise. The image resolution cells where the measurements are possible are known as Permanent (or Persistent) Scatterers (Ferretti et al 2001). Persistent Scatterer InSAR (PSI), overcomes the decorrelation problems by identifying resolution elements whose echo is dominated by a single scatterer in a series of interferograms (Hooper et al 2007). In fact, PSI is an extension to the conventional InSAR techniques addressing the problems related to decorrelation and atmospheric noise. Since the reflected signal is the coherent sum of all wavalets backscattered within the resolution cell, the decorrelation also depends on the contribute of single scatterer, which can be constructive or destructive. In fact, if one of the scatterers contributing to the pixel is much brighter than the others, the largest contributor to the phase is the wavelet from the brighter scatterer and

there is little interference from the other Scatterers (Hooper 2006). In general, Persistent Scatterers are represented man-made features such as buildings edges, roads, etc. (Usai, 1997) or natural features such as outcrops.

Ferretti et al., (2000, 2001) proposed the pioneer algorithm PSInSAR™ for Persistent Scatters computation. Progressively, alternatives Multi Temporal InSAR (MT-InSAR, Zhang et al., 2011) algorithms have been developed such as SBAS (Berardino et al., 2002), IPTA (Werner et al. 2003), SPN (Arnaud, et al., 2003, Duro et al., 2003), CPT (Mallorquí et al., 2003), StamPS (Hooper et al., 2004), PSP-IFSAR (Costantini et al., 2008), QPS (Perissin et al., 2007) and SqueeSAR™ (Ferretti et al., 2011). Pioneers PSI methods have been very successful urban areas studies, where buildings provide strong backs scattering waves. However, in non-urban areas, very low density of measurement points was identified and thus not very suitable for most of the natural hazards application (i.e. landslide risk assessment). Second generation of MT-InSAR algorithm, also account for those areas where not a predominant signal from a distinct object can be detected, but rather, the whole area is characterized by a coherent deformation signal. This type of measurement points are known as Distributed Scatterers (Ferretti et al., 2011) and are in general represent by barely vegetated fields. One of the peculiarities of MT-InSAR algorithms is that the signal has to be coherent during the entire time series. If from one point of view, this allows to have higher precision of displacement measurement, for very long time series or in very dynamic environments, it may represent a limitation (longwall mining, open pit mining, seasonal snow cover, etc.). To overcome this problem, the latest algorithms identify the Temporary Coherent Scatterers, extracting information also for those areas where a

statistically coherent signal is detected over a fraction of time (F. Novali et al., 2011, Ferretti et al., 2012, Sowter et al., 2013).

All the afore mentioned algorithms of MT-InSAR can vary and based on different assumption (large baseline, small baseline, functional temporal model dependent, functional temporal model independent, single master, multi master, phase unwrap, etc.) and account for different scatterers types (Pesistent, Distributed, Temporary, etc.). Since this study deals with post-processing application of MT-InSAR, it is independent from the algorithm employed. For this reason, only the general concepts of MT-InSAR are introduced, leaving to the user the choice of the most suitable algorithm according to purpose of the study.

Figure Figure 14 shows a general framework of MT-InSAR. First the archive of Single Look Complex Images have been focused and co-registered to ensure that each ground target contributes to the same (range, azimuth) pixel in all the images in the data stack. Then a master is selected and all the interferograms can be computed using a DEM to account for the topographic contribute. Hence, the MT-InSAR algorithm core, start from the PS selection based on pixels with a stable electromagnetic behavior within the data stack. In particular PS can be defined by both phase and amplitude stability. Existing methods for selecting PS candidates rely on thresholding pixel amplitude variability with time, defined as the ratio of the standard deviation of the amplitude over its mean (Ferretti et al., 2001, Hooper, 2006). At this point, the DEM error is estimated and his contribute can be subtracted to each PS candidates phase.

Once the topographic contribute is removed, the atmospheric artifacts needs to be estimated in order to isolate the deformation term. The basic

concepts are that the atmosphere can be considered uncorrelated in time while correlated in space. This means that the atmospheric phase screen is completely different on each acquisition. While in space, it is demonstrated that the mean distance of correlation is of about 1 km (Hansen, 2001). Thus, the estimation of the atmospheric contribute can be done by high-pass filtering the data in time and then low-pass filtering in space. After the estimation, the atmospheric phase contributes in each interferogram are interpolated and then subtracted from the remaining phases in order to finally obtain the Persistent Scatterers.

Persistent Scatterers are thus generally provided with displacement time series and elevation information, plus parameters indicating the quality of the measurements (such as coherence and standard deviation).Usually, time series of displacement are fitted by a linear regression in order to evaluate the average annual velocity [mm/year]. Conventionally, negative values of displacements refers to objects moving away from the satellite, while positive displacements refers to objects moving towards the satellite. It is necessary to highlight that PS are unwrapped from a reference point within the scene and that is often selected based on its radiometric characteristics. In fact, the selection of the reference points is crucial since it will affect the quality of the whole dataset. Thus, post-processing analysis and interpretation, must always take in account that MT-InSAR are relative measurements and check the reference point, in order to identify if located in areas affected by deformation.

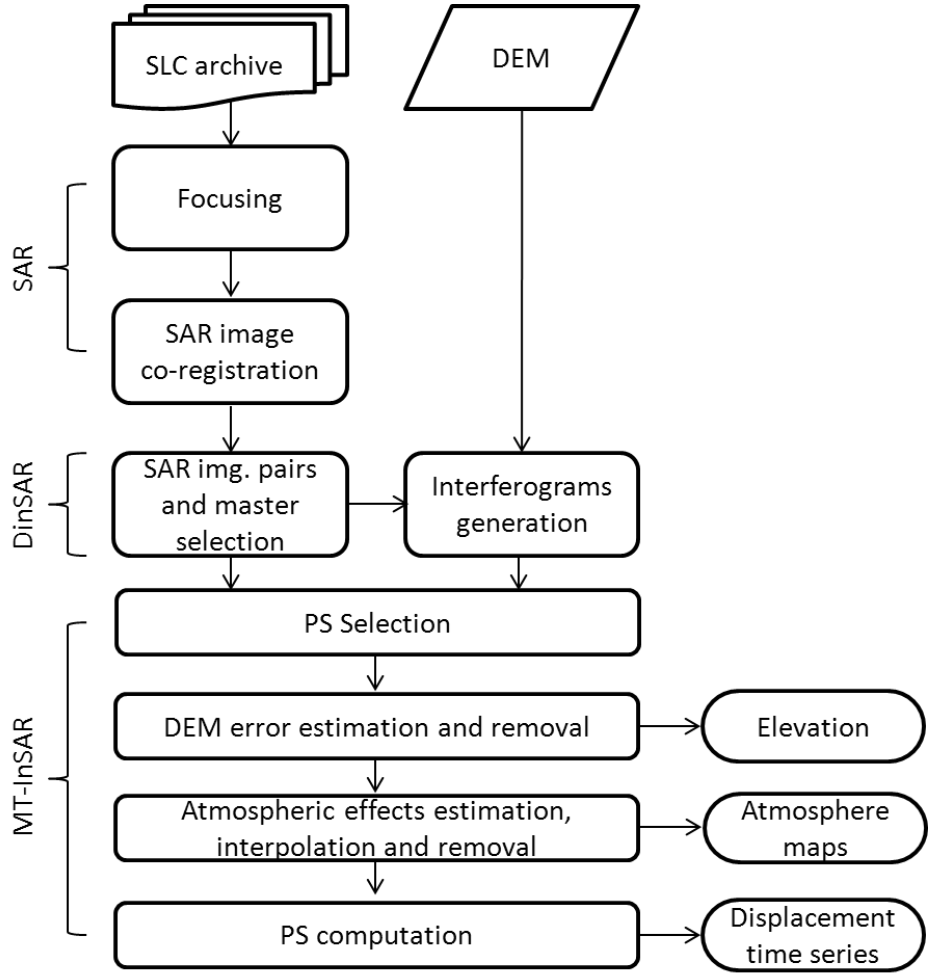

Figure 14. Processing chain of a general MT-InSAR.

In addition to Persistent Scatteres, the latest's MT-InSAR algorithms also evaluate Distributed Scatterers (DS) and Temporary Coherent Scatterers (TCS). In particular, DS correspond to areas that contribute to the signal captured from the antenna. In other words, a general deformation trend is found over differently sized areas, as opposite to PS, that contribute to the signal as single scatters. As an example, typically DS are expected to be found within agricultural fields, while high density of PSs are expected in urban areas. TCS are measurement points where a deformation trend is found but the where the coherence has been lost

during the time (i.e. an object on the surface that is not visible during the entire time span). TCS, for example, can be found in areas affected by seasonal snow cover. The limitation of TCS is that a mean velocity can be evaluated, but no time series of displacement can be extracted. In addition, it is not known "when" and "for how long" the object was affected by deformation.

3 Tools for PSI post-processing

3.1 Velocity components extraction

InSAR measurement represents the component of ground deformation projected to the LoS direction. The module and sign of LoS displacement is dependent on the relationships between acquisition geometry (ascending or descending), local geomorphology, (i.e. slope and aspect) and the real direction of movement. This is a critical issue when dealing with landslides, since only a fraction of slope movement can be captured in the LoS, especially for slopes facing parallel to the azimuth direction (near North or South). Moreover, the same slope movements can be recorded by InSAR with opposite sign and different module from ascending and descending orbits, making the interpretation of slope dynamics not immediately intelligible. Datasets should therefore be post-processed in order to homogenize information and to extract the most significant data on a geomorphic perspective.

Typically, there are two options to evaluate the velocity components.

1) The first option (*double orbits*) can be used when no-prior information on the direction of the deformation are known and when datasets from complementary orbits are available (ascending and descending). In this case, after the establishment of common scattering elements from both orbits, the two velocity from ascending and descending geometry, are combined to compute the bi-dimensional velocity in the East-West plane. In general, the velocity in a three-dimensional system can be evaluated by knowing its components from the (MATTM, 2010). It is possible to set a

reference s`ystem where the East-West correspond to the X axes, the vertical direction correspond to the Y axes and the North-South direction correspond to the Z axes. Accordingly, the resultant velocity is described by equation (12).

$$\vec{V} = V_x \cdot \vec{s}_x + V_y \cdot \vec{s}_y + V_z \cdot \vec{s}_z \quad (12)$$

Where $\vec{s}_x$, $\vec{s}_y$ and $\vec{s}_z$ are the versor.

Anyway, SAR systems measure the deformation rate along the LoS and for a fixed deformation in the three-dimensional reference system, the portion of the deformation measured along the LoS is defined for ascending and descending orbit:

$$\begin{cases} V_{asc} = V_x \cdot s_{x_{asc}} + V_y \cdot s_{y_{asc}} + V_z \cdot s_{z_{asc}} \\ V_{desc} = V_x \cdot s_{x_{desc}} + V_y \cdot s_{y_{desc}} + V_z \cdot s_{z_{desc}} \end{cases} \quad (13)$$

Since only two orbits are available, only two equation can be write to solve a problem made of three unknown parameters, thus the problem is undetermined. Since, due to the acquisition geometries of SAR satellites that is near North-South, only a small portion of the component along this direction is measured. Therefore, if we consider the North-South portion negligible, the problem can be solved in two dimension (East-West and vertical) as reported from equation (14) (MATTM, 2010):

$$\begin{cases} V_{asc} = V_x \cdot s_{x_{asc}} + V_y \cdot s_{y_{asc}} \\ V_{desc} = V_x \cdot s_{x_{desc}} + V_y \cdot s_{y_{desc}} \end{cases} \quad \textbf{(14)}$$

Equation (14) indicates that East-West and vertical components of the velocity can be evaluated using complementary datasets (ascending and descending). SAR image from different orbits are affected differently from the topography and complementary PS do not precisely overlap. Therefore it is necessary to define couples of comparable measurement points from ascending and descending.

2) The second option (*single orbit*) can be used only if information on the direction of the deformation are known, for example from alternative monitoring systems and an in-depth knowledge of the phenomena. The advantage of this method is that it can be applied using one single geometry (ascending or descending).
   A common approach, for landslide hazard, is to assume a movement direction parallel and downward to the slope surface (Colesanti and Wasoski, 2006, Cascini et al., 2010, MATTM, 2010, Zhao et al., 2012, Zhao et al. 2013, Tantianuparp et al., 2013, Cascini et al.. 2013,). Based on this assumption, the three components of the deformation and its modulus can be evaluated from $\vec{r}$ (the LOS unit vector) and $\vec{u}$ (the slope unit vector):

$$\vec{r} = \begin{bmatrix} r_{east} \\ r_{north} \\ r_{vert} \end{bmatrix} = \begin{bmatrix} -sin\delta cos\theta \\ sin\delta sin\theta \\ cos\delta \end{bmatrix} \quad \textbf{(15)}$$

$$\vec{u} = \begin{bmatrix} u_{east} \\ u_{north} \\ u_{vert} \end{bmatrix} = \begin{bmatrix} -sin\alpha cos\beta \\ -cos\alpha cos\beta \\ sin\beta \end{bmatrix} \quad (16)$$

Where δ and θ are respectively the look angle and the azimuth angle of the satellite. The slope unit vector can be evaluated from aspect and slope maps, derived from the Digital Elevation Model (DEM). In fact, in equation 16, α is the slope angle measured from the horizontal plane and β is the aspect angle.

The deformation along the slope direction defines as (Zhao et al., 2012):

$$d_{slope} = d_{los}/(r_{east}u_{east} + r_{north}u_{north} + r_{vert}u_{vert}) \quad (17)$$

In the real case, the assumption that the deformation is paralleled the slopes, is not always true as for the case of rotational landslides, ground settlements, etc. Consequently, erroneous results (also caused by DEM resolution) can be potentially misinterpreted.

In this study, the two afore mentioned models to extract velocities' components used in literature (MATTM, 2010) have been implemented as tools for ArcGIS™. In addition, an alternative method of PS coupling from double orbits has been presented (GEO-PSIC).

3.1.1 Double orbits method: resampling grid

As anticipated, in order to use double orbits method, and apply evaluate the velocity component solving the (14), it is necessary to define couples of comparable measurement points from ascending and descending dataset. A grid based approach has been proposed as nation-

wide guidelines (MATTM 2010). The method consists in create virtual PS for both orbits from a resampling grid overlapping the study area. In particular, PSs are averaged within the resampling grid (Figure 15) and the results are assigned to the cells' centroid (known as "virtual PS").

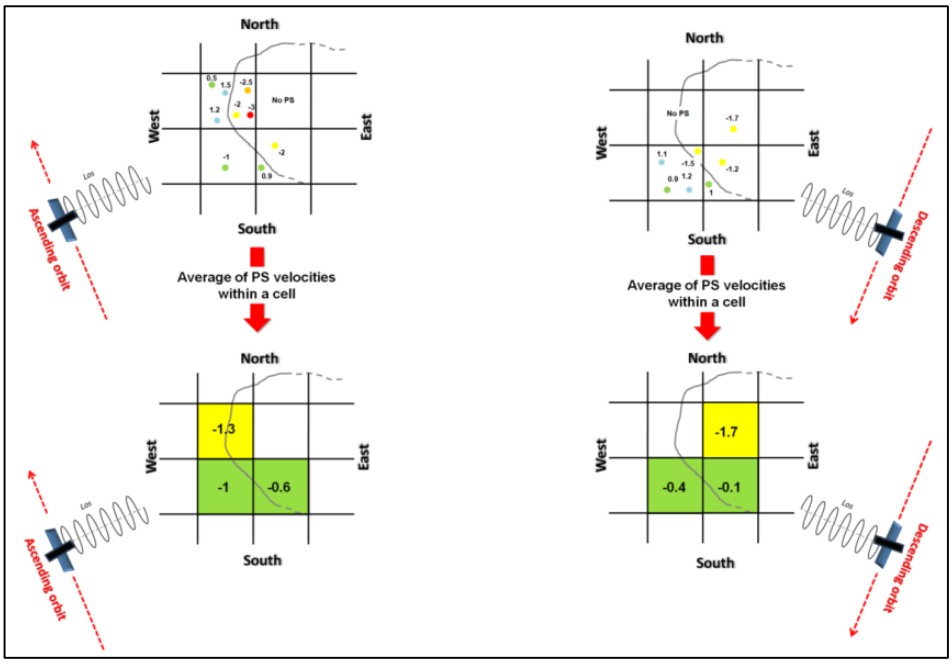

Figure 15. Resampling grid method for velocity components evaluation. Approach usable with double orbits.

Once the virtual PS are computed, the velocities from ascending and descending orbits refers to the same area, that for simplicity is represented in Figure 16 as a scattering object (i.e. building). Figure 16 shows that real displacement (red arrow) is measured with different modulus and different sign from the complementary orbits. In particular in descending geometry, it is recorded as a movement toward the satellite, while in ascending geometry is recorded as a movement away from the satellite.

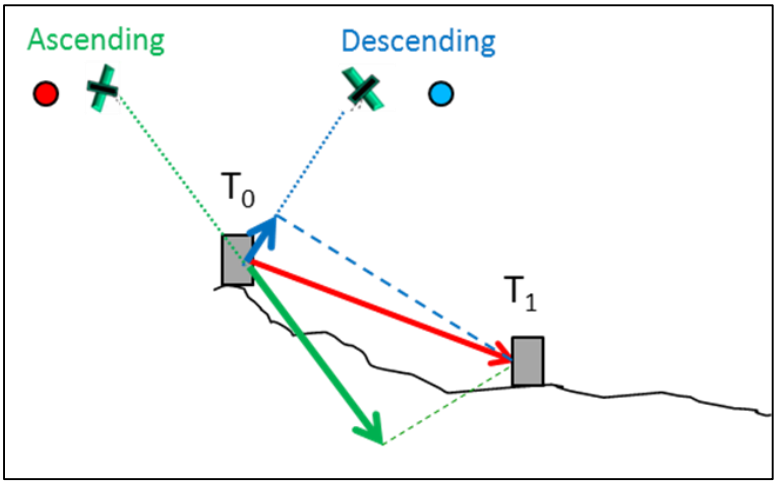

Figure 16. Geometric computation of resultant velocity from ascending and descending orbits.

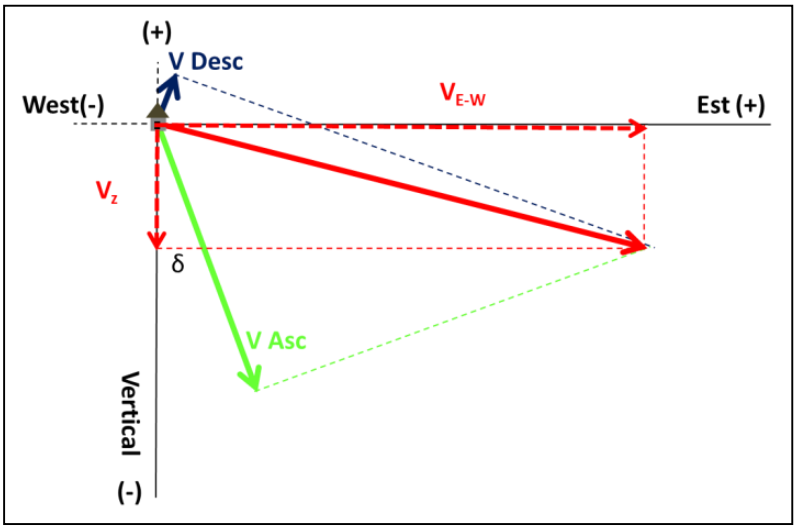

Figure 17. Geometric computation of the East-West component and Vertical component of the velocity.

In order to compute the components evaluation it has been used the explicit form of (14). The solution has been implement using the look angle and azimuth angle as parameters, instead of the versor used in (14). Equation (18) and (18) account for the azimuth angle and evaluate component of the V_{los} in the East-West direction, in order to rigorously

apply the decomposition shown in Figure 17. Equation (20) and (21) are used to calculate the East-West components and the vertical components.

$$V_{losEO\_Desc} = V_{losDESC}/cos(-\theta_{desc}) \quad (18)$$

$$V_{losEO\_asc} = V_{losASC}/cos(\theta_{asc}) \quad (19)$$

$$V_{EW} = \frac{\left(V_{losEO_{desc}}/cos\delta_{desc}\right) - \left(V_{losEO_{asc}}/cos\delta_{asc}\right)}{(sin\delta_{desc}/cos\delta_{desc}) - (sin\delta_{asc}/cos\delta_{asc})} \quad (20)$$

$$V_v = \frac{\left(V_{losEO_{asc}}/sin\delta_{asc}\right) - \left(V_{losEO_{desc}}/sin\delta_{desc}\right)}{(cos\delta_{asc}/sin\delta_{asc}) - (cos\delta_{desc}/sin\delta_{desc})} \quad (21)$$

Where θ is the azimuth angle and δ the look angle.

A tool for ArcGIS™ has been implemented in order to automatize the whole procedure (from the resampling grid creation to the velocity components evaluation). The Graphic User Interface (GUI) allows the selection of the metadata for both descending and ascending dataset (Figure 18).

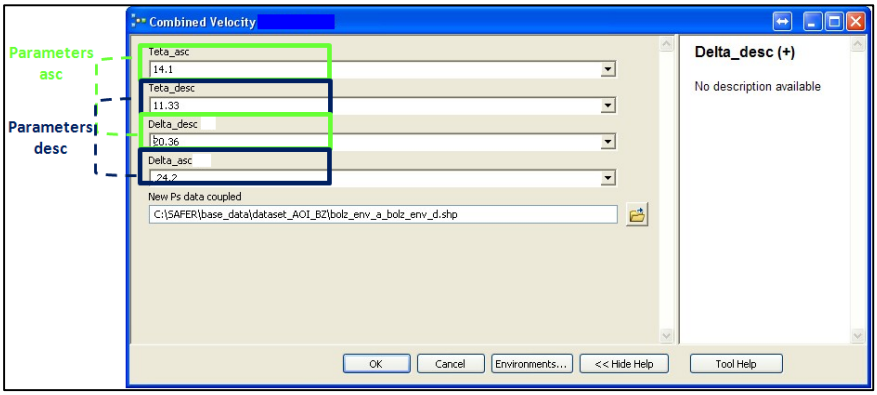

Figure 18. Graphic User Interface (GUI) of the grid method for ArcGIS™. Metadata (azimuth angle and look angle) required as input data.

As visible from Figure 15, the methods is strictly dependent from the size of the resampling grid. Accordingly, deformation velocities of geomorphic units smaller than the resampling grid (or falling only partially within the cell) can be underestimated and smoothed. In other worlds, using the resampling grid there is a probability to couple PSs belonging to very different slope surfaces and, possibly, different slope instability phenomena.

3.1.2 Double orbits method: Geomorphic Persistent Scatterers Interferometry Coupling (GEO-PSIC)

In order to avoid smoothing effects of PS measurements due to the resampling grid in areas of geomorphic interest has been presented a new approach based on geomorphic criteria. This tool, named Geomorphic-based Persistent Scatterers Coupling (Geo-PSIC), has been developed in collaboration with the European Academy of Bolzano (EURAC – Institute for Applied Remote Sensing). GEO-PSIC aims to couple "true" complementary PS, without any resampling and averaging process. The scope is to avoid the combination of features measured on different geomorphic units that can remarkably deteriorate the quality of the

resulting displacement rate components of the investigated phenomenon. To this end, GEO-PSIC couple PSs (ascending and descending) with a relation that can be one-to-one or one-to-many. In particular, both Persistent and Distributed Scatterers can be coupled according to geomorphological and geometric criteria, (i.e. slope and aspect similarities and relative distance). This method has been implemented in a PostgreSQL/PostGIS geo-db and on a web-platform that allows the end-user to upload the PS_{los} database and download the PS_{WE} and PS_{Vert}. The data input required are the PS database (ascending and descending geometry) and their relative's orbital parameters (δ and θ). The PS datasets should be from the same satellite and on the same temporal range. In addition, DEM of the area of interest is required since each PS has to be tagged with slope and aspect parameter attributed by location.

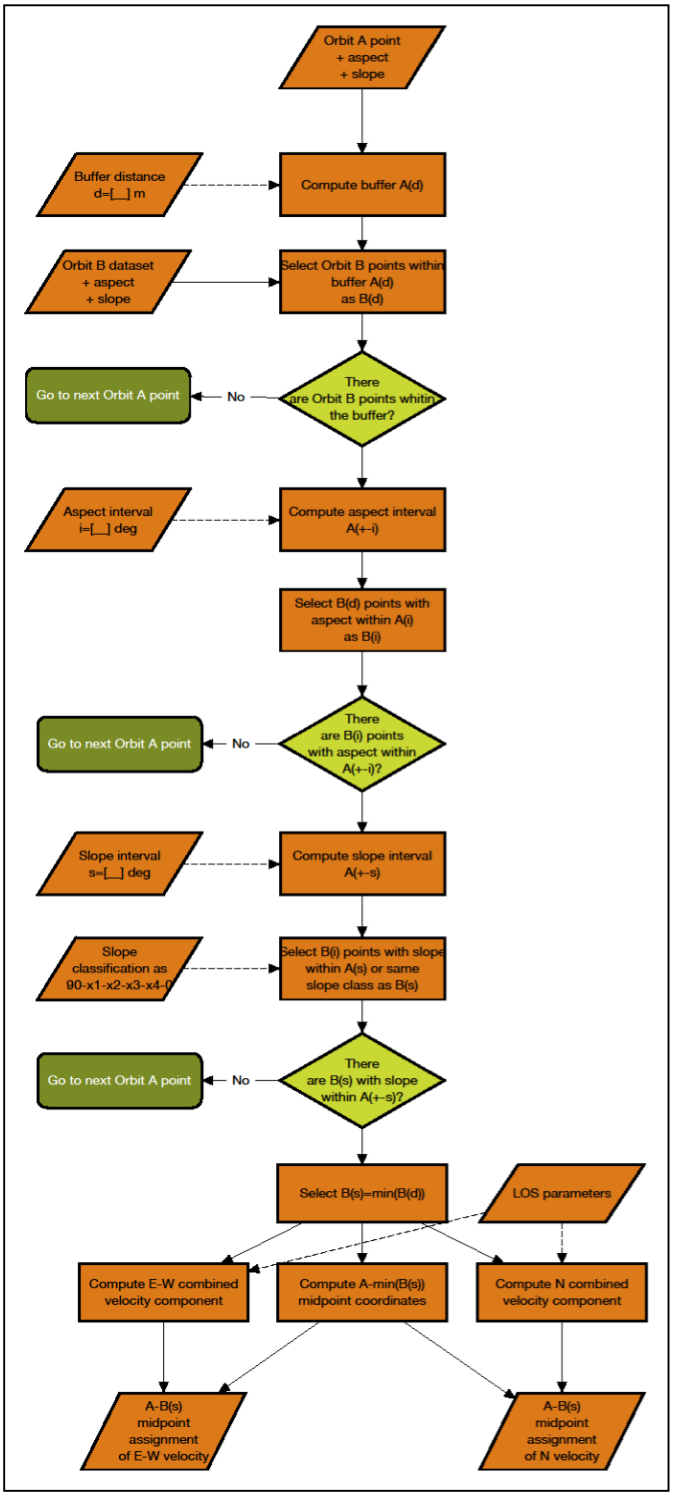

Figure 19. GEO-PSIC model architecture.

Consequently, the outputs of the model is affected by the DEM spatial resolution that has to be selected considering the geomorphology and the roughness of the topography. In fact, using very High-Resolution DEM (VHR-DEM) with highly rough surfaces, PSs can be improperly classified in different geomorphological units

According to the GEO-PSIC model workflow (Figure 19), slope and aspect values from the DEM are attributed to each PS. For each PS from one dataset (e.g. Ascending orbit), is verified if any PS from the complementary orbit exists within a specified distance (Figure 20- left)

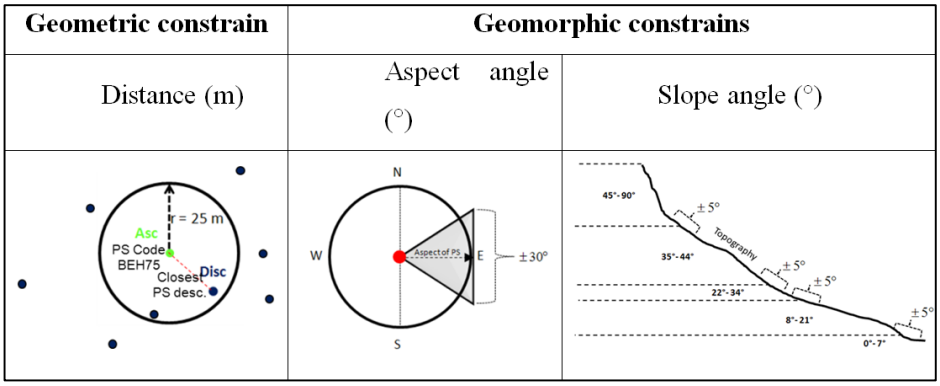

Figure 20. Geometric (left) and geomorphic constrain of GEO-PSIC. Aspect angle class (centre) and slope angle classes (left).

If PS from the complementary orbit is found, a check of reciprocal geomorphic parameters is performed in order to define if the PSs computed for the different orbits belong to the same surface for the investigated area. Namely, these rules consist in checking the correspondence according to slope classes and aspect intervals (Figure 20– center, right). Number and wideness of both can be selected according to characteristics of phenomena. In this work, we used aspect intervals of ±30°, from the reference PS, while for slope classification we used not equally spaced classes in order to avoid the ineffectual

oversampling of classes from 45° to 90°. It is also important to point out, that in the class 45° – 90° is mainly affected by shadowing and thus by a lack of sampling.

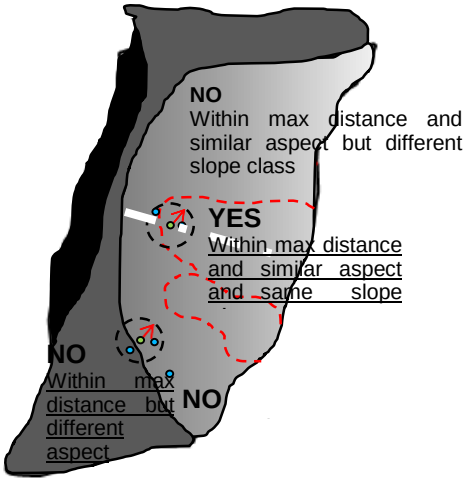

Figure 21. Example of the aspect angle constrain on the PS selection in GEO-PSIC.

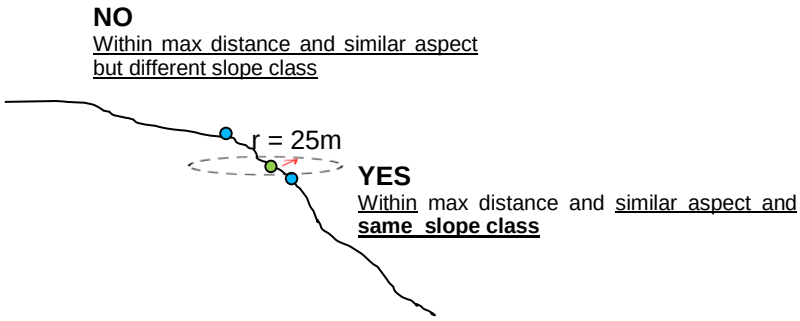

Figure 22. Example of the slope angle constrain on the PS selection in GEO-PSIC.

For each couple of ascending and descending PS filtered, is finally computed the calculation of East-West and vertical components of the

displacement using the equations (18) to (21) Both computed components are assigned to a new PS, planimetrically located at the midpoint of the coupled ascending and descending PSs. As a result, PS outputs database (vertical components and East-West components) are not regularly distributed over an equally spaced grid.

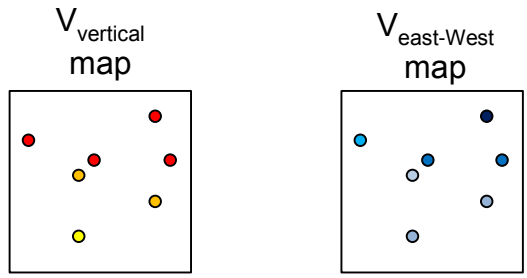

Figure 23. Outputs database of vertical components and East-West components. The spatial distribution of PS is not regular and equally spaced as for the resampling grid method.

3.1.3 Single orbit method: slope back-projection method

When only one geometry is available, it is possible to back-projects the *LoS* deformation along the movement direction, if this latter is known a-priori. Often the movement direction is estimated from the topography, assuming that the deformation follows the slope direction. To automatize the procedure, has been implemented a tool that can be easily used in ArcGIS™. The model inputs are:

3) DEM;
4) Azimuth angle (θ),
5) incidence angle (δ),
6) PSI database in one single acquisition geometry (ascending or descending).

Figure 24 shows geometrically the back-projection model and how the topography is used with the metadata of the SAR image (azimuth angle and incidence angle) to evaluate γ (the angle between the LoS and the aspect) and φ (the angle between the line of sight and the topographic surface). Firstly, the V_{los} is back-projected along the aspect direction:

$$V_{aspect} = V_{los}/\cos\gamma \quad (22)$$

$$V_{slope} = V_{aspect}/\cos\varphi \quad (23)$$

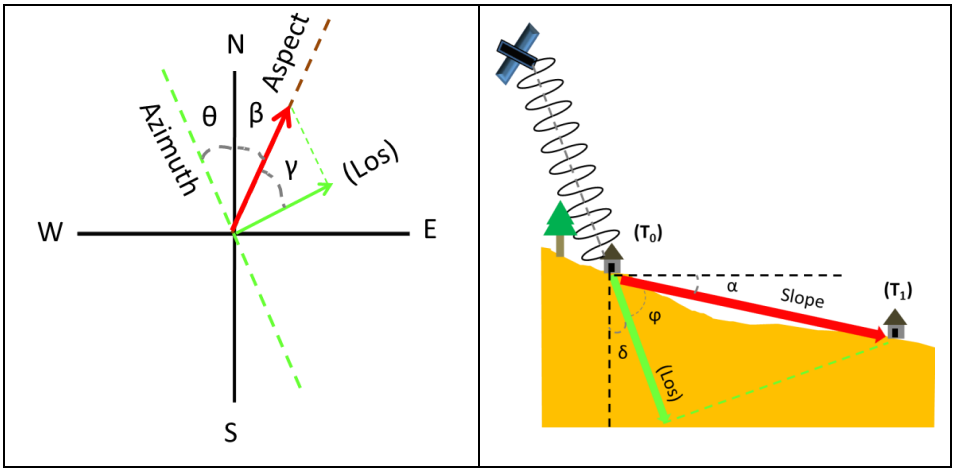

Figure 24. Back-projection method. left) Evaluation of the V_{aspect}; right) evaluation of the V_{slope}.

Once the (23) is applied, the V_{slope} is the "real" deformation vector in the three-dimensional space from which, if required, it is possible to extract the East-West, North-South and vertical components. It is important to highlight that this method is not rigorous the uncertainty introduced can be much higher the real deformation. The errors introduced within the model are mainly related to the fact that:

7) The assumption that the movement direction is parallel to the slope is not always true
8) Results are highly influenced by the DEM quality and spatial resolution

It is probable in fact, that very high resolution DEM (i.e. lidar DEM) produce unreliable back-projected results. Further, it should be considered that back-projecting V_{los} along the slope (V_{slope}), also amplify the inaccuracy of the measurements, typically represented from the standard deviation σ.

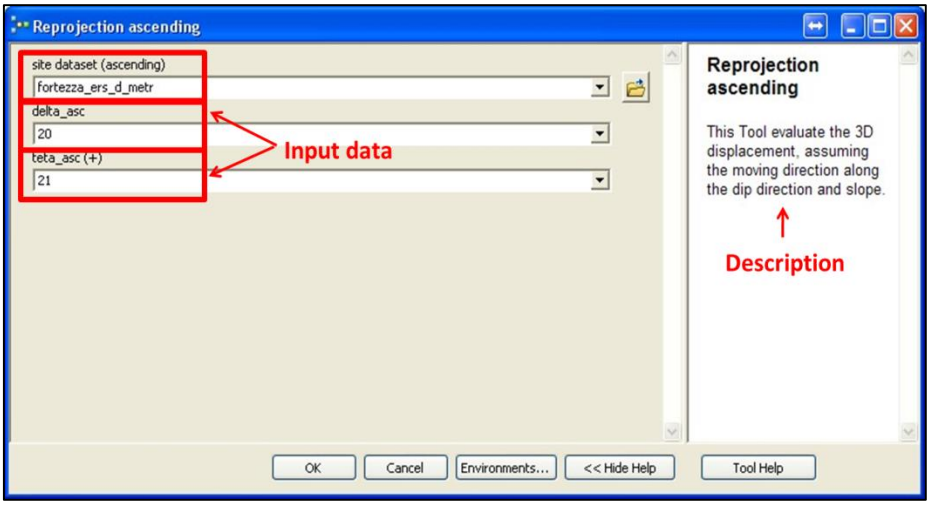

Figure 25. Figure 18. Graphic User Interface (GUI) of the back-projection method for ArcGIS™.

3.2 Time Series Analysis

As anticipated, in general a linear regression model is fitted to data to evaluate the average deformation rate per year (mm/y) of the entire time series. Some authors (Meisina et al., 2008; Cigna et al., 2011) pointed out that the analysis of a few relevant time series may provide useful information on slope dynamics. However, due to high number of measurement points populating PSI database, the visual analysis of single time series is very time consuming and almost impossible to carry out at small scale. To overcome this issue, as part of this work, a paper has been co-authored (Berti et al., 2013) where it is presented PS-Time, a software for automatic classification of displacement time series. This statistically-based software is freely available for research purposes (http://www.bigea.unibo.it/it/ricerca/pstime).

PS-Time is based on a sequence of statistical tests that allows to automatically classifying PSI time series into six distinctive target trends (Figure 26):

- Type 0: uncorrelated – displacement varies erratically in time.
- Type 1: linear – displacement increases linearly in time with constant velocity.
- Type 2 – quadratic: velocity varies continuously in time.
- Type 3 – bilinear: time series is segmented in two linear tracts of different velocity separated by a breakpoint in which the function is continuous.
- Type 4 – discontinuous with constant velocity: time series is segmented in two linear tracts of similar velocity separated by a breakpoint in which the function is discontinuous.

- Type 5 – discontinuous with variable velocity: time series is segmented in two linear tracts of different velocity separated by a breakpoint in which the function is discontinuous.

As an example of their significance on landslides studies, type 0 (uncorrelated) may refers to stable areas (i.e. dormant landslides, areas never affected by landslides, etc.). Type 1 (linear) refers to active slow-moving landslides, creep but moving at constant rate. Type 2 and 3 may represents an acceleration (or deceleration) of a preexisting (or recent) landslide. The differences between class 2 a class 3 are in the motion change rate since in type 2 it is gradual, while in type 3 is net (Figure 26).

The first step in the analysis (Figure 27) is an ANOVA *F* test for the significance of the linear regression (Davis, 1986). The PS displacements are plotted against time and fitted by a linear regression model. If the linearity test fails the time series is directly classified as "uncorrelated" (type=0). Otherwise, if linear regression is significant the time series is tested against a bilinear model. If significant breakpoint exists in the time series, it is checked if there is a discontinuity at the breakpoint and if there is a change in velocity. According to the results of the statistical tests the time series are classifies as 3 (bilinear) in no discontinuity is detected, otherwise in 4 if together with discontinuity is there is no change in velocity and in 5 if a change in velocity exists. On the other hand, if no significant breakpoint is found, the time series is fitted with a quadratic function. If the quadratic term is significant the time series is classified as type 2 (quadratic) otherwise as type 1 (linear). All statistical tests are based on probability thresholds which have been calibrated by the authors, by a visual classification of more than thousands of time series. The expert-based classification has been used together with the

PS-Time classification, to construct a ROC curve and establish the most effective thresholds. A detailed description of all statistical tests and PS-Time architecture, can be found in the paper published by Berti et al. (2013).

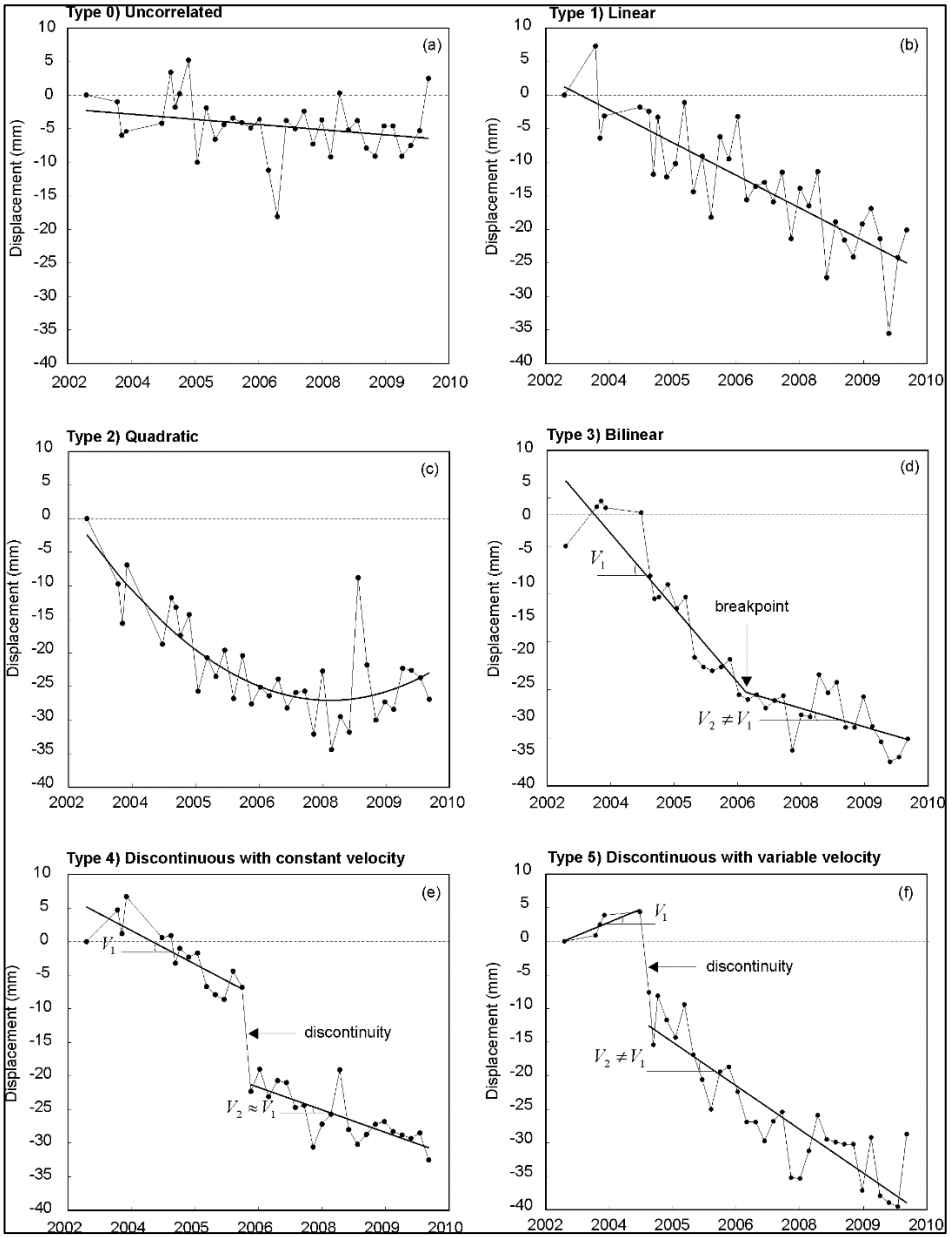

Figure 26. Time series classes of ground displacement detectable with PS-Time (Berti et al., 2013).

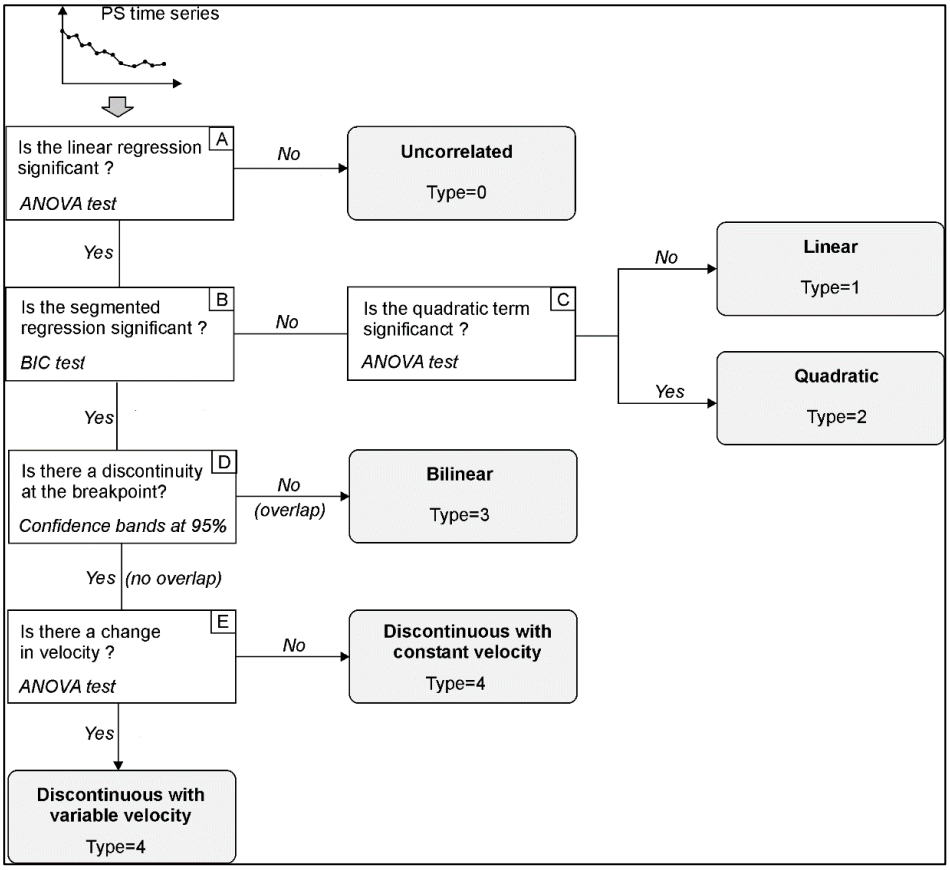

Figure 27. PS-TIME simplified workflow for the automatic classification (modified after Berti et al. 2013)

However, since classes 4, and 5 are very unusual and the classes 2 and 3 have a very similar significance, for most of the study they can be all grouped together in a simplified class of "bilinear".

Additionally for each time series, descriptive parameters are retrieved which can be used to characterize the magnitude and timing of changes in ground motion (i.e. date of acceleration/deceleration, velocity before the change in motion, velocity after the change in motion, seasonal amplitude). Figure 28 shows the Graphic User interface of PS-Time, through which it is selected the PSI dataset (in .csv format), and the values for the probability thresholds. As a default the software

parameters are set based on the calibration described in Berti et al. (2013). The output of PS-Time is a text file (.csv) with the PSs codes and all the descriptive parameters described previously in this chapter, which can be easily joined to the PSI dataset into any GIS environment.

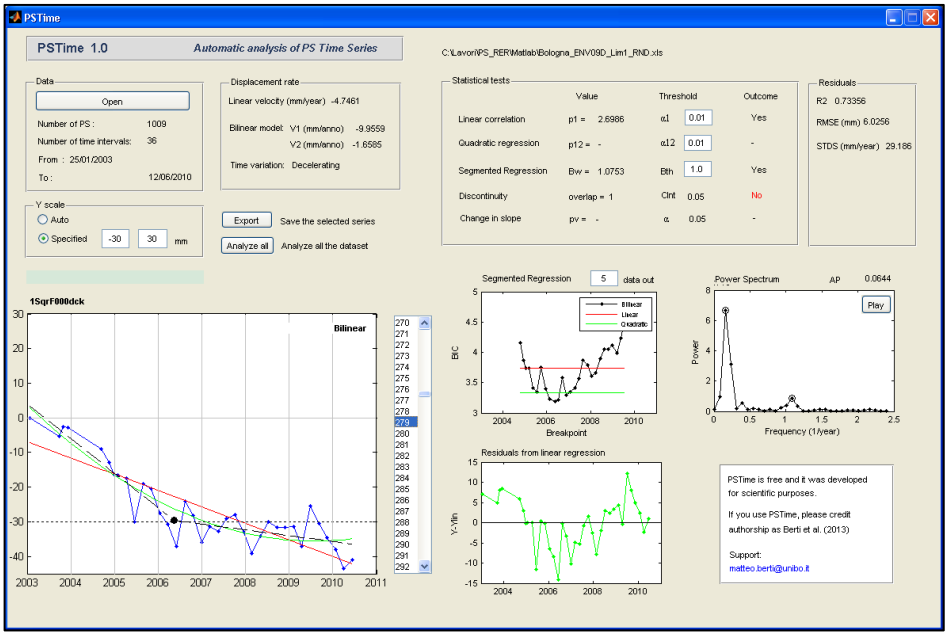

Figure 28. Graphic user interface PS-Time.

3.3 Cluster analysis

Due to the large number of features, small-scale interpretation of PSI dataset is highly computational power demanding. A possible approach to reduce the information redundancy is to identify significant areas characterized by similar deformation. Milone and Scepi (2011) identified clusters of similar time series trends using the Clustering for Large Applications (CLARA) algorithm, introduced by Kaufman and Rousseeuw (1990). Morelli et al., (2010) applied the Getis–Ord G_i^* statistic for the creation of iso-kinematics map that have been also used to identify tectonic uplift activity (Perrone et al., 2013). Lu et al., (2012) combined the use of the kernel density (Silverman, 1986) with the Getis–Ord G_i^*statistic to identify automatically slope movements reflecting in concentrations of high-velocity PSs. In this proposed approach, referred from the authors as PSI Hotspot and Cluster Analysis (PSI-HCA), the G_i^*statistic is used to evaluate the clustering level of PSs, while the kernel density function (Silverman, 1986) is used to estimate PS density based on these derived G_i^* values. The G_i^*index at i PS and for j neighbor is calculated as:

$$G_i^*(d) = \frac{\sum x_j + x_i - n_{ij}\,\bar{x}^*}{S^*\{[(n \cdot n_{ij}) - n_{ij}^2]/(n-1)\}^{0.5}} \quad (24)$$

Where n indicated the total number of PS and n_{ij} the number of PS within a predefined search distance d. The velocity of the PS is represented by x , its average and standard deviation from the whole dataset velocity are represented by $\bar{x}^*$ and S^*.

Using the velocity as a weighting factor, the result is a measure of high-velocity PSs concentrations, with respect to the PSI data set. Positive G_i^* index refers to clusterization of PS moving towards the satellite while negative value refers to clusterization of PS moving away from the satellite. However, at this stage, the output dataset are still high computational power demanding and spatially discontinuous. In order to create clusters map, Lu et al. (2012) applied the kernel density (Silverman, 1986), a non-parametric probability density function of a random variable defined as:

$$f(x) = 1/nh \sum_{i=1}^{n} K((x - X_i)/h) \quad (25)$$

Where K the is the kernel, $x - X_i$ is the distance from each i-th PS and the bandwidth h represent the smoothing parameter. The Kernel density is here used to create a smoothing surface fitting the G_i^*index values and thus derive a population of Hot and Cold spots (clusters moving towards or away from the satellite) starting from a finite data sample. PSI-HCA results into a low computational power demanding map which is easier to use for rapid small-scale mapping of landslides.

4 Application to Landslides

4.1 Application to Regional landslide recognition

4.1.1 Introduction & state of the art

The use of remote sensing has proven to be very valuable for landslide hazard assessment. In particular, a typical remote sensing landslide study can be differentiated in the following phases: Detection; Classification; Monitoring of the landslide activity in time.

This phases should be followed by the analysis and prediction in space and time of slope failures (Mantovani et al., 1996). Tofani et al., (2013) within the framework of the Safe-Land (an FP7 EU-funded project) prepared a questionnaire to collect information about the use of remote sensing among end-users and researchers involved in landslide studies in Europe. Results highlighted that detection is usually performed using optical and radar images while for the monitoring phase, radar images are preferred.

Table 1. Landslide velocity classes and InSAR applicability (modified after Cruden and Varnes, 1996).

Class	Description	Typical Velocity (lower extreme value per class)	Detectable with MT-InSAR
7	Extremely Rapid	5 m/sec	No
6	Very Rapid	3 m/min	No
5	Rapid	1.8 m/hour	No
4	Moderate	13 m/month	No
3	Slow	1.6 m/year	No
2	Very Slow	16 mm/year	Partially
1	Extremely slow		yes

In general, considering the satellites nowadays in orbit (L, C and X Band) and the repeat-pass (days to month), the landslides that, typically, can be monitored with InSAR, are within the "extremely slow" and "very slow" classes (Table 1).

In particular, the first report addressing InSAR as a tool for landslides detection is found in Scanvic et al. (1993). Since then, many examples of InSAR, applications to landslide studies have been presented (Carnec et al., 1996; Singhroy et al., 1998; Singhroy and Mattar, 2000, Kimura and Yamaguchi, 2000; Allievi et al., 2003, Catani et al., 2005; Corsini et al., 2006, Meisina et al. 2008, Lu et al. 2013, Bianchini et al., 2012). The introduction of PSI InSAR algorithms has greatly favored regional landslides studies. This is due to fact that: 1) PSI datasets structure is prone to be used for different types of geospatial analysis; 2) PSs are easier to interpret compared to interferograms; 3) PSs are returned only in coherent areas, reducing the ambiguity in the interpretation of deformation due to the atmospheric noise. The main problem related to the interpretation of PS data over regional areas is the great amount of data to be analyzed, so that authors have proposed different types of automatic analysis of PSs. For example (as discussed in section "Cluster analysis"), Lu et al., 2012 aim to identify clusters of LoS velocity mapping using the G_i^* index and kernel density. Notti et al., (2008, 2010) identify "anomalous areas" with a minimum of 3 PS within a distance of 50 meters, characterized by average LoS displacement rates over to ± 2 mm/yr. Berti et al., 2013 focused their attention rather on the shape of the deformation's time series (discussed in section "Time Series Analysis"), classifying automatically entire PSI dataset. A further approach for landslides inventories update, is the activity matrix (MATTM 2010, Cigna et al., 2013), which define landslides activity based on the

deformation rate captured from different satellite and thus referred to different time ranges. However, when using the activity matrix a V_{ACT} velocity thresholds should be set *a priori*. Examples of V_{ACT} velocity thresholds reported from the authors are in the range tween ±1.5 and ±4.0 mm/y. Moreover, Bianchini et al., 2012 and Righini et al., 2011 distinguishing slow from very slow phenomena using a V_{los} of ±10 mm/y. Cascini et al., 2013 propose the DInSAR-Damage matrix, which is an evolution of the activity matrix, introducing data concerning survey-recorded damages as indicators of movement. As a result, they classify landslides in "dormant" and "active" landslides, where the "active" class includes reactivated and suspended phenomena (Cruden and Varnes, 1996). The DInSAR-Damage matrix use the V_{slope} to establish if a landslide is moving or is stable and the threshold is variable within the dataset, depending on the inaccuracy of the PS. The literature review highlighted that automatic or semiautomatic post-processing routines are needed to extract information from large dataset aimed to identify areas with deformation trends characteristic of slope movements. The post-processing tools presented in the previous Chapter, are here applied to different geological context to detect and characterize the potential active landslides.

4.1.2 South Tyrol

4.1.2.1 Objectives and General Settings

Post-processing routines are tested in South Tyrol, a geographic region located in Eastern Alps, in northern Italy (BZ). The mountainous landscape derives from a complex geological and structural settings constituted by sedimentary, magmatic and metamorphic rocks belonging

to the basement and to the marine stratigraphic succession, dating from the Permian up to the Cenozoic. The area is dived in Southern-Alpine and the Austro-alpine domain (Klebelsberg, 1935; Bosellini et al., 2002; Stingl and Mair, 2005) by the transpressive Periadriatic Seam (i.e Insubric Line) (Laubscher, 1989). The Austroalpine domain is predominantly represented by metamorphic rocks, such as gneiss, paragneiss and mica-schist, which are followed by a Permo–Triassic stratigraphic succession with locally embedded volcanic units. In other hand, the Southern-Alpine sector is characterized by magmatic basement (Oligocene to Pliocene) followed by a carbonatic or terrigenous succession (Mesozoic–Cenozoic). The geomorphic structures of the area (i.e. sub-vertical slopes, valleys, crests, landslides, alluvial fan, debris fan, rock glaciers, moraines, cirque glacier, etc.) are the results of the combination of tectonic, lithological and climatic factors. Within the study area, there are several Deep-Seated Gravitational Slope Deformation (DSGSDs) which are the consequence of the slope stress release due to the most recent post-deglaciation (Würm). In addition, gravitational processes, such as landslides, are widespread in the study area and in general mass movements have been favored from intense extensional tectonics. Even if all landslides types (Cruden and Varnes, 1996) can be found in the study area, the attention of this study is on slow-moving and extremely slow-moving landslides. These landslides often interact with infrastructures, with potential loss of money for ordinary and extraordinary maintenance. In few cases, they might also evolve into catastrophic events.

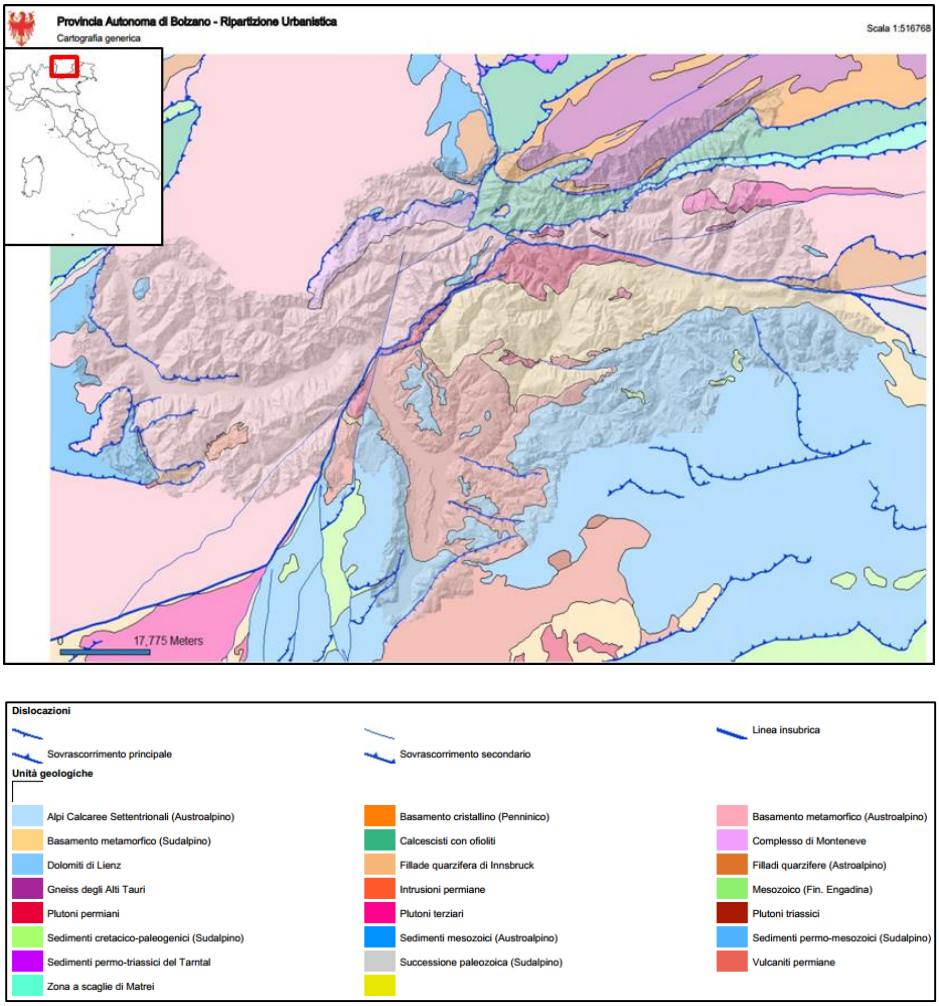

Figure 29. Simplified geological map of South Tyrol. Source: Geobrowser of the Autonomous Province of Bolzano (legend in Italian).

In particular, this study focused on the western sector of South Tyrol, in the Venosta valley, where nine most critical area have been identified with the aim of InSAR data and a-priori knowledge of active deformations. The Venosta Valley belongs to the Austro-Alpine domain and outcrops are mainly represented by Micaschists, paragneisses, phyllites and marbles in the upper portion and by granitoid gneiss, phyllites, porphyroides, marbles and green shales in the lower portion. In

the Southeastern sector of the study area, the metamorphic basement contacts with the Permian Plutonic rocks trough the Insubric Line.

Nine critical areas have been mapped by visual interpretation from the SqueeSAR™ datasets as areas where further investigation may be required (Figure 30). In some of these areas, landslides mapped within the IFFI project (Italian Landslides Inventory) can be found (Figure 31).

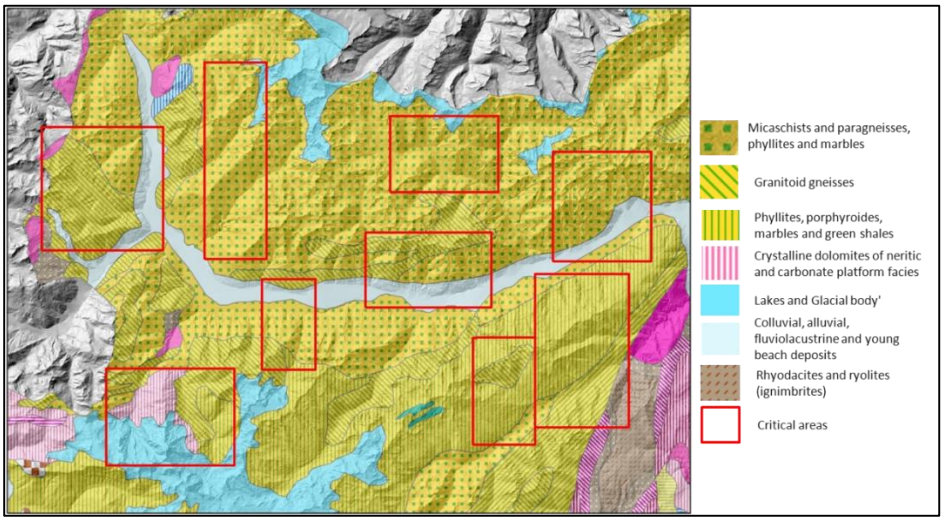

Figure 30.Geology of the Venosta Valley and critical areas.

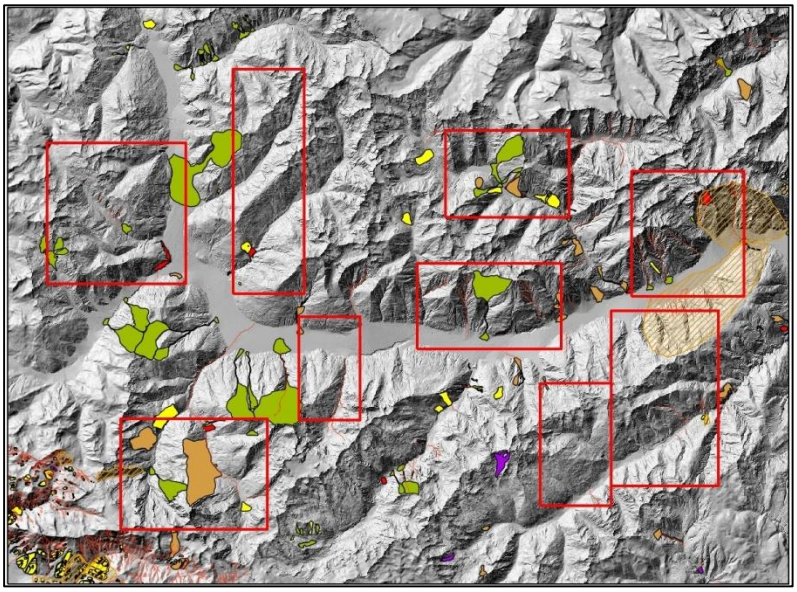

Figure 31. Landslide inventory of the Venosta Valley (IFFI).

4.1.2.2 Datasets & Methods

The PSI dataset used in for the analysis have been made available within the framework of the European project "Services and Applications for Emergency Response" (SAFER). In particular, two data stacks (ascending and descending) composed by 38 and 37 RADARSAT-1 SAR images respectively, where processed by T.R.E. s.r.l. using their own SqueeSAR™ proprietary algorithm. In particular the dataset covers the Venosta Valley (an area of about 4000 km^2 in the Western sector of South Tyrol) and refers to a time span from March 2003 to March 2006. The results of the SqueeSAR™ processing in terms of average velocity [mm/year] and standard deviation [mm/year] are shown in Figure 32, Figure 33, Figure 34 and Figure 35. Velocity are displayed between $\pm 5\ mm/y$ in order to highlight also extremely slow moving landslides that according to the Cruden and Varnes classification (1996) are below $16\ mm/y$. When interpreting InSAR data, it is very important to analyse the velocity together with the associated standard deviation, which typically increase with the distance from the reference point. This is evident since several "extremely slow" moving landslides can have a velocity comparable to its standard deviation.

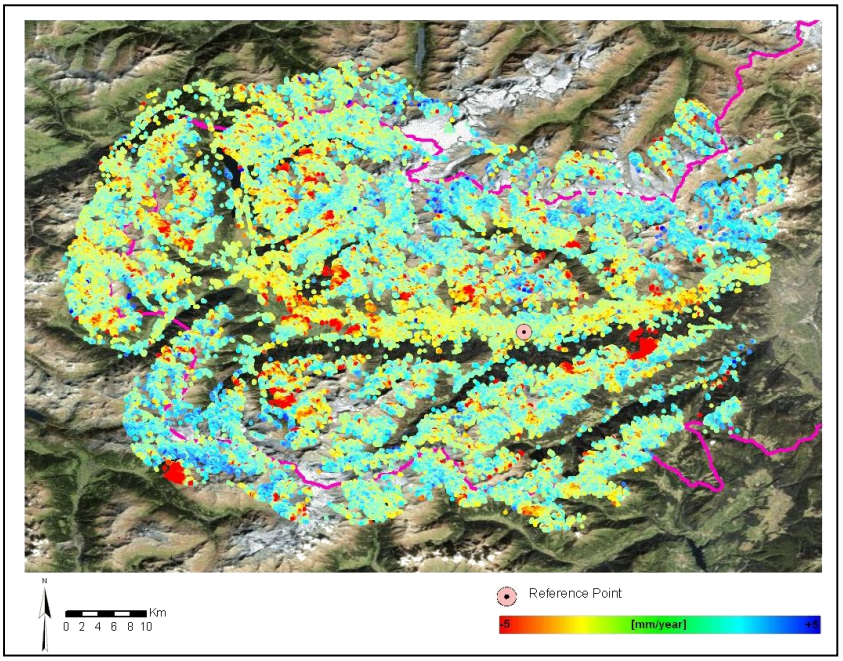

Figure 32. PS velocity of the descending geometry and location of the reference point. Satellite: RADARSAT; Algorithm: SqueeSAR™.

According the Figure 33 and Figure 35, the maximum value of standard deviation within the descending dataset is about $1.8\,mm/y$ while in ascending dataset the standard deviation reach in the North-Eastern sector a standard deviation of about $6\,mm/y$. Is it possible to note that the standard deviation increase as the distance from the reference point increase, since it also depend from the cumulated number of link between the Persistent Scatterers Candidates (PSC) needed for the phase unwrap.

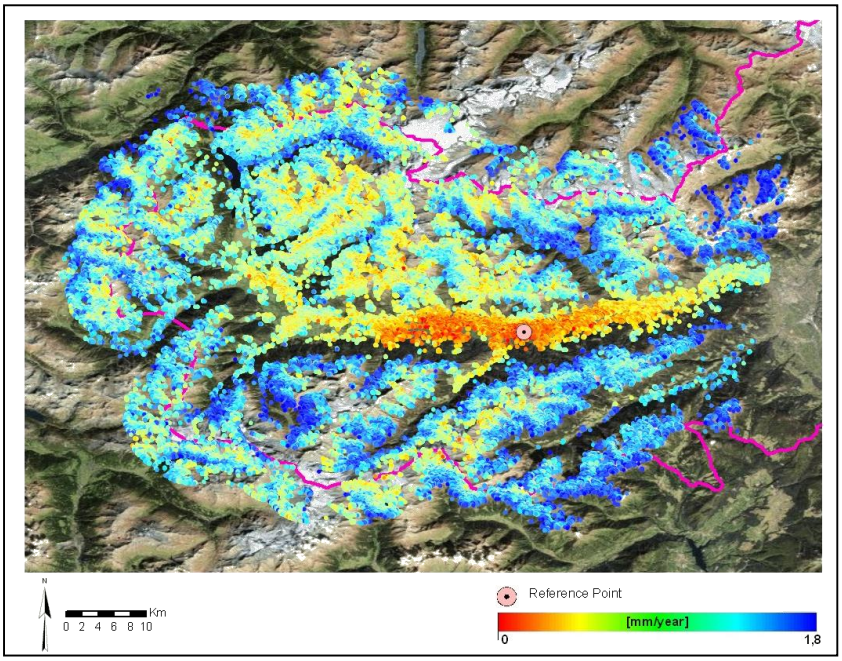

Figure 33. PS standard deviation of the velocity (descending geometry).

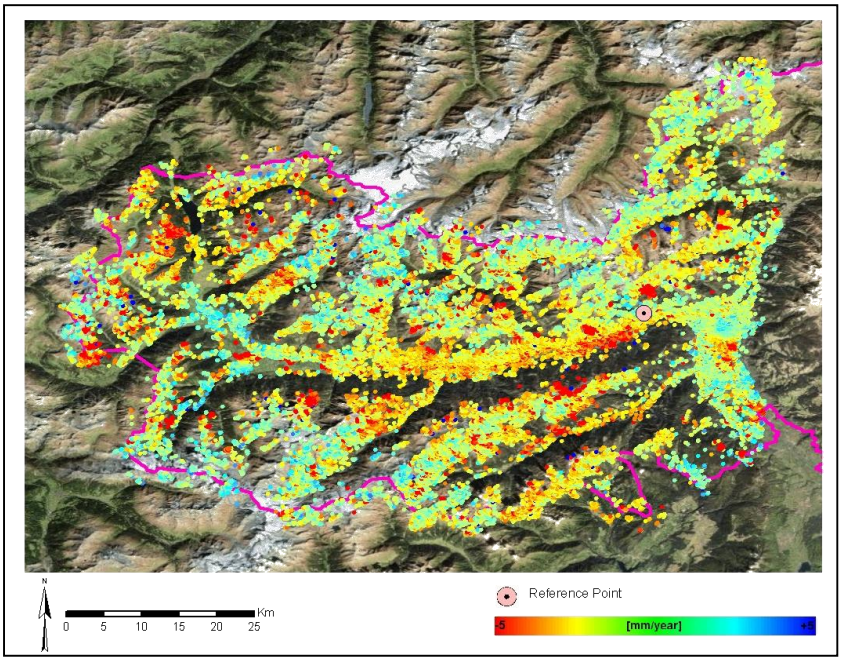

Figure 34. PS velocity of the ascending geometry and location of the reference point. Satellite: RADARSAT; Algorithm: SqueeSAR™.

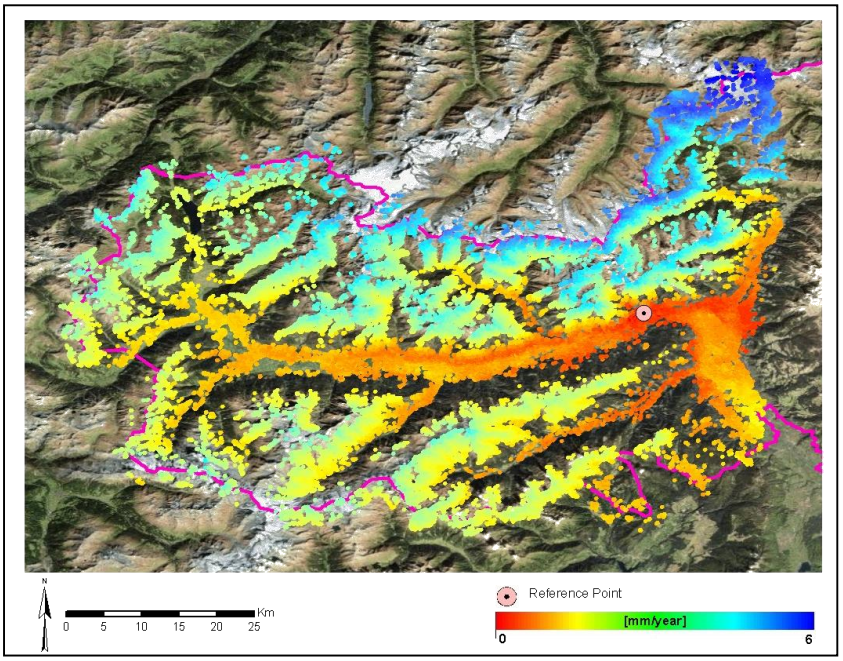

Figure 35. PS standard deviation of the velocity (ascending geometry).

4.1.2.2.1 Hot Spot Analysis

In order to test the automatic mapping of critical areas, the Hot Spot Analysis was applied to the RADARSAT descending dataset. The results are strictly dependent from a distance parameter used as to limit the search radius to find PSs clusters. Since this analysis is aimed to detect landslides, 200 meters has been set as maximum search distance, considering to be a reasonably values for defining spatially correlated deformations and reducing at the same time the probability to clusterize together PSs belonging to different geomorphic units. Figure 36 show the result of the Hot Spot Analysis where cold spots (blue) indicate areas moving toward the satellite while hot spots (red) indicate areas moving away from the satellite. It is important to highlight that the output of this analysis is a continuous map, with absence of "no-data" area and where each pixel is represented by a value of "magnitude" that depends from

the density of points and degree of clusterization velocity values. Unfortunately these values do not have a physical significance and it varies for each dataset. Also, a map with only significant Hot and Cold spots, a threshold has to be applied to mask all areas stable and/or with not particular interest. In this study, it has been used a trial and error approach, overlapping the Hot Spot map with the landslide inventory and checking the geomorphic units from the ortho-photos and the Lidar DEM. Even if this is a qualitative approach, about 20 hot spot and 14 cold spot, have been identified and are available to be checked at local scale to define if further investigation are required.

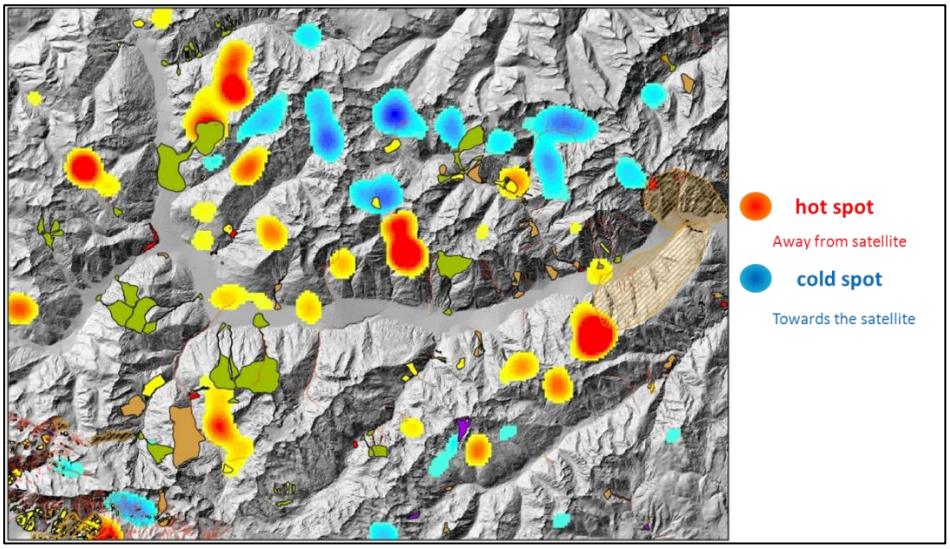

Figure 36. Hot Spot Analysis of the descending dataset. The cold spots (blue) indicate areas moving toward the satellite while hot spots (red) indicate areas moving away from the satellite.. Other coloured polygons are landslides mapped within the National Landslide Inventory (IFFI). It can be noticed that many hot spots are located outside mapped landslide areas, indicating an added value of PSI data for updating landslide inventories.

It is possible to note that while some of the spots correspond to previously mapped landslides, several spots put the attention over

towards areas not classifies as landslides. This is the results of several factors. In fact it has to be considered that:

- Landslide inventories include active a dormant landslides;
- The National Landslide Inventory (IFFI) in this area is not very detailed and incomplete;
- The HS analysis map all types of deformation/displacement (i.e. subsidence, rock glaciers, landslides, ground settlements, etc.)
- The HS analysis also produce several false positive

4.1.2.2.2 Velocity components extraction

The East-West and vertical components of the PS velocity have been computed using Geo-PSIC (Figure 37). The average PS density over the whole study area is of about 170 PS/km2 in the descending geometry and about 150 PS/km2 in the ascending geometry. For being a regional analysis, covering mostly montaneous areas, they can be considered high density datasets. If from one point of view, high number of PSs leads to have more information available to analyse, from another point of view, for regional scale analysis, their use in standard workstation can be crucial. When evaluating the velocity components the number of PSs decrease drastically with both approach, the resampling grid and Geo-PSIC (Table 2). The main contribution to this reduction of PSs number, is due to the fact that PS decomposed can be evaluated only in area were both ascending and descending are available. Unfortunately due to geometrical distorsion of SAR images often areas visible in one geometry are not visible in the opposite geometry, end vice-versa.

Table 2. Statistics of Geo-PSIC analysis at regional scale.

	PS asc	PS desc
	108000	117000
PS decomposed obtained with Geo-PSIC	11580	
% of PSs with respect to the input PS datasets	5,2%	

The geomorphic approach proposed with Geo-PSIC, compared with the resampling grid, allows to obtain the most significant PS decomposed, favourinvg PSs with a geomorphic similitude.

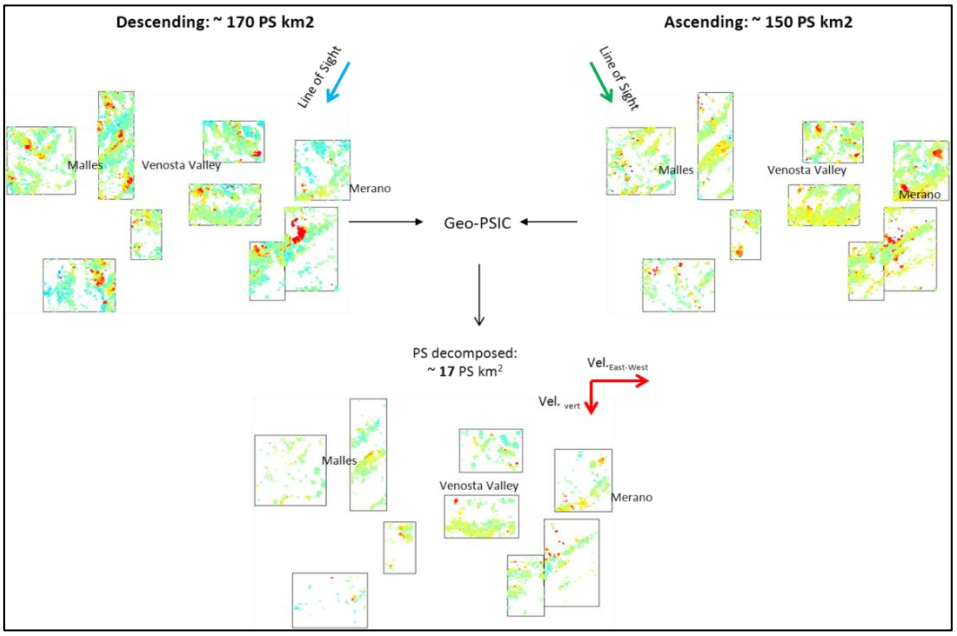

Figure 37. Application of Geo-PSIC for the selection of the PS couples for the evaluation of the velocity components.

In order to test the effectiveness of Geo-PS, the resempling grid approach has also been applied to the same dataset to extract the velocity components, and the results have been compared. Fot the processing with Geo-PSIC it was used a serch distance radius of 25 m, while for the Resampling grid a pixel size of 50 x 50 m (comparable with a circle

having a radius of 25 m). By comparing the results of the whole datasets for both techinques (resampling grid and Geo-PSIC) it can be observed that for regional analysis the two methods are practically equivalent. In fact as expected, comparing separetly the vertical components and East-West components of the velocity, very similar results can be found between the two methods (Figure 38, Figure 39).

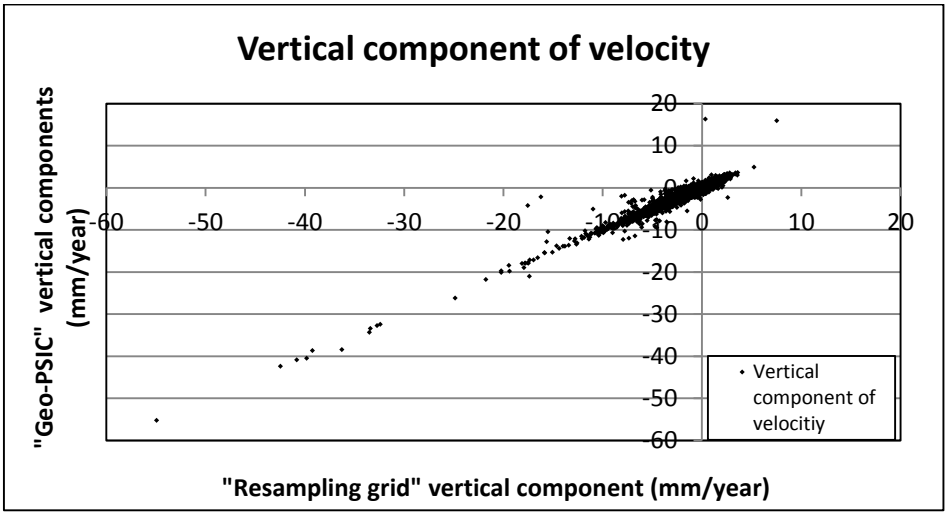

Figure 38. Comparison of the vertical component from the "resampling grid" method and from "Geo-PSIC".

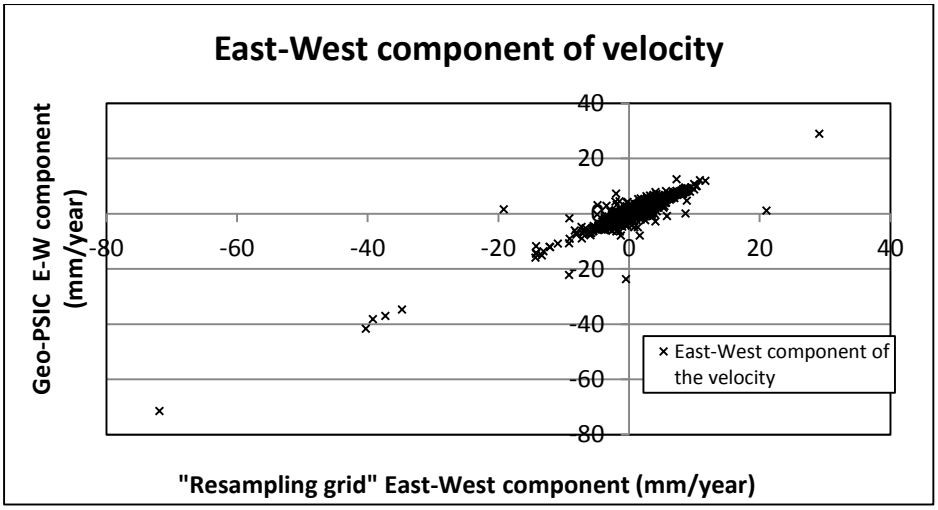

Figure 39. Comparison of the East-West component from the "resampling grid" method and from "Geo-PSIC".

Additionally it has been verified at regional scale the improvement from using our proposed approach, Geo-PSIC. To this end, first the cells of the resampling grid method, have been overlayed with the results from Geo-PSIC. It was found that over a total amount of 11512 $PS_{resampling\ grid}$, only 9581 are also overlayed by $PS_{Geo\text{-}PSIC}$, meaning that 16.8% of the $PS_{resampling\ grid}$ are discarderd by Geo-PSIC. In other words, 16.8% is the amount of points that are returned by the resampling grid even if in extreme geomorphic conditions (belonging to different geomorphic units) (Table 3).

Table 3. Measurement points discarded by "Geo-PSIC" due to particular geomorphic condition, but returned from the "resampling grid" method.

Tot $PS_{resampling\ grid}$	11512	
	$PS_{res.\ grid\ \&\ Geo\text{-}PSIC}$	$PS_{descarded}$ (different geomorphic unit)
n° PSs	9581	1931
% of tot	83,2%	16,8%

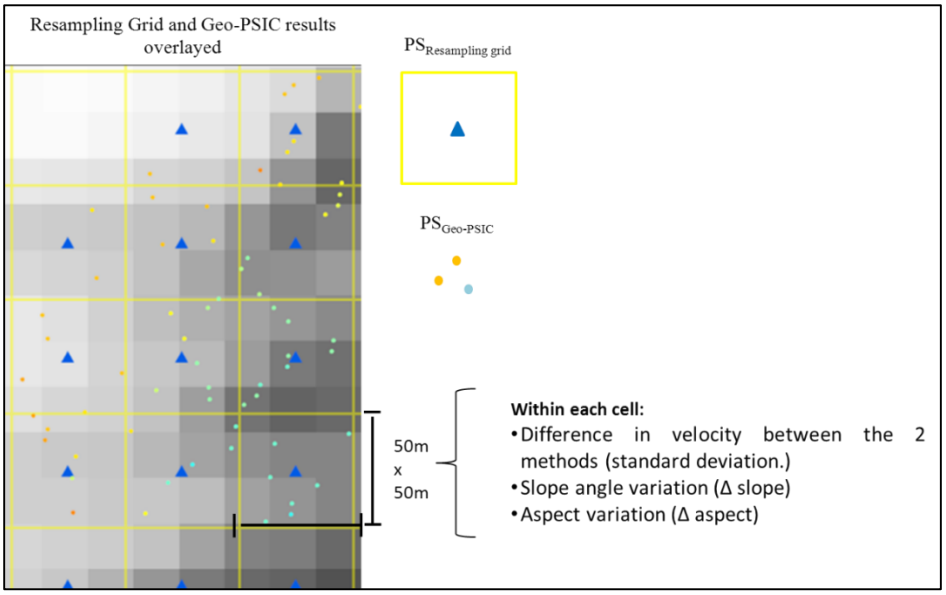

Figure 40. Overlay of the "resampling grid" results and the Geo-PSIC results. Extraction for each single cell of: 1) variation of velocity; 2) variation of slope angle; 3) variation of aspect angle.

Figure 41 shows the $PS_{res.grid}$ discarded from Geo-PSIC, for each class of slope angle variation within a cell (Figure 40). The distribution curve is asimmetric and it can be observed the most of the areas have little slope angle variation, in particular about 2°. Of course the reults also depend from the DEM resultion, which in this study was 20 m. Very high resultion DEM can cause the opposite effect, that means that rough surface can locate PS in different slope angle ad aspect angle classes, even if they belong to the same geomorphic unit.

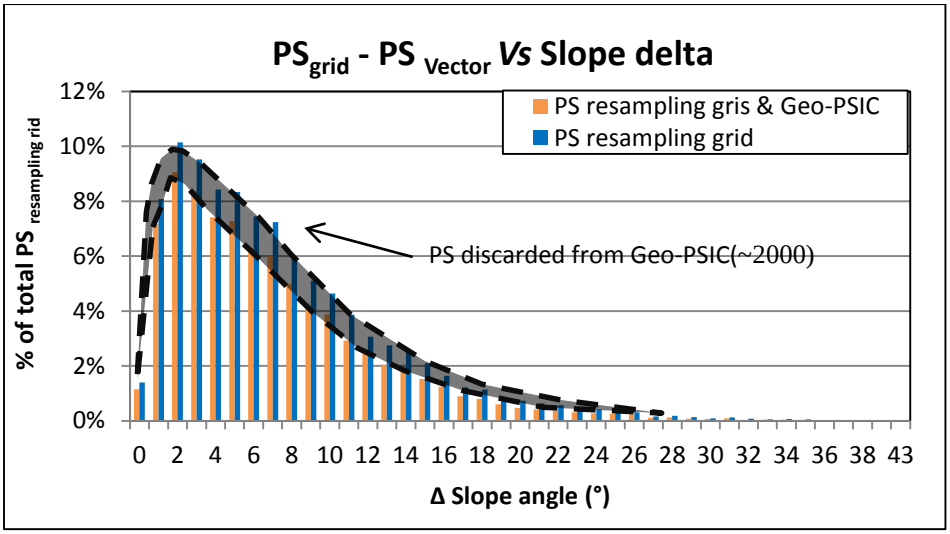

Figure 41. Measurement points from the resampling grid method and discarded from Geo-PSIC thanks to the introduction of geomorphic rules.

It should be noticed that there is a clear direct proportional relation between the minimum variation of the velocity within each single cell, and the corresponding variation of slope angle. In other words, Figure 42 highlight that differences in the evaluation of the velocoty between the two methods, increase with the variation of slope angle classes. In particular the more abrupt is the local geomorphology (high slope angle variation) the bigger are the differences between the resampling grid and Geo-PSIC. The increase of difference in velocity for high slope angle variation also prove the smoothing effect typical of the resampling grid method.

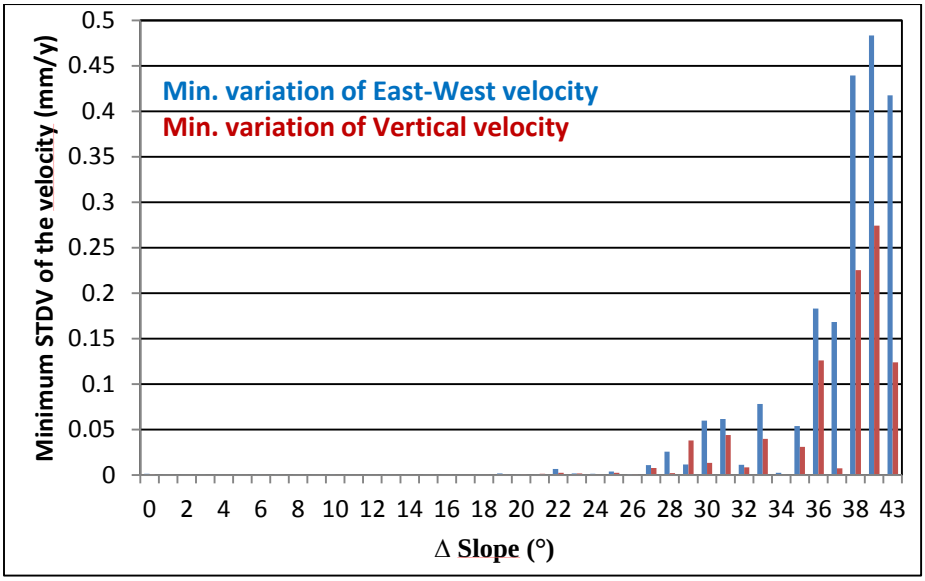

Figure 42. Minimum variation of the velocity within each class of variation of slope angle.

4.1.2.2.3 Time Series Analysis

The RADARSAT-1 ascending dataset of the Venosta Valley has been processed with PSTime in order to determine the deformation types of all the measurement points. The results (Table 4) indicate that among about 100000 measurement point analyzed with PSTime, 60% do not show any correlation between time and deformation, In other words, 60% pf the PS represent "stable" areas. It has to be stressed out that this is a statistic definition, but there can be stable areas even in presence of PS time correlated (i.e. type 1,2,3,4 and 5), or unstable areas in presence of PS "uncorrelated" with time (i.e. moving reference point, movement direction near-North-South, etc.). It is evident tha the "uncorrelated class" (which the normal distribution is tipically ceneterd on "zero") has a much higher probability tha is referred to stable targets. About 7% of the PS results to be linear, 15% are quadratic and 17% are bilinear. Only about 0.1% of the measurement points have a step in the time series. Usually steps can be used also to identify possible unwrapping phase.

However since from class 2 to class 5, all time series can be described by 2 segments, all PS have been riclassified in 3 simple classes: uncorrelated, linear and bilinear.

Table 4. Time series classes statistics from PSTime processing in the Venosta Valley.

TOT PS (RADARSAT-1 ascending)	**98455**	
0 (Uncorrelated)	59974	60.92%
1 (Linear)	6782	6.89%
2 (Quadratic)	14766	15.00%
3 (Bilinear)	16826	17.09%
4 (Bilinear + step & constant velocity)	63	0.06%
5 (Bilinear + step & change in velocity)	44	0.04%

Figure 43 shows the map of the AOIs in South Tyrol and the spatial distribution of the deformation trend types.

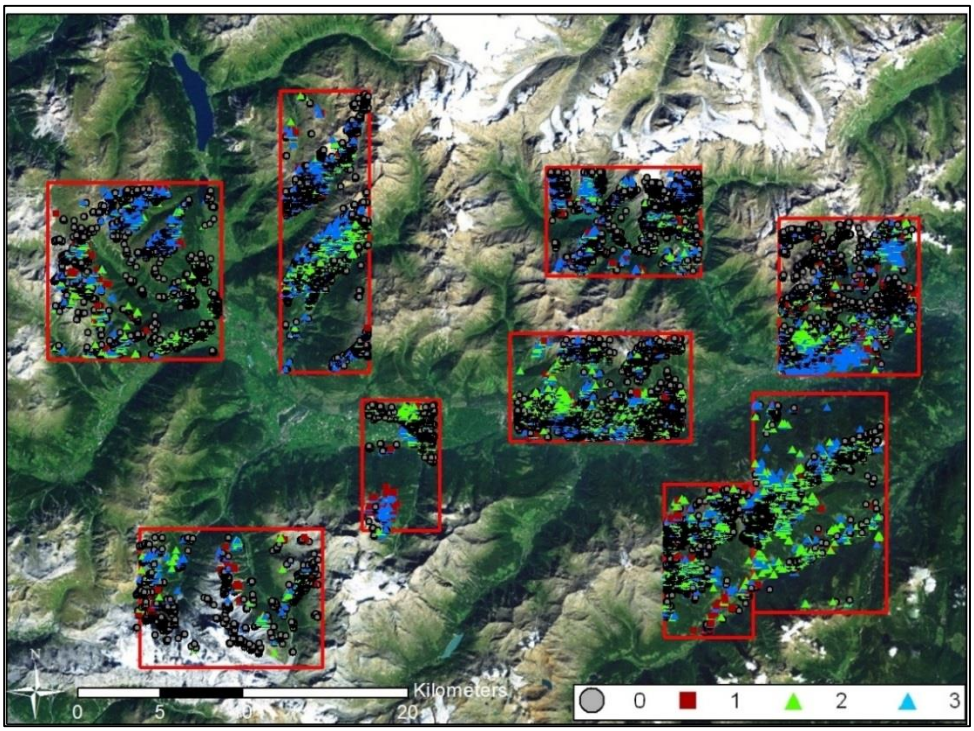

Figure 43. Time series classes of the dataset RADARSAT-1 ascending, over the Venosta Valley in the "critical areas". It can be noticed that deformation types are not randomly distributed on space, but they tend to be clusterized toghether.

It should be noted that the time series classes are not randomly distributed on space, but they tend indeed to be clusterized toghether. This allow the user to focus the attention over the areas with an omogeneous defomation trend to understand the dynamics and the motivations for that behaviour. In these cases, local scale anaysis should be addressed.

4.1.2.3 Results & Discussion

Deformation over the Western sector of South Tyrol have been analised using the MT-InSAR post-processing techniques proposed in this thesis. A first identification of 9 main deformation units was carried out from visual interpretation of the average displacement rate along the line of sight of the satellite. The hot spot analysis was also carried out to automatically identify areas of deformation toward and away from the satellite. The resulting map identified an higher number of clusters, in particular about 20 hot spot and 14 cold spot were identified. However the output is a continuous map. The users has 2 options:

1) Qualitative: use the Hot Spot map as continuous raster, for the geomorphic interpretation, together with others map layers (i.e. orthophotos, landslides inventories, geological maps, DEM)
2) Quantitative: Define, for each Hot Spot map, a threshold to discretize the hot and cold spots and assign "no-data" to the pixels that can be considered stable.

Both the approaches require a geomorphic knowledge of the area from the user. In the first case the geomorphologist is required to draw *n* areas of interest where the deformation indicated from the Hot Spot map, find a geologic or geomorphic significance. However the user, even in this phase should define the AOIs following geologic/geomorphic boundaries. In the second case, the experience of the geologist has to drive the calibration of the threshold setting, by a trial and error approach, with the aim to minimize the number of false positives and true negatives. The velocity components have been evaluated with Geo-PSIC. $PS_{Geo\text{-}PSIC}$ returned to be about 5% of the 2 parents datasets (ascending and descending). The PS coverage and PS density drive the results of the outputs in terms of spatial distribution. Unfortunately, in extreme geomorphic condition as the Alps, several slopes can be only moniterd from one geometry. Other areas are seasonally affected by snow cover, resulting in coherence loss and thus measurement points loss. As a direct consequence, the PS distribution is notably lower then the input PS datasets. However, geo-PSIC has the potentiality to filter the the data that are in different geomorphic unit, enanching the geomorphic interpretation for AOIs, mapping. To validate the effectivness of Geo-PSIC, a camparison has been carried out with the resampling grid. The analysis has shown that the resampling grid in about 17% of the cases, has averaged within the single cell of analysis, also PS in different surface units. The time series analysis was carried out to support the identification similar deformation phenomena in time. In fact, based on the hypotesis that surface deformation (i.e. landslides) have a trend correlated in the near-space domain, with PSTime it has been possible to classify, in a relalatively short time, all the measutrement points. The results has shown that about 60% of the measurement points are from the

"uncorellated" class, which can be considered stable. The remaining PS that are distruted between the classes "linear"(7%), "quadratic" (15%) and "bilinear" (17%) have a clusterized pattern mainly affecting slopes, rather then the valleys and following geomorphic lineaments (i.e. crests). However as anticipated, the geology of the Alps can lead into data loss. However, the post-proccessing tools tested provided additional information, that can help the users to identify at regional scale, areas where more investigation are needed, at local scale, considering the average velocity, the velocity components, and the looking at the distrubution of time series analysis. Time series analysis it is also fundamental to highlight any possible accleration of landsides.

4.1.3 Northern Apennines

4.1.3.1 Objectives and General Settings

The study area is geographically located in the Centre-Northern part of Italy, in the Emilia-Romagna Region. In particular has been studied an area extent of about 3500 km2 in the mountaneous area of the Reggio-Emilia, Modena and part of the Bologna province, which belong to Northern Apennienes. Elevation starts from few tens of meters above the sea level, at the conjuction between the Apennines and the Padana Plain, and exceed 2000 meters, in the internmost sector of the Apennine Chain, towards the Tuscany Region border (i.e. Monte Cimone, 2165 m a.s.l). The climate is mediterranean with most of the precipitation occurring in the spring and in autumn. The second order rivers present in the study area are the Secchia, the Panaro and the Reno. The Northern Apennines are a fold-thrust belt originated during the Tertiary by the collision between the Apulia (or Adriatic) microplate related to the African plate and the Briançonnais microplate (Sardinia-Corsica massif), related to the European plate (Boccaletti et al., 1971; Scandone, 1979; Mantovani et al., 1985; Dercourt et al., 1986; Carmignani et al., 2004). The main geological domains are the Ligurian Domain, Epiliguarian Domain and Tuscan Domain (Figure 44). From a geological perspective, in the Emilia-Romagna region crop out marine, transitional and continental sedimentary rocks, Late Triassic to Holocene in age, arranged in a complex structural setting resulting from the formation of the Apennines mountain chain (Abbate et al., 1970; Emilia-Romagna SGSS, 2006, Rossi et al., 2010). The lithological and the structural settings control the morphology of the area (Figure 45).

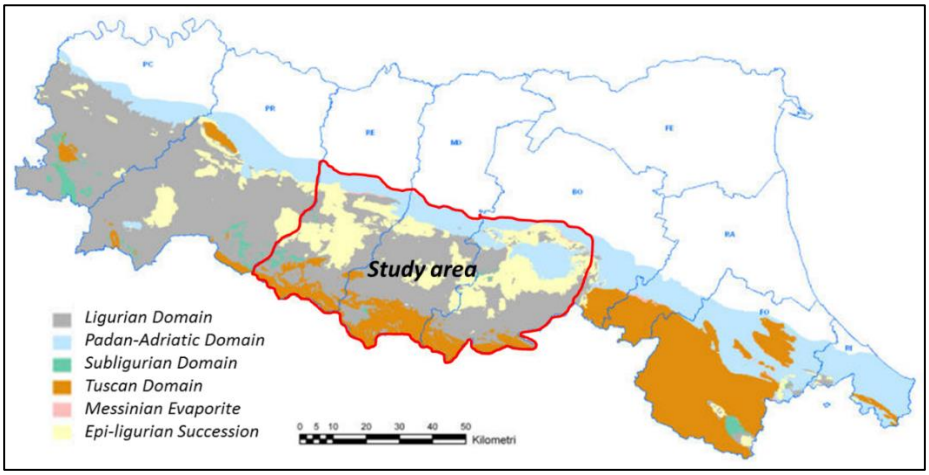

Figure 44. Map of Geological-Structural Domains of the Emilia Romagna Region (modified after: http://ambiente.regione.emilia-romagna.it/). The study area is highlighted in red.

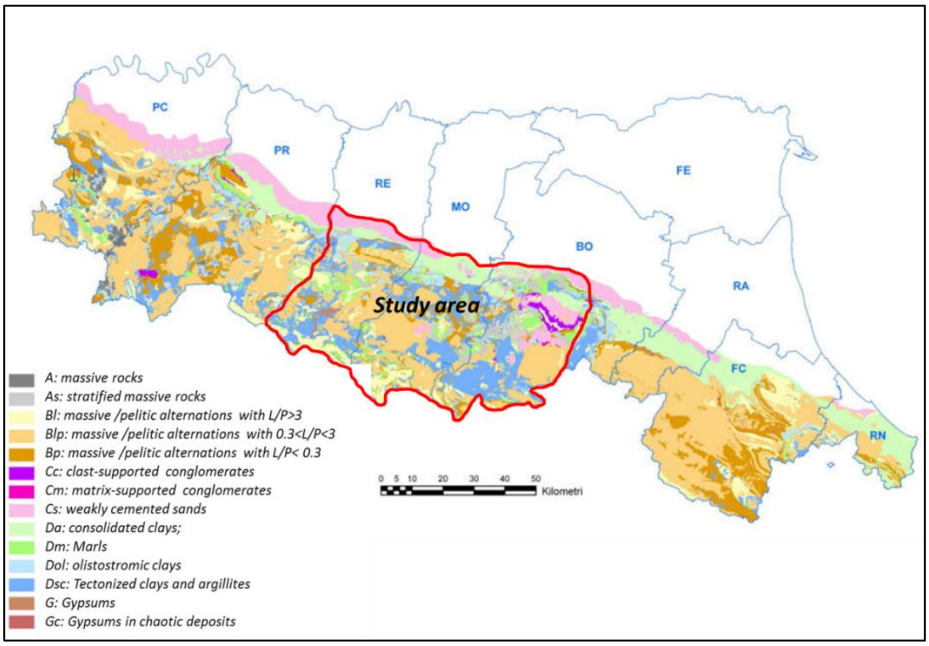

Figure 45. Lithotechnical map of the Emilia Romagna Region (modified after: http://ambiente.regione.emilia-romagna.it/).

Landslides are abundant, in fact about 25% of the hills and monuntains are affected active or dormant landslides. In Emilia Romagna Region, the gradual evolution of slopes over thousands of years, resulted in 70.037

landslide mapped, from which, 38178 are classified as active and 31859 as dormant or stabilized landslides. Typically periods of dormancy are alternated with reactivation phase, that may correspond to exceptional climatic events (i.e. rainfall and rapid snowmelt). The most frequent landslide types in the study areas are shallow and deep-seated slides, earth flows, mudflows, rockslides and complex landslides (Cruden and Varnes, 1996). Here landslides, which may be present since the Mid-Holocene (Leuratti et al. 2007), are also facilitated from the contact bewteen formations with different lithotechnic characteristics, such as sandstones and claystones (Figure 45). In this study, postprocessing routines proposed in Chapter 3, have been used to:

- Identify areas affected by deformation not mapped within the landslide inventory of the Geological Service of the Emilia Romagna Region (Servizio Geologico Sismico e dei Suoli – SGSS);
- Identify areas classified as stable within the landslide inventory, and propose further investigation aimed to an update of the landslide activity;
- Test the effectiveness of the automatic mapping (i.e. Hot Spot Analysis) versus the visual interpretation and manual mapping of MT-InSAR data;
- Classify the deformation trend of all targets in the sudy area, with the aim to identify areas affected by similar deformation trend and deceleration or acceleration of the deformation;
- Evaluate the Vertical and East-West component of the velocity of the deformation velocity to characterize the direction of the deformation;

- Evaluate where the landslide direction is truly parallel to the slope direction, as it is often assumed in literaure when using the "back-projection " method for velocity components estimetion (Section 3).

Some of the research presented in this section, have been carried out in the framework of the agreement with the Civil Protection of the Emilia Romagna Region "ASPER – RER", entitled "Supporto all'analisi di Dati Interferometria Permanent Scatters".

4.1.3.2 Datasets & Methods

The landslides of Emilia Romagna Region have been studied with different datasets, of different satetellites, different scales and processed with different MT-InSAR algorithm. In particular have been analised the ERS, Envisat and RADARSAT-1. In particular, the ERS and Envisat datasets have been processed in the framework of the PST-A project (Piano Straordinario di Telerilevamento). This is a nation-wide project founded by the Italian Environmental Ministry. The datasat analize cover the entire region and have been processed with the PSP-IFSAR algorithm (Costantinti et al., 2008). For the regional analysis, all single frame of PSI data, have been grouped and merged by satellite type and geometry. According to Table 5, over 770000 Persistent Scatterers have been analysed, spanning a time interval of about 15 years. The number of images processed can be different for each frame, and varies between about 30 images to about 70 images.

Table 5. Datasets from the PST-A projects used for the regional analysis. Single frame have been grouped and merged together, per satellite and geometry.

Satellite	Geometry	PS n°	Time range
ENVISAT	Ascending	248349	2003-2010
	Descending	324847	
ERS	Ascending	41097	1992-2000
	Descending	157896	

The datasets of the PST-A where also used for the statistical threeshold calibration of PS-Time. In particular, random time series over the area represented in Figure 44 and Figure 45, have been manually classified and compared with the automatic classification of PS-Time, using the ROC curve method (Green and Swets, 1966). A detailed description of this analysis can be found in Berti et al,. (2013). However the algorithms used within the PST-A project, did not include the evaluation of Distributed Scatterers and Temporary Scatterers, limiting the analysis to the solely Persistent Scatterers. Unfortunately, landslides studies using only Persistent Scatterers, often leads into lack of data in the areas of interest. This is particularly evident in the Apennines, where landslides often take place over low reflectivity geological units (e.g. clays) and over vegetated areas. To limit this problem, an area of about 2000 km^2 (mainly covering the province of Modena) was analised with a last generation algorithm and an up-to-date dataset. In particular, two RADARSAT-1 data stacks, comprising of 112 scenes in descending orbit and 124 scenes in ascending orbit, have been processed with SqueeSAR™. The time coverage lasts from April 2003 to November 2012, with an average temporal frequency of 1 scene/month.

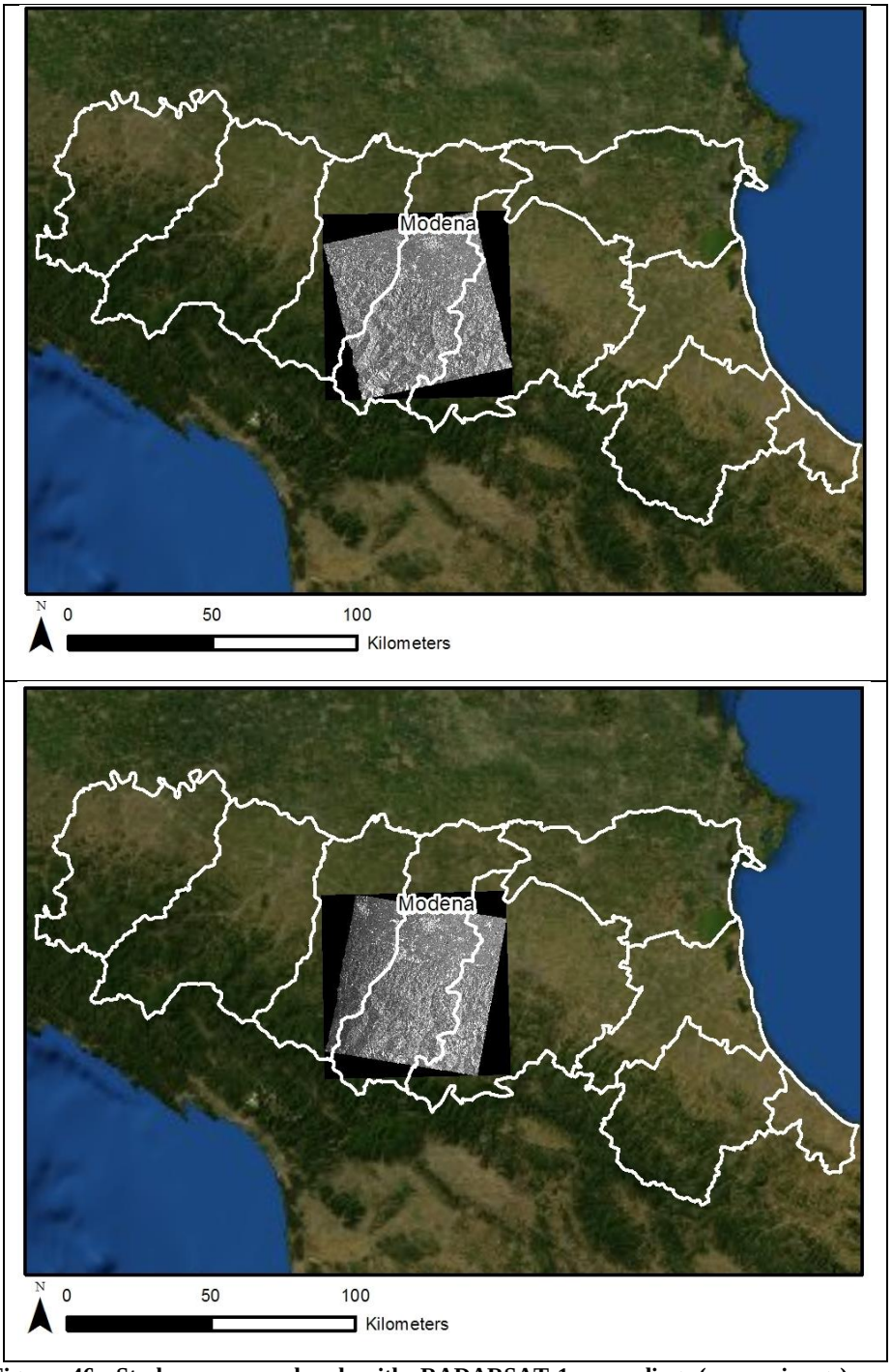

Figure 46. Study areas analysed with RADARSAT-1 ascending (upper image) and descending (lower image). The with polygon highlight the whole Emilia Romagna Region, and the coverage of the PST-A data sets.

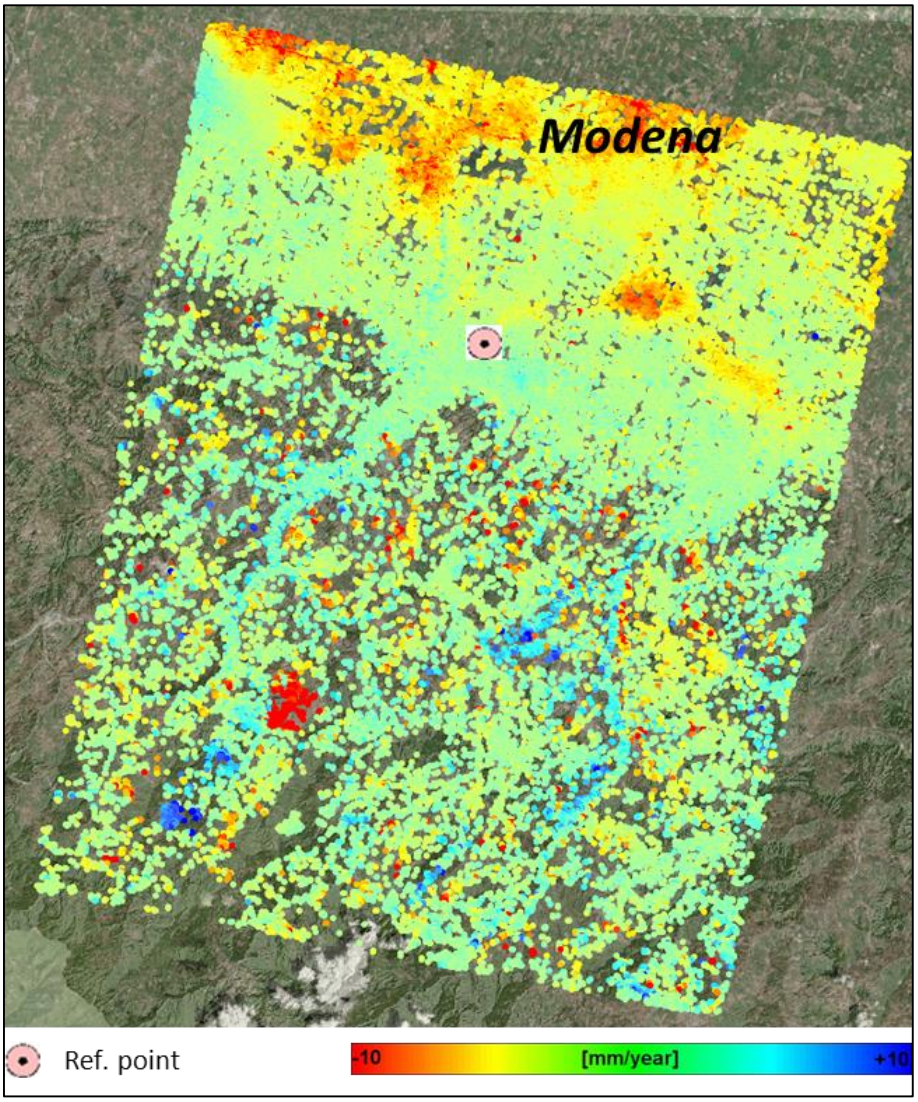

Figure 47. RADARSAT-1 descending data set. Algorithm: SqueeSAR™.

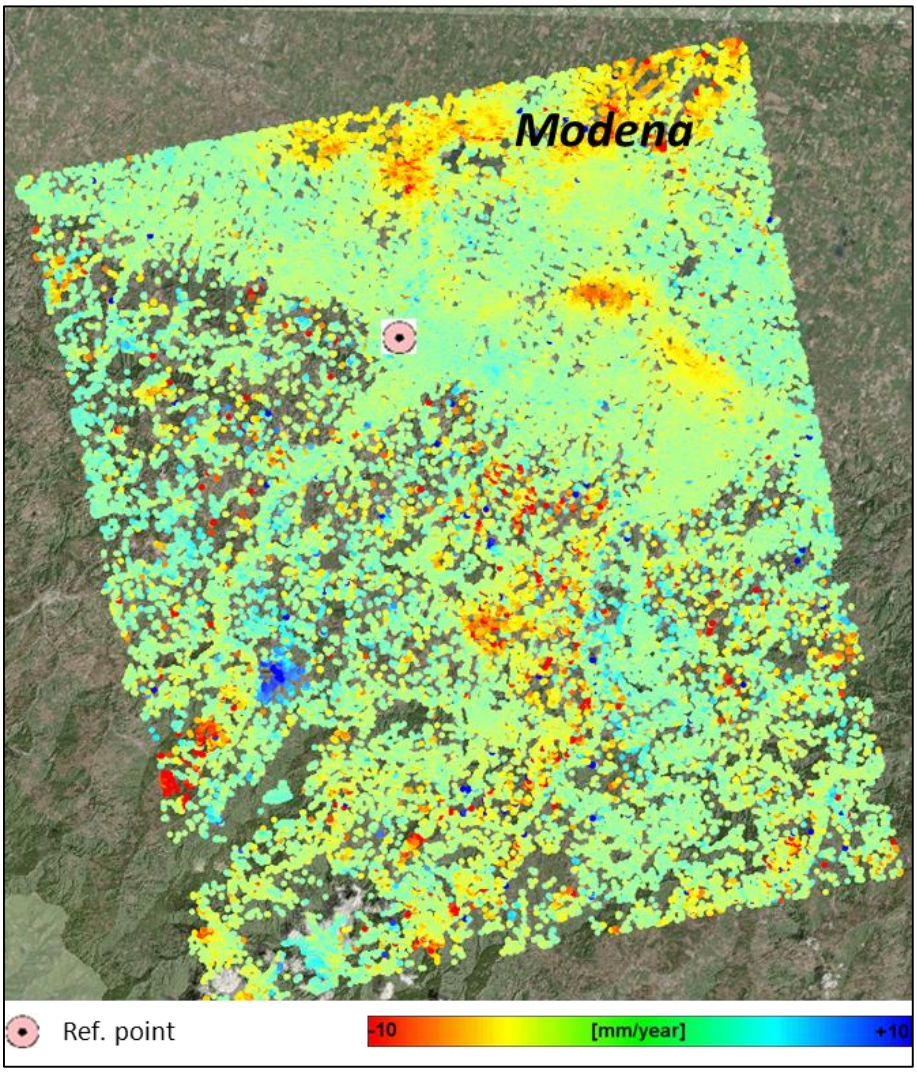

Figure 48. RADARSAT-1 ascending data set. Algorithm: SqueeSAR™.

The analysis with RADARSAT-1, processed with a very high number of images (over 120 per geometry) and with the latest algorithm developed from T.R.E., allow also to determine which is the impact of the datset quality/type on the finale results, compared with the PST-A data analysis. In addition, on the RADARSAT-1 data set, T.R.E. has also computed:

- Acceleration of the deformation trend of each measurement point

- East-West and Vertical components of the velocity

The method used for the computation of the velocity by T.R.E it is based on the resampling grid, but measurement points within each single cell are averaged based on the coherence. In addition, for each decomposed measurement point, the time series of the displacement and a new reference point are returned. This allow a value of standard deviation for each decomposed measurement point.

4.1.3.2.1 Hot Spot Analysis

The Hot Spot Analysis was applied to the RADARSAT-1 descending dataset covering mainly the mountainous area of in the province of Modena (Figure 47). SqueeSAR™ dataset, being also populated by Distributed Scatterers, can have a very high density of measurement points. If from one perspective, more points means more information, from the other perspective, they can be computer resource demanding and difficult to handle with standard personal computers. Appling the Hot Spot Analysis, the main deformation process can be rapidly identified, providing a lighter raster product easier to use as a layer in any GIS environment.

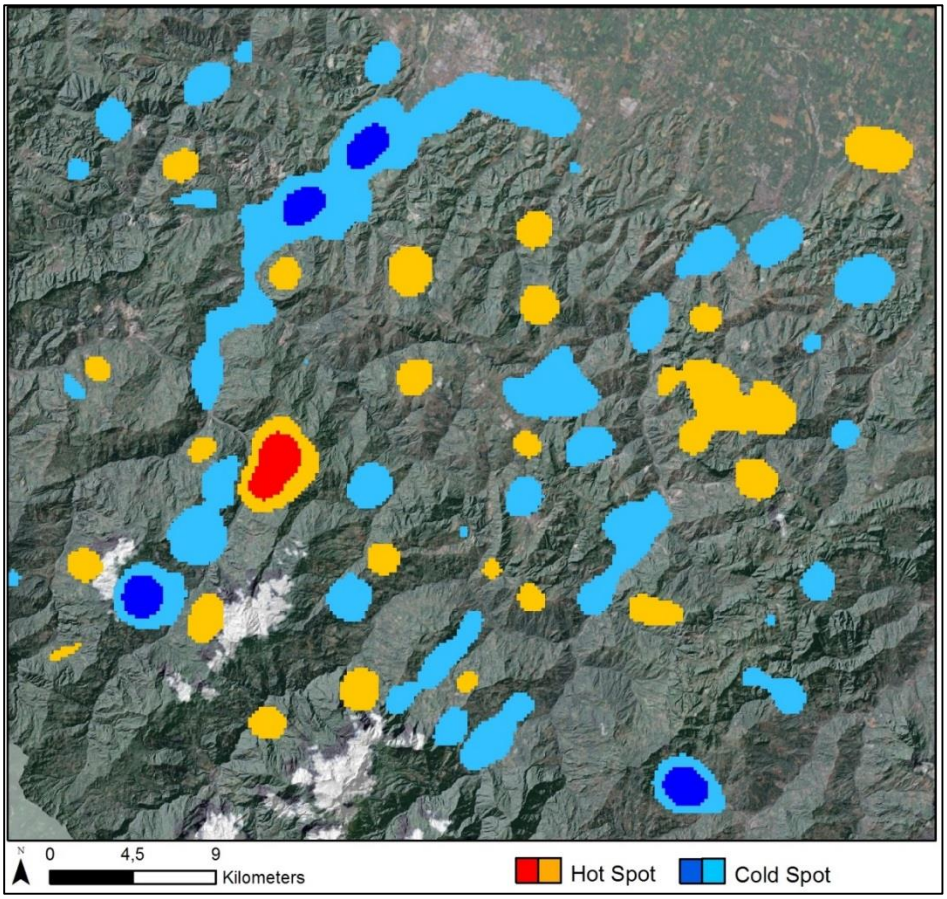

Figure 49. Automatic classification of potential active landslide with the Hot Spot Analysis. RADARSAT-1 descending.

The cluster analysis (G_i^*index) was applied using a distance parameter of 200 meters, considering to be a value representing the typical distance of spatial correlation of the acting deformation phenomena. The resulting Hot Spot Map (Figure 49), from continuous type, has been reclassified into five classes highlighting different magnitude of spots. Blue and cyan indicate high and low magnitude of Cold Spots (moving toward the satellite, while red and orange indicate high and low magnitude of Hot Spots (moving away from the satellite). However the magnitude is only in part related to the velocity of the deformation, since it also depend

from the clusterization and density of the measurement points. Over 30 Cold Spots and 25 Hot Spots can be identified on the study area. In this case study it has been decided to not compare the Hot Spot Analysis with the landslide inventory, (which may not reflect the MT-InSAR data) but rather with a manual classification of the areas considered affected by deformation. Thanks to this approach it has been possible to define that the Hot Spot Analysis can return "*true negative*" and "*false positive*" spots.

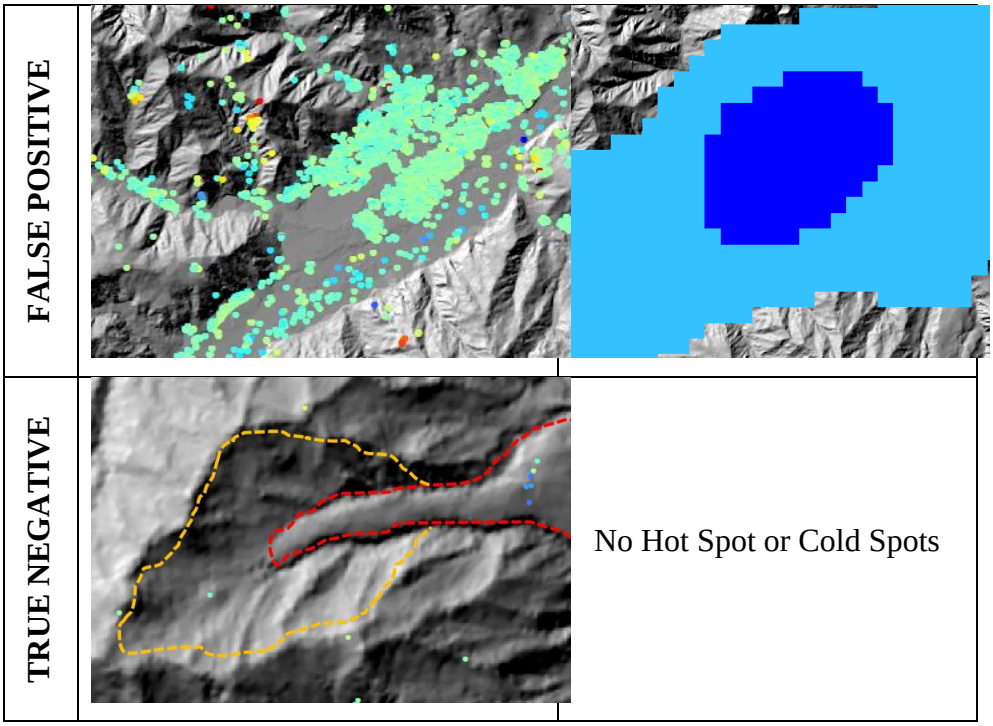

Figure 50. Example of "false positive" and "true negative" generated from the automatic mapping using the Hot Spot Analysis, RADARSAT-1 descending dataset.

Figure 50 shows two example of a "false positive" (upper image) and a "true negative" (lower image). In this example, the "false positive" is due to the high density of measurement points in one area, with a low positive velocity (within the instrumental error). This can happens in

cases where villages (high number of reflectors) are surrounded by agricultural fields or vegetated areas (low number or measurement points, mainly distributed Scatterers).

4.1.3.2.2 Velocity components extraction

This section show the application of the velocity component extraction in single orbit applied at regional scale. In addition, for study area covered by the dataset RADARSAT-1, we estimated where the back-projection method (single orbit) is reliable. To this end, first the east-west components have been evaluated, and the angle between their resultant vector and the horizontal plane has been estimated (γ). If the assumption of deformation parallel to the slope direction (used in the back-projection method) is true, then γ should be near equal to the slope angle.

4.1.3.2.2.1 Single orbit

The tool developed for the extraction of the velocity component using a single orbit was applied to the both the ENVISAT descending and ascending datasets. To this aim a DEM with 20 meters of spatial resolution was used to extract the geomorphic parameters (slope angle and aspect angle) together with the satellite metadata. In particular, since the area include different frames, average values azimuth angle (12.39°) and look angle (23.13°) where used for the descending dataset (Figure 51). On the other hand, for the ascending dataset the average values of 13.72° and 22.76° were used for azimuth angle and look angle respectively. As evident from Figure 51 and Figure 52, the back-projection method produce a "salt and pepper" result which is due by noise amplification. This effect depends from the value of the velocity along the LoS, the slope exposure, slope angle and DEM resolution. In particular, values of back-projected velocity are much less reliable for slope near North-South oriented. This is due to the fact that SAR signal is

not sensitive to the slope directions parallel to their azimuth direction (which is near North-South). Furthermore, it has to be taken in account that landslides do not always moves along a direction parallel to the slope angle. It is important to highlight also that this method amplify the noise and the trends that are related to derive of the datasets rather than a real deformation.

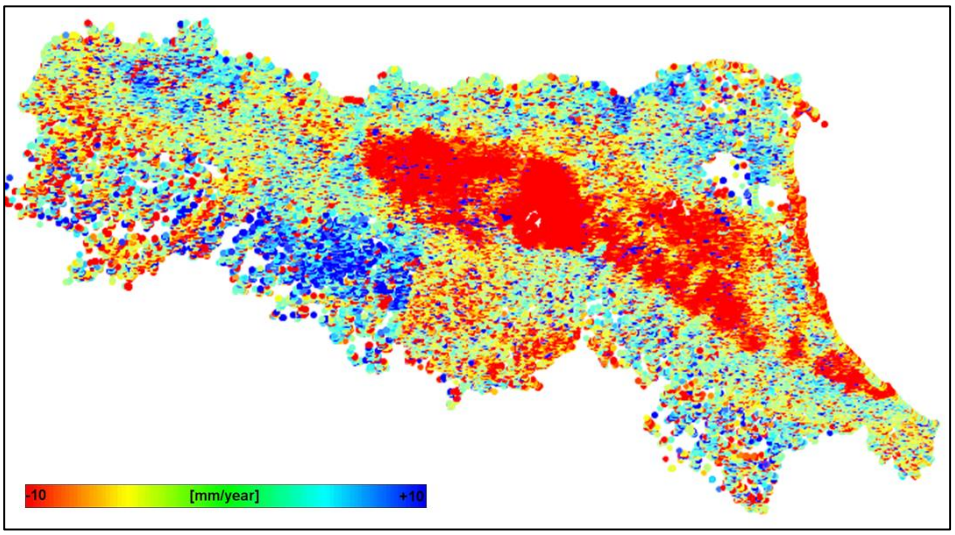

Figure 51. Back-projection of the velocity LoS along the slope direction. The results 3D vector is displayed. Envisat descending.

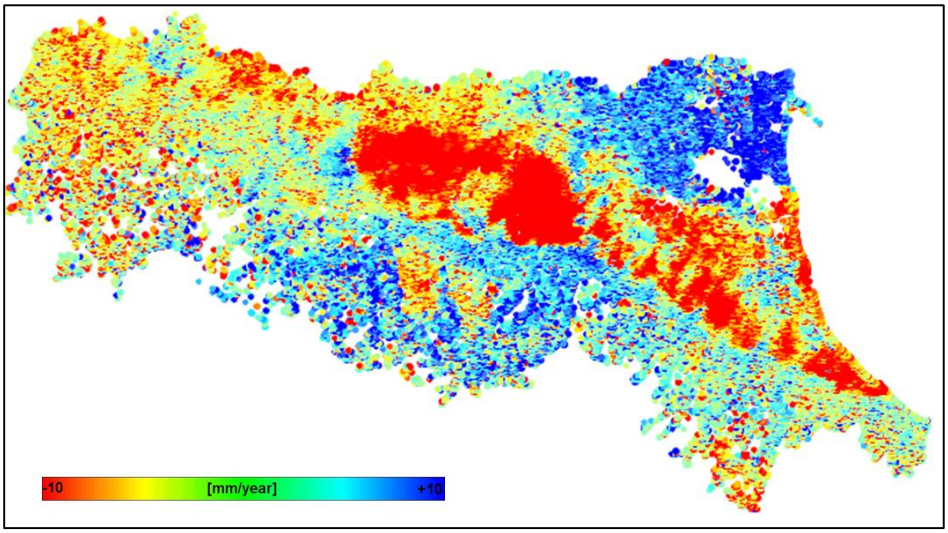

Figure 52. Back-projection of the velocity LoS along the slope direction. The results 3D vector is displayed. Envisat ascending.

In order to verify where this assumption is reliable or not, a further study discussed in next section was carried out. This approach is based on the extraction of bi-dimensional velocity component (East-West and vertical).

4.1.3.2.2.2 Double orbit

For the RADARSAT-1 dataset, the East-West and vertical velocity components have been evaluated at the time of the InSAR processing by T.R.E. using the resampling grid method. Based on this results, the resultant of the two velocity components (East-West and vertical) can be evaluated by a simple trigonometric calculation. Also it is possible to evaluate the angle between the resultant vector of the deformation and the horizontal plane (Figure 53).

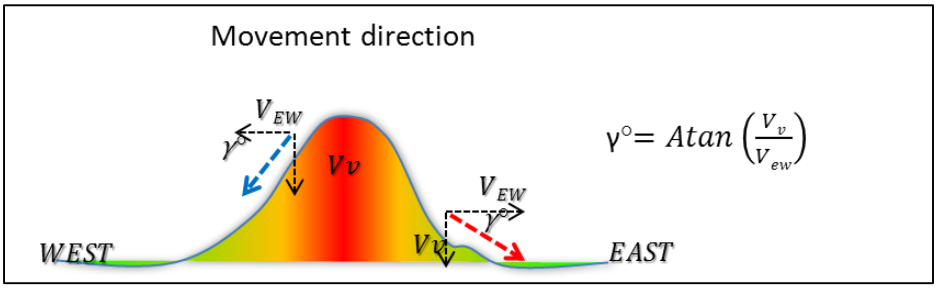

Figure 53. Calculation of the angle (γ) representing the movement direction, from the velocity components.

Figure 54 shows the results of the computation of the angle of movement direction in the East-West direction. A value of γ=90° means that the movement direction is vertical, while a movement completely horizontal will have γ=0°. It is possible to observe that most of the measurement points in the Po Plain (near Modena) shows a deformation mainly vertical. This is in agreement with the well-known subsidence affecting these areas. Ideally, if a landslide moves parallel to the slope direction, the γ angle and the slope angle should be similar (Figure 53).

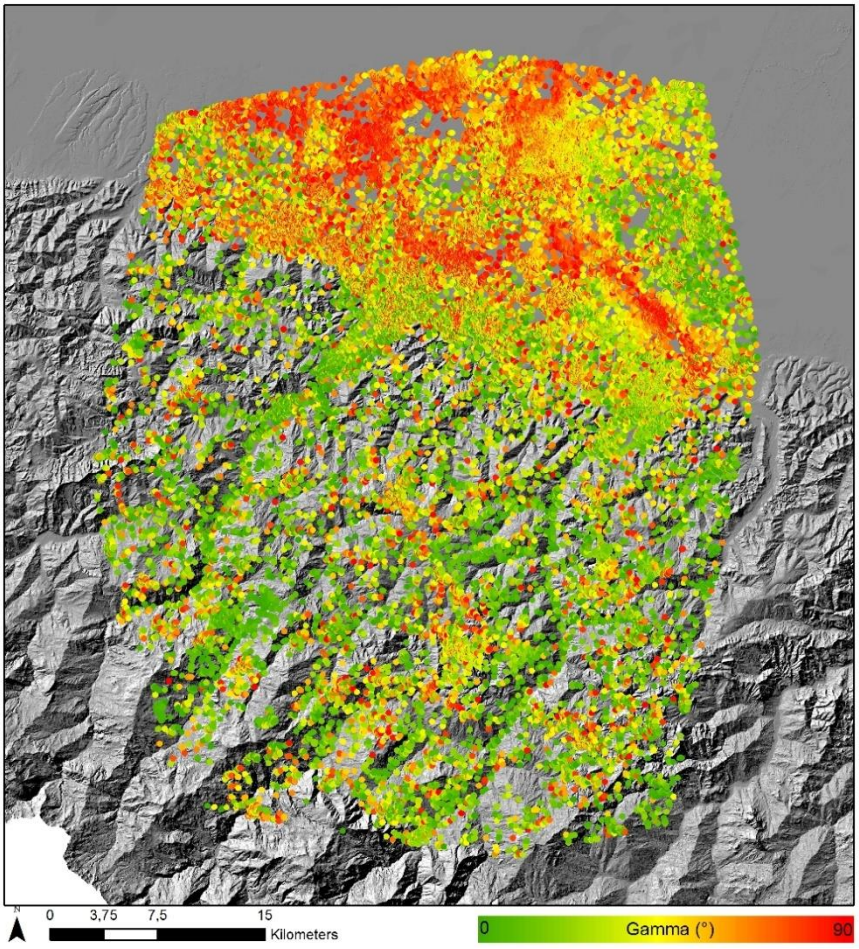

Figure 54. Direction of movement (γ) computed for all decomposed measurement point. RADARSAT-1.

In order to verify the reliability of this statement, a statistical analysis of γ was carried out within 63 selected AOIs. In particular, the AOIs were selected where evident signal of deformation was found in the RADARSAT-1 dataset. It is important to highlight that since the resultant of the deformation (Figure 53) is in the East-West plane, and no North-South components are present in it, the slope gradient to be compared must also to be evaluated in the East-West plane (Figure 55).

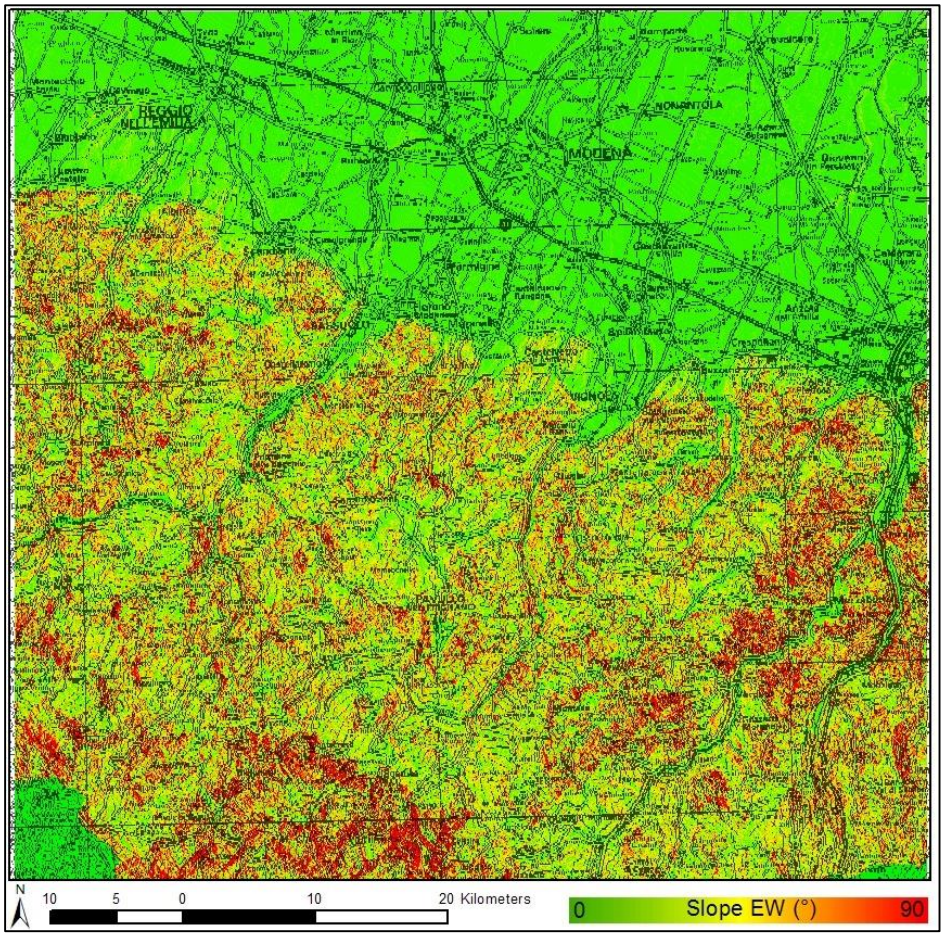

Figure 55. East-West slope gradient of the terrain.

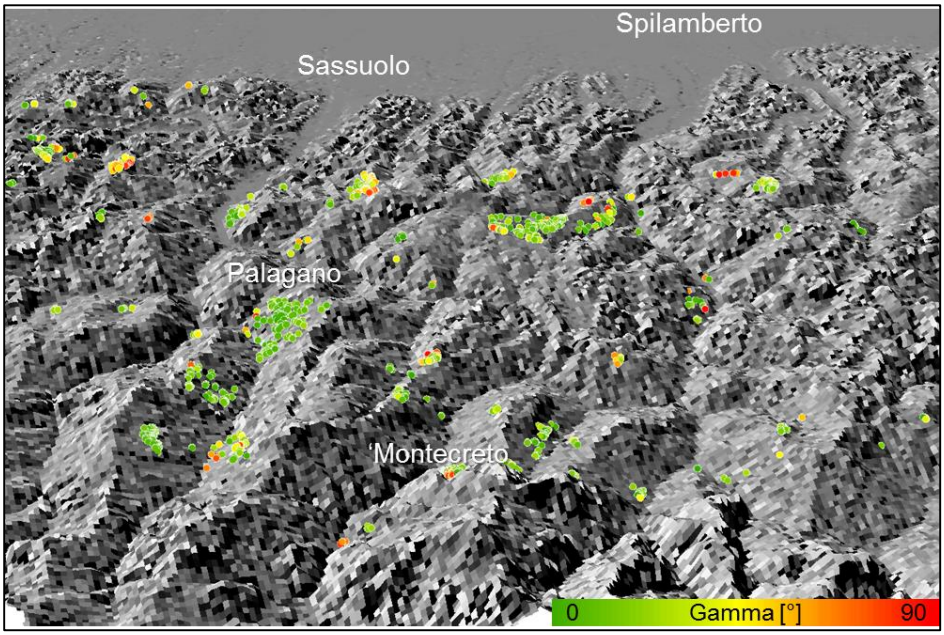

Figure 56. Measurement within the AOIs identified at regional scale, showing the angle of movement direction (gamma).

At this point, an average of the γ value and of East-West slope gradient was carried out within the 63 selected AOIs in order to define were these 2 parameters shows similar values. Extended results are found in Table 6.

Table 6. Average of angle of movement direction (γ) and East-West Slope gradient within each selected AOIs. Piola, which shows a very high variation between the two values is highlighted.

AOI ID/note	*n*PS	Avg Slope Dx (°)	Avg γ (°)	AOI ID/note	*n*PS	Avg Slope Dx (°)	Avg γ (°)
Barighelli di sopra	93	4	41	lama del corvo	10	6	37
Valestra montelago	1	8	7	Mezzolato	4	14	3
Not relevant	1	11	4	Mocogno	5	10	10
Prediera - Caldiano -	64	7	32	Moncerrato	6	11	15
near active landslide	1	2	37	Montecreto.	75	8	32
Allegara - Prignano	4	7	20	Monteombraro	89	6	30
Badland_gully, soil slip	8	7	12	Monticello -	15	9	22
Baiso - Piscina de calanchi	49	5	58	Mulino della piana	4	8	3
Valestra montelago	5	10	18	Pompeano.	13	9	8
Boccassuolo -	54	5	36	Piola	3	9	69
Bombiana -	7	4	29	Monteorzello	7	8	64
Ca del grosso	1	14	19	Prognano	1	14	35
Ca guidi	43	6	42	Puzzole .	9	3	64
Calanchi\badlands,	28	9	22	Regnano	8	8	22
Casa vernese (Montecreto).	5	9	29	Regnano -	7	3	26
Casina - Villa Bonini	5	3	8	Riolo	6	6	18
Castellaro - Bivio zoppo.	13	7	11	Riolunato	7	4	71
Castellaro - Sestola.	27	7	14	Roncolo	6	5	14
Castelluccio - Montese	15	9	20	Roncoscaglia.	35	9	24
Cava	2	15	37	serra di migni.	12	11	20
fosso moranda.	2	10	39	sestola	15	14	20
Active landlside	4	11	34	Sommavilla	4	14	23
Active landlside.	2	4	37	Svolta	1	12	34
Casa Giannini. Panaro.	1	5	14	Castelvecchio	29	10	20
Prignano sulla Secchia.	1	10	36	Active landlside	97	6	11
Prignano sulla ecchia.	4	7	35	Vaglia -Borro	25	12	19
Landlside dell'oca.	8	4	30	Vergato– Bologna	6	8	11
Lotta.	19	6	18	Via cast.. Polinago	1	7	42
Gaiato	10	12	47	Vesale. Sestola	8	9	28
Nuova estense	42	8	27	Alberelli (MO)	1	7	55

Active landlside	5	7	28	Zocca	3	1	15
Gully erosion/badland.	2	13	39	Zocca2	2	6	30

It is possible to represent in a dispersion graph, the γ value and the East-West slope gradient, which have been evaluated at each measurement point. Figure 57 shows clearly that there is no clear correlation between the two parameters, suggesting that it is discouraged to use the back-projection method. In this case, it can be better to use the mono dimensional data (along the line of sight).

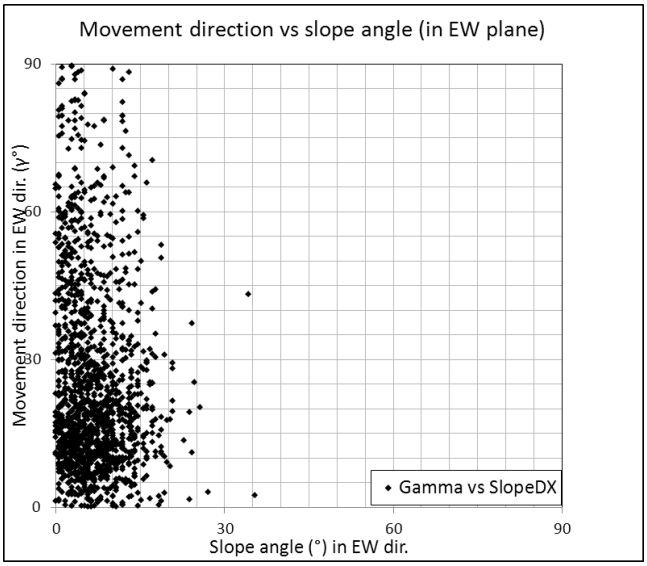

Figure 57. Movement direction evaluated from MT-INSAR vs East-West gradient of terrain.

As an example, it can be shown the case of "Piola", which is one of the AOIs from Table 6 that has among the highest variability between the two parameters (Figure 58).

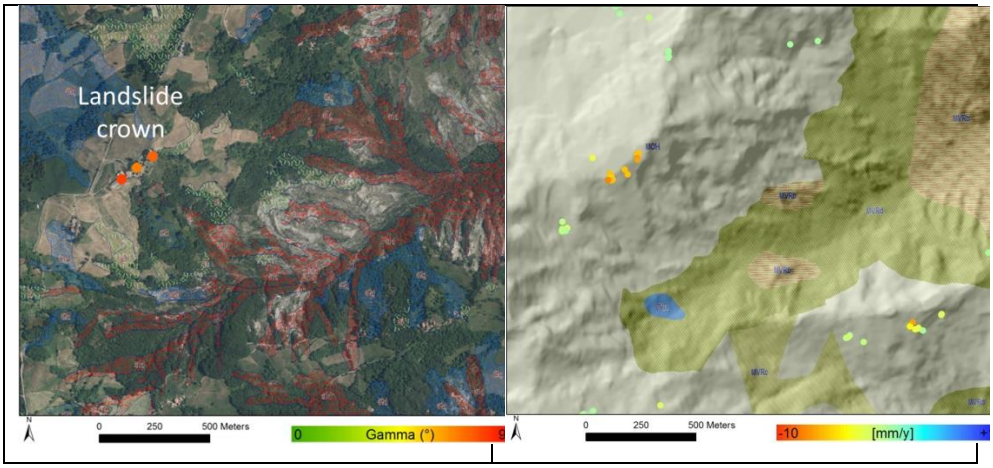

Figure 58. Piola AOI. The movement direction indicates a deformation mainly vertical, while the East-West slope gradient near zero (horizontal). It is possible to see that Piola is located above a crown of a complex landslide which may act as a retrogressive phenomenon.

Structures in Piola are affected by an evident vertical deformation. However, looking at the terrain shade of this area, it can be observed a mainly flat topography. This is not surprising if we consider that Piola is located on top of a landslide crown, which is even classified as active in the regional landslide inventory. The active landslide probably has a retrogressive component, activating the area located on the upper part of the slope. The vertical deformation indicate a roto-translational cinematic of the landslide.

4.1.3.2.3 Time Series Analysis

In general, in a regional landslide scale study, it is expected most of the area being stable (a part from specific studies over specific areas). As a consequence, an Mt-InSAR monitoring study, with a regular distribution of measurement points, should be mainly characterized by PS with no signal of deformation and rather indicating stable areas. A similar finding has been reported by Berti et al (2013) who showed that most of the MT-InSAR time series are of "uncorrelated type". These results are reported in Figure 59.

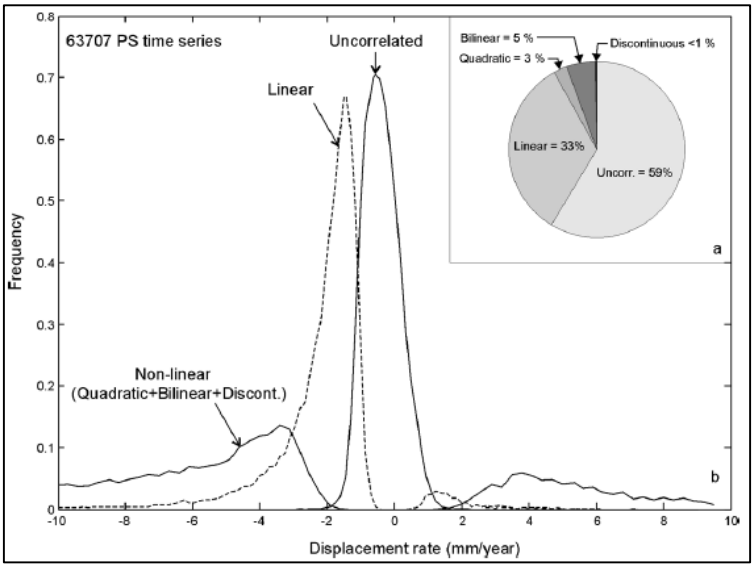

Figure 59. Frequency distribution of time series type classified using PS-Time. Dataset (ENVISAT descending) from PST-A project, Area: Northern Apennine (BO). (Berti et al., 2013).

The "uncorrelated" class shows a Gaussian distribution, centred on 0 mm/y" and within the range of ~ 2 mm/y. According to the PS-Time algorithm, this means that statistically, there is a very low probability that a measurement point classified as "uncorrelated (in this case within ± 2 mm/y), is in reality affected by an active deformation. In other word, in our perspective this can be an index to characterize the overall precision of the measurement points. It is interesting to note that 2 mm/y is a value empirically used often in literature as threshold to discriminate active landslide from stable landslide (Notti et al., 2008, 2010, Catani et al., 2012). The time series analysis with PS-Time has been carried out for the two dataset RADARSAT-1 (ascending and descending geometry) and then compared with the results obtained within the project "ASPER RER 2012", processing the ERS and ENVISAT datasets for the whole Emilia Romagna Region. Results of RADARSAT-1 post-processing are shown in Figure 60 and Figure 63. In particular the time series types are

represented. The results of the classification from the ascending dataset are summarized by the pie chart in Figure 61. It can be noted that most of the time series are “uncorrelated” (37%) which are followed by the linear (34%), the bilinear (23%) and quadratic (6%). The time series with a discontinuity are less the 1% and usually correspond to measurement affected by unwrapping errors. Additionally, the acceleration type can be evaluated. In particular, measurement points that are of “uncorrelated” type will have a null velocity, measurement points with a linear deformation trend will have a constant velocity, while bilinear and quadratic types are both affected by a change in velocity (acceleration or deceleration). The results are summarized in Figure 62 from which is possible to note that targets showing acceleration and target showing deceleration, are almost equally distributed (17% and 12%).

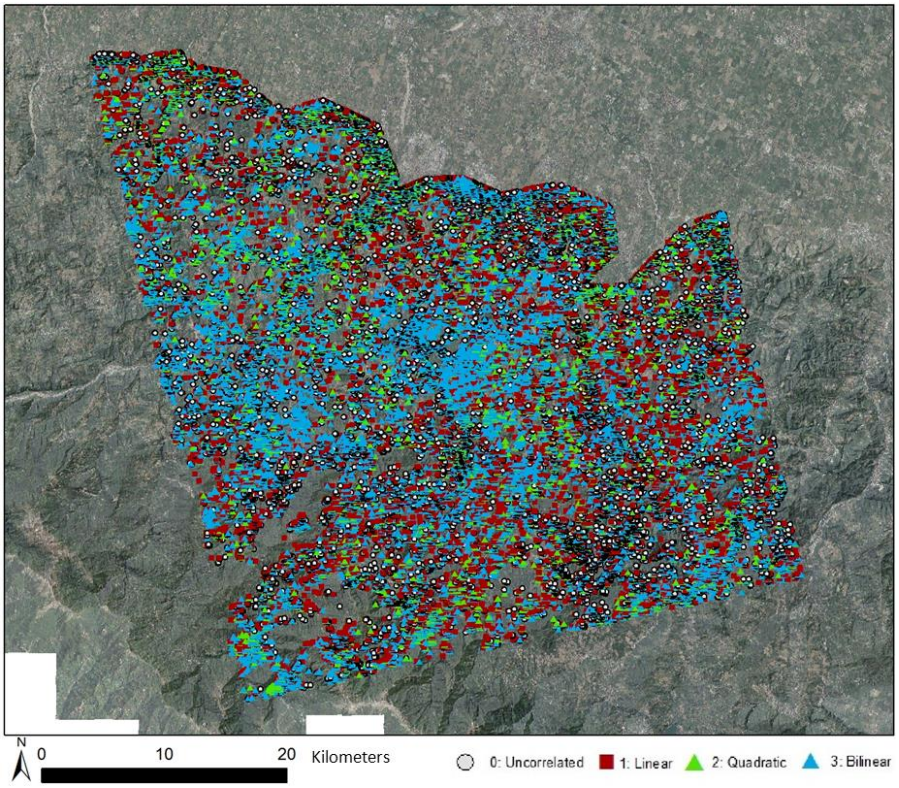

Figure 60. Classification of the time series analysis of the dataset RADARSAT-1 ascending.

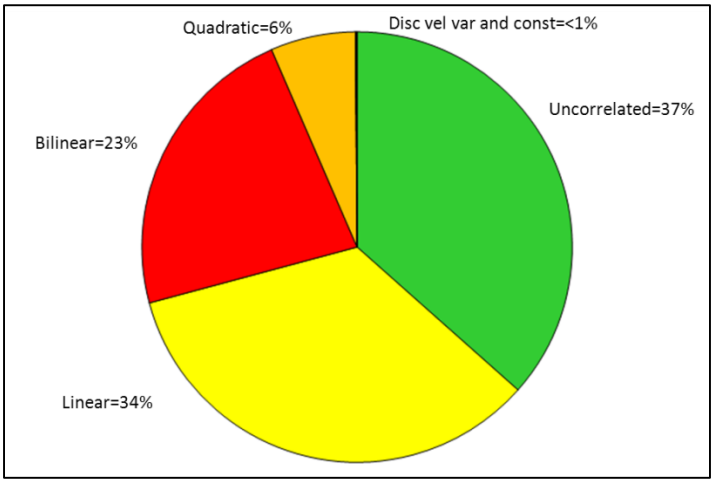

Figure 61. Pie chart showing the proportion of the time series classes within the RADARSAT-1 ascending dataset.

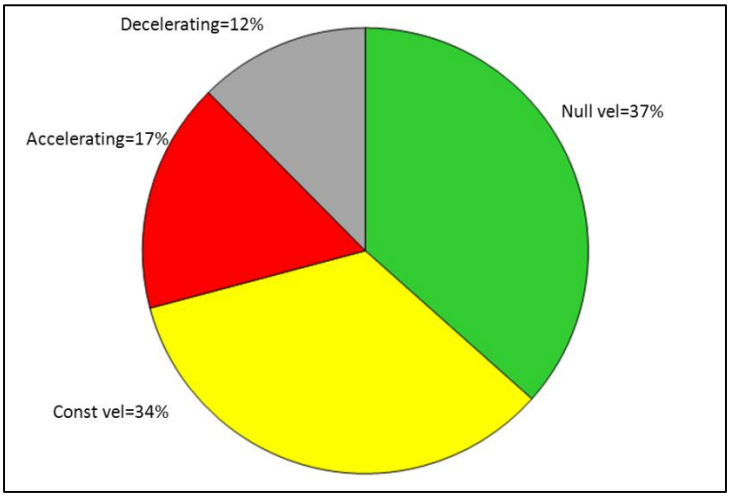

Figure 62. Pie chart showing the proportion of the deformation rate (acceleration, deceleration, null velocity and constant velocity). RADARSAT-1 ascending dataset.

The time series analysis applied to the descending dataset, shows a slightly different result. Figure 63 show clearly that in the area are present significantly less measurement points showing "linear" deformation compared to the ascending dataset.

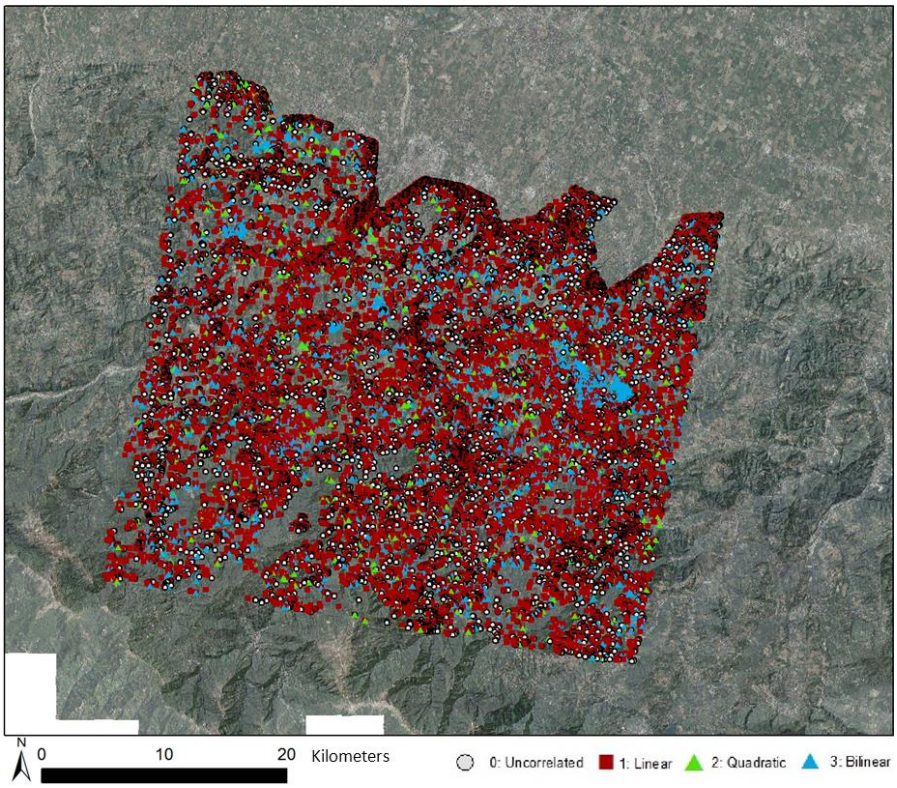

Figure 63. Classification of the time series analysis of the dataset RADARSAT-1 descending.

The detailed proportion of the time series classes can be read from the pie chart presented in Figure 64. Targets with linear deformation trend are 43%, which is about 10% more than the results found in the ascending dataset. However, since the "uncorrelated" class show a similar proportion (35%), it is reasonably to not correlate this effect to a derive of the reference point. The PS-Time algorithm have shown to be very sensitive to even small variation in the time series, so that systematic errors in the displacements, can potentially affect the overall statistical result, and be misleadingly interpreted as deformation. This has not to be considered a weakness of the Ps-Time algorithm, but it implies before its application, a critical analysis of the datasets quality has to be carried out.

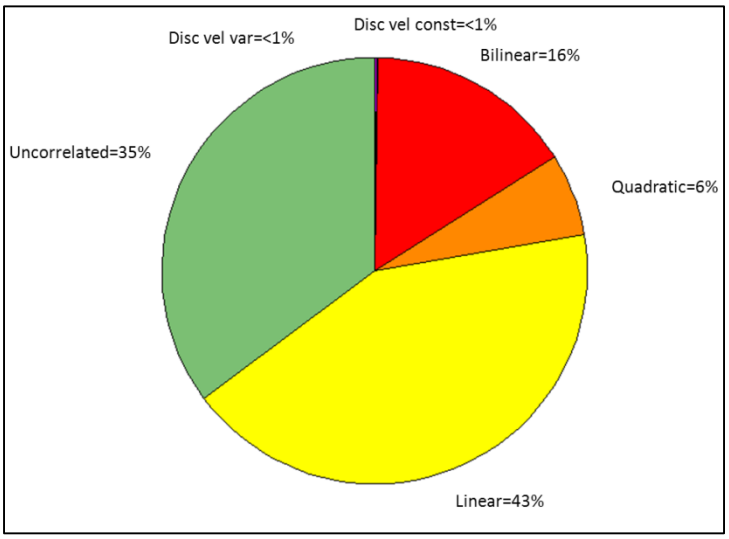

Figure 64. Pie chart showing the proportion of the time series classes within the RADARSAT-1 descending dataset.

Even in the descending dataset the measurement points showing acceleration (13%) and the measurement points showing deceleration, are almost equally distributed.

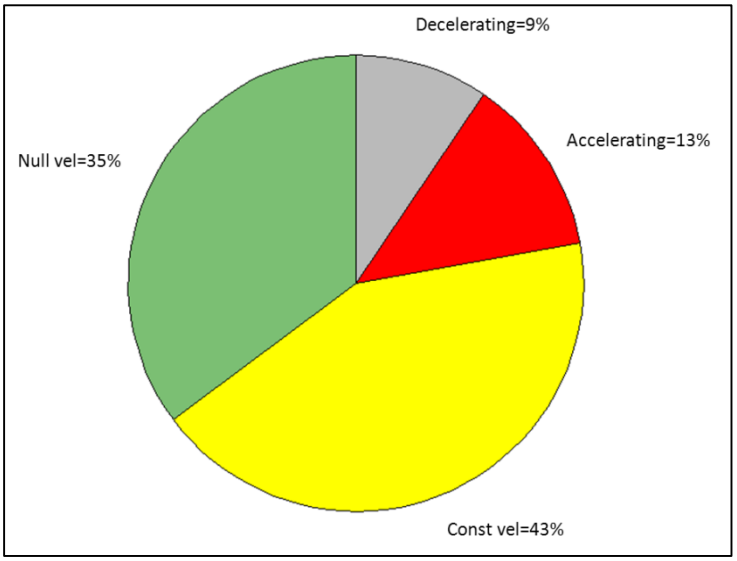

Figure 65. Pie chart showing the proportion of the deformation rate (acceleration, deceleration, null velocity and constant velocity). RADARSAT-1 descending dataset.

Based on the assumption the distribution of the "uncorrelated" time can be used to evaluate the quality of the MT-InSAR dataset, the frequency distribution of the time series classes within the velocity, was carried out for the RADARSAT-1 ascending dataset (Figure 66).

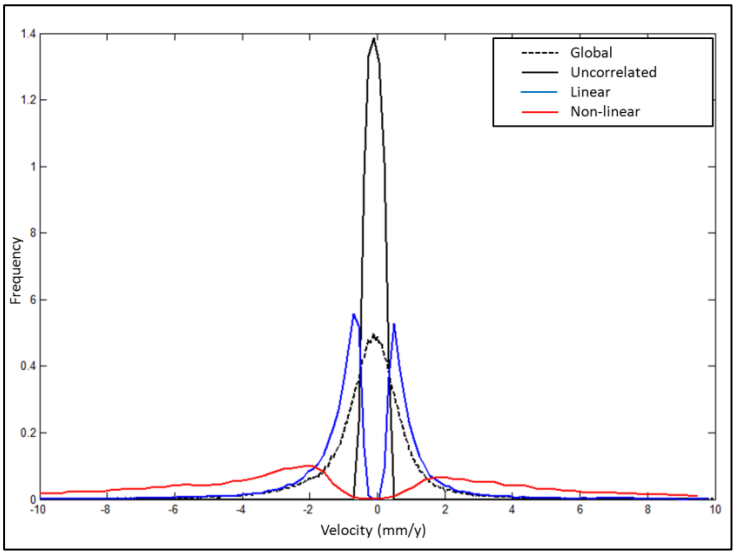

Figure 66. Frequency distribution of time series type classified using PS-Time. Dataset RADARSAT-1 descending.

It is interesting to note, that RADARSAT-1 descending dataset, which is composed by 112 images and processed with the SqueeSAR™, has very narrow Gaussian distribution of "uncorrelated" with extremes velocity values of ~0.5 mm/y. This means that statistically the dataset has a higher precision and lower noise. However from an operation point of view, based on the experience, the "correlated" time series having a velocity lower than 2 mm/y should be used very carefully as a possible indication of active deformation.

4.1.3.3 Results & Discussion

The post-processing routines proposed in this work can all provide a support to the landslide inventory update. In the simplest approach, it can be applied the matrix approach to the definition of the landslide activity. Assuming to use the velocity threshold (2 mm/y) found with PS-Time from Berti et al., (2013), the landslide activity can be update by crossing the MT-InSAR dataset and the landslides inventory. The

landslides containing measurement points with average higher than 2 mm/y will be classified as active. In other hand, dormant landslides will contain measurement points showing average velocity lower the 2 mm/y. Figure 67 shows that according to the matrix approach, 72% of the active landslides should be reclassified into dormant while 49% of dormant need to be reclassified as active.

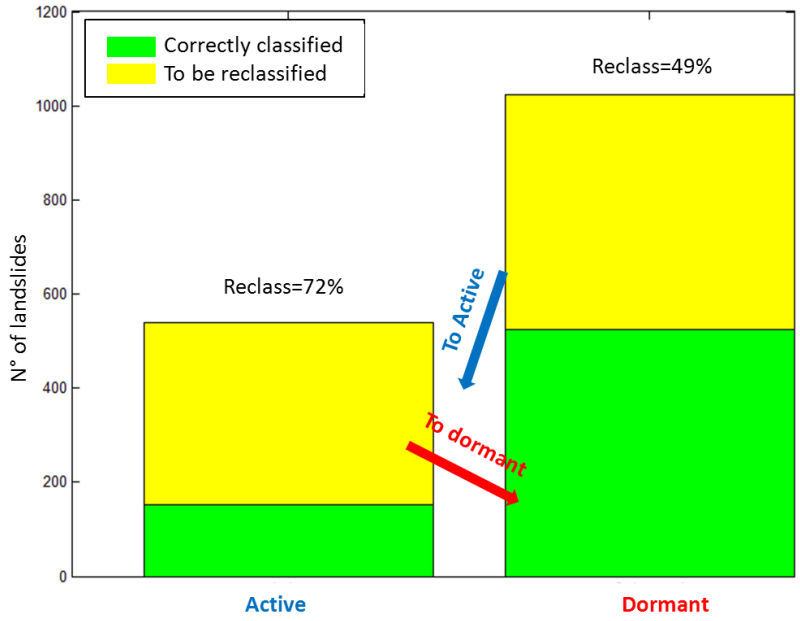

Figure 67. Number of landslides from the inventory that need to be reclassified according to RADARSAT-1 descending dataset. Activity threshold set at 2mm/y.

It should be pointed out that automatic inventory update can leads into erroneous classification. The following factors should be taken in account since they can drive the results of the activity update:

1) Not every landslide contain the same distribution of measurement points. Very few points cannot be significant while many points (i.e. belonging to different geomorphic subunit of the landslide) can leads into a lower and averaged velocity of deformation;

2) Landslide dipping near-North-South can only partially be measured by InSAR. As a consequence, even PS with velocity < 2mm/y, can indicate activity;
3) Non-linear deformation. PS that activated recently, can show only a mild average annual velocity, but a much higher velocity in the purely active phase. To this end PS-Time it is valuable, since it allows to discretise the time series in segments of different velocity.
4) Inventories can be incomplete or some landslide can be only partially mapped. By crossing landslide inventory with MT-InSAR dataset, only the landslide already mapped will be update. Since MT-InSAR can reveals extremely slow deformations with high precision (~2mm/y), there can be several areas active previously unknown.

Based on the author experience, it advisable that regional scale analysis should only highlight potential areas of deformation, rather than automatically update landslide inventories (i.e. matrix approach). To this end the user can decide if use clustering approach (i.e. Hot Spot Analysis) or manual classification based on visual interpretation of MT-InSAR products. In the northern Apennines, thanks to the availability of different types of data sets over the same area both the approach were applied (Hot SpotAnalysis and manual mapping) a user-based classification has been carried out, identifying b y visual interpretation whereas MT-InSAR could indicate an active deformation process, which is in agreement with the local geomorphology. This manual classification was necessary to:

- Evaluate the contribute of SqueerSAR™ (and thus of thus of distributed and temporary scatterers) on the landslide mapping in the Apennines
- Compare the results with AOIs mapped using the PST-A data sets
- Evaluate the effectiveness of the automatic hot spot analysis.

In regional analyis both Geo-PSIC and PS-Time can be used to support the identification of potential active landsldes. The use of the velocity component in fact, compared to the use of velocity in the LoS, allow an easier verification of the dynamics of the deformation with the geomorpholgy. In fact, to achieve a proper AOIs mapping, updated ancillary data are requires, as ortophoto, DEM, geological map, landslide inventory, etc. (Figure 68).

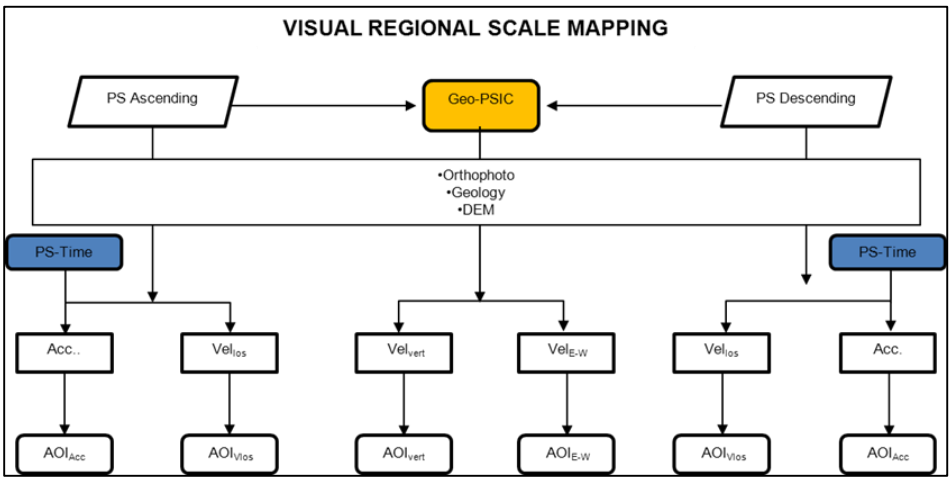

Figure 68. Integration of Geo-PSIC and PS-Time in the regional mapping of potential active landslides.

Table 7 shows a summary of the classification carried out by visual interpretation of areas wich may represent ative landslides and that requires further investigations (i.e. fieldwork, damage to buildings and

infrastrucure assessment, geomorphic evidences, in situ monitoring systems, etc.).

Since within the PST-A project database, no acceleration were computed, the comparison of non-linear deformation can only be based on PS-Time classification, and of course on measurement points that have a significant average velocity. In fact a non linear deformation, can still be recognisable using the average velocity, if a significant linear regression fits the displacements distribution (time series).

Table 7. Potential areas affected by landslides mapped by visual interpretation of RADARSAT-1 data set (SqueeSAR) and ENVISAT (PSP-IFSAR, from PSAT-A).

	Mean velocity		Velocity components				Acceleration			
	Line of Sight		Vertical		East-West		(T.R.E.)		PS-Time	
Asc.	115	16	31	7	96	12	77	-	18	2
Desc.	112	25					79	-	21	3
	Rsat	Envisat	Rsat	Envisat	Rsat	Envisat	Rsat	Envisat	Rsat	Envisat

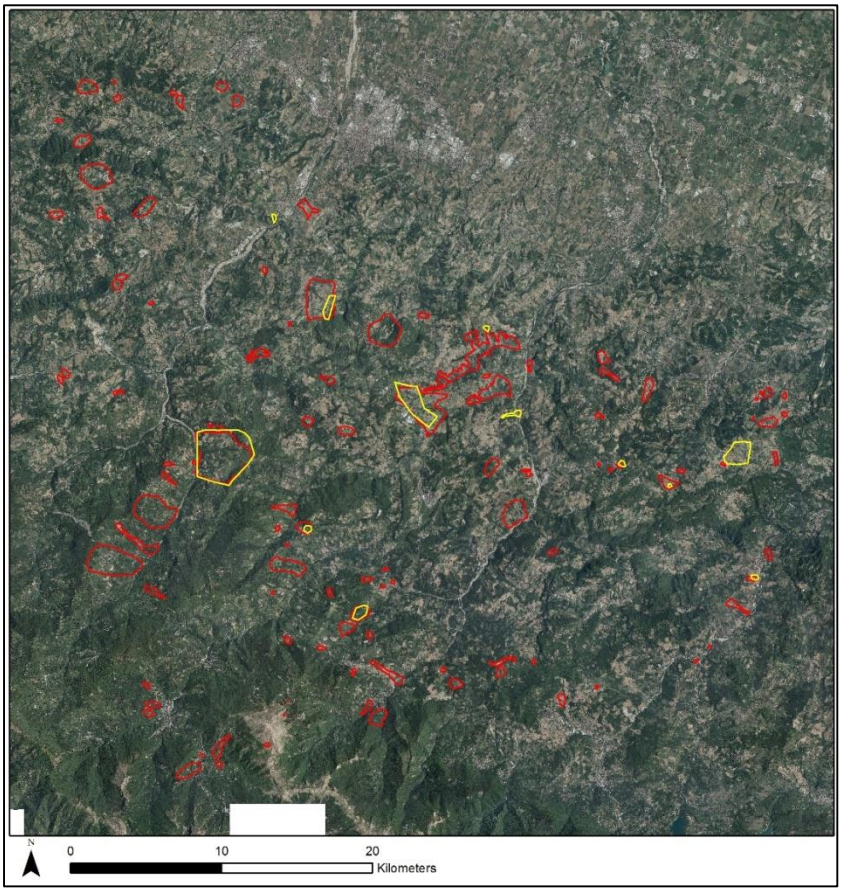

Figure 69. Potential active landslides from visual interpretation of RADARSAT-1(red polygons) and ENVISAT. (yellow polygons), both in ascending geometry.

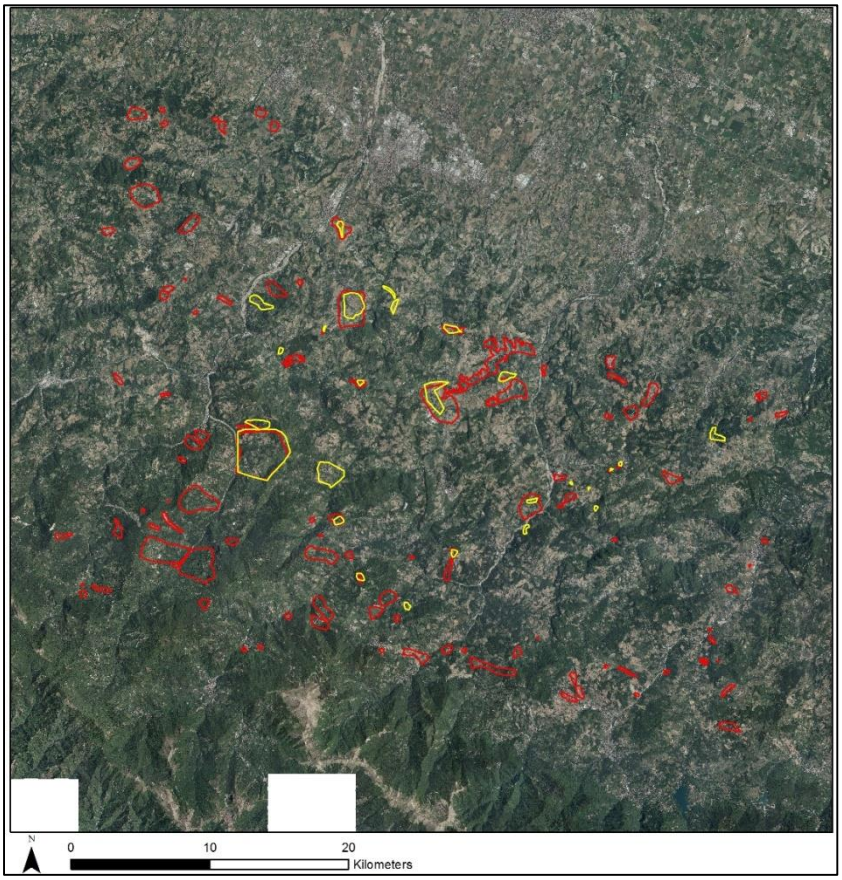

Figure 70. Potential active landslides from visual interpretation of RADARSAT-1 (red polygons) and ENVISAT (yellow polygons), both in descending geometry.

Figure 69 and Figure 70, show that using SqueeSAR™ data, about 6 time more potential active landslides can be identifyed, just analysing the average annual velocity. However the visual interpretation of large dataset cover large areas is time consuming and in first analysis the Hot Spot Analysis can be an option. The challenge is to find threshold of magnitude for the cluster discrimination, which balance the false positives and the true negatives spots. The comparison bewteen the automatic analysis (Hot Spot) and manual analysis (viasual interpretation) is presented in Figure 71. In general there is a good agreement between the automatic classification and the manual

classification, and the prediction tend to be more successful for larger phenomena. On the other hand, very localized deformation are not well predicted. This is due to the fact that localized deformation is not represented by a not statistically significant number of measurement points, and no clusters can be found.

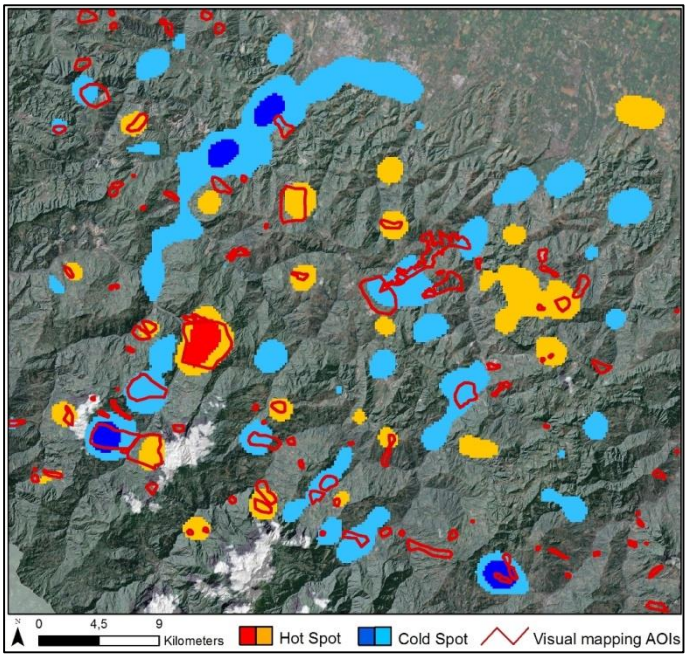

Figure 71. Comparison between Hot Spot Analysis and manual mapping by visual interpretation. RADARSAT-1.

In a regional scale study, after the identification and classification of potentially active landslides, a second phase of analysis should follows. This phase is intended to be mainly carried out at local scale, aiming to further investigation such as geomorphic surveys, damages surveys, ancillary data, in-situ monitoring, etc.).

4.2 Application to Slope-Scale stability analysis

4.2.1 Introduction & State of Art

Historic deformations are very valuable for site-specific landslides studies (Rossi et al. 2010) allowing the investigation of slope dynamics deformations, and thus to take decision on remedial works or mitigation efforts. When large landslides are studied, the use of conventional monitoring techniques (i.e. total stations, GPS, extensometers, inclinometers, etc.) can be resource intensive, especially where the investigation has to cover large slope failures for long periods (Giordan et al., 2013, Calò et al. 2014). In that sense, since about 2 decades, authors applied with success the InSAR technique to site-specific landslide studies (Fruneau 1996, Refice et al., 2000). The applicability of InSAR for landslide monitoring is increasing within latest years thanks to the "second generation" of X-band SAR systems (i.e. COSMO-SkyMed, TerraSAR-X). In particular, these satellites have a short repeat pass (CSK up to 1 day in constellation mode) and high spatial resolution (CSK <1 meter in "spotlight" mode). Consequently, higher number of measurement points are extracted from MT-InSAR algorithm, improving the landslide mapping and investigation. In addition, the reduced repeat pass allow to measure very variable deformation pattern and seasonal deformation. In other words, also non-linear deformation can be conveniently monitored. In perspective, it is important to have the necessary tools for time series analysis. The new constellation of satellite, with high frequency of acquisition, allows to use InSAR for the so-called "continuous monitoring" with the ambition to become a tool for quasi-real-time monitoring. However, sometimes landslide do not provided the best reflectivity condition for InSAR monitoring, in

particularly when highly vegetated. To overcome this problem, a network of artificial corner reflectors can be installed over and outside the landslide body (Iasio et al., 2011, Corsini et al., 2012, Crosetto et al., 2013) and be used in conjunction with GPS measurements (Zhu et al. 2014). MT-InSAR has proven to be applicable also for long-term monitoring of landslide post-failure deformation (Greif et Vlcko, 2012), for creep monitoring (Suncar et al. 2012) and for landslide geomechanical modeling (Calò et al., 2014). It has also to be considered that distinguish the mechanism and the affected areas of slow-moving landslides is challenging. InSAR provide very high precision datasets over wide areas, which, through post-processing analysis, can be used to support the characterization of the deformation.

4.2.2 South Tyrol

4.2.2.1 Objectives and General Settings

A second step of the InSAR-based landslide analysis is required after the detection of potential active landslides at regional scale. At this level of analysis, the InSAR data should be used to define more precisely the active zones from the stable zones and define the landslide spatio-temporal dynamics. In order to be successful, InSAR data should be analyzed in conjunction with other thematic layers, such as geology, geomorphology and with any of the ancillary information available (field surveys, in-situ monitoring data). The knowledge of temporal evolution of the landslide will help to make decision on possible remedial work. However, the aim of the slope scale analysis with InSAR data is to provide a better picture of the active phenomena, allowing planning aware-further investigation, reducing costs for redundant or ineffective in situ monitoring. Notti et al., (2013), used to show the velocity components (vertical and East-West) along the main axes of displacement of the landslides to identify variations along the landslide profile. To the author knowledge, works on time series analysis of site-specific deformation, are still lacking. In this section, the MT-InSAR have been post-processed to define, at selected landslides in South Tyrol, the direction of the displacements, the modulus of the displacements and the temporal evolution of the landslide. In addition, successful examples of local scale application of the post-processing methods proposed (PS-Time and Geo-PSIC) are presented.

4.2.2.2 Datasets & Methods

The post-processing routine have been applied to the datasets presented in section "application to Regional Landslide recognition – South Tyrol". The two data stacks (ascending and descending) processed with SqueeSAR™ are composed by 38 and 37 RADARSAT-1 SAR images respectively, and cover a period from 2003 to 2006. The specific site analyzed in this section are located in the western sector of South Tyrol.

4.2.2.3 Tools

Two over the three post-processing techniques have been applied to specific-sites in South Tyrol. The Hot Spot Analysis is mainly used for regional scale analysis of landslides, in particular for the detection and mapping of active landslides. For this reason, it was not applied at slope scale analysis, since no additional information are added. In other hand, the velocity components have been applied and used to define the angle of movement direction. The time series analysis has been used to define if a landslide is:

1. Accelerating: the landslide can potentially leads into a higher risk scenario
2. Decelerating: it might be an indication that the causal factors have been removed or that the landslide is stabilizing.

4.2.2.4 Results & Discussion

4.2.2.4.1 Val Mazia

4.2.2.4.1.1 Geological and Geomorphological Settings

The study area, which has an extent of about 50 Km^2, is located in the Val Mazia, a secondary valley of the main valley "Vinschgau" (Val Venosta). In particular is analyzed the slope facing Southeast and bordered to the bottom from the "Rio Saldura", a tributary stream of the

Adige river. The average slope angle is about 30° and with an elevation starting at about 1700 m (Rio Saldura) to about 2800 ma (mountain crest). In the IFFI landslides inventory, no landslides are mapped in this area. However, in the upper part of the slope, starting from the elevation of about 2600 meters, there are evidences of double crests, indicating the possible presence of a Deep Seated Gravitational Slope Deformation (DSGSD) (Figure 72).

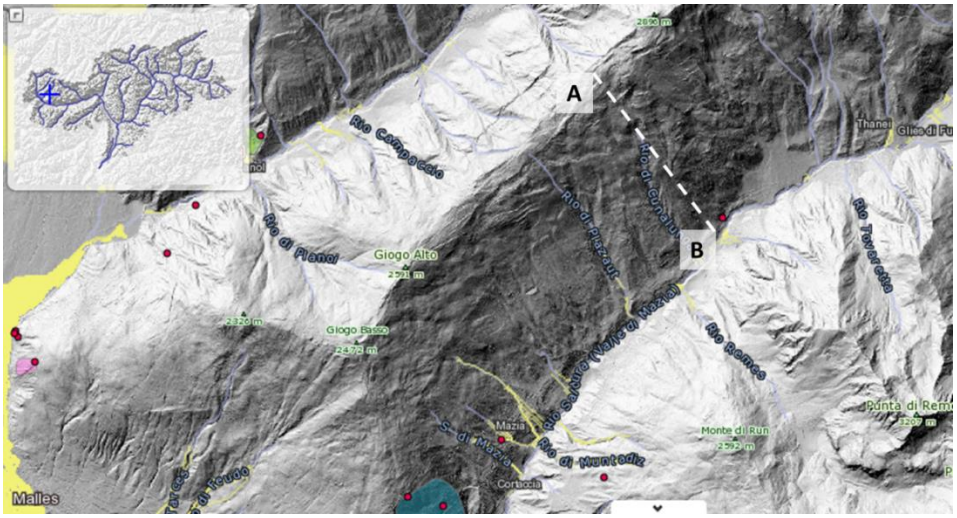

Figure 72. Hill shade view of the study area topography (Val Mazia). The profile section analysed (A-B) is represented by dashed line.

From a geologic point of view, the area is located in the Austro-alpine domain and outcrop mainly metamorphic rocks, Phyllites, Micaschist and Gneis (Figure 73). However, due to the geomorphic exposure of the slope and to the geological material, the site result to be reflective and visible from both satellite orbits, allowing carrying out quantitative analysis on the movement direction.

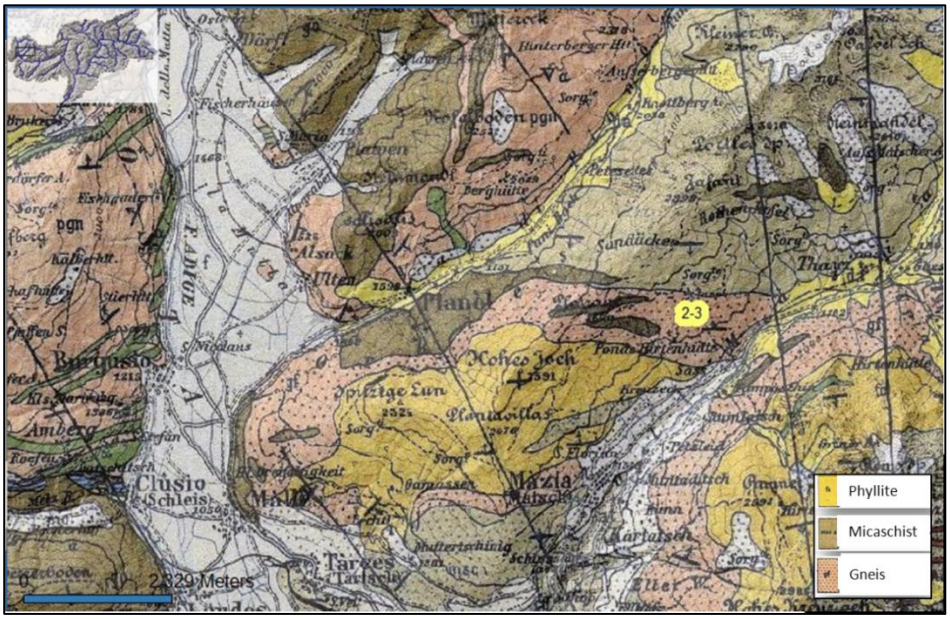

Figure 73. Geological map in scale 1:100000. Source: Geobrowser (Autonomous Province of Bozen).

4.2.2.4.1.2 Ground deformation pattern

SqueeSAR™ data shows deformation over the study area, in both datasets, ascending and descending (Figure 74 and Figure 75). The modulus of the deformation varies from about five mm/y in the "line of sight" in the crest area, and tend to "zero" at the base of the slope. Unfortunately, due to the vegetation cover, the lower zone of the slope is lacking of measurement, with a consequence that in that area the deformation cannot be estimated. Due to the South-East exposure of the slope, the deformation is measured as negative from the ascending satellite (movement away from the satellite) and as positive from the descending dataset (movement toward the satellite). Thanks to the combination of the two geometries, components of the velocity can be estimated. The velocity components can be used together to evaluate the

angle of movement direction (γ) of the landslide as described in Chapter 3.

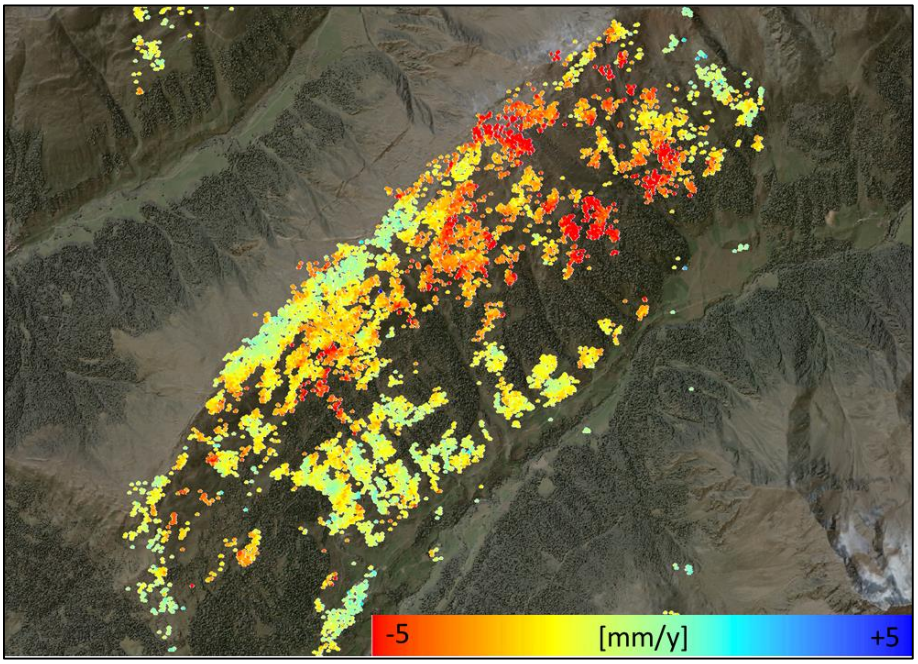

Figure 74. Average annual velocity of the RADARSAT-1 ascending dataset, stretched between ±5 mm/y.

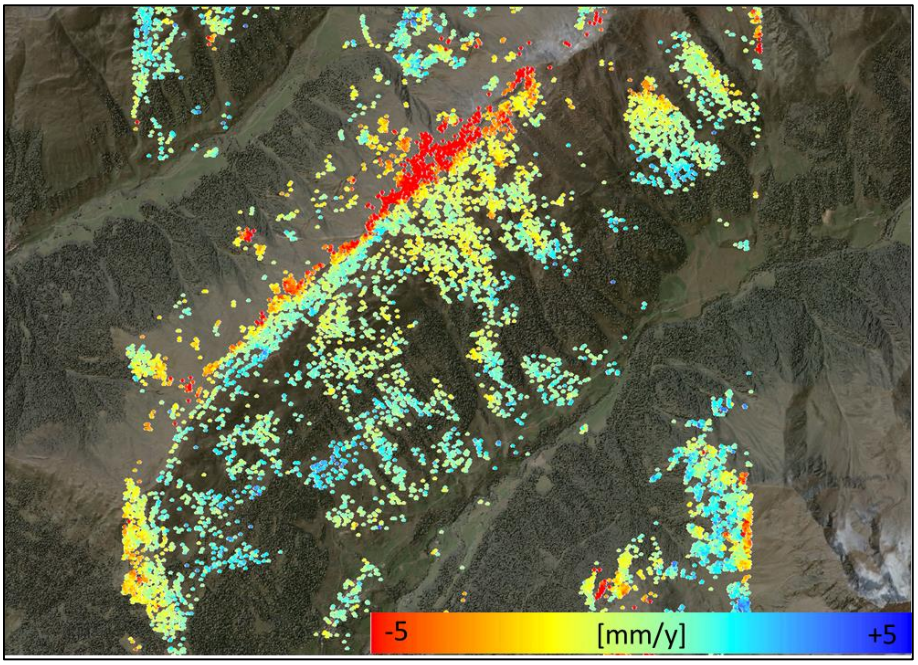

Figure 75. Average annual velocity of the RADARSAT-1 descending dataset, stretched between ±5 mm/y

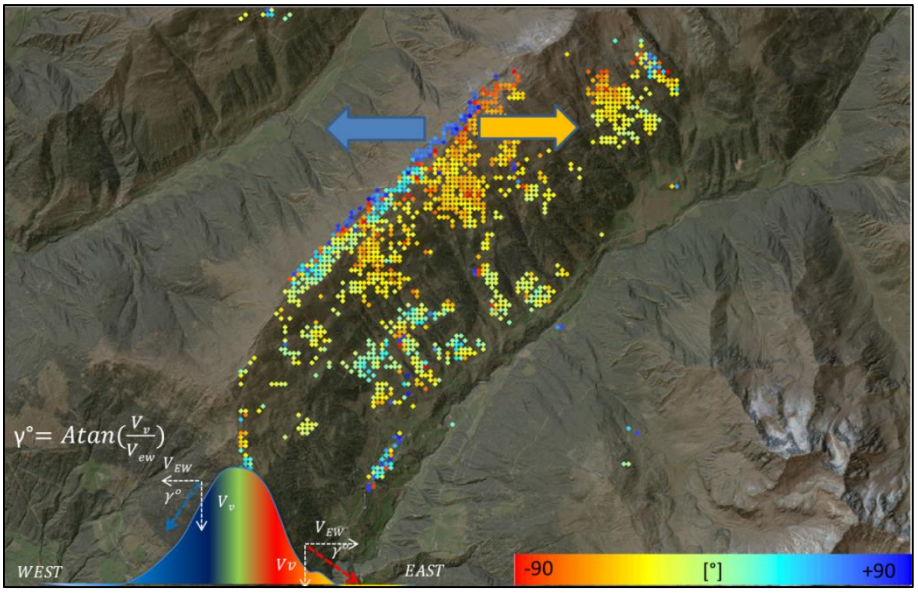

Figure 76. Movement direction angle (γ) evaluated from the velocity components. Blue indicates a direction toward West, while red indicate movement toward East. The colour

gradation is proportional to the angle of direction where: 0°=horizontal movement; 90°=vertical movement.

The use of the γ is advantageous to identify the cinematic of the landslide and thus have an idea of the sliding surface (i.e. Roto-translational, translational, etc.). The direction of movement of the Val Mazia test site, are shown in Figure 76. Several consideration can be drawn from these results:

1. The crest is affected by two distinct DSGSD of which one is dipping to South East (in the direction of the Val Mazia) while another DSGSD dips to the opposite slope direction (Nort-West).
2. The Val Mazia DSGSD has a roto-translational movement dynamic. The upper zone moving predominantly vertical (~85°-~70°), the medium zone is moving almost parallel to the slope (~30°), while the lower, has very little deformation but with horizontal direction.

In addition, the velocity components are plotted along a profile (A-B) of the DSGSD (Figure 72). The InSAR data shows that in the upper part of the DSGSD the velocity of deformation is mainly vertical (~6 mm/y), toward the middle portion on the slope, the movement is almost parallel to the slope. The intersection point of the V_{vert} and $V_{East\text{-}West}$ is where the two velocity components are similar. In other words, in that portion of the slope, the movement direction follow a 45° angle γ. From this point, toward the base of the slope, the East West component is predominant, until the DSGSD toe, where the vertical component is null.

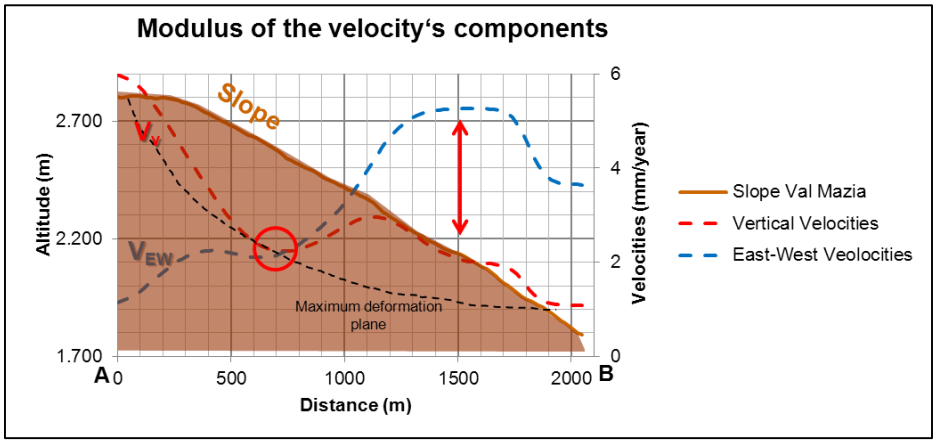

Figure 77. Cross section A-B along the DSGSD of the Val Mazia. The vertical component and East-West component is plotted along the cross section, enhancing the roto-translational cinematic.

To characterize the deformation type in the time domain, the time series analysis with PS-Time was carried out. In particular was analyzed the RADARSAT-1 ascending dataset, that due to the acquisition geometry and the geomorphology, resulted to be more sensitive to the deformation and returning am higher number of measurement points (slope parallel to the line of sight). It is interesting to note that the correlated time series are clustered in the Northern sector of the studied slope, while in the southern area, the uncorrelated are predominant (Figure 78). In particular, in the most active area, the time series shows a "bilinear" or "quadratic" deformation trend, indicating in both case a non-linear deformation. Furthermore, in order to determine if is an acceleration or a deceleration, causing the non-linearity of the deformation, was evaluated the difference in velocity between the two segments of each time series. Following this approach it is possible to plot the points that have an increasing velocity (and thus an acceleration, identified with red dots), or a decreasing velocity (identified with blue dots). All measurement points showing a linear deformation trend, or uncorrelated, will have a

"constant" velocity, that of course for the "uncorrelated" is equal to "zero". Figure 79 shows that the area is affected by a general deceleration.

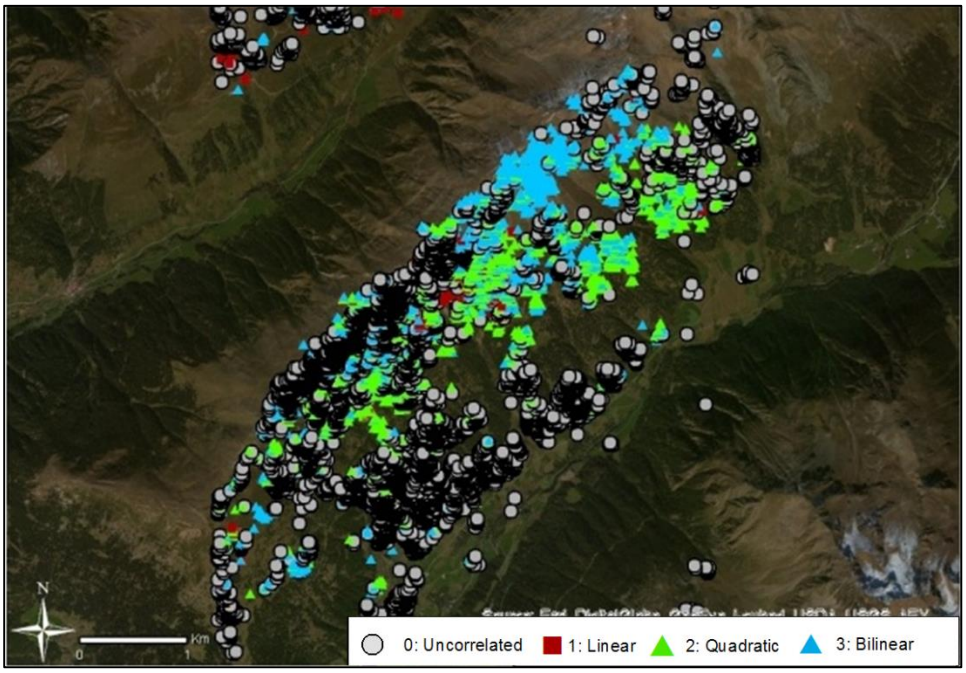

Figure 78. Time series classification of the RADARSAT-1 ascending dataset, from PS-Time. The correlated time series are clustered in the Northern sector of the studied slope, while in the southern area, the uncorrelated are predominant.

Following this approach it is possible to plot the points that have an increasing velocity (and thus an acceleration, identified with red dots), or a decreasing velocity (identified with blue dots). All measurement points showing a linear deformation trend, or uncorrelated, will have a "constant" velocity, that of course for the "uncorrelated" is equal to "zero". Figure 79 shows that the area is affected by a general deceleration.

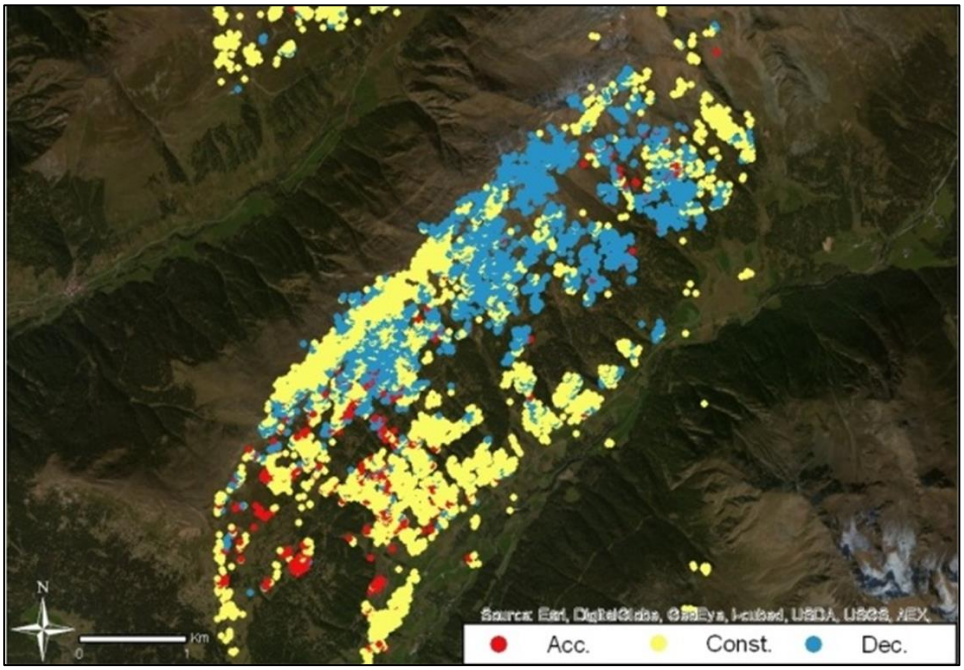

Figure 79. Acceleration (red), deceleration (blue) and constant velocity, computed with PS-Time for the RADARSAT-1 ascending dataset.

4.2.2.4.1.3 Discussion

DSGSD are common in the Alps and they are linked to the tension unload that slopes suffer after the last glaciation. The Val Mazia DSGSD was not mapped on the landslide inventory and thus probably was not prior known. InSAR has proved in general to be very valuable for detecting such slow movement affecting large portion of slopes. In addition, the post-processing routines presented in this study, provide more detailed information on the cinematic of the landslide, and the temporal dynamics. Like for most natural phenomena, deformations are correlated in space, since there is a high probability that similar deformation types are found within a certain distance. Both the post-processing methodologies applied shows that the results are not randomly distributed. In fact:

1. PS-Time highlighted a cluster of correlated (specifically "bilinear") measurement points, in the northern sector of the slope, and in particular in the upper zone. This area correspond to the most active area, while the area in the southern-western zone of the slope, mainly "uncorrelated" measurement points are returned. The computation of the change in velocity of deformation, suggest that the active area, is actually showing a mild deceleration (~2 mm/y).
2. The velocity components, and consequently the evaluation of angle of movement γ shows a clear distribution of near vertical (90°) deformation in the crest area that tend gradually to the horizontal movement direction (DSGSD toe), describing a roto-translational cinematic.

It important that test sites have a good measurement point's coverage, in order have a sort of continuous information over the landslide. While in general at the Val Mazia site, both the satellite geometries shows a god coverage, the lower portion of the slope is missing measurement points. In fact, the analysis of the velocity components along the profile is not fully reliable, since the results depends from a neighborhood velocity interpolation (Figure 77).

4.2.2.4.2 Parcines

4.2.2.4.2.1 Geological/geom. Settings

The study area has an extent of about 15 km^2, and is located at 8 km East from Meran (Figure 80).

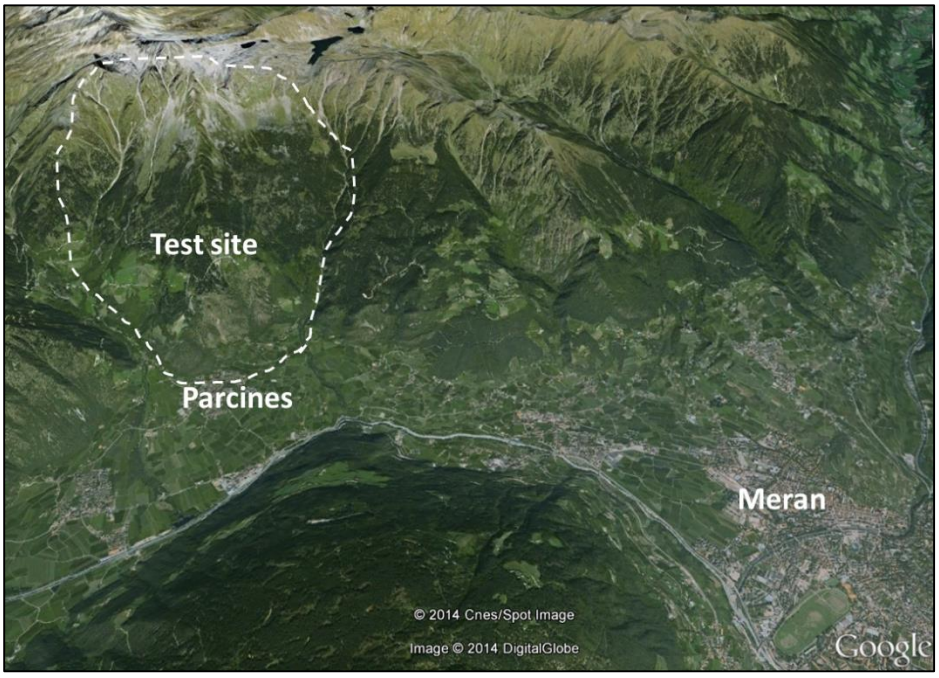

Figure 80. Geographic location of the test site. Source Spot Image: Google.

The two slopes analysed to test the various tools for the velocity components computation, are delimited at the bottom from two large debris fan reaching the Adige River. From a geomorphic point of view, study area is in adverse condition for InSAR monitoring. In fact slopes are facing near South direction and thus deformation are expected mainly parallel to the satellite azimuth. In these conditions, only a small component of the displacement is measured from the satellite. The geological map of Meran (1:50000) shows that the main features outcropping are the quaternary post-glacial deposit (diamicton), the diamicton from the late-Pleistocene, the orthogneiss and paragneiss. In

the upper zone of the study area are present a series of debris fan which are generated from the avalanches and snow melt.

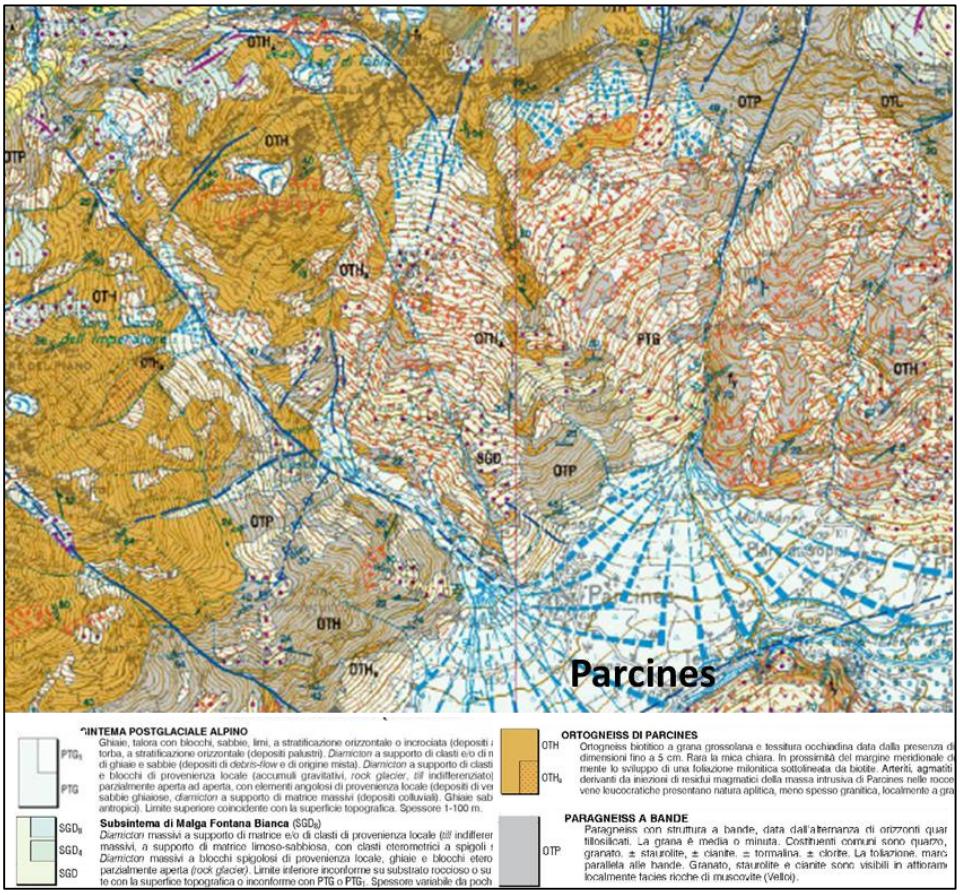

Figure 81. Geological map 1:50000 of the study area. Legend in Italian (CARG project. Source: ISPRA, http://www.isprambiente.gov.it/Media/carg/13_MERANO/Foglio.html).

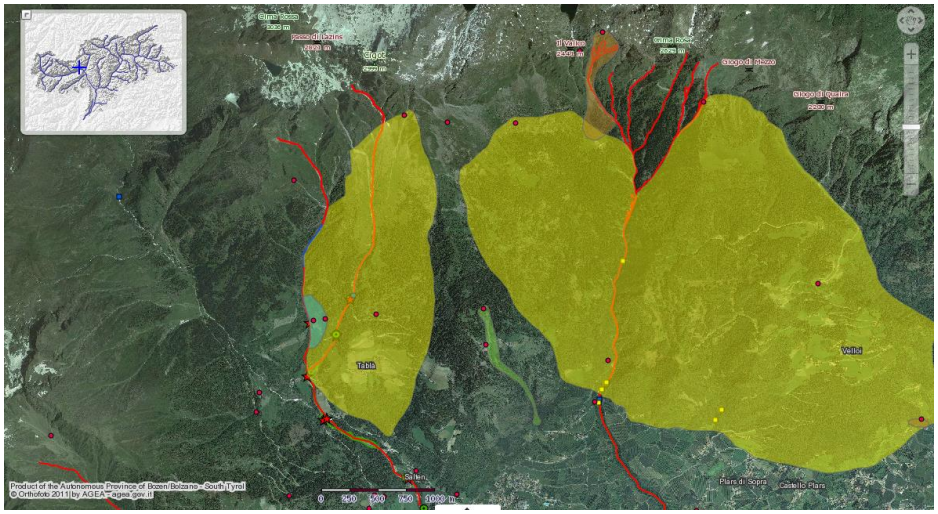

Figure 82. Landslide inventory of the Autonomous province of Bolzano. In the study area are mapped the left units, as rock falls/toppling, while the unit on the left side is classified as DGPV.

4.2.2.4.2.2 Ground deformation pattern

Over the study area. a narrow crest acting as a watershed, identify two distinct geomorphic units: a western unit and an eastern unit (Velloi). The velocity of deformation shown in captured from RADARSAT-1 shows that slope movement are present in both the units. In particular Figure 83 shows the velocity from the descending while Figure 84 shows the velocity from the ascending orbit. In general velocity over the western unit is mild (~3 mm/y), while the eastern unit shows a larger active portion moving at higher rate (8-15 mm/y). Since both slopes are exposed near North-South, the real displacements over these areas are expected to be higher than the displacements measured from the InSAR. This is due to the little sensitivity of the InSAR to movement parallel to the satellite azimuth. However, the descending dataset has shown a higher sensitivity to the movements' active over these areas. Based on this considerations, the evaluation of the velocity back-projected along the slope, has been applied to the ascending dataset. (Figure 86).

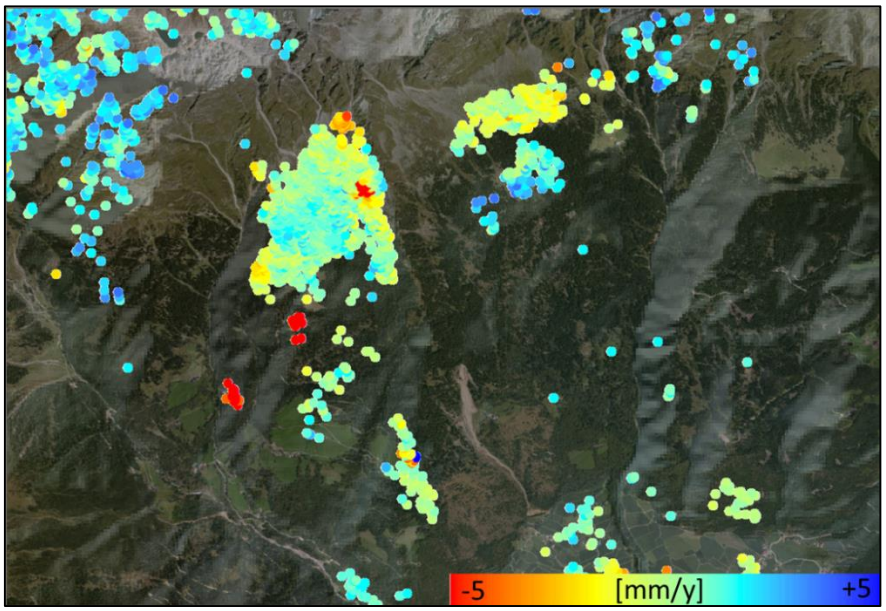

Figure 83. Average annual velocity. RADARSAT-1 descending.

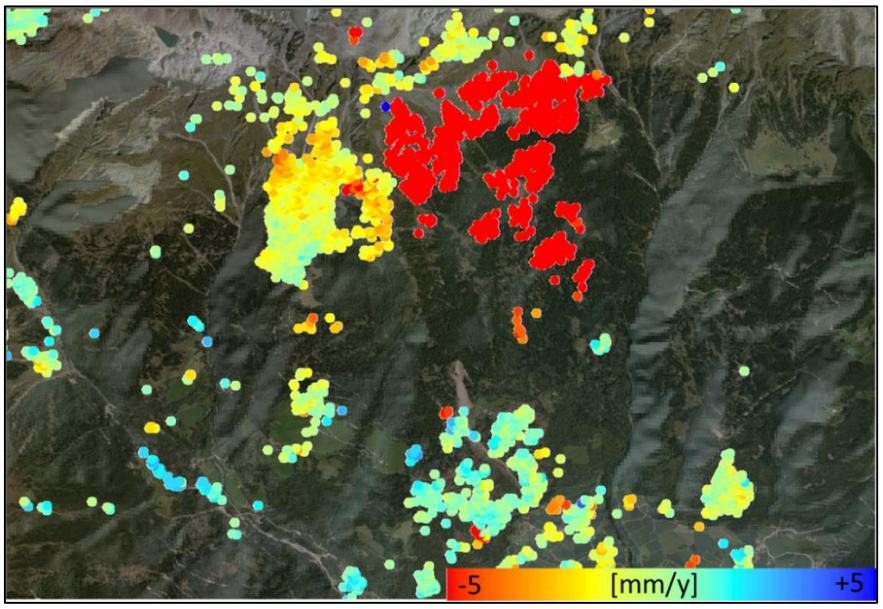

Figure 84. Average annual velocity. RADARSAT-1 ascending.

The particularly abrupt local geomorphology and the presence of distinct active sub-units, made this test site suitable for testing the three available

methods for the evaluation of the velocity components. First, the method for back-projection (used when only one single orbit is available) is compared with Geo-PSIC (the double orbit novel approach proposed in this study (Figure 85). It is evident that the assumption that the mass movement is parallel to the slope direction, generate unexpected values of velocity (Figure 85a) creating a "salt and pepper" effect. In other hand, the velocity components evaluated combining ascending and descending orbits (i.e. Geo-PSIC) shows good and intelligible results. In particular it can be observed that a high vertical component exist in the study area, in particular in the eastern sector. The East-West component shows that both the sub-units have a horizontal component predominant in the East direction (positive value of velocity). It can be observed from the Figure 85b that the western sub-unit show a very localized phenomena having a horizontal component predominant in the West direction. This type of deformation can also be found in correspondence of boulders.

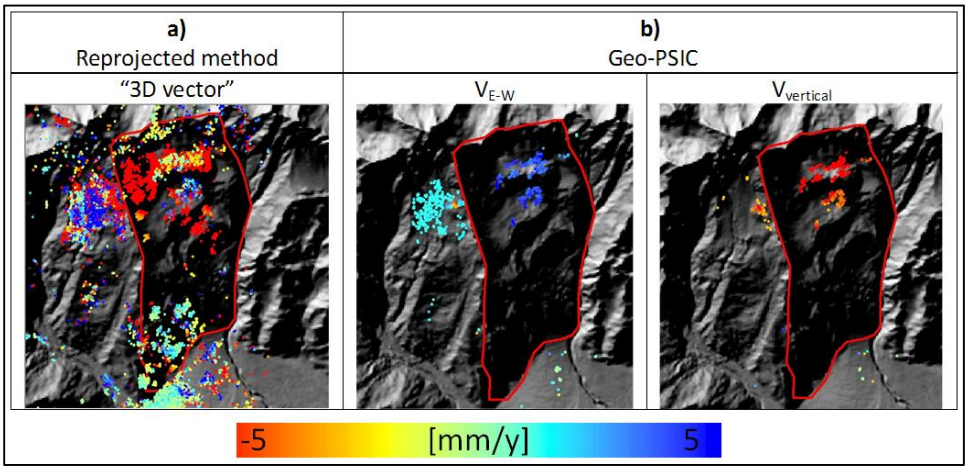

Figure 85. Comparison of the methods for the evaluation of the velocity components. a) velocity back-projected along the slope; b) $V_{East-West}$ and $V_{vertical}$ evaluated with Geo-PS.

Once established that the use of double orbit produce sensibly better results than the back-projected method, both double orbits methods are

compared. The aim was to test the effectiveness of geomorphic criteria introduced by Geo-PSIC, with the method used in literature, the resampling grid. Figure 86 shows that while overall the resampling grid produce results similar to Geo-PSIC, at very local scale, results can be different. It can be noted that the little local deformation, visible also from the velocity in the line of sight results, is highlighted by Geo-PSIC but averaged by "the resampling grid".

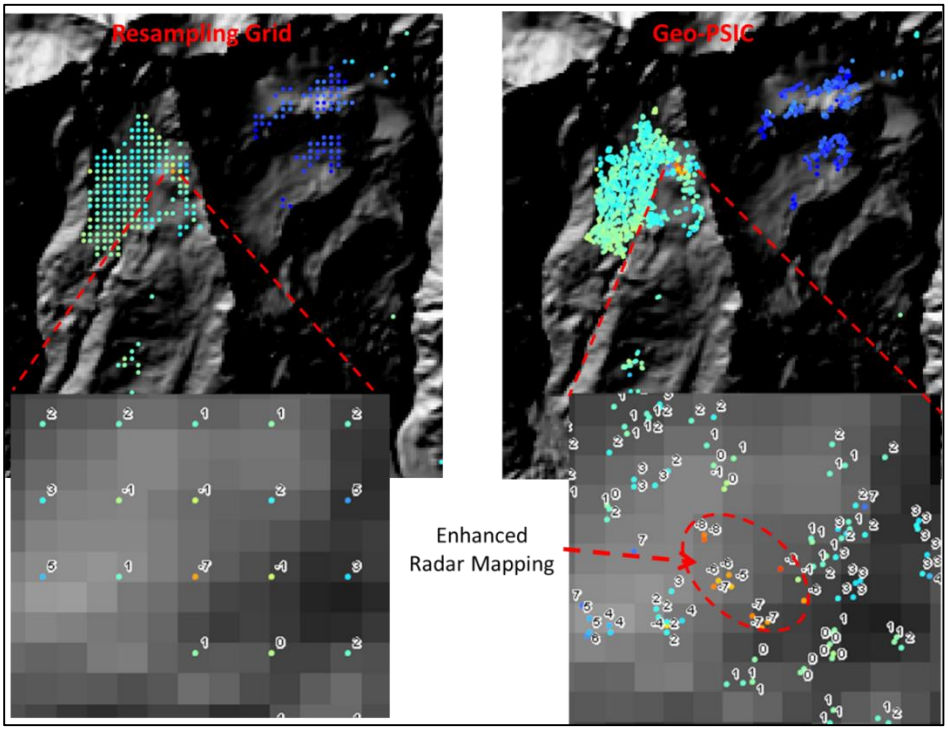

Figure 86. Comparison of the two methods for the velocity components extraction, based on double orbit use. The resampling grid (left) and Geo-PSIC (right).

4.2.2.4.2.3 Discussion

The test sites of Parcines, have shown that most of the movements are found in the quaternary deposits. In particular most the activity is found in correspondence of debris. However, in addition to the debris displacements, the eastern sector (Velloi) is affected by a deep seated landslide, and further in-situ investigation may be required. The methodological test carried at Parcines, has shown that back-projected method produce data not always intelligible, characterized by a sort of "speckle". This effect is due to the roughness of the topography. In fact, when computing the aspect angle and slope angle, any surface roughness present in the DEM, will return a correspondent values, that could be not realistic of the main slope angle. As a consequence, the best results are expected at low resolution of DEM, in particular in Alpine geomorphic condition, governed by high energy relief and abrupt change of local morphology. However, in this test site a resolution of 20 meters was chosen, but still the results are very poor. Additionally it has to be considered that the landslide do not always moves parallel to the slope, but rather they can move in correspondence tectonic or structural planes. Another cons to take in account in the back-projection method, is that even the noise is amplified. In example, measurement point that shows velocity around 1 mm/y, if located in slope near North- South can shows velocity of hundreds of mm/years. As a matter of facts, this effect applies to active measurement points and stable one. The results is a map characterized by high uncertainty, low intelligible and difficult to interpret. The use of double orbit produce a minor number of measurement points compared to the resampling grid, but since no

assumption are made, it is a rigorous approach and very little uncertainty is associated with it.

Geo-PSIC has also been tested with the resampling grid method presented in literature. Goo-PSIC highlighted very localized phenomena identifying a cluster of measurement points moving at about 7 mm/y. In other hand, the resampling grid produced a smoothed effected over the same local phenomena, hiding this area from any visual interpretation (only one measurement points with velocity indicating activity. In conclusion, for very local scale analysis, and in geomorphic conditions as the Alpines, the use of Geo-PSIC instead of the resampling grid can be beneficial. Also, it is scourged any application of the back-projection method, that has the effect to increase exponentially even the noise, making the interpretation hard. If no double orbit is available, the author suggest to use the line of sight results instead.

4.2.3 Northern Apennines

4.2.3.1 Objectives and General Settings

In this section site-specific landslide are analyzed in the Northern Apennines. In particular are selected two test sites from the database of potential active landslides compiled in the previous stage of analysis (regional scale analysis). Similarly to the objectives described for the study in South Tyrol, the aim is to define the extent of the active landslides, to characterize their dynamics and define if the landslides are experiencing acceleration, deceleration or are moving at constant rate. Objectives of this section were also to verify if the post-processing routines are applicable in Alpine as well as in Apennines environments.

This test was necessary to determine if calibration are needed before to apply the proposed post-processing routines to different geomorphic conditions. It has to be highlighted that InSAR is not proposed as a unique solution for monitoring site-specific landslide, but it has to be analyzed in conjunction with traditional in-situ measurement. However, the InSAR can help to identify critical area, and define favorable location and distribution of geotechnical measurements.

4.2.3.2 Datasets & Methods

The two RADARSAT-1 datasetes analized at site specific scale are comprising of 112 scenes in descending orbit and 124 scenes in ascending orbit, with a near montly acquisition. The algorithm used is the latest version of the SqueeSAR™, which provide also measurement points in area coherent for a limited period of time (Temporary Scatterers). The time coverage lasts from April 2003 to November 2012. The post-processing routines have been applied to characterize the landslides, define its activity and its cinematic. In particular, for the velocity component evaluation was decided to use the "resampling grid" for the geomorphic condition of the Northern Apennines, which are generally smooth compared with the Alpines environments. Non-linear deformation are also investigated to define if the landslide is actually decelerating, accelerating or moving at constant rate.

4.2.3.3 Tools

As for South Tyrol test sites, two over the three post-processing techniques proposed have been applied to characterize landslide in Apennine geomorphic environment. In particular have been applied the

"resampling grid" for the computation of the velocity component and PS-Time for the study of the deformation time series. The velocity components where then used to evaluate the angle of movement direction, in order to identify the landslide cinematic (i.e. roto-translational, translational, near vertical, etc.). using the angle of movement direction, the east-west component and vertical component, are summarized in one single interpretative layer, and gives a more direct picture on the landslide type. However, in order to identify the modulus of the displacement (or velocity) the East-West component and Vertical component can still be analyzed separately.

PS-Time was used to identify measure of deformation correlated in time, check their degree of clusterization and, if significant, then to define if the geomorphic unit studied is stabilizing, accelerating or moving at constant rate.

4.2.3.4 Results & Discussion

4.2.3.4.1 Palagano

4.2.3.4.1.1 Geological/geom. Settings

The study area is located in Apennine area of the Modena province and has an extension of about 6 km2. The slope dips toward west and is delimited to the bottom by the Dragone stream, a tributary stream of the Secchia River. According to the geological map "Cartografia Geologica (CARG), the few outcrops that can be found in the area of interests, belong to the Montevenere Formation (MOV). In particular, MOV is constituted by arenaceous-calcareous rocks alternated with fines fractions.

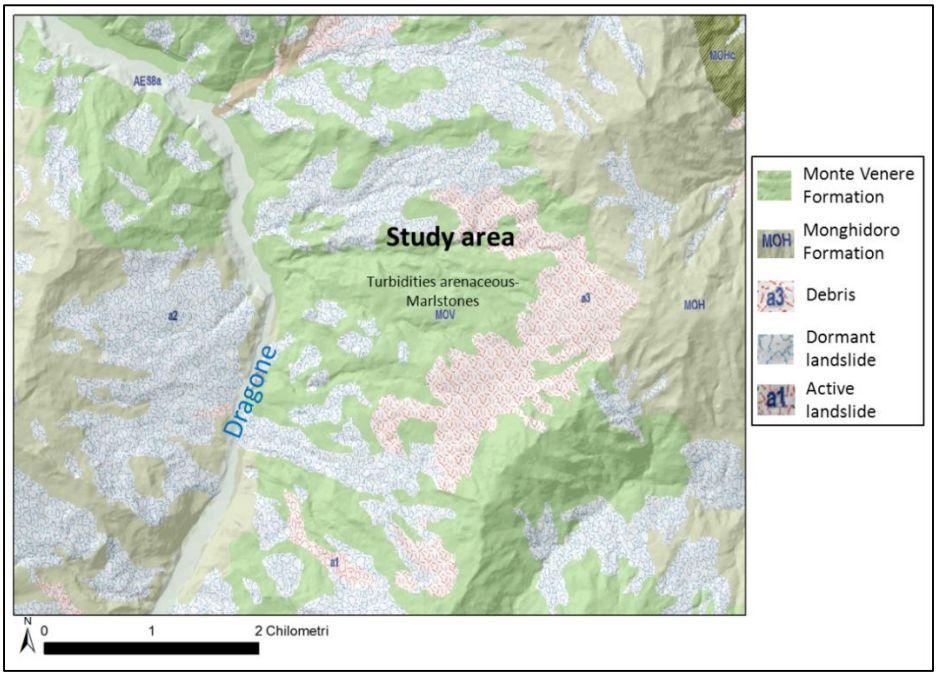

Figure 87. Geological map (CARG, 1:50000) of the study area of Palagano (MO).

In the surrounding area, turbidites from the "Formazione di Monghidoro" is found as well. However, most of the study area is covered by significant quaternary deposits, such as ancient landslides bodies and debris. In contrast to smooth geomorphology, steep areas can be found, due to the different competence of different facies existing within the MOV. In the upper part of the study are, the MOV is overlaid by the Monghidoro Formation, made of turbidites arenaceous-pelitic at the bottom and fining-upward to pelitic turbidites (Figure 87). Together with the geological map, it can be observed that within the study area several dormant landslide and debris have been mapped. Some other unpublished work, mention that outcrops at the bottom of the slope, show very high deformation and poor geomechanical properties, suggesting the hypothesis of the slope being affected by a DSGSD. Figure 88 shows the geological map 1:10000 of the study area and it include the quaternary

landslides deposits. In this map, most of the study area is classified as a dormant DSGSD or rockslide, with minor landslide subunits of "undefined" type. Some very local area are also classified as "active" landslide of "undefined" type. In Figure 88 are also highlighted two profiles were cross sections and displacement have been analyzed. The red circle indicate the location of the time series of displacement shown in this section (Figure 90 and Figure 92)

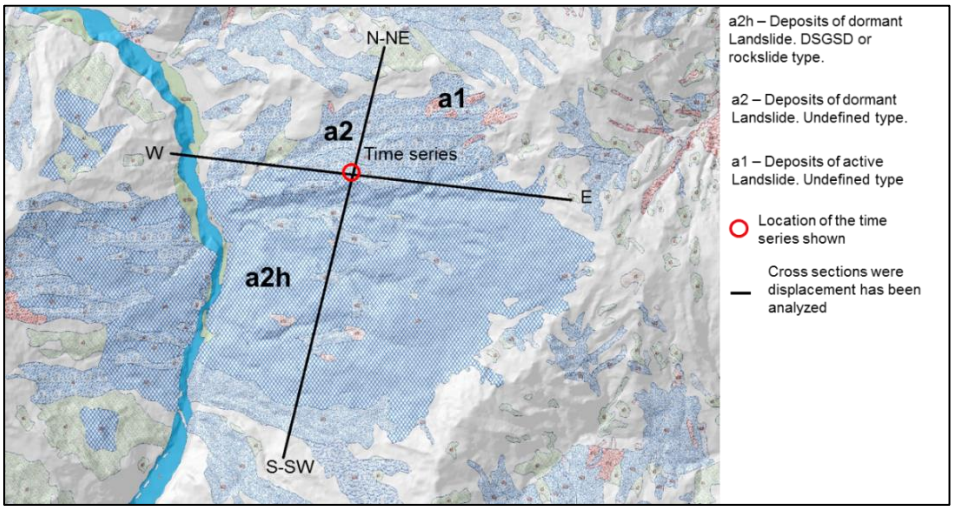

Figure 88. Geological map 1:10000 with detailed landslide inventory and cross section were the cumulated deformation has been analysed.

4.2.3.4.1.2 Ground deformation pattern

The average annual velocity of deformation for the RADARSAT-1 descending dataset is shown in Figure 89. All measurement points within the slope studied, show clearly evidences of deformation. Modulus of velocity are about 15 mm/y for the time span considered (2003 – 2012), which leads in about 150 mm of cumulated displacement. Deformation are found in the areas mapped as dormant landslide, in areas covered by debris but also in zones where no landslides or quaternary deposits are mapped in the official inventory maps.

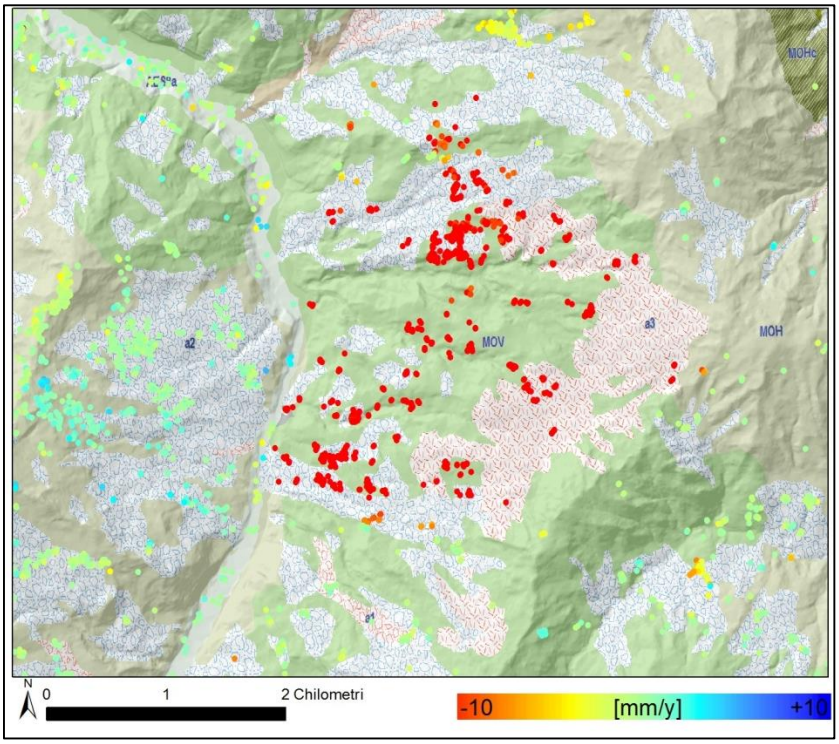

Figure 89. Average annual velocity of the measurement points in study area of Palagano (MO). RADARSAT-1 descending dataset.

Figure 90 shows the deformation time series (descending) of the area indicated with the red circle in Figure 88.

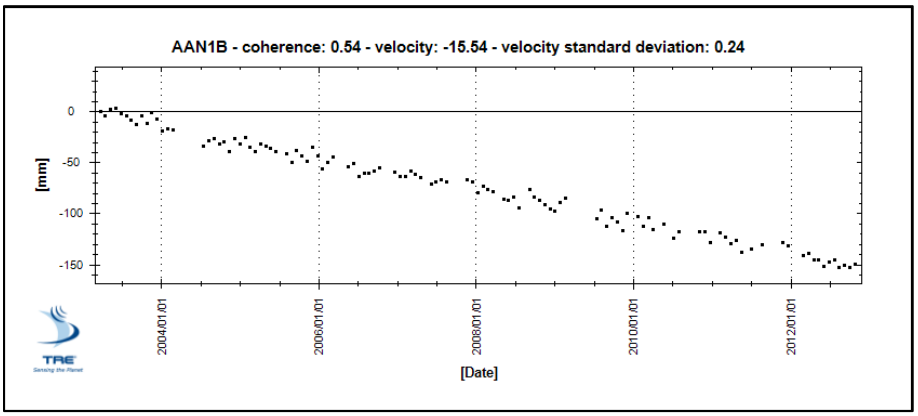

Figure 90. Time series of displacement of a measurement point located in the red circle in Figure 88. Line of sight descending dataset.

Analogous deformation pattern is measured from the ascending geometry (Figure 91). Similarity is also found in the modulus of the velocity of deformation in the two geometry (ascending and descending). This is also related to the exposure of the slope, which is near East-West. Under this geomorphic condition, most of the real deformation can be measured from the InSAR, about the same portion of it can be captured from the ascending and descending orbit. In other words and according to the local geomorphology, it is expected that the real deformation can be totally measured by the East-West and vertical component, while the North-South can be considered negligible.

Both the datasets, ascending and descending shows a slightly higher deformation rate in the central portion of the study area, over an area classified as "undefined dormant landslide". The time series of the displacement measured at that location are the one represented in Figure 90 and Figure 92. It is interesting to note that while both ascending and descending shows a similar deformation velocity over that area (15 mm/y), the East-West components reach a higher value (22 mm/y). In the other hand, the vertical component is almost negligible (2 < mm/y). In this portion of the slope, the InSAR dynamic are in agreement with a translational movement, while toward the upper portion of the slope there is a slightly roto-translational movement. However the low density of measurement points, do not allow to define the dynamic in any portion of the landslide.

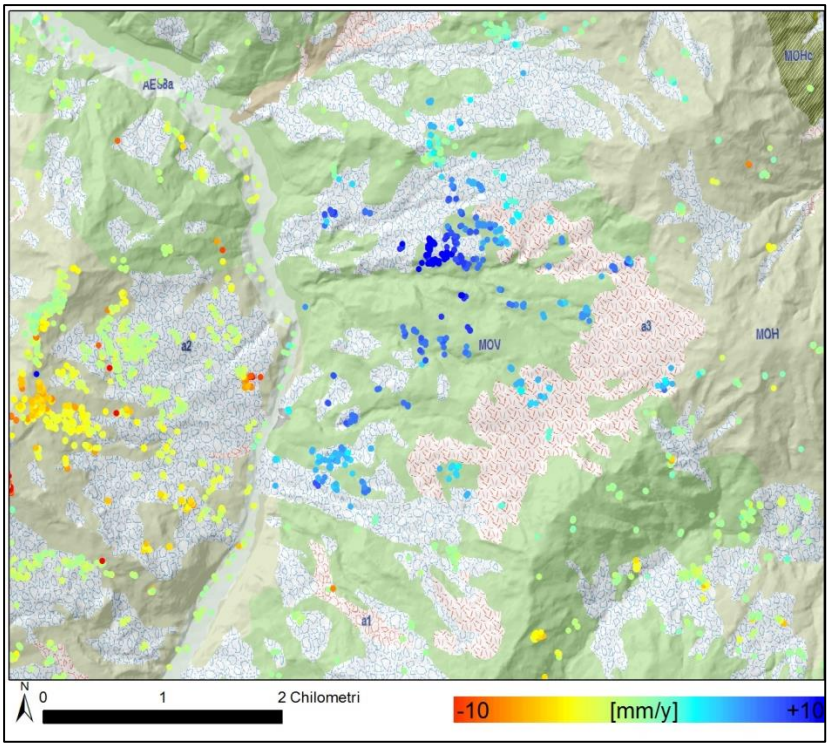

Figure 91. Average annual velocity of the measurement points in study area of Palagano (MO). RADARSAT-1 ascending dataset.

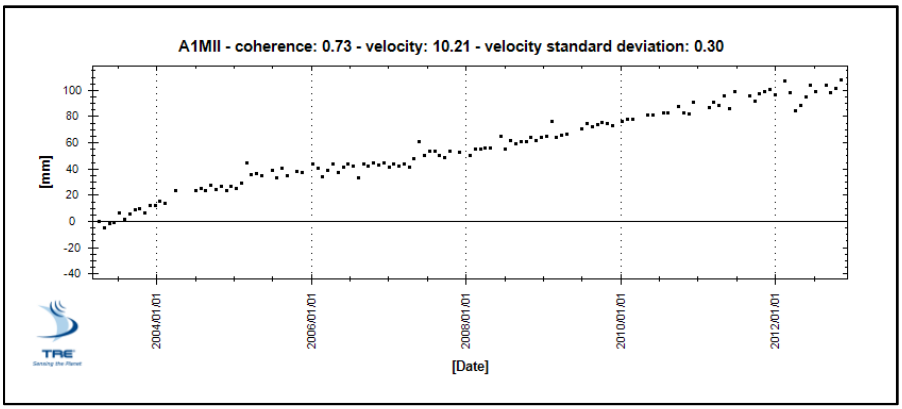

Figure 92. Time series of displacement of a measurement point located in the red circle in Figure 88. Line of sight ascending dataset.

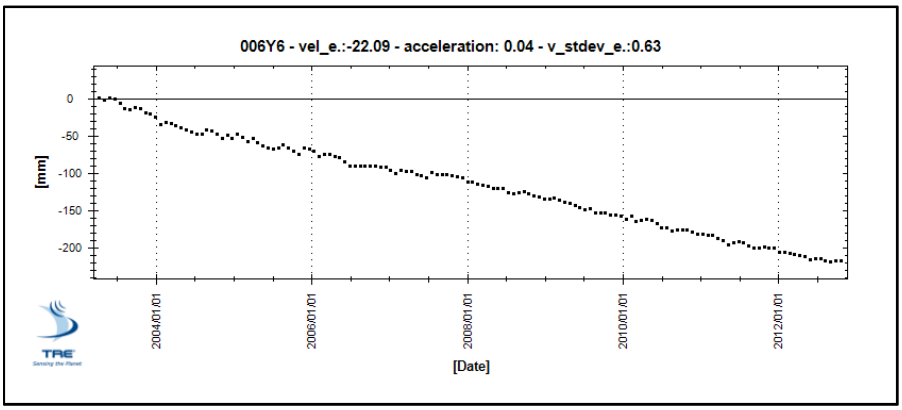

Figure 93. East-West displacement of the measurement point located in the red circle in Figure 88.

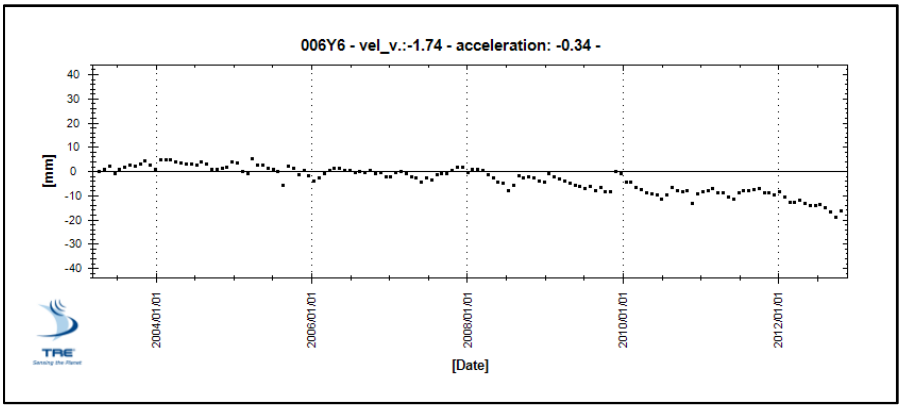

Figure 94. Vertical displacement of the measurement point located in the red circle in Figure 88.

It can be deducted from the combined observation of Figure 93 and Figure 94, that the horizontal component is sensitively higher than the vertical one. In order to study the type of movement over the whole study area, we calculated the direction of movement trough the angle "gamma" (°). Figure 95 shows the angle of moving direction of the measurement points that can be extrapolated to characterize the landslide. It should be noticed that the distribution is not optimal and Permanent Scatterers are found in particular in urban and outcrops areas. The deformation at Palagano, in general, is nearly horizontal and just very little amount of deformation is found in the vertical component. However, a small variation of gamma (and thus V_{EW} and V_{vert}) is detectable. In particular, relatively higher values of movement direction are found in the upper part of the landslide (East) while they tend to "zero" (and thus near horizontal) at the bottom of the slope (near Dragone Stream).

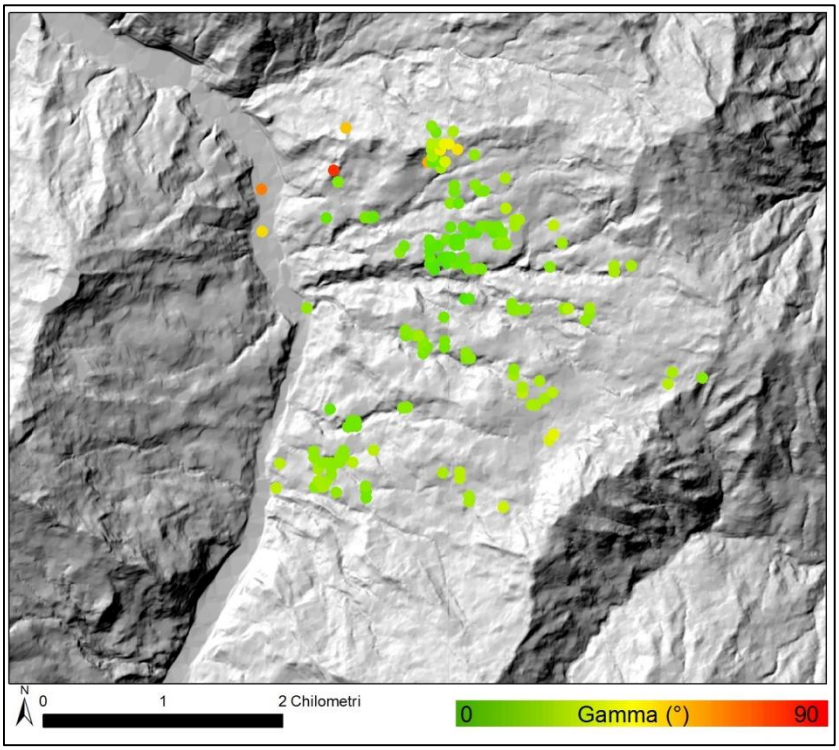

Figure 95. Angle of the movement direction (gamma) at the study area of Palagano (Mo).

To characterize the deformation of the study area in the time domain and detect if clusters of similar deformation pattern were recognizable, both the datasets (ascending and descending) were processed with PS-Time. The results of the time series types are shown in Figure 96 and Figure 97. All the measurement points within the study area resulted to be correlated, that means that a deformation is detected. However there is not a distinctive deformation type that characterize the area. In fact different deformation types (linear and bilinear) are classified within short distances (hundreds of meters). Also it has to be highlighted that different geometries has shown slightly different statistics of deformation types. In particular the ascending dataset show a higher number of bilinear compared to the descending, which has a higher number of linear. As mentioned in this work, the explanation is related to the high

sensitivity of PS-Time and the datasets that even if only slightly different, they can affect sensibly the results.

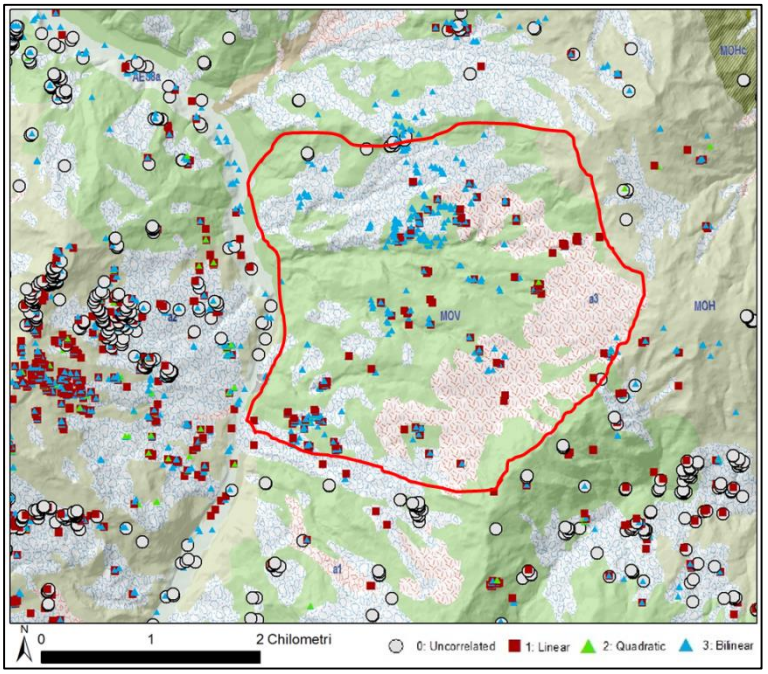

Figure 96. Time Series analysis carried out with PS-Time with the ascending dataset.

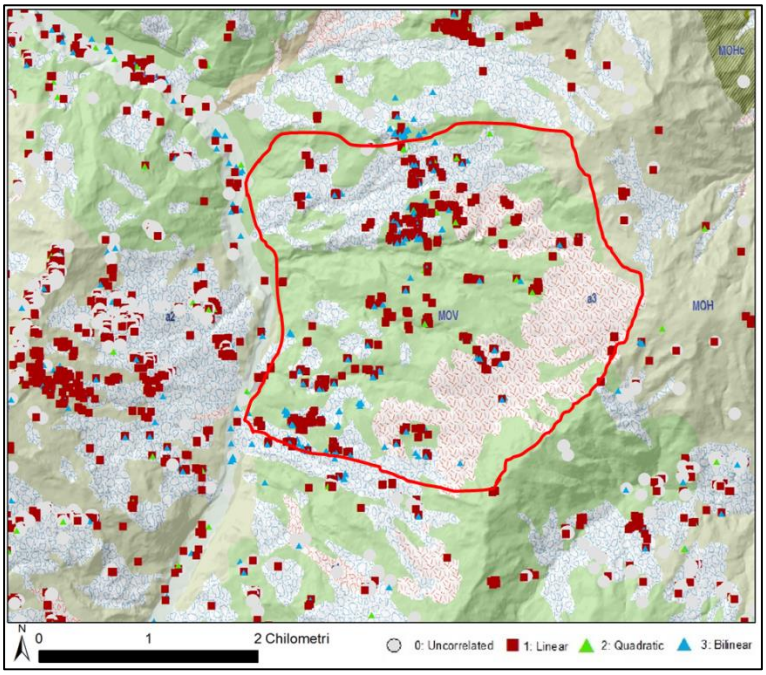

Figure 97. Time Series analysis carried out with PS-Time with the descending dataset.

The cumulated displacement was analysed along two sections, one along and one across the DSGSD (see Figure 88 for trace of sections). Along the sections we plotted the cumulated displacements that in satellite measured in the period of time from March 2003 to October 2012 (Figure 98). Each blue lines represented in the graph from upper image in Figure 98, indicates the cumulated displacement at a specific time. The total displacement at the end of the satellite acquisition (October 2012) is indicated with the red line. The topographic profile shown under the displacement graph, indicate the location where the deformation is happening. It is possible to note that the highest deformation is found in the area from the centre of the landslide to the SSW sector. Another area characterized by a higher deformation rate, is found near the NNE sector. Figure 99 shows the cross section analysis carried out on the same descending dataset, but along the landslide (near E-W direction).

While it can be noted that different portion have different magnitude of deformation, due to the relatively low density of measurement points, it was not possible to identify if sub-units based on different velocity.

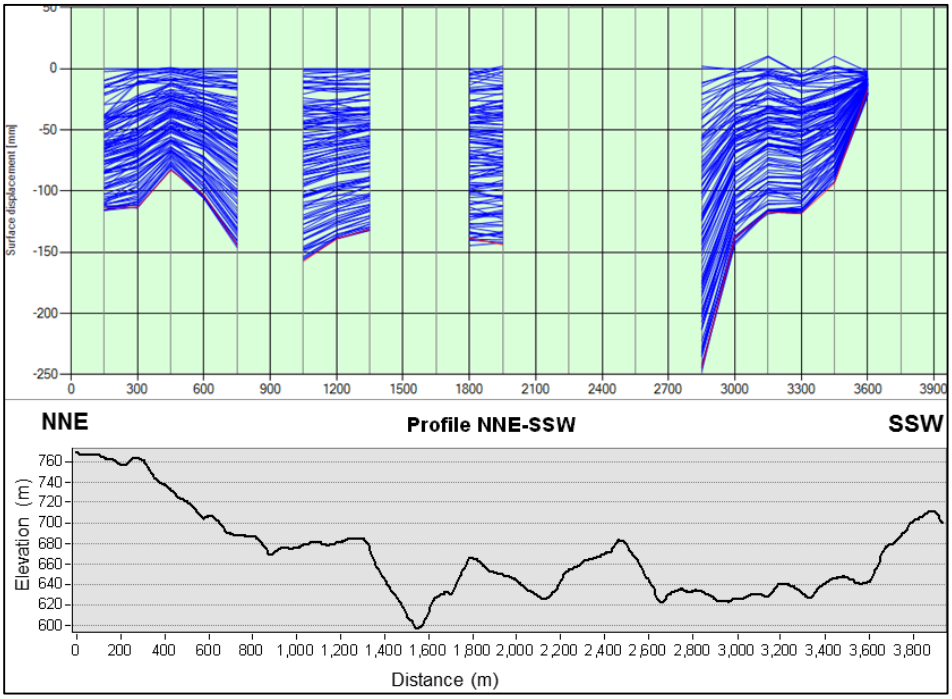

Figure 98. Cross section NNE-SSW. Up) cumulated deformation along the profile (Figure 88) from March 2003 to October 2012; down) topographic profile. Descending dataset.

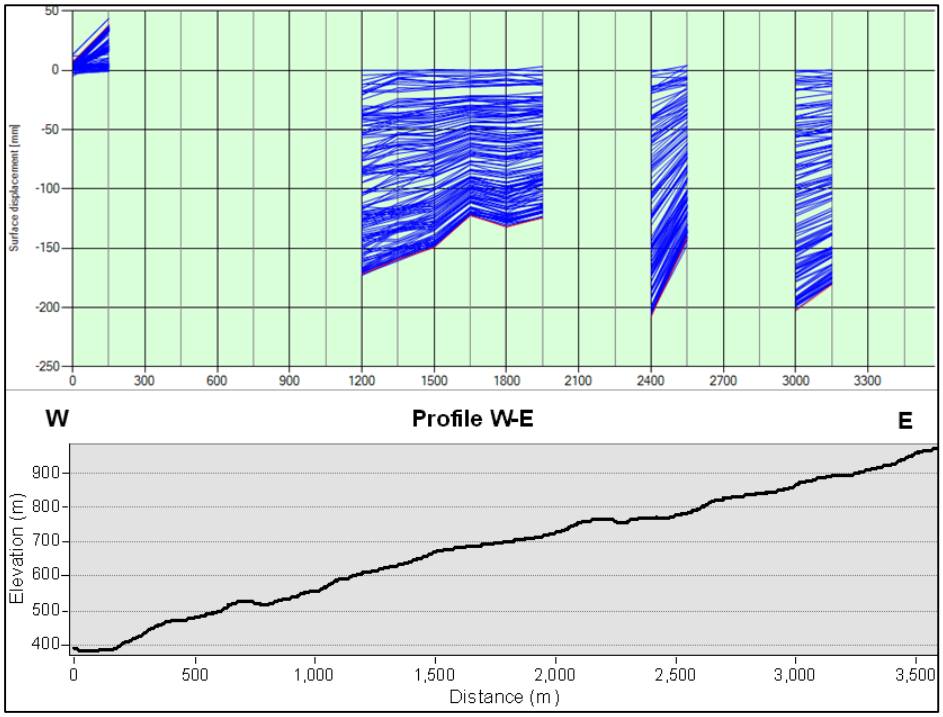

Figure 99. Cross section W-E. Up) cumulated deformation along the profile (Figure 88) from March 2003 to October 2012; down) topographic profile.

4.2.3.4.1.3 Discussion

The analysis has highlighted that an active DSGSD/rockslide affect the study area. The velocity reach the 25 mm/y and has a component mainly horizontal, suggesting a translational sliding. A portion with a slightly higher vertical component is found toward the upper part of the slope, indicating that a roto-translational dynamic could exists. However the lack of measurements in this area has limited the analysis. The time series analysis has proved that all measurement points area "correlated" thus are indices of an active deformation phenomena. However, even if there seems to not be a distinct deformation target over this area, the time series analysis isolated the "uncorrelated" measurement points. The cross sections showing the cumulated deformation, are shown that all the wide

area is moving and that 2 local area have a slightly higher deformation magnitude (Near NNE and near SSW). The profile E-W do not provide dense measurements but has proved to highlight that all the area is active and also suggest a higher deformation at the centre of the AOI.

4.2.3.4.2 Montecreto

4.2.3.4.2.1 Geological and Geomorphological. Settings

Montecreto is a small village located in the Apennines of the Modena province. The study area has a mean altitude of about 900 m.a.s.l. and extension of about 1 km^2. The slope dips toward west and is delimited at the bottom by the Scoltenna Stream, which is a tributary stream of the Panaro River.

In the study area, outcrop rocks from both the Umbro-Tuscan domain and Ligurian Domain. In particular, the "Monte Cervarola" Sandstones (CEV2) represents the main formation while in the Northeastern sector are found also claystones variegated with limestones (AVC) and the marls from the "Monte San Michele" formation (MSM). The geological map is shown in Figure 100. According to the landslide inventory, the slope where the village of Montecreto is covered by slope debris and the landslide inventory has no previous indication or awareness of active mass movements in that area. However, the local geomorphology suggest that the area might have been affected in the past by slope movements.

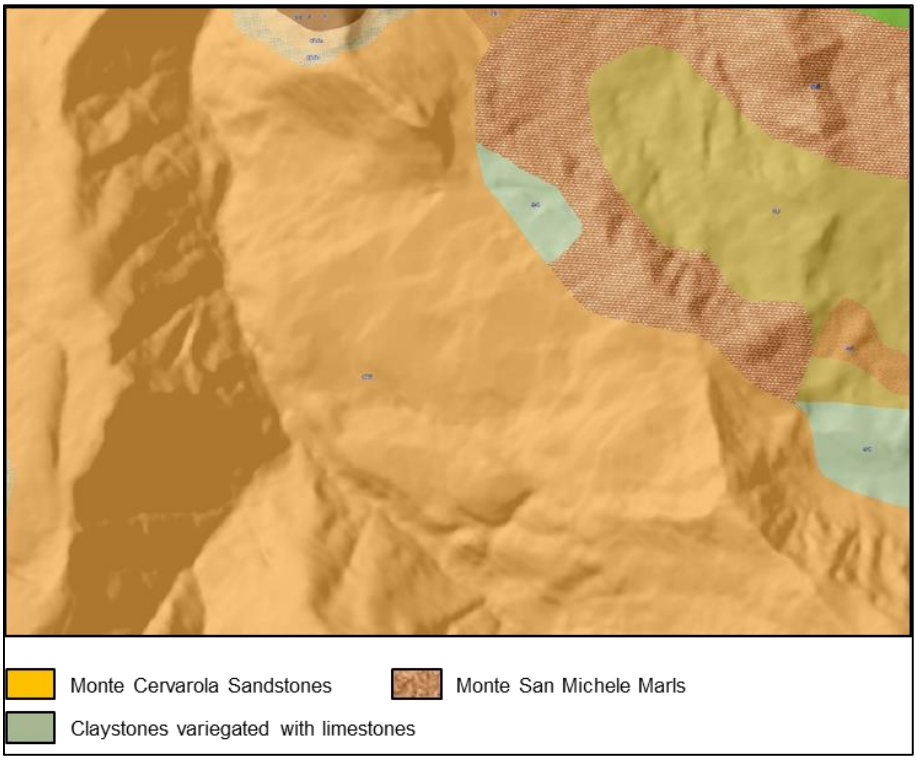

Figure 100. Geological map. Source: Web Map Service of the Emilia Romagna Geological Service.

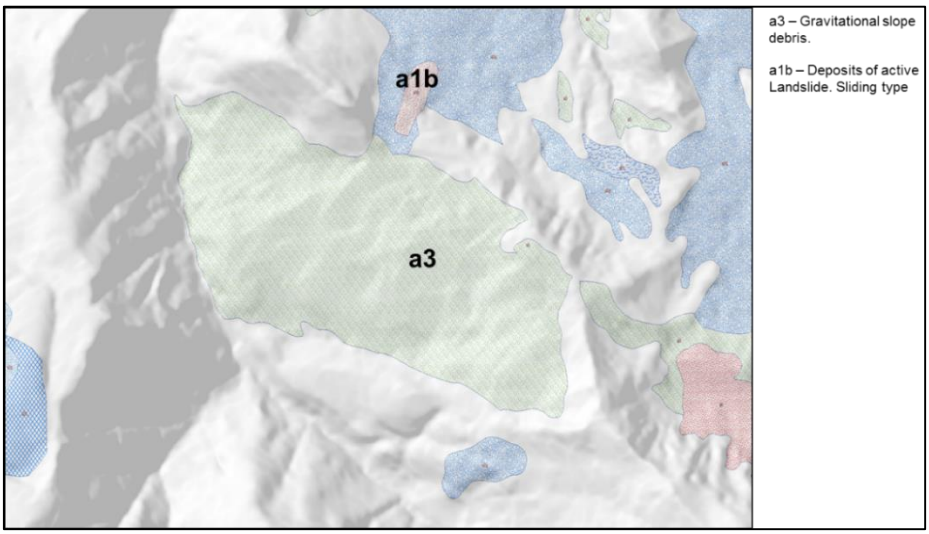

Figure 101. Geological map 1:10000. The landslide inventory is included.

4.2.3.4.2.2 Ground deformation pattern

The average annual velocity over the Montecreto study area is shown in Figure 102 and Figure 103. Mean annual velocity is mild but in both the geometries, there is an evident pattern of higher velocity deformation from the surrounding areas. In order to further investigate the deformation in that specific area, were carried out average time series of all measurement points in the area that shows evidence of activity (Figure 102 and Figure 103). The average time series were evaluated by averaging per each date, all the displacement in the study area. It is important to highlight that this type analysis has to be carried out carefully and only after a check of time series within the study area. In fact, if different deformation trend affect the study area, the average will result in a smoothing effect and the information might be lost. In the other hand, the average time series can be a very useful tool in areas with a distinctive deformation trend. Furthermore, they reduce noise affect and represent a general deformation trend of the study area. Figure 102(up) shows the average time series computed for the ascending dataset. It is interesting to note that the deformation is not linear. After a period of activity from 2003 to 2004, the displacement are almost stabilized for about 4 years. A reactivation of the slope movement is measured at the beginning of 2009. According to the time series, it is possible that a phase of stabilization is reached again at the beginning of 2012.

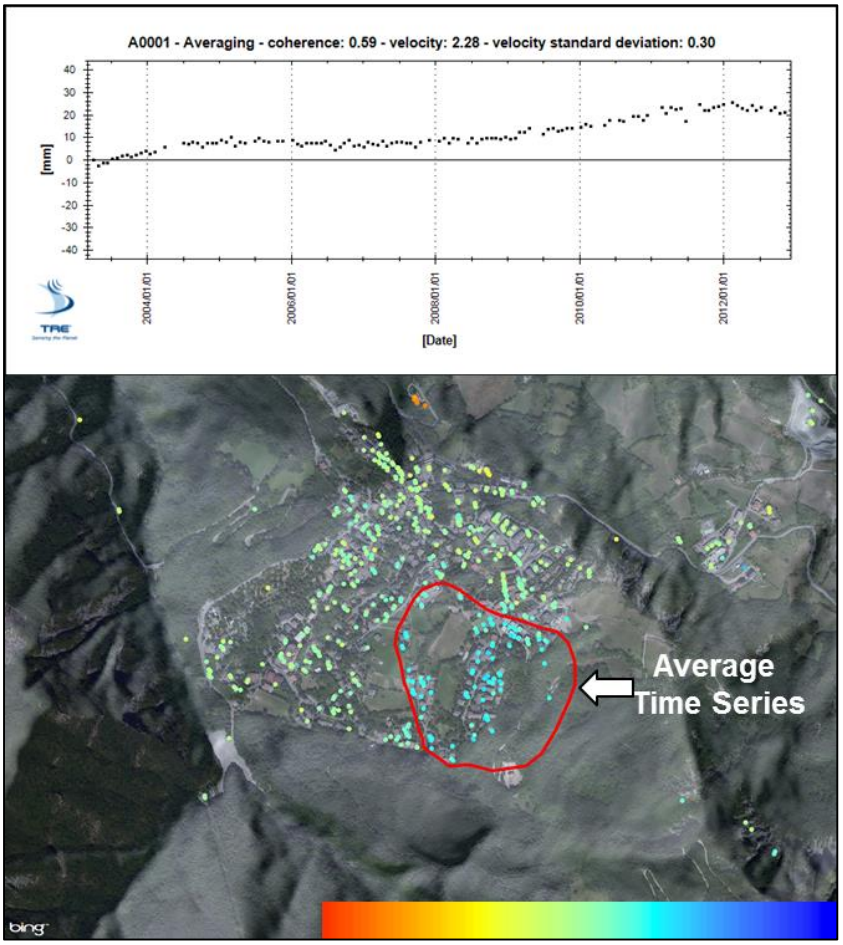

Figure 102. Average annual velocity of the ascending dataset. The red polygon highlights the AOI where was computed an ``average time series`` of displacements (top of the image)

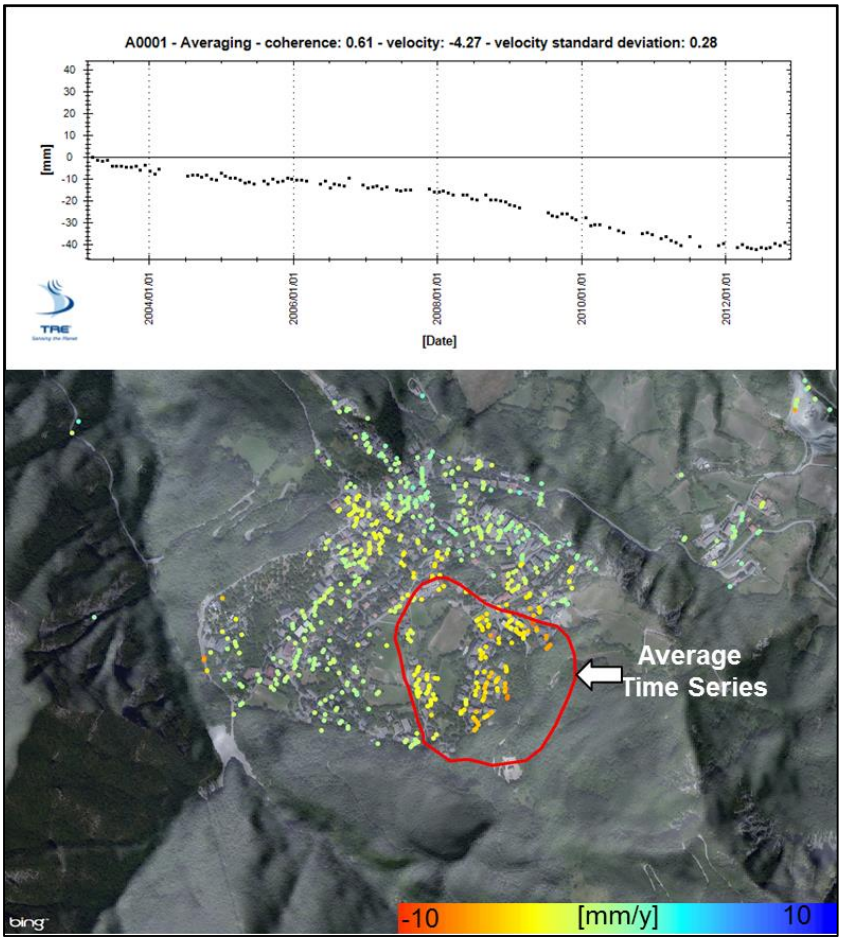

Figure 103. Average annual velocty of the descending dataset. The red poligon highlight the AOI where was computed an ``average time series`` of displacements (top of the image).

Evidences of deformation are highlighted also from the descending orbit (Figure 103). As expected the sign of the deformation is inverted with respect to the ascending geometry (movements are toward West and thus away from the satellite in descending geometry). It is interesting to note that the descending average time series (carried out over the same study area) shows a very similar deformation pattern (Figure 103). In fact, a first stage of activity is followed by a deceleration phase and again by an

acceleration between 2008 and 2009. Around 2012, the study area of Montecreto, experienced a second stabilization phase. These results encourage using MT-InSAR not only for detection but also for accurate landslide monitoring. It has to be highlighted that the results reached in this study, have been achieved with 24 days repeat satellite. A higher frequency of acquisition (i.e. 4 days) will allow to measure even higher frequency variation in deformation trend.

Figure 102 and Figure 103 shows that the same non-linear deformation is measured from both satellite geometries, confirming the different stages of activity. Any doubt that could be raised interpreting non-linear deformation from one single geometry is abolished when both geometries indicate the same deformation trend.

An automated time series classification of the ascending and descending datasets was carried out with PS-Time. The results shown in Figure 104 and Figure 105 prove that in the study area a “correlated” and in particular a “non-linear deformation exists.

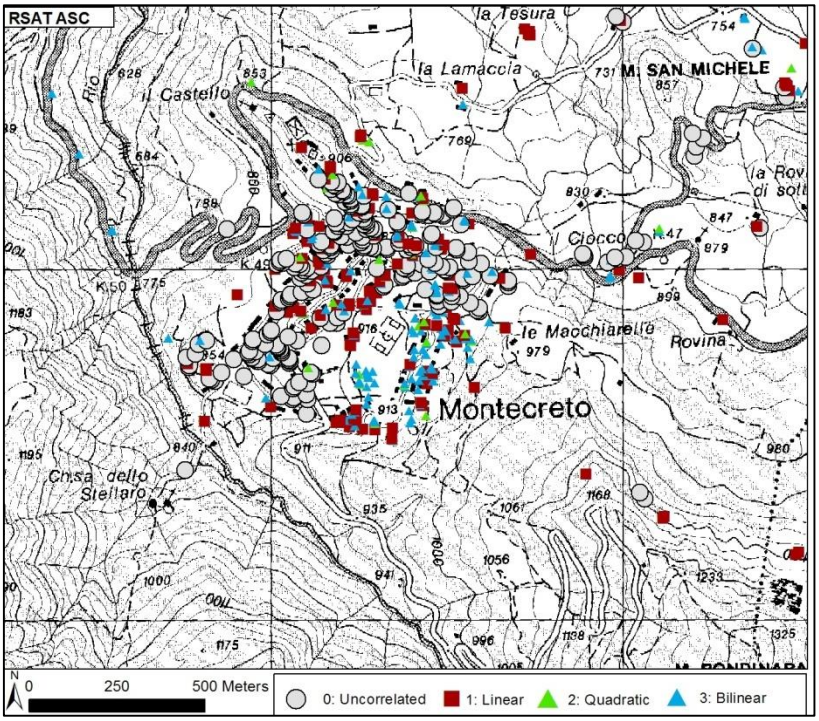

Figure 104. Time series analysis of the RADARSAT-1 ascending dataset.

In fact, measurement points classified as “bilinear” are clusterized at the same location where the average time series was computed, highlighting a non-linear deformation. It has to be highlighted that while the deformation time series over Montecreto will be better assessed by 4 segments, PS-Time only allows the discretisation of the time series in 2 segments. As a consequence, only major stages of deformation will be accounted in the result.

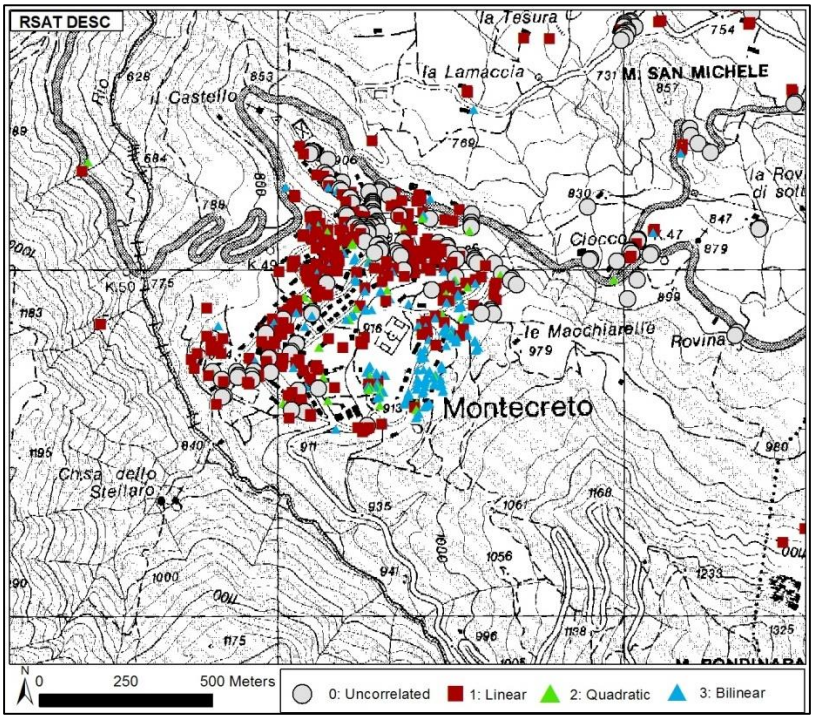

Figure 105.Time series analysis of the RADARSAT-1 descending dataset.

In order to characterized the dynamics of the slope movement affecting the study area, The velocity components have been calculated. The East-West component is predominant while the vertical component is almost negligible. These results can be summarized by the angle of movement direction expressed by "gamma" (Figure 106). In fact, over the active area, the gamma angle shows values around 10° indicating a movement mainly translational. Velocity components values are about -7 mm/y in the East-West component and around -1 mm/y in the vertical component.

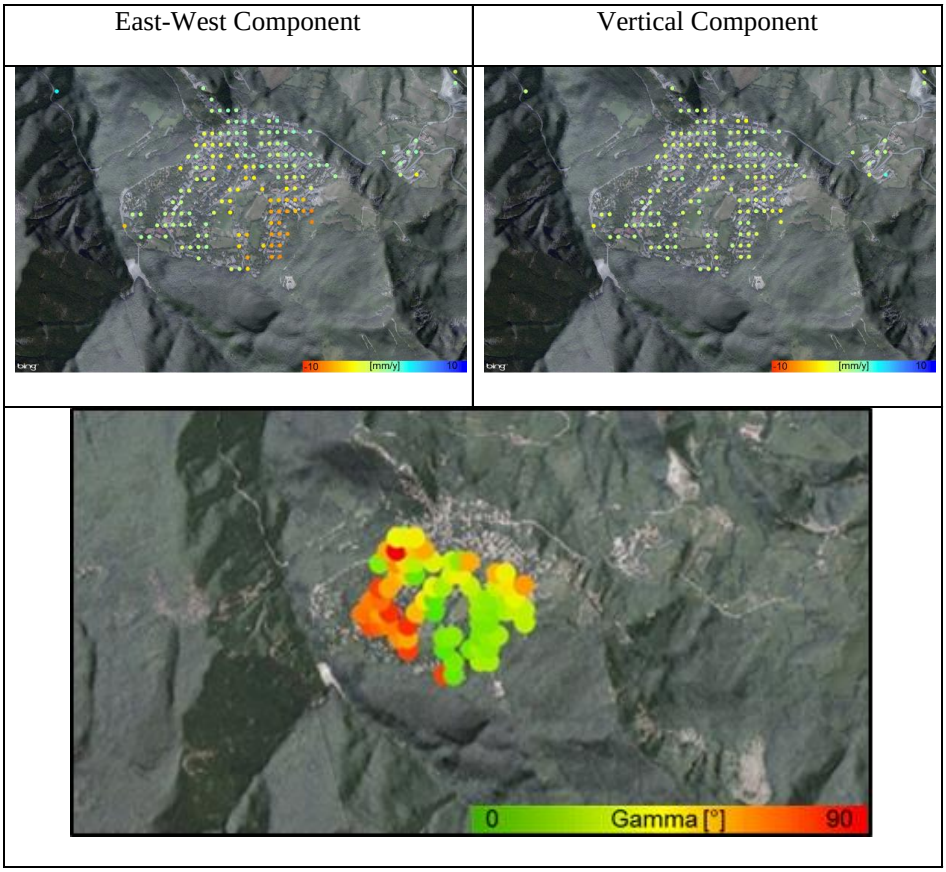

Figure 106. Velocity components and movement dynamics. The upper right image shows the East-West component of the displacement velocity while the upper left shows the vertical component (color scale ±10 mm/y); Bottom) By merging both the components, can be evaluated the angle of movement direction (gamma). Green indicate movement near horizontal while red indicate movement near vertical.

4.2.3.4.2.3 Discussion

The post-processing analysis of SqueeSAR™ data has provided additional information useful to characterize the deformation in space and time domain. The time series analysis carried out with PS-Time has shown that a non-linear deformation is active over the area of Montecreto. Since the same cluster of non-linear deformation is found in both ascending and descending geometries, it is possible to conclude that the signal measured from the satellite it is related to a ground deformation. In the area where PS-Time has highlighted clusters of non-linear deformation, has been computed an average time series of displacement. The average time series, which has been computed for both satellite geometries, has allowed to identify a distinctive temporal deformation trend and has reduced the noise associated with the measurements. Both the trends have shown that over the Montecreto area, the deformation had multiple stages. In particular from 2003 to 2012 have been measured 4 stages, characterized by a deceleration in 2004, an acceleration around 2008and again a stabilization at the beginning of 2012. On a recent work, Berti et al., (2013) have applied PS-Time over the same study area. In particular the authors analysed a dataset characterised by a lower quality (lower number of images, less frequent images acquisition, first generation algorithm). They found that PS-Time highlighted a cluster of bilinear measurement points over the study area. However, in that specific case was found that the reference point was located in a subsiding area, and all the dataset was affected by a drift in velocity. The authors also carried out a similar analysis but after the correction the drift in velocity from all the time series. The results turned the measurement points over Montecreto into the “uncorrelated”

class since the linear regression for the time series was not statistically significant (Figure 107).

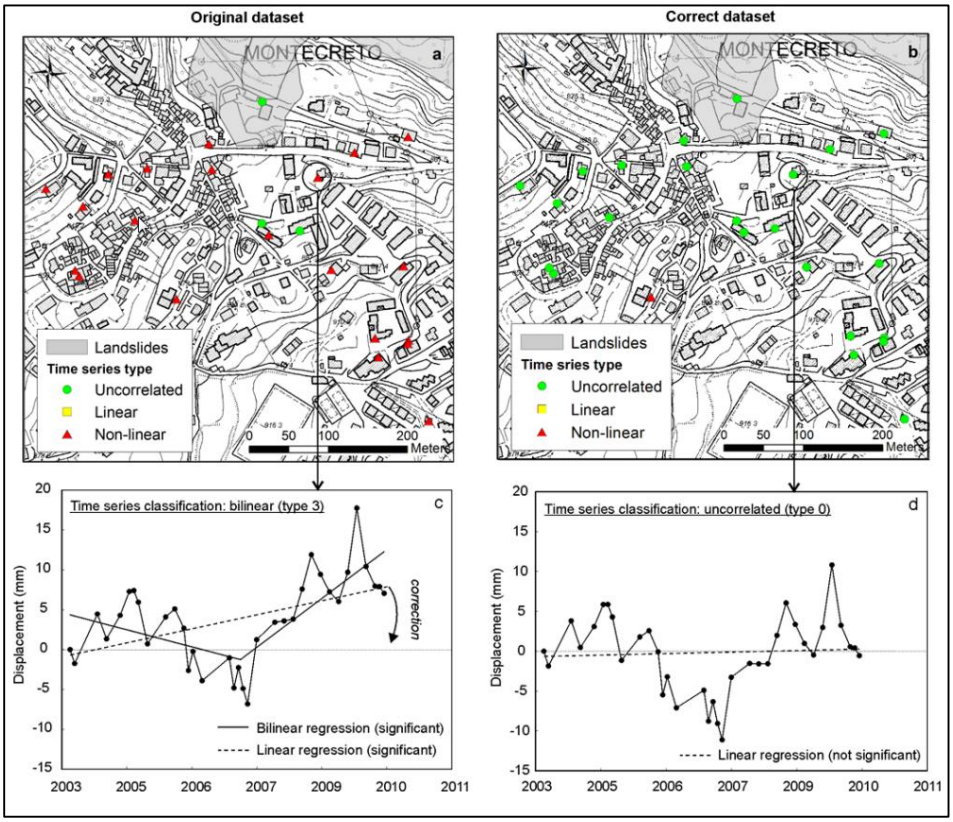

Figure 107. Comparison of time series classification in the area of Montecreto (Modena province, northern Apennines of Italy) obtained by the original and corrected dataset (ENVISAT descending, from PST-A). After Berti et al., (2013).

As visible from Figure 107, a breakpoint within the time series is visible, but due to the dataset quality, was not possible for the authors define if a deformation was affecting the area of Montecreto or if the breakpoints were related to some noise effects. Thanks to the analysis carried out with RADARSAT-1 was possible to confirm the presence of an active non-linear deformation.

The computation of the velocity components has allowed to define the kinematics of the deformation. Among all the measurement points over

the study area, the modulus of the East-West velocity component is predominant (~7 mm/y) while the vertical component is negligible (~1 mm/y). In order to better understand these results, was evaluated the angle of movement direction. As a results the movement is near horizontal (~10°). It has to be noted that the area surrounding the active deformation zone, clusters of measurement points indicating a vertical movement are found (gamma=~90°). These values are not in reality representing a vertical deformation because are the results of a trigonometric calculation of velocity values close to 0 mm/year (Figure 106). It is recommended to analyse the angle of deformation only for measurement points where a significant deformation can be detected. In fact, PS-Time classify these measurement points as "uncorrelated" indicating that they do not represent any deformation.

The kinematic analysis can be carried out only where enough coverage of measurement exists. Unfortunately in the upper part of the slope studied there are no data, because of the land cover is predominantly vegetated.

5 Application to man-induced subsidence.

5.1 Introduction & State of Art

Underground excavation can induce significant subsidence at surface topography interacting with the environment and man-made strucures and infrastructures. However different undergroud excavation types can have different subsidence dynamics, in particular in term of magnitude and timing of the subsidence. A particular case is represented by the longwall coal mining technique. It is well known that longwall mining generates fractures into the overburden inducing severe subsidence and potential damages (Can et al., 2011, Deck et al., 2003; Duzgun, 2005; Kratzsch, 1983; Perski and Jura, 2003; Saeidi et al., 2009). Subsidence can interact with man-mad features such as buildings and infrastructures and utilities, but as a consequence of fracturing, also natural features can be affected, such as drainage systems and underground water resources (Can et al., 2012, Altun et al., 2010; Li et al., 2010). Specifically, drainage system within the area of influence, can expereince water infilatration due to the increased vertical permeability. In the other hand, when subsidence happens in urban areas, building and infrastructures can be affected and damaged if located in the "area if influence" wich is generated from the excavation. The "area of influence", also known as "application area" (NSWDMR, 2003), define the interaction betweeen features and subsidence, and represent the surface that is likely to be affected by the underground mining. The Angle of Draw (AoD), which identifies the "area of influence", is still the standard way to estimate subsidence impacts (Seedsman 2004). Holla & Barclay (2000) proposed

an empirical relation between the AoD and the "width to depth ratio", showing a large variability (~2° to ~60°) even within a single coal-field and average value of 29°. Nevertheless, a precautionary value of 35° has also been suggested for Southern Coalfields (Holla & Barclay 2000, NSWDMR 2003). More in general, for NSW Coalfields, when local data are not available, a cut-off-point is taken as a point on the surface defined by an angle of draw of 26.5 degrees from the edge of the extraction (MSEC, 2007). However underground excavations induce both vertical and horizontal displacement that can extend from several hundreds to thousand meters from the mine layout. This type of deformation (mainly horizontal and at measurable over long distance) is known in literature as "far-field deformations". Krogh (2007) observed in NSW Coalfields, horizontal displacements extending over 1 km away from the mine workings, and in extreme cases up to 3 km. Therefore the AoD's evaluation is still questionable due to its large variability dependents from geological settings, and to the fact that the subsidence is asymptotic. To this regard, often the standard cut off point of 20 mm of displacement is used, while other authors define the AoD based on precision of the surveying equipment, rather than a threshold of displacement. It is evident that the AoD's variability directly affects the outline of "influence area" and its estimation should be based on accurate monitoring data. To this regardr, InSAR has been formerly used to monitor subsidence induced by underground mining (Carnec et al., 2000; Wegmuller et al., 2000; Strozzi et al., 2001; Herrera et al., 2007; Ng et al., 2009; Perski et al., 2009).

While typically longwall mine layout are located outside from cities, tunnel excavation are often carried out in urban areas or in presence of buildings in the area of influence. As a consequence, even a minor

deformation, can create large economic losses. In these contexts, very precise monitoring systems are required to determine the surface area affected by displacement and the rates of movement.

5.2 Long-Wall mining induced Subsidence

5.2.1 Objectives and General Settings

In longwall mining, usually several panels of coal are extracted in progression (multiple longwall mining) and after one panel is mined out, the next panel start to be excavated. A series of pillar are left in place between adjacent panels, in order to reduce the collapse in the mine and thus the related surface subsidence (Figure 108).

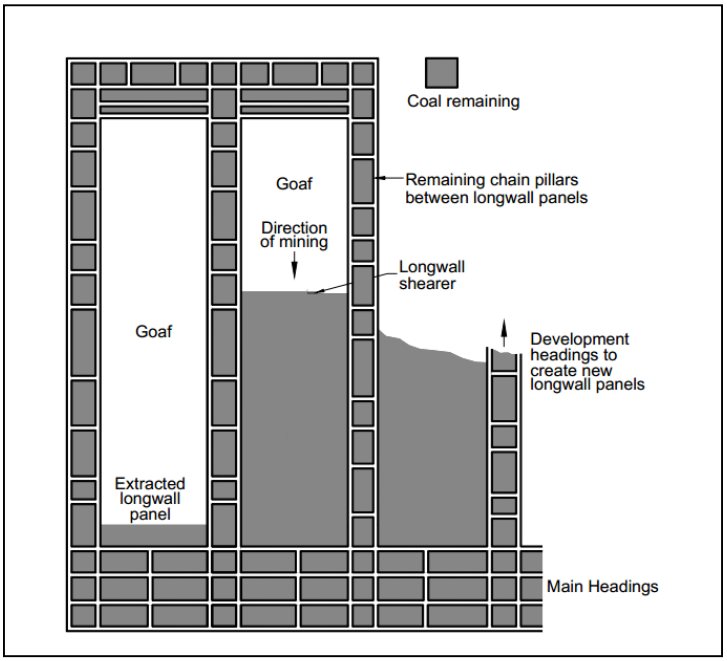

Figure 108. Layout of a typical multiple longwall mining (after MSEC, 2007).

In general coal panels are more than 1000 m long and about 200 m wide. The thicknes and the depth of the panels, depend from the local geology and the position of the coal layer in the stratigraphy. During the excavation, hydraulic supports are installed backward to the shearer to avoid the collpase of the roof during the excavation. However, when the shearer advance according to the excavation plan, the hydralic supports are are also moved toghether. As a consequence, in the area were the support are removed, the roof will be free to collapse within the goaf, inducing sudden fracture within the overburden that leads in a surface deformation that extent above the over the "area of influence". In other words, the outline of the "area of influence" define the limit of zero subsidence and thus separate the stable area from the subsiding area (Figure 109).

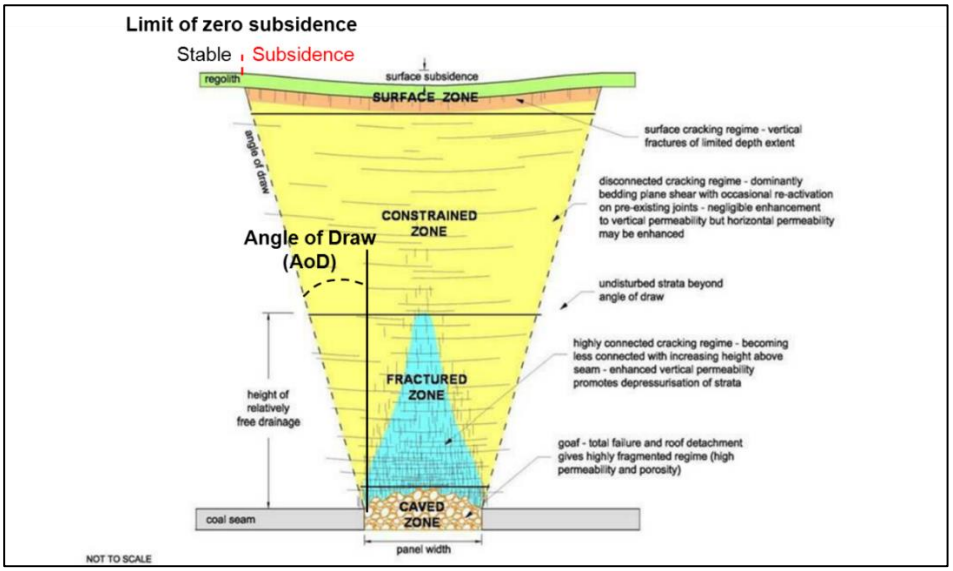

Figure 109. Conceptual Model of caving and the nature of fracturing, and the related area of influence in surface affected by subsidence (modified after NSWDP, 2008).

The relation between the area of zero subsidence and the excavated longwall panel are explained by the angle of draw (AoD) and are visible in Figure 109. In these contexts bothe deformation are expected, vertical and horizontal. In particular the vertical component reach the maximum value at the centre of the subsidence bowl and tend to zero moving toward the limit of zero subsidence. The horizontal component is zero at the centre of the bowl and maximum at a point located between the centre and the border of zero subsidence, known as “tilt”. However the dynamics of the subsidence bowl are more complex in case of multiple longwall panels extraction.

The objectives of this study were:

1. characterize the response of the topographic surface to multiple longwall extraction per every year monitored
2. Study time-dependant deformation at any point in surface.

3. Evaluate with InSAR, the value of angle of draw that account for the far-field deformation
4. Validate the value of angle of draw with numerical modeling
5. Compare the results of tne numerical modeling using the InSAR based angle of drwa, (AoD_{InSAR}) with the tipically value used in literature ($AoD_{literature}$)
6. Determine where InSAR can be used as source of data for subsidence modeling calibration. 7

The calibration of numerical model with InSAR can be very valuable, since miners typically use numerical modes to carry out subsidence prediction and risk analysis (Lloyd et al. 1997, Luo et Cheng 2009, Keilich 2006, NG et al. 2010).

The test site is the Metropolitan Mine, an underground coal mine located in the Southern Coalfields of New South Wales (Australia), about 40 km South of Sydney and operating since 1988.

Figure 110. Geographic location of the Metropolitan Mine (NSW).

At present, about 3 meters thick of coal are mined out from the Bulli Seam (DeBono et Tarrant, 2011) using the longwall procedure. The Bulli

Seam is stratigraphically the top seam in the Illawarra Coal Measures (Hutton, 2009), and is overlain by the Narrabeen Group (late Permian late Triassic) consisting of about 300 m of sandstones, claystones and shales. The Middle Triassic quartz sandstone and Hawkesbury Sandstone are the upper formation extending over most of the area (Figure 111).

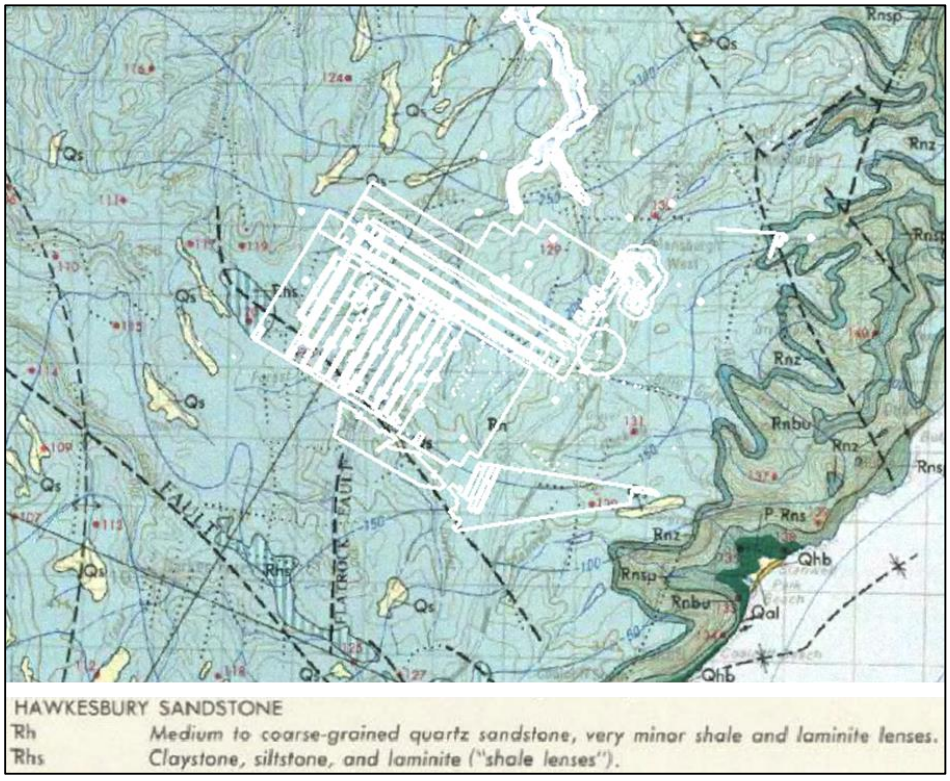

Figure 111. Geological map 1:100000 of the study area. The Metropolitan mine layout is indicated with white lines.

The depth of the cover at the Bulli Seam varies from 400 m to 520 m depending on the local surface topography (DeBono et Tarrant 2011). The stratigraphic profile is shown in Figure 112.

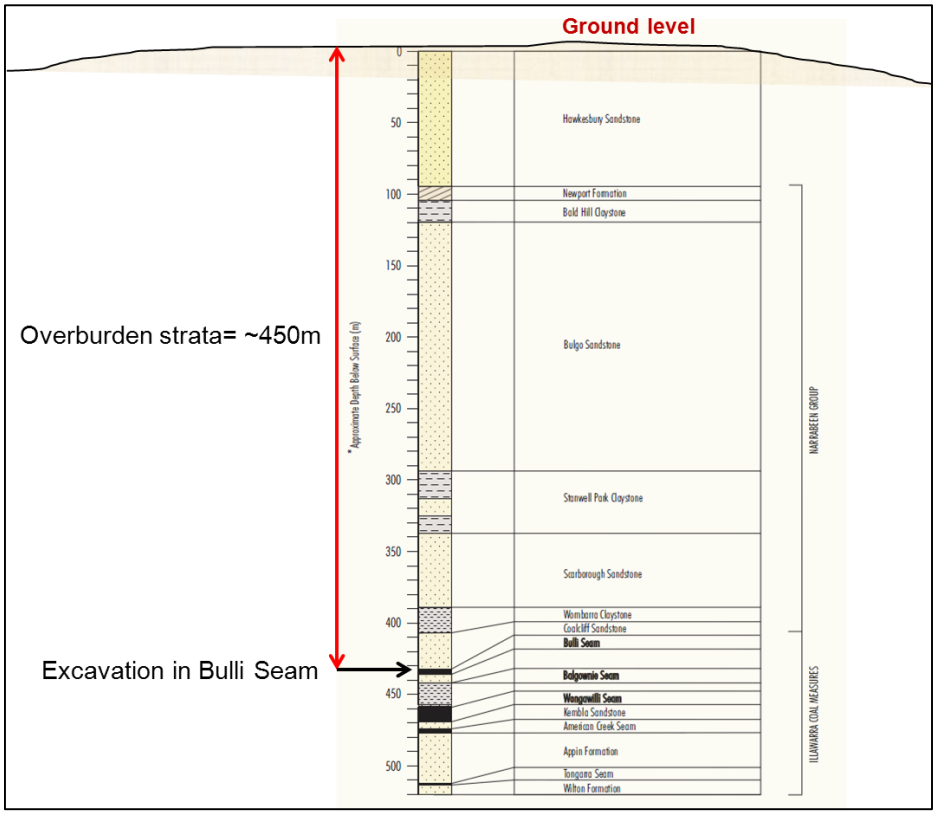

Figure 112. Stratigraphic profile at Metropolitan Mine. The actual working seam is indicated (Bulli Seam), with about 450 meters of overburden, made of predominantly sandstones.

The excavation of the mine layout presented in this study, started in July 1995 with the extraction of the longwall 1 (Figure 113) and finished in April 2010 with the extraction of the longwall 18 (DeBono et Tarrant, 2011, Morgan et al., 2013). Accordingly, the longwall mining progression is from South East to North West. On the other hand, the extraction direction of each single longwall is from South West to North East (DeBono et Tarrant, 2011).

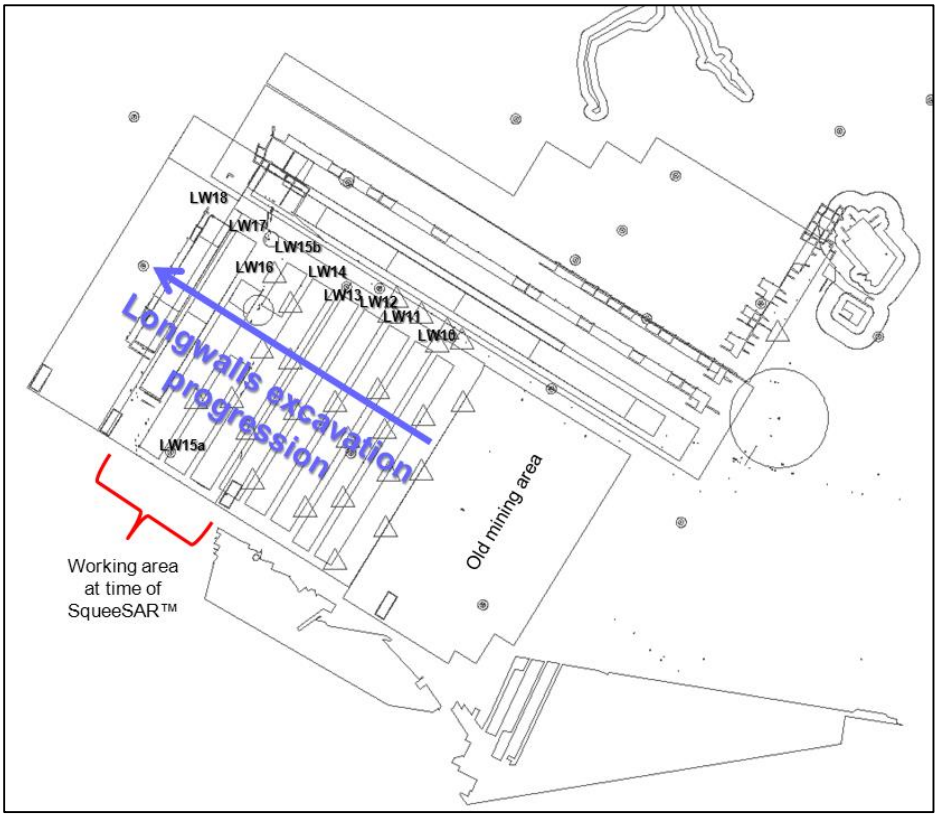

Figure 113. Mine layout at Metropolitan Mine. Longwalls are enumerate progressively according to the extraction sequence. The longwalls extracted during the ERS satellite monitoring are highlighted.

5.2.2 Datasets & Methods

Post-processing routines of MT-InSAR data have been applied to a longwall mine located in New South Wales (Australia) in order to define the evolution of the subsidence bowl.

However MT-InSAR can have some limitation in longwall mining monitoring, because of the very high and sudden deformation expected at the centre of the subsidence bowl (order of meters). As a general rule, it is known that MT-InSAR can only monitor deformation that are of the order of fractions of the RADAR wavelength (max = $\frac{\lambda}{2}$), even if with

recent algorithms, thanks to a high spatial coverage of measurement points, thus threeshold can be widely exceded. However, in order to overcome this problem, the standard DInSAR was used to characterize the centre of the subsidence bowl, while the MT-InSAR was used to characterize the area of zero subsidence, thanks to the very high precision of this technique.

The validation of the AoD_{InSAR} was carried out with "Surface Deformation Prediction System" (SDPS 6.1g) (Agioutantis and Karmis, 2013) a numerical model developed for longwall mine operation. The SDPS software was chosen since it has tested extensively and has given excellent correlation between predicted and actual measured subsidence, for a number of case studies (VPI&SU, 1987; Karmis et al., 1989; Newman et al., 2001, Karmis et Agioutantis 2004). Finally, the predicted and the observed "area of influence" have been compared. The time series analysis was carried out with PST-Time to identify over the study area, the zones affected by the typical deformation belonging to different phase in longwall mine operations (Figure 136).

Two stacks of ENVISAT radar imagery were used for the SqueeSAR™ analysis. The two data sets consisted of 44 images acquired along an ascending orbit and 43 images acquired on a descending orbit. Both data sets were acquired on a 35-day repeat interval and cover the time period from June 2006 to September 2010, corresponding to the extraction time of longwall 13 to longwall 18 (Figure 113). A DInSAR processing was also carried out bt T.R.E. in order to extract single interferograms. SAR image pairs for the DiNSAR analysis have been selected minimizing the nornmal baseline (B_n) and the temporal baseline (B_t), in order to reduce decorrelation effects (Table 8).

Table 8. Single interferograms processed. Bt= Temporal baseline; Bn=Normal baseline.

INTERFEROGRAM	Usability	MONTHS OF THE SLAVE ACQUISITION
20061001_20061105_Bn-45_Bt-35	Very_poor	Nov-06
20061210_20070218_Bn-199_Bt-70	Very_poor	Feb-07
20061210_20070603_Bn-183_Bt-175	Poor	Jun-07
20070429_20070603_Bn+159_Bt-35	Medium	Jun-07
20070429_20070708_Bn+38_Bt-70	Medium	Jul-07
20070603_20070708_Bn-121_Bt-35	Medium	Jul-07
20071021_20071230_Bn-156_Bt-70	Poor	Jul-07
20071021_20071125_Bn+230_Bt-35	Very_poor	Nov-07
20070708_20070812_Bn-31_Bt-35	Poor	Dec-07
20080413_20080622_Bn-70_Bt-70	Very_poor	Jun-08
20080622_20080831_Bn-77_Bt-70	Medium	Aug-08
20080622_20080831_Bn-77_Bt-70	Medium	Aug-08
20090222_20090503_Bn-102_Bt-70	Very_poor	May-09
20090503_20090712_Bn+64_Bt-70	Medium	Jul-09
20090607_20090712_Bn-228_Bt-35	Medium	Jul-09
20090503_20090816_Bn+58_Bt-105	Medium	Aug-09
20100103_20100207_Bn+406_Bt-35	Very_poor	Feb-10
20100314_20100523_Bn+82_Bt-70	Medium	May-10
20100418_20100523_Bn-199_Bt-35	Very_poor	May-10
20100523_20100627_Bn+22_Bt-35	Good	Jun-10
20100627_20100905_Bn-23_Bt-70	Poor	Sep-10
20100801_20100905_Bn+278_Bt-35	Very_poor	Sep-10

5.2.3 Ground deformation pattern

SqueeSAR™ data approach resulted in measurement point densities of 191 and 135 points per square kilometre for the ascending and descending data sets, respectively. A large area of subsidence was observed directly over the areas of active operations at the Metropolitan mine, with displacement rates up to -34 mm/year detected along the satellite LOS. Figure 114 shows movement saturated at ±10 mm/year to adequately represent and characterize the subsidence feature.

While the spatial coverage of measurement points was good throughout most of the Area of Interest (AOI), there is a gap in the results within the centre of the subsidence feature. This is due to the high subsidence rate experienced in the area over the longwall mined at the time of the SAR image acquisition. With these types of deformation (sudden and non-linear), MT-InSAR techniques fails and do not provide measurement points, because of the coherence loss over time. Figure 114c and Figure 114d shows the vertical and East-West velocity components respectively. The East-West component shows that positive values (blue) are found on the western sector of the mine layout while negative values (red) are found on the central/e

astern sector of the mine layout. This is a typical deformation pattern indicating the presence of an horizontal component toward the centre of a subsidence cone.

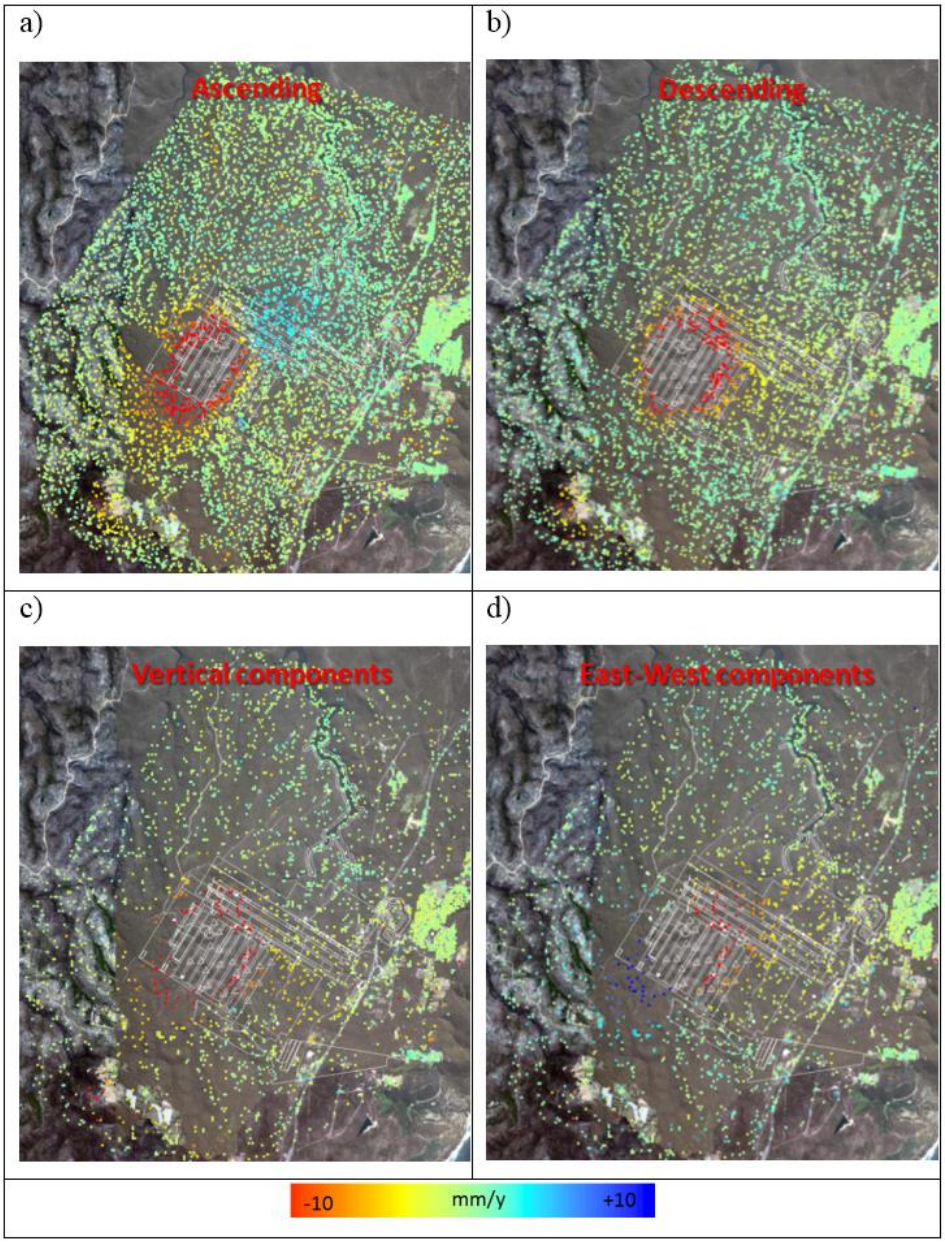

Figure 114. Average annual velocity of deformation for a) the ascending dataset; b) the descending dataset; c) the vertical component of the velocity; d) East-West component of the velocity.

5.2.3.1 Characterization of the subsidence bowl

As anticipated, in multiple longwall mining, the subsidence can be thought as a bowl that dynamically moves over the study area with time. In order to characterize these dynamics, it is preferable to analyse the cumulated displacement due to the fact that no linear regression are fitted to the time series to evaluate average velocity. This approach is recommended when analysing non-linear deformation. By displaying the cumulated displacement at different dates (every year) it has been possible, by visual radar interpretation, to draw a line dividing the stable areas from the deformed areas, in the western sector of the mine layout. This direction correspond to the mining progression (Figure 116). By setting an arbitrary reference point perpendicular the limits of zero subsidence, it is possible to evaluate the velocity of the subsidence bowl, that form a sort of waves moving over the study area. The reference point for the distance measurements, has been located on the border of the old mine layout (Figure 116). Since the dates for every "limit of zero subsidence" are known (from MT-InSAR time series), it has been possible to estimate a velocity of the moving subsidence bowl, which is about 300 m/y. Figure 115 show the propagation in time of the area of zero subsidence defined by means of radar interpretation of MT-InSAR.

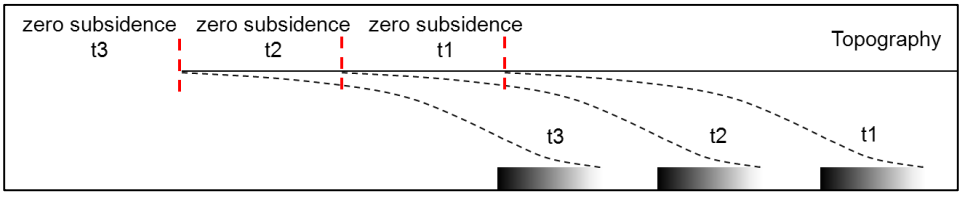

Figure 115. Scheme of the identification of the limit of sero subsidence, per every year, using MT-InSAR techniques.

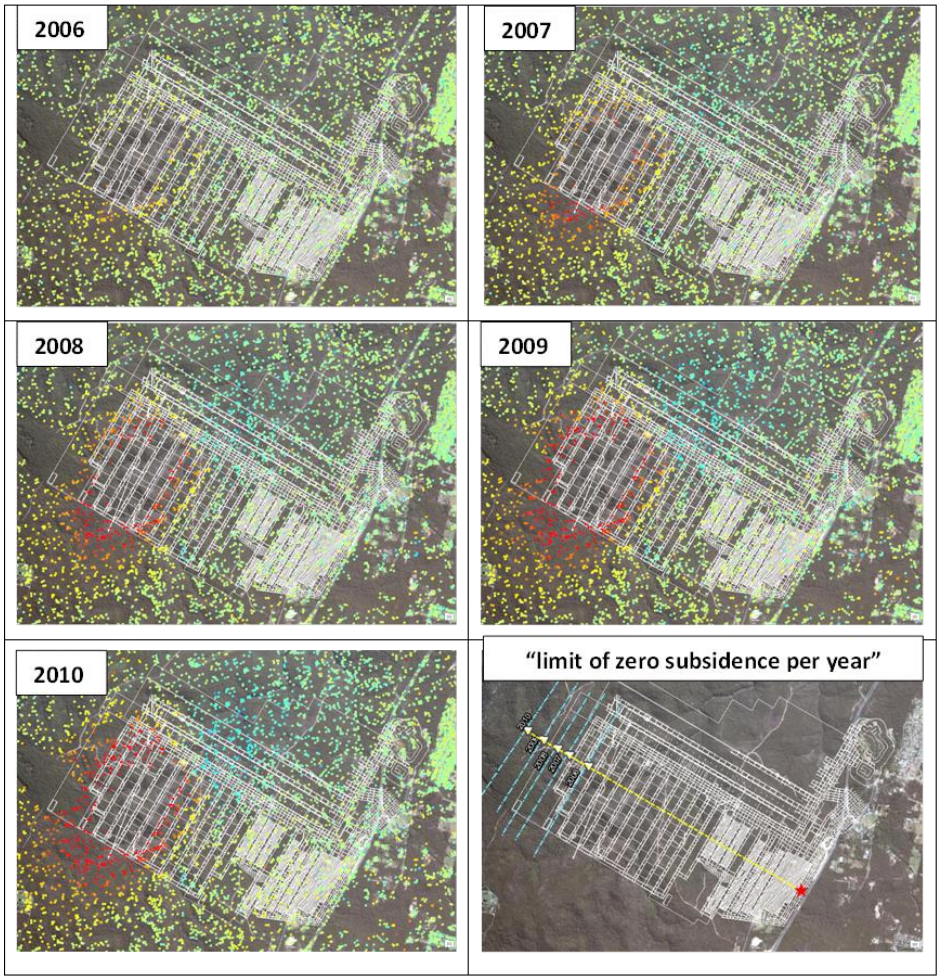

Figure 116. Radar interpretation of the limit of area subsidence (front of the subsidence bowl) for any year during the acquisition. It possible to note the advance of the front of the subsidence bowl, in the direction of the mining progression.

The interferograms, even if do not provide very precise measurements, have the advantage to be used to characterize a sudden event by analysing using as master and slave, images before and after the event. The advantage is that if a small B_t is selected for DInSAR analysis, the results reflect the deformation in in that specific interval. As a consequence, DInSAR is precious when dealing with deformation

variable in space and time, such as in the mining sector and provide a sort of instantaneous velocity. Each single interferogram has been visually interpreted to identify for any date, the location of the maximum subsidence.

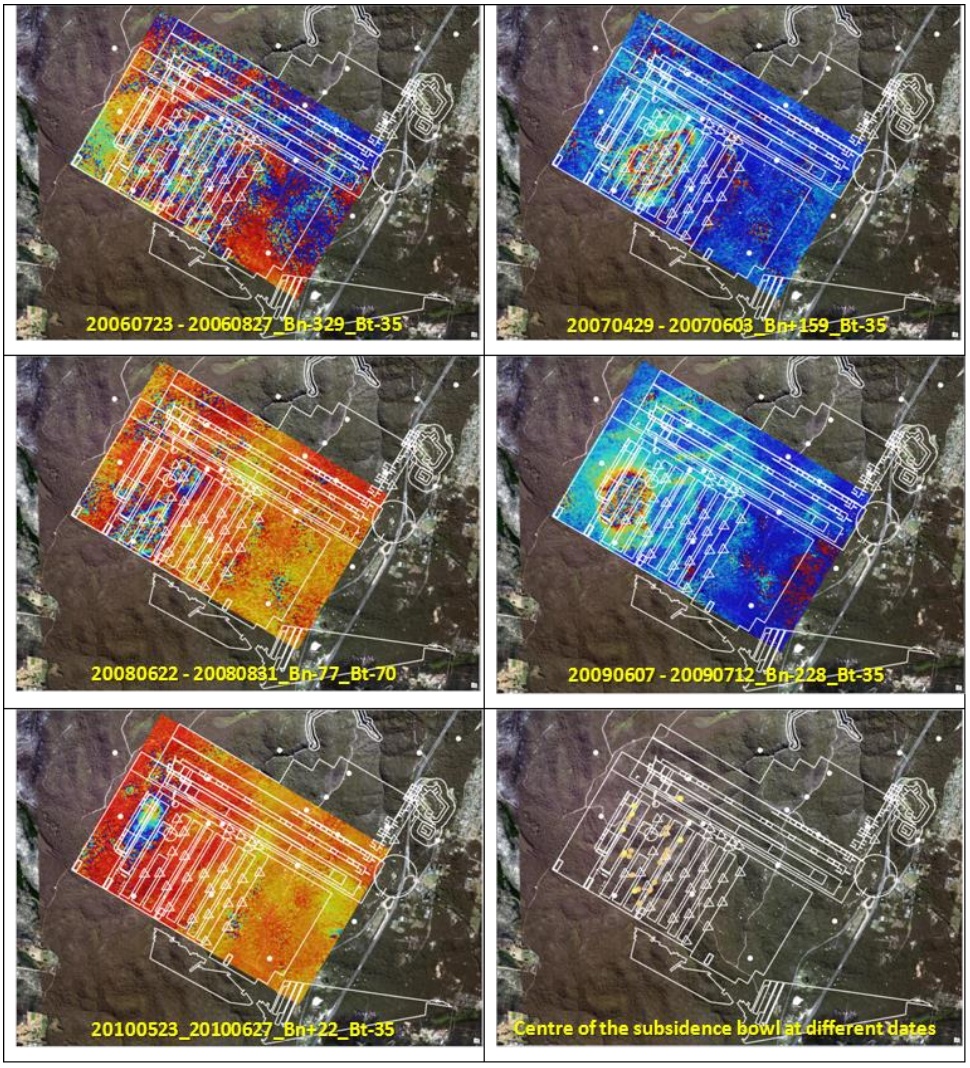

Figure 117. Interferograms used for the interpretation of the maximum subsidence at different dates.

Most of the interferograms processed have a very low coherence, due the high deformation rate over the mine layout. However, by identifying the

maximum deformation on the interfergrams, it has been possible to evaluate the velocity of the movement of the subsidence bowl centre with the same approach used for the subsidence bowl front. The distance of the centre has been measured from the same reference point. Since the excavation date of the longwall are known, it has been possible to create a graph showing the position at each date of the excavation, of the subsidence bowl front and subsidence bowl centre. It is interesting to note that all they shows the same velocity that is about 300 m/year (Figure 118).

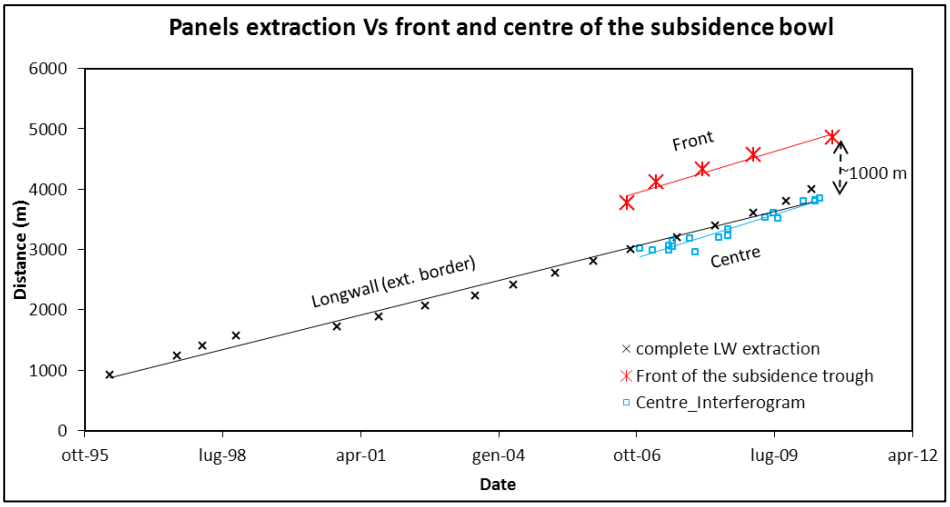

Figure 118. Advancing velocity of the longwall extraction, of the subsidence bowl front and subsidence bowl centre.

Figure 118 shows also that the front of the subsidence advance together with the centre of the subsidence bowl and at constant 1000 m from the external border of the longwall panel. Figure 119 shows a simplified scheme of the relative position of the front and the centre of the subsidence bowl, and the external border of longwall. By knowing the depth of the panel (Figure 120), a simple trigonometric relation allowed

to evaluate the angle of draw (63°) which will defines the areas affected by subsidence in surface.

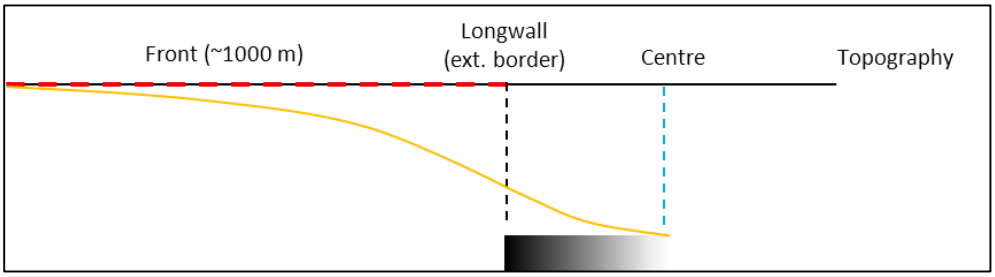

Figure 119. Scheme of the relative position of the front and centre within the subsidence bowl, and the longwall external border.

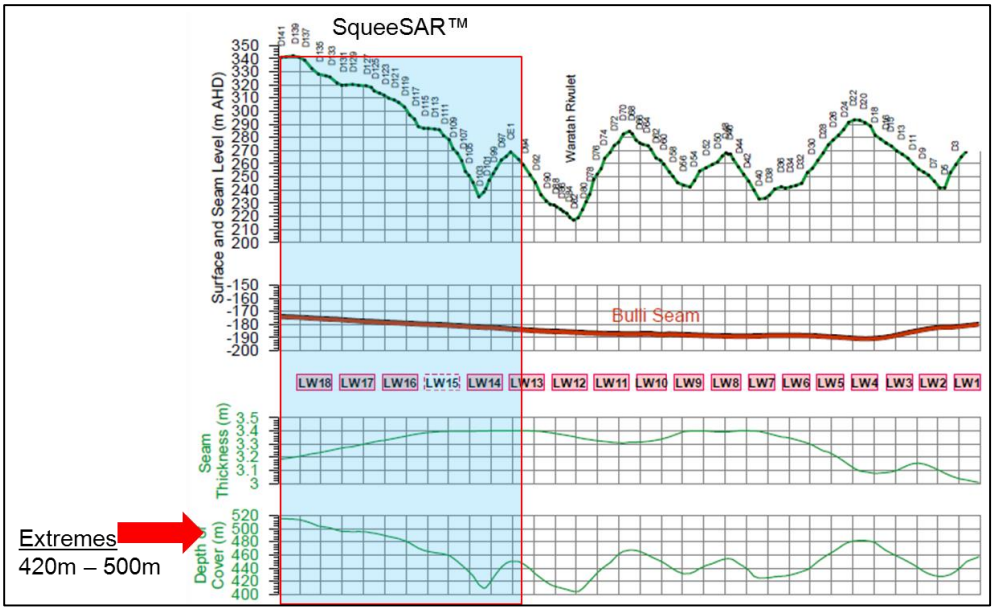

Figure 120. Variation of surface topography, depth of the Bulli Seam, seam thickness, and depth of the cover (overburden). The area mined during the SqueeSAR™ acquisition is highlighted. Modified after DeBono et Tarrant (2001).

5.2.3.2 Time series analysis

PS-Time was used to carry out an automated classification of MT-InSAR time series and to characterize the effect of the subsidence bowl in the area surrounding the mine layout. The results (Figure 121) shows clearly that a cluster of measurement points showing acceleration is located at the front of the mine layout, while points showing deceleration are located at the rear of the mine layout.

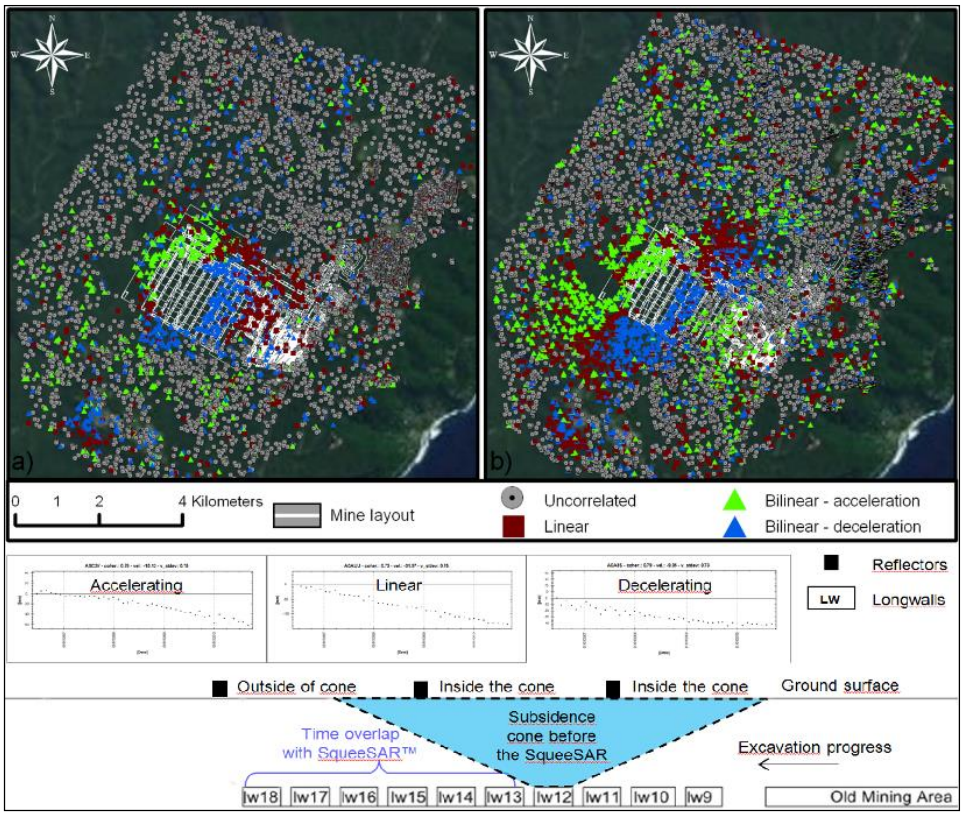

Figure 121. Results of the time series classification with PS-Time of a) descending dataset and b) ascending dataset. Both geometries show a clear localization of measurement points showing acceleration (front of the mine excavation direction) while measurement points showing deceleration are located at the back of the mine layout, over old longwalls. c) Schematic cross section of influence areas for each longwall during the InSAR monitoring dates. The cone represents the areas affected by subsidence at the beginning of the InSAR monitoring. Objects outside the cone and in front of the mine layout, will result in acceleration since reached by the subsidence cone after.

A cluster of measurement points can be found over the old mining area. The schematic cross section in Figure 121c provide an explanation for the localization of these clusters of different deformation types. The blue cone represents the areas affected by subsidence at the beginning of the InSAR monitoring. Since the cone advance along the direction of mining progression, objects that at the start of SqueeSAR™ acquisition were

located outside from the cone, will show acceleration. In the other hand, the measurement points that were located inside the cone at the beginning of the acquisition but outside at the end, will exhibit deceleration. The points that have linear deformation trend, are the ponts that are affected by the subsidence during all the acquisition, The "linear points" can be found in fact along an axes around the centre of the subsidence trough, and over the old mining area, where residual deformation exists for several years.

5.2.4 Numerical modeling

SDPS uses the influence method to define the subsidence profile. In particular, at any point (P) at the surface, the subsidence can be evaluated by equation (26):

$$S(x,s) = \frac{1}{r}\int_{-\infty}^{+\infty} S_o(x)\exp\left[-\pi\frac{(x-s)^2}{r^2}\right]dx \qquad (26)$$

where:

r = the radius of principal influence = h/ tan(β);

h = the overburden depth;

β = the angle of principal influence;

s = the coordinate of the point, P(s), where subsidence is considered;

x = the coordinate of the infinitesimal excavated element;

So(x) = m(x)a(x) (the roof convergence for excavated element);

m(s) = the extraction thickness;

a(x) = the roof convergence (subsidence) factor

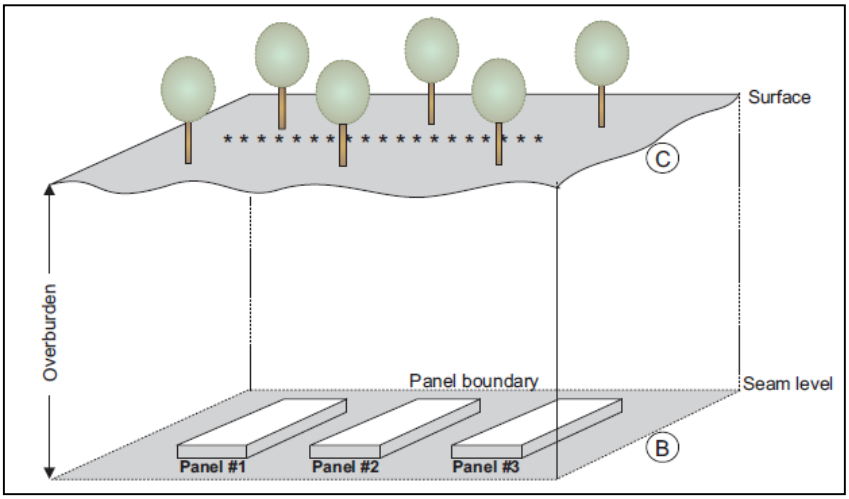

Figure 122. Input geometries of the SDPS numerical model. (Source. SDPS Reference guide, version 6.1, 2013).

In order to evaluate the subsidence with SDPS at Metropolitan Mine, the input parameters needs to be estimated:

1. Points coordinates: the subsidence was modeled at the same location of the SqueeSAR™ measurement points. With this approach, ther results are directly comparable.
2. Elevation: SqueeSAR™ dataalso have the elevation in the attribute table.
3. Mine geometries: the coordinates of the longwalls borders can be types into SDPS
4. Extraction thickness: 3 meters (DeBono et Tarrant, 2011)
5. Percentage of hardrock: from the stratigraphy.
6. Angle of Influence: is the complementary of the "angle of draw".

The percentage of hardrock in the overburden has been evaluated applying the classification of Brown (1981) shown in Figure 123.

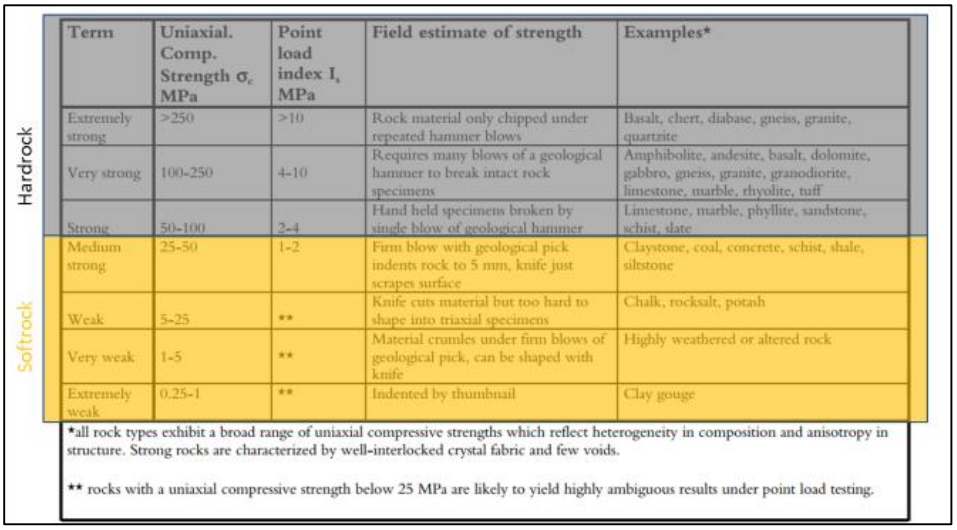

	Term	Uniaxial. Comp. Strength σ_c MPa	Point load index I_s MPa	Field estimate of strength	Examples*
Hardrock	Extremely strong	>250	>10	Rock material only chipped under repeated hammer blows	Basalt, chert, diabase, gneiss, granite, quartzite
	Very strong	100-250	4-10	Requires many blows of a geological hammer to break intact rock specimens	Amphibolite, andesite, basalt, dolomite, gabbro, gneiss, granite, granodiorite, limestone, marble, rhyolite, tuff
	Strong	50-100	2-4	Hand held specimens broken by single blow of geological hammer	Limestone, marble, phyllite, sandstone, schist, slate
Softrock	Medium strong	25-50	1-2	Firm blow with geological pick indents rock to 5 mm, knife just scrapes surface	Claystone, coal, concrete, schist, shale, siltstone
	Weak	5-25	**	Knife cuts material but too hard to shape into triaxial specimens	Chalk, rocksalt, potash
	Very weak	1-5	**	Material crumles under firm blows of geological pick, can be shaped with knife	Highly weathered or altered rock
	Extremely weak	0.25-1	**	Indented by thumbnail	Clay gouge

*all rock types exhibit a broad range of uniaxial compressive strengths which reflect heterogeneity in composition and anisotropy in structure. Strong rocks are characterized by well-interlocked crystal fabric and few voids.

** rocks with a uniaxial compressive strength below 25 MPa are likely to yield highly ambiguous results under point load testing.

Figure 123. Classification of hardrocks and softrocks, based on Brown (1981).

In particular, Brown (1981) proposed a rocks mass classification based on the uniaxial compression strength (σ_c) and point load index (I_s). Also example of typical rocks within each single strength class are indicated. Since no information are available on σ_c and I_s, the rock types were used to identify the strength class (Figure 123). By knowing the stratigraphy at metropolitan mine (Figure 112) it possible then evaluate the percentage of hard rock in the overburden (Table 9).

Table 9. Estimate of the percentage of hardrock in the overburden, according to the classification proposed by Brown (1981).

Geological Formation	Thickness	Hardrocks
Hawkesbury	90	X
Newport Formation	10	X
Bald Hill Claystone	18	
Bulgo Sandstone	170	X
Stanwell Park Claystone	40	
Scarborough Sandstone	50	X
Wombarra Claystone	20	
Coakliff Sandstone	22	X
Total thickness	**420**	**332**
% of Hardrocks	**~80**	

Once every parameter has been established, two numerical model have been carried varying the AoD and keeping as constant all the remaining parameters. In particular a numerical model was assessed using the AoD_{Insar} while a second result was obtained using the $AoD_{26.5}$, which is the value of angle of draw used in literature when no other data are available (Figure 124).

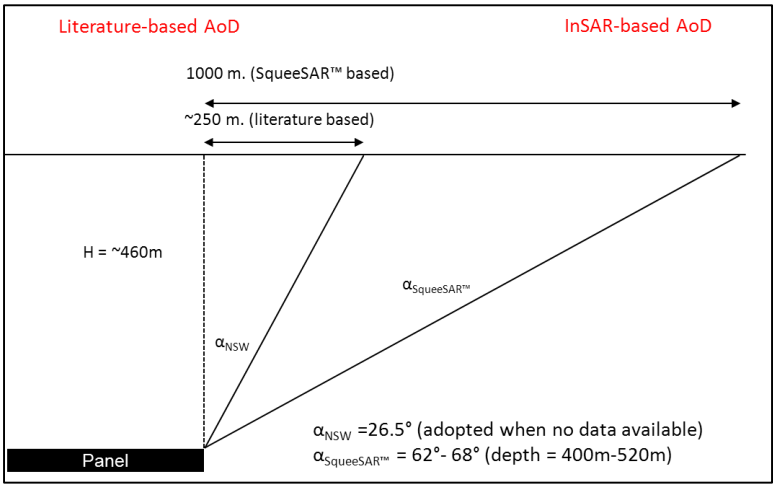

Figure 124. Comparison of the two angle of draw used for the numerical simulation with SDPS.

5.2.5 Results & Discussion

The subsidence was evaluated with SDPS at the same location of the PS/DS from SqueeSAR™ to allow a direct comparison. Figure 125 shows the results of the simulation carried out using the angle of draw from literature (26.5°) and the angle of draw evaluated in this study by means of InSAR characterization. East-West and vertical component of the subsidence has been assessed separately. It is evident that using $AoD_{26.5}$, the area of influence is sensibly underestimated, in both the components. In other hand, using the AoD_{InSAR} the results are very similar to the observed. In order to provide a better comparison of the above mentioned results, an interpolation of the deformation was carried out, and the contour line indicating 20 mm of total displacement are represented.

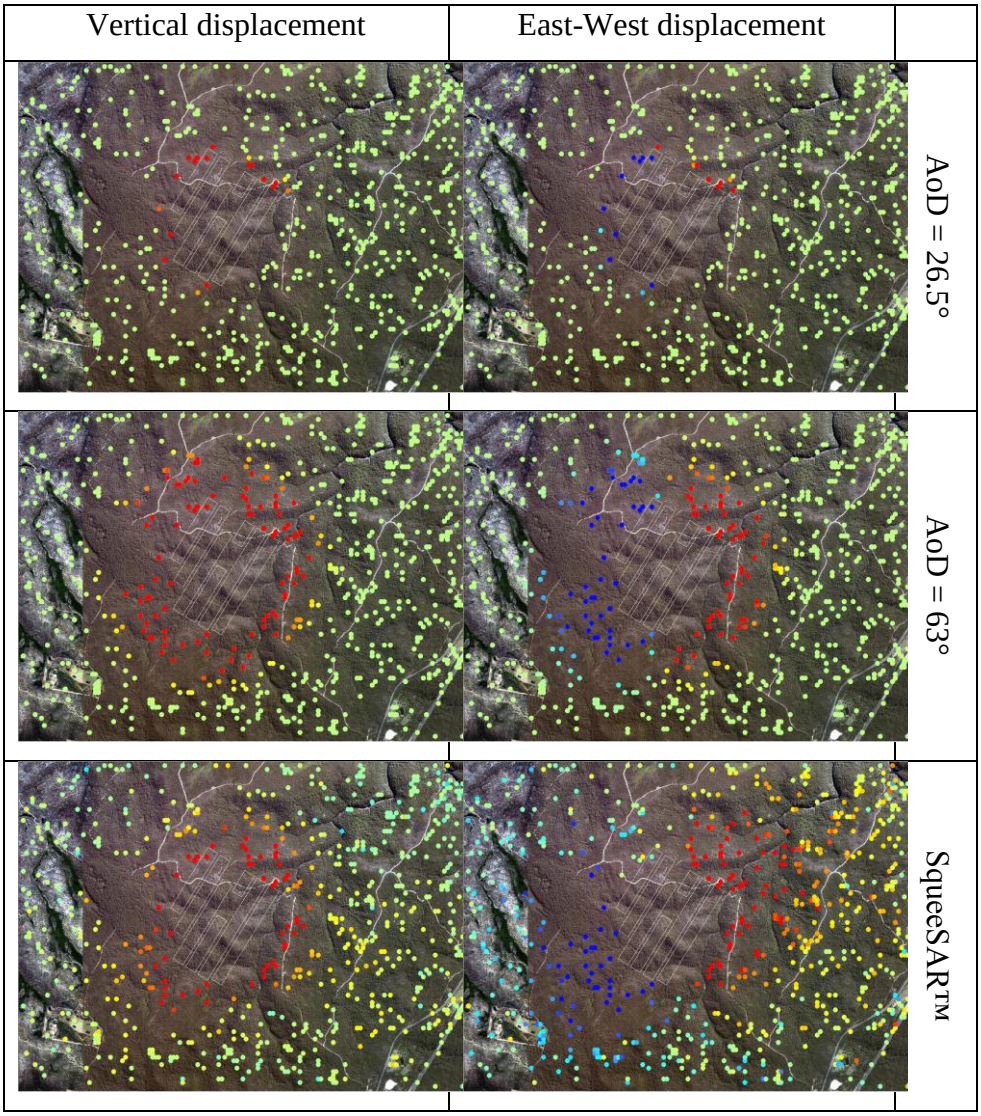

Figure 125. Comparison of the numerical modelling results. The East-West and vertical component of the subsidence are compared with the SqueeSAR™ data. It is evident that the simulation carried out using AoD evaluated with InSAR provide results very similar to the "measured".

It is important to note that 20 mm is the limit of the subsidence often assumes in literature as "zero subsidence" (Figure 126).

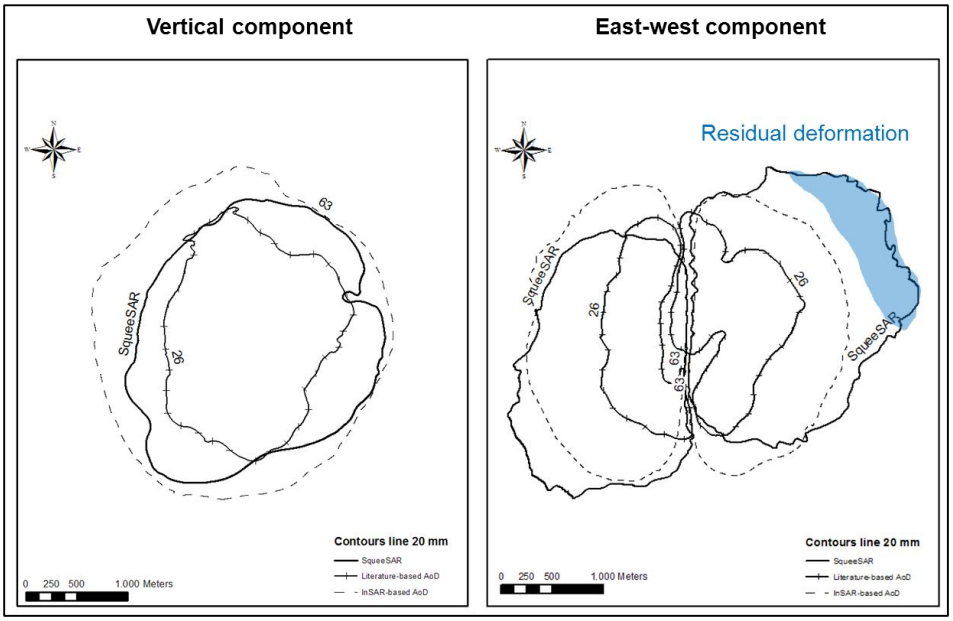

Figure 126. Contour lines comparison of 20 mm of subsidence for numerical modelling using $AoD_{26.5}$, AoD_{63} and the SqueeSAR™ data. Residual deformation can be observed over the old mine.

Figure 126 confirms that using the AoD_{InSAR} the results are closer to the observed. However, the best improvement is found on the East-West components rather on the vertical components. This can be explained by the fact that the InSAR calibration has been carried out at the limit of zero subsidence, where most of the deformation is horizontal. It can also be observed that the area indicated with blue, on the East-West component is not due to the fact that the results do not fit, but it is due the residual deformation over the old mining area, that was not introduced in the model (because antecedent the SqueeSAR™ analysis).

5.3 Underground tunneling induced Subsidence

5.3.1 Objectives and General Settings

Tunneling above urban is crucial because of the element at risk exposed to the potential subsidence. This means that even small deformation often cannot be ignored. The objective of this section was to define if the MT-InSAR and in particular the post-processing routine (PS-Time) can be successfully used to detect even very small deformation surface at the time of the tunnelling. The study area is located in North Vancouver, Canada (Figure 127).

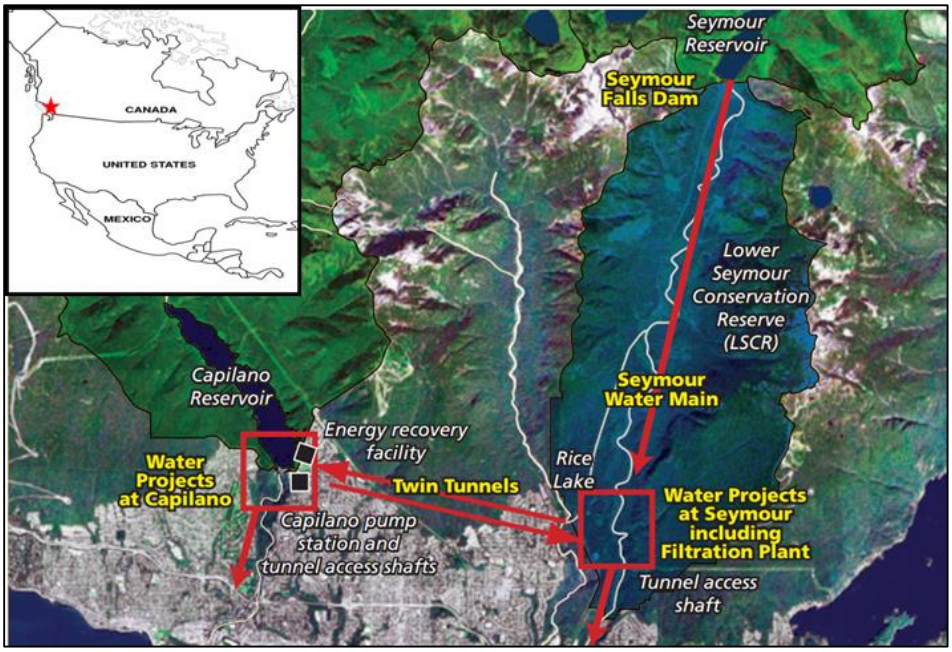

Figure 127. Geographic location of the study area. The water filtration plant of the Seymour-Capilano reservoir is illustrated.

In 2004, the project owner, Greater Vancouver Regional District, awarded the construction contract for the Seymour-Capilano Filtration Plan to Germany-based Bilfinger Berger. The filtration is to treat the water coming from both the Seymour reservoir and the water from the

Capilano reservoir, that will be conveyed through the Twin Tunnels (Figure 127). The contractor chose two 3.8 m diameter TBMs to bore the Twin Tunnels in intrusive granitic rock with strengths of 200 – 265 MPa.

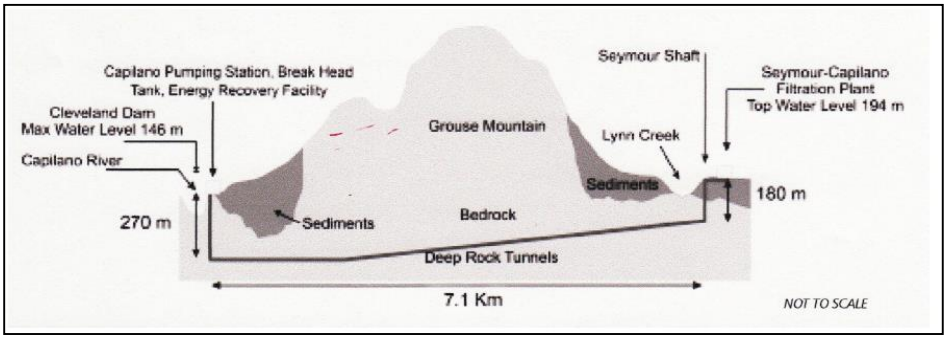

Figure 128. Cross section along the twin tunnels conveying the water from the Capilano reservoir, to the Seymour Water Filtration Plan. Tunnels have been excavated in intrusive granitic rocks and at the TBMS entrance, sediments deposits of the order of hundred meters are found (Source: http://tunneltalk.com/Seymour-Capilano-Apr09-Twin-tunnel-restart-comes-at-a-high-price.php).

MT- InSAR is suited for monitor deformation over urban areas, as they provide an overview of the entire affected area and can measure movement rates with millimetric precision. An area of about 10 km^2 was studied, in particular where the shaft excavation of the Seymour-Capilano water filtration plant was started in 2004. To characterize the relationship between the tunnel excavation and the ground deformation it is necessary to process a radar dataset covering the period of excavation.

5.3.2 Datasets & Methods

For this work a Radarsat-1 data stack, comprising 58 descending images from March 2001 to June 2008 was processed using the SqueeSAR™ algorithm (Ferretti et al., 2011). To better characterize the deformation in the time and space domains, an in-depth time series analysis is essential.

To this end PS-Time was used to classify the time series and define if an sudden acceleration was captured from the satellite after the tunnels excavation.

5.3.3 Ground deformation pattern

The results of the SqueeSAR™ processing are shown in Figure 129. The coverage and the density of points is very high, due to the presence of buildings and infrastructures in the AOI. It is possible to see that a very mild deformation is detectable near the area of the excavation of the Twin Tunnels (east of the area). Interestingly, by post-processing the SqueeSAR™ data with PS-Time, a large cluster of bilinear deformation can be found at the location of the Twin Tunnels entrance. This suggest that in that area, a disturbing factor has played a role on the history of all measurement points and thus on the ground surface (Figure 130). In order to define which type of deformation has been experienced over this area and over which extent, the was also computed the study of the acceleration, It is possible to note that all the vast majority of measurement points in the AOIs is affected by an increase of velocity.

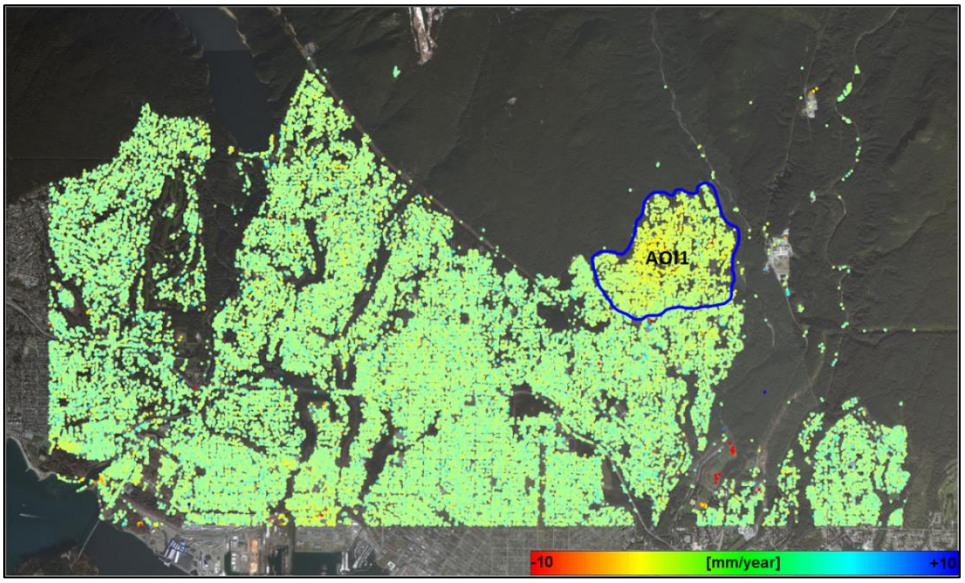

Figure 129. Average annual velocity of deformation calculated over the entire time series. The AOI is highlighted in blue.

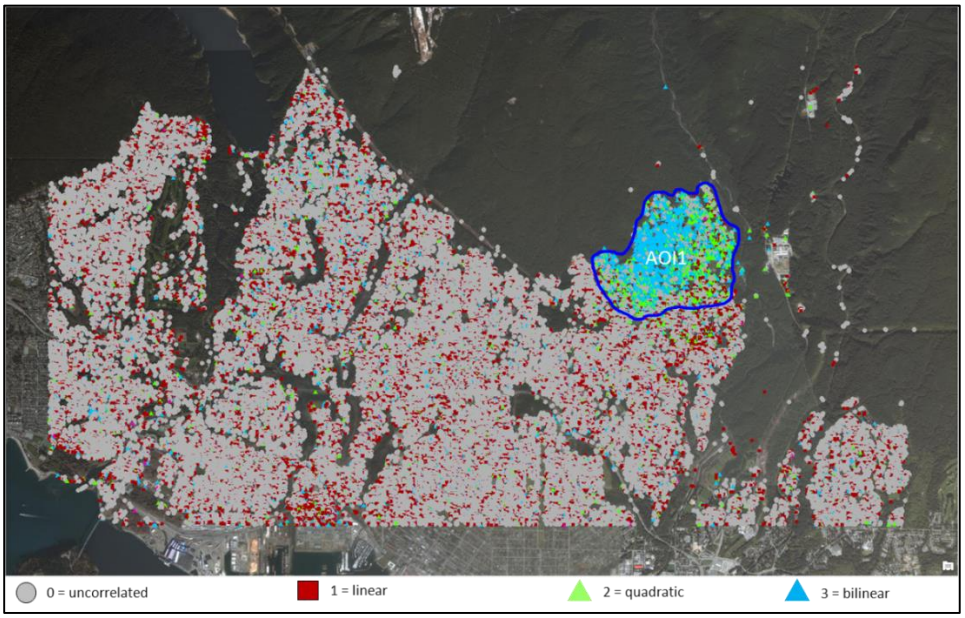

Figure 130. Time series classes obtained processing the MT-INSAR with PS-Time. Within the AOI, there is an high concentration of non-linear deformation.

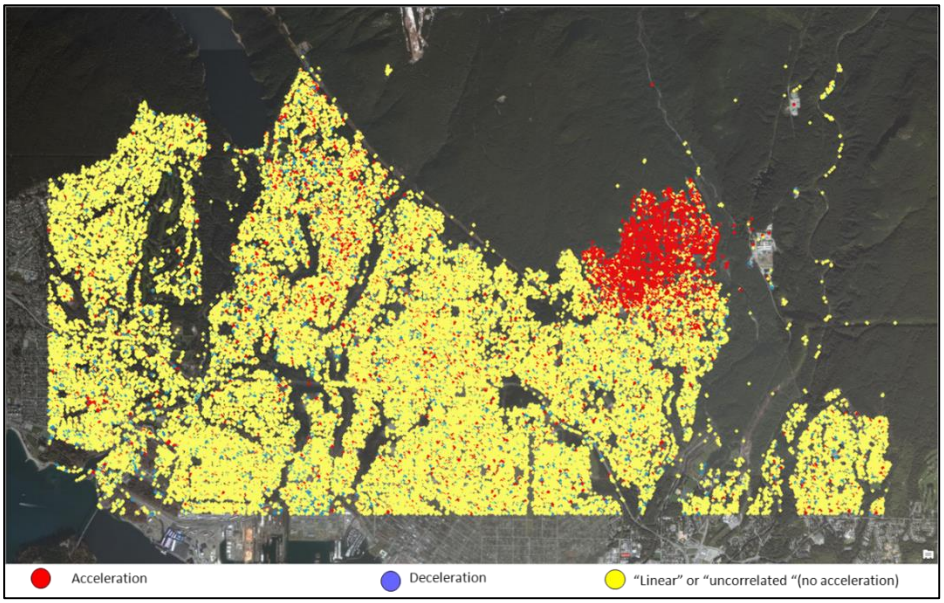

Figure 131. Acceleration history of the measurement point evaluated with PS-Time. Around the entrance of the Twin Tunnels above Grouse Mountain, most of the measurement points shows acceleration.

While computing the acceleration, also the date corresponding to the instant of acceleration and the velocity before and after the event are computed. PS-Time provide a very useful information in this context since it allows to clearly define the relation between the tunnels excavation and the subsidence. It is possible to represent the velocity of deformation before and after the phenomena who triggered the deformation. To this end, Figure 132 shows the velocity captured by the SAR satellite before any deformation event. As it is possible to note, all the area was totally stable (green) before a triggering event event but was definitely active after the acceleration date (Figure 133).

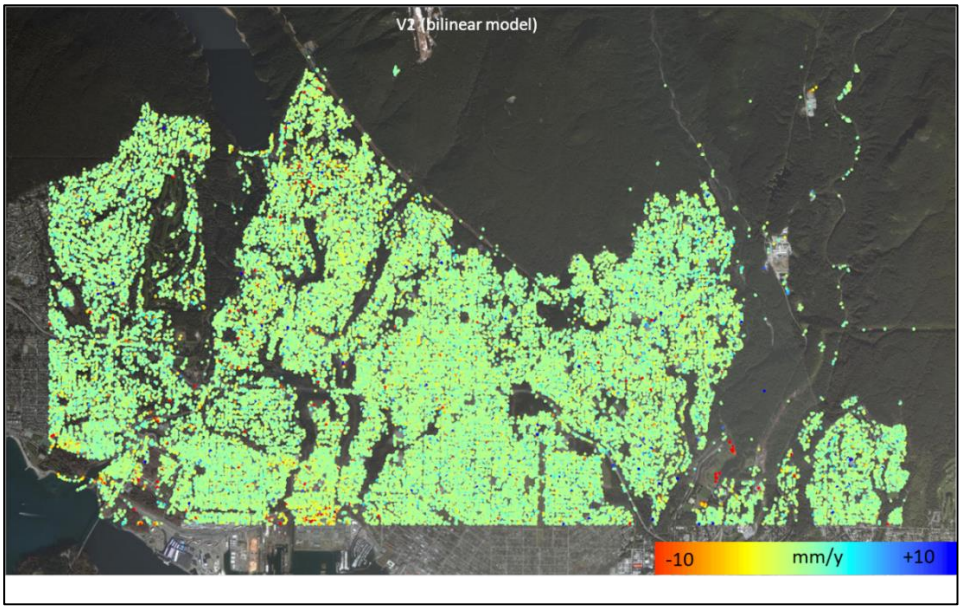

Figure 132. Average velocity of the first segment of the time series (before the acceleration date).

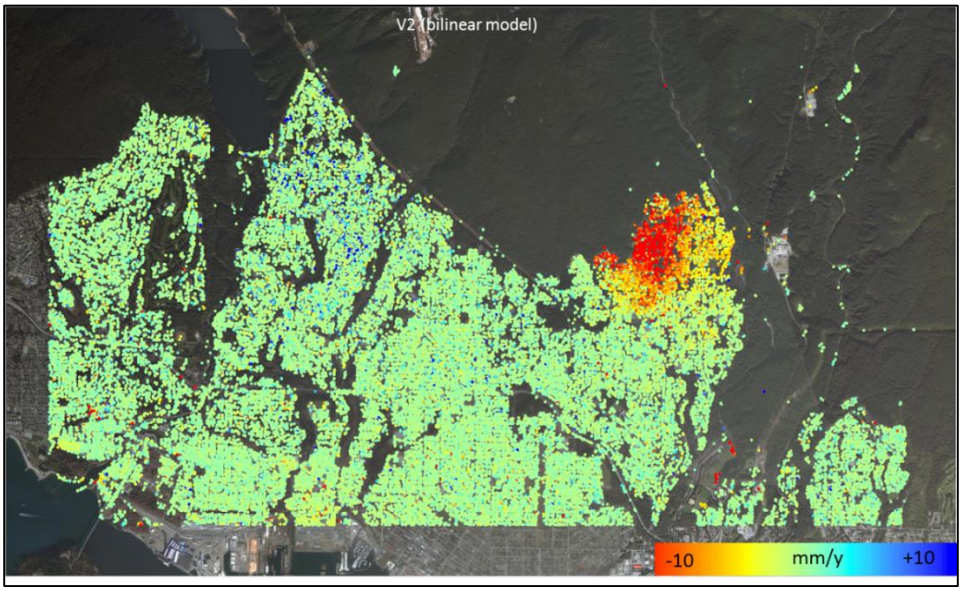

Figure 133. Average velocity of the second segment of the time series (after the acceleration date).

In order to fully characterize the deformation and to define if any relation exist between the tunnel excavation and the subsidence registered, the analysis of the distribution of the acceleration dates was carried out. By interpolating only the dates of acceleration, it is possible to observe a regular distribution of the acceleration. In particular, acceleration started before at the South-East of the AOI and reach later the North-West of the AOI. This direction is similar to the direction of the Tunnels excavation (Figure 134 left).

Figure 134. Distribution in space of the date activation of the subsidence; Right) Time series of three different sector of the study area. It is evident the different date of activation of the deformation.

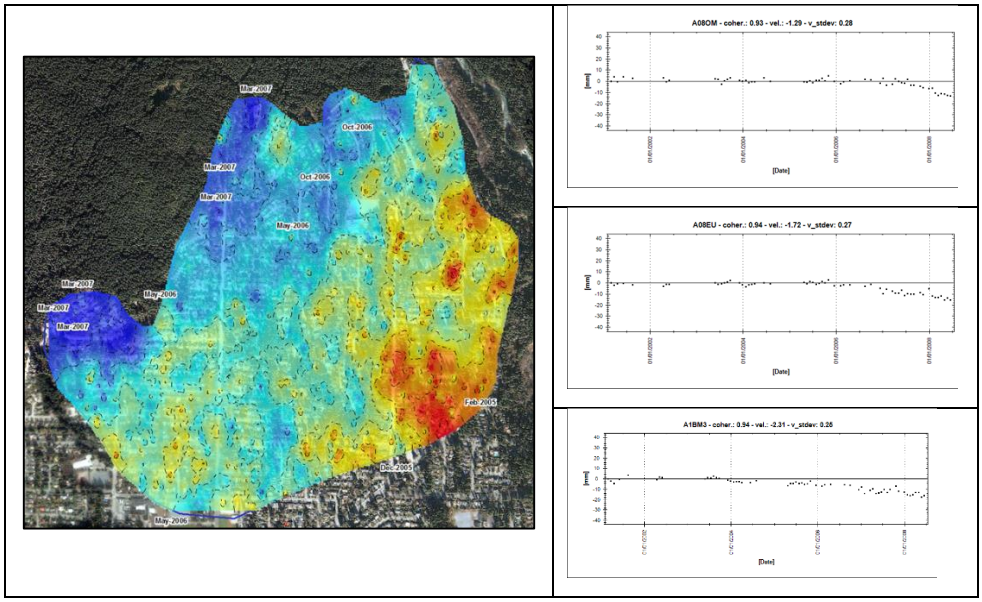

5.3.4 Results & Discussion

The time series analysis showed that within the area investigated, 56% of measurement points are characterized by a bilinear deformation trend, 25% by a quadratic trend, and 7% by a linear trend, indicating that a

change in deformation rate was present for a vast majority of points. In addition, 78% of the points accelerated mostly in 2006, corresponding with the date in which excavation of the tunnels started (Figure 135).

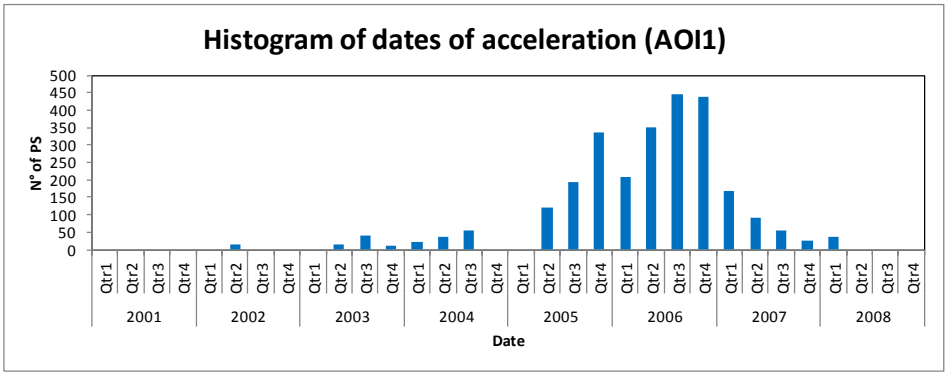

Figure 135. Histogram of the measurement points showing acceleration within the difference period of time.

In general, total deformation of up to ~ 40 mm was preceded by a phase of stability at the ground surface. The stability has been followed by the triggering event. Due to the specific location, and thanks to the time series analysis was possible to define that the tunnels excavation triggered the subsidence in the AOI. In fact, most of the date of subsidence activation are measured in 2006, which correspond with the working period of the Twin Tunnels. PS-Time has proved to be a powerful tool to identify non-linear deformation, acceleration and date of the event. Also it allowed to have pictures of the deformation happening before and after the event.

6 General discussion

6.1 Landslides

Landslides studies can benefit from the introduction of MT-InSAR techniques. Starting from a regional scale analysis, several potential landslides can be detected. Among this areas, showing deformation from satellites, often there are areas that are not known as active or even not classified as landslide. Other times, there might be some ground evidences (geomorphic, geologic or damages to man-made structures) of gravitational phenomena, but without any monitoring evidence. This can happens when very large areas (in particular if deep seated such as DSGSDs, rockslides, etc.) move together at very slow displacement rate, without generate damages to structures located above the active landslide. To this end, MT-InSAR is unique, since it provides a relatively low cost, monitoring data over large area at very high precision. However some limitations apply to use of MT-InSAR as a routine for landslide hazard and risk management. The most important limiting factor is that only "extremely slow" and part of the "very slow" moving landslides (Varnes, 1996) can be monitored without having problems of coherence loss and phase unwrapping (Table 1). While extremely slow and very slow moving landslides often are associated to a low risk in terms of life's losses, if protracted for long time, they can leads in economic losses and services disruption. Thus for slow moving landslides, MT-InSAR still provide a unique possibility for mapping and update of landslide inventories. Another limitation is due to the fact that landslides are often covered by vegetation which do produce a strong

backscattered signal to the satellite. The consequence is that few measurement points are returned over vegetated areas, or non-reflective in general. Also the geological condition can play an important role on the measurement point distribution. For example clays are characterized by a low reflectivity, while sandstone, limestone, granitic rocks etc., are prone to produce a strong backscattered signal to the satellite. As a consequence different geological contexts provide a different InSAR applicability. Most of the landslide in the Apennines are found in clays and quaternary deposits and are often vegetated. Most of the measurement points are thus found along roads or in correspondence of buildings. In fact from this study, was found that a large amount of small villages located in the Apennines, are built over landslide body often classified as ancient or dormant, but MT-InSAR revealed them as active. These areas, being built over disturbed material with poor geotechnical characteristic, are prone to re-activate and slowly moving at near-constant rate for years.

In other hand, Alps has proved to be in general suitable for the in terms of reflectivity due to the presence of outcrops. However two other limitation affects the Aps. One is represent from the abrupt geomorphology. Very steep slope generate geometrical distortions on radar SAR images (i.e. layover and shadowing) that leads in loss of information in that area. Another limiting factors is found in areas exposed at seasonal snow coverage. One of the basic principle of the MT-InSAR is that a measurement point has to be statistically coherent for the entire time span. Where snow cover seasonally the measurement point, the coherence is lost, and phase history of the deformation cannot be extracted. However, to limit this effect, recent algorithm have been developed to evaluate the average velocity for Temporary Coherent

Scatterers (TCS). In these case, the time series of the deformation cannot be evaluated and not either the period of time when the point has been coherent, but only the average velocity. Unfortunately Temporary Scatterers were not been developed yet at time of the processing of the South Tyrol dataset. The analysis showed that MT-InSAR in South Tyrol is very suited for the monitoring and detection of the several DSGSDs present in Alpine environment.

Regarding the use of the Hot Spot Analysis for regional scale mapping of active landslide, it has to be highlighted that this technique should be only used as very first step of analysis, to identify the main deformation. As a result of this work, it has been observed that some relevant deformation, are not detected by the HS analysis, because of the low density of measurement points and thus low clustering. Since the density of measurement points depends from a series of factors (land cover, velocity of the landslide, wavelength, spatial resolution, number of images processed, etc.) the detection of active landslides cannot be totally automated. Also, some false positive can be returned over clusters of points in urban areas, but affected by very mild velocity (i.e. <2mm/y). The velocity in fact is continuous and stable measurement points can have velocity in a range around zero that depends from the dataset precision. However, based on the experience and on the time series analysis with PS-Time (Berti et al., 2013), was found that measurement points within the range ±2 mm/y, can be reasonably considered stable. It has to be stressed that these consideration are valid when the reference point used for the MT-InSAR processing is located in a stable area.

However, for a proper identification of potential active landslides, it is recommended that a geoscientist analyse the data carefully (visual interpretation, geomorphic analysis). The landslide identification also is dependant from the dataset quality and distribution of measurement points. In this work, thanks to the availability over the Northern Apennines, of two datasets characterized by different quality (second generation algorithm vs first generation algorithm, long time series vs short time series, etc.), was carried out a comparison of dataset effectiveness for landslide landslides detection. Table 10 shows the results of the potential active landslides mapping, using the two different datasets: a recent SqueeSAR™ analysis of RADARSAT-1, and the ENVISAT dataset available from the PST-A project, processed with the PSP-IFSAR. The analysis was carried out using different information such as: 1) mean annual velocity along the line of sight; 2) velocity component's (East-West and vertical); 3) acceleration (evaluated with PS-Time and when available with the value available from the data-provider). The results show a higher effectiveness of the RADARSAT-1 processed with SqueeSAR™, then the ENVISAT available from the PST-A project. As an example, ENVISAT allows to classify only 10% of the landslide classified with RADARSAT-1 in the descending geometry.

Table 10. Comparison of MT-InSAR effectiveness for landslides detection over the Northern Apennines (MO). Potential landslides were identified using average line of sight velocity, velocity components, and acceleration. The acceleration analysis, when possible, was carried out based on both PS-Time outputs and the acceleration computed by the MT-InSAR data provider (T.R.E.).

	Mean velocity		Velocity components				Acceleration			
	Line of Sight		Vertical		East-West		(T.R.E.)		PS-Time	
Asc.	115	16	31	7	96	12	77	-	18	2
Desc	112	25					79	-	21	3
	Rsat	Env	Rsat	Env	Rsat	Env	Rsat	Env	Rsat	Env

These results prove the higher quality and higher spatial coverage provided by the SqueeSAR™ data, which include also Distributed Scatterers.

Comparison of MT-InSAR effectiveness for landslides detection over the Northern Apennines (MO). Potential landslides were identified using average line of sight velocity, velocity components, and acceleration. The acceleration analysis, when possible, was carried out based on both PS-Time outputs and the acceleration computed by the MT-InSAR data provider (T.R.E.).

Regarding slope-scale analysis, the time series analysis is particularly important. In the Alps, there are examples of rockslides that after moving for years (hundreds to thousands) suddenly accelerate leading into catastrophic rock avalanche (i.e. Val Pola). This types of phenomena are prone to produce very high risk, and in this context, the use of PS-Time for the identification of acceleration in the displacement rates, is very valuable. Even if landslides types and kinematics over the Apennine and the Alps are very different, the distribution of the velocity in the two

different geological contexts are very similar. This is not surprising since, as anticipate MT-InSAR basically monitor the extremely slow moving landslides, which are present in both the areas, and saturate the maximum detectable deformation detectable by means of InSAR.

The methods for the velocity components evaluation has shown that the use of double orbits provide the best results. In fact, the back-projection assumes that the movement is parallel to the slope angle. In this work it has been proved that this assumption is not always correct and that the results is strictly dependant from the DEM resolution. Furthermore, when re-projecting the displacement from line of sight to slope direction, also the noise is amplified. In the other hand, in abrupt geomorphic condition, such as in the Alpine areas, Geo-PSIC helps to identify the velocity components even for very localized phenomena, such as for boulders. In conclusion there are no particular reasons to not use Geo-PSIC in any geological and geomorphic condition, since in the worst case produce results similar to the resampling grid. From the analysis of the velocity components and the angle of the landslide movement direction (identified as “Gamma”), it was noted that in the Apennine, most of the landslide monitored with MT-InSAR, has a notably predominant horizontal component rather than the vertical component. This is in agreement with the gentle slopes typical of the Apennines where landslide body move almost translational. However a higher vertical component is found in the direction of the landslide crest. It has to be mentioned, that these considerations are affected by the distribution of the measurement points that often are found in correspondence of buildings and roads less in the detachment area of the landslides. In fact, most of the landslides in the Apennines are roto-translational and can shows at the landslide crest near vertical surface. In these conditions,

satellites can hardly identify measurement points, due to the geometrical distortions and other source of coherence losses. The evaluation the angle of movement direction has proved to be useful to characterize the landslide type. In fact, translational or roto-translational landslide can be distinguished if a good coverage of both ascending and descending is available. However, when using the angle "gamma" for the characterization of the movement direction, it should be paid attention to limit the analysis at the PS that indicate a deformation rather than PS stable or near-stable. The reason is because since the movement direction is based on a trigonometric role, the module of the velocity do not account in the results. As a consequence, even PS with values close to 0 mm/y will return a value of "gamma". In this case, the movement direction do not have a physical meaning. A possible approach could be to combine the use of "gamma" with PS-Time, and calculate the movement direction of the deformation only to "correlated" measurement points.

PS-Time can be used to classify large data and to identify homogeneous deformation pattern. It has proven to be very useful to identify non-linear deformation, acceleration deceleration and date of the change in motion. However, PS-Time work perfectly with deformation characterized by maximum 2 phases of activity. When the time series is characterized by *n* acceleration (or deceleration), the time series would be better mathematically described by a *n+1*-segment. Also, PS-Time should be used very carefully due to its sensitivity to the data quality. It is possible that the same area monitored from 2 different satellite geometries (ascending and descending) provide slightly different results. An example is given by the RADARSAT-1 dataset of the Apennine area (Figure 60, Figure 63). While these are very high quality dataset, still the

time series classification can be different. PS-Time in fact is so sensitive that a small variation, in the time series of displacement, can turn into a statistically significant displacement trend. Other case can be represented when the reference point has a very low derive, which might be not significant from a geological point of view, but will affect all the classification of "uncorrelated" and "correlated". In particular, most of the "uncorrelated" will be classified as "correlated" (i.e. linear, bilinear, etc.). The sensitivity of PS-time has to be taken in consideration when analysing very large dataset, that they could be affected by these types of problems. The result will be a "salt and pepper" effect of the time series classes than can confuse the end-user. However, since natural phenomena are correlated in space, if a clear deformation pattern exists, that area will be mainly characterized by one type of deformation pattern or will show an higher concentration. In fact, PS-Time become very useful at local scale, where looking at single phenomena it is possible to identify the deformation type, if there is an acceleration in the landslide, or if the remedial works have been successful (deceleration, stabilization), and the extent of it.

6.2 Man-Induced subsidence

MT-InSAR has been used in conjunction with DInSAR to estimate the subsidence dynamics over a longwall mine in New South Wales , Australia (the Metropolitan Mine). The strength of the combination of these two interferometric technique is due from the millimetric precision of measurements provided from the MT-InSAR and the possibility to study the deformation happening between two desired date (Differential Interferograms). DInSAR provide a lower precision but has the

advantage, that can be used also for non-linear deformation, and thus also over area where the MT-InSAR could not successfully applied to decorrelation problems. In particular in thus study it has been demonstrated that the front of the subsidence bowl can be measured with very high precision (mm). In other words, by defining the front of the subsidence, the limit between the stable zone and the subsiding area, is drawn. By doing this analysis at any time of the available history of deformation, the velocity of the front can be estimated. However, in order to fully characterize the subsidence bowl, also the centre of it has to be identified in each period of time. Since in longwall mining the maximum vertical deformation is expected to take place at the centre of the bowl (above the longwall mined out), a DInSAR analysis was carried out. It is recommended that for the smallest temporal baseline is selected for the interferograms generation, in order to measure a sort of instantaneous deformation. The small Bt interferorams, should be always taken in account, in particular in very dynamic areas, such as underground or open pit mining. In addition, from a SAR point of view, larger temporal baseline leads in temporal decorrelation and thus in measurement loss. The time series analysis with PS-Time has provided a very powerful approach to explore the deformation patter of the whole areas and identify areas characterized by different deformation type. In fact, different deformation type are always linked to different phenomena and PS-Time has allowed to understand the spatio-temporal dynamics. In fact, thanks to the classification of the deformation type of all measurement points in bilinear-accelerating, linear, bilinear-decelerating, and "uncorrelated" it has been possible to locate any point at ground surface over the typical deformation curve in longwall mining. According to this curve, points within the area of influence (in particular

above the mine layout) will be affected by three different phases (Jarosz et al., 1990). The first phase is the initial subsidence, Deformation at this position starts ideally from a stable prior condition (Figure 136), thus an acceleration in the displacement rate is expected. However at phase 1, only a little percentage over the maximum expected subsidence is reached. The main phase refers to the metric subsidence that take place after the panel is mined out and the roof has collapsed within the goaf. This severe deformation propagate to the ground surface and can take place in few weeks (phase 2). After the phase 2 (main subsidence) is ended, and after the longwall extraction has moved in other area, a residual deformation is experienced for years. It has to be noted that the amount and timing of the residual subsidence is time-dependant and in particular depends from the geological and geomorphic settings. The deformation in this phase, first show an evident deceleration and then slowly tend to the asymptote.

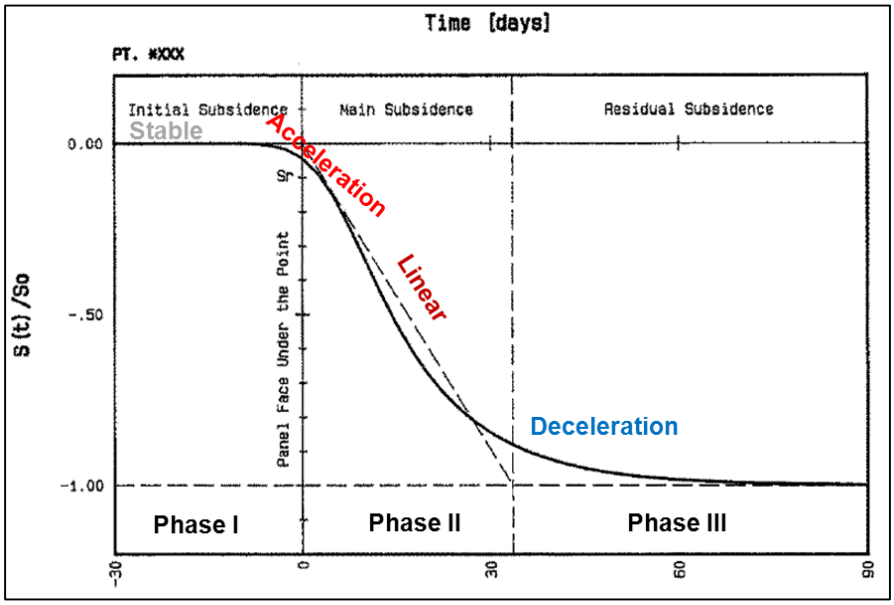

Figure 136. Development of subsidence over time, at a specific location within the mine layout for an hypothetical longwall extraction (modified after Jarosz et al., 1990).

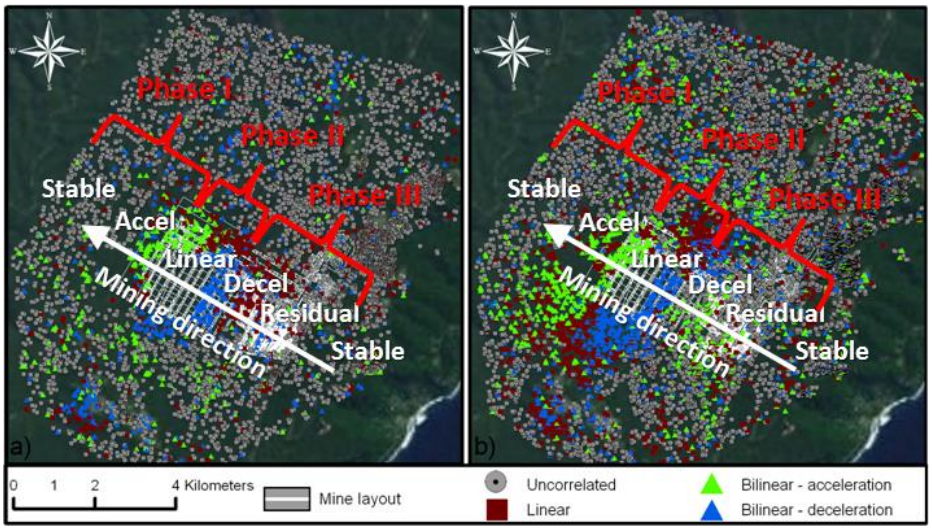

Figure 137. Interpretation of the typical deformation phases over longwall mining obtained from the time series analysis (PS-Time).

Thanks to the time series analysis carried out with PS-Time was possible to interpret the MT-InSAR data according to the typical curve (Figure 136) of deformation for a point affected by longwall mining induced subsidence. While Figure 136 show the deformation of a single point in time domain (after the extraction of the underneath longwall), in multiple longwall mining, it is possible to imagine the same graph in space domain. In other words, a point located at surface along the axes of the longwall progression, will be affected by the wave of the approaching subsidence bowl. This effect has been clearly understood and verified in this work by the evaluation of the dynamics of the subsidence bowl. It has been demonstrated that the longwall mining create a sort of bowl that move over the area as a wave, with distinct subsidence centre and front. Merging these information with the time series analysis and with the curve represented in Figure 136 it is possible to interpret the results and identify on the maps the different area concerning the three phases of the

subsidence and the relatives states of deformation trend (Figure 137). It is interesting also to note that e residual deformation is detected by the SqueeSAR™ analysis over the old mining area, indicating that subsidence can take several years before the stability in reached. However when more panels are mined out at the same time, their mutual effects at ground surface are cumulated and their interpretation become challenging.

Interesting results have been found also regarding the angle of draw at metropolitan mine. Was found and validate with numerical modelling, that the AoD can reach values over 60° while often in literature it is mentioned that typical AoD are about 26° degree. The AoD directly identify the areas that will be affected by the subsidence after the longwall extraction. It is evident that a correct knowledge of this angle it is necessary in order to mitigate the subsidence related risks (environmental, economics, etc.). The MT-InSAR could have thus a double benefit for the miners: 1) subsidence monitoring and 2) calibration of numerical models. In fact miners, in order to get accepted any further mine layout, they are requested to submit a Subsidence Management Plan (SMP) highlighting the effects of the future excavations at the surface and at the element at risk.

The subsidence induced by tunnelling it is in general of a smaller magnitude, In fact, as opposite to the longwall mining, no material is left to collapse within an empty space (i.e. the goaf). The subsidence can be related the sediments assessment and/or to any water loss. However in North Vancouver thanks to the MT-InSAR and the post-processing analysis a not negligible deformation was detected, with acceleration in the period of the workings at the Seymour-Capilano Filtration Plan. Also,

studying the direction of the progression of acceleration date, was found that it correspond to the direction of the Twin Tunnels excavation. Thanks to an in-depth analysis supported by the post-processing routines, it has been demonstrated that the deformation in surface has been triggered by this large engineering project.

7 Summary and conclusion

The objectives of this thesis were to develop post-processing tools for MT-InSAR data, and test them in different fields of application such as tunneling, underground mining and landslides. For the landslides related applications, further objectives were to test them at different scale of analysis (regional scale and slope-scale) and different geomorphic/geologic environment (Apennine and Alpine). For the man-induced subsidence analysis, it was expected to carry out numerical modeling and integrate the InSAR data into the geomechanical subsidence models.

In Chapter 1 of this thesis was given an introduction on interests that both the scientific community and the private sector has given in the latest years to the InSAR. The main reasons why nowadays there is a need for post-processing tools of MT-InSAR is also addressed.

Chapter 2 briefly reviews the basic principles of SAR, classical InSAR and Differential InSAR. The main InSAR applications and drawbacks are also briefly reviewed. At the end of the chapter are in introduced the MT-InSAR basics and explained how the limitations introduced by DInSAR are overcame.

Chapter 3 discuss the three main tools for post-processing analysis proposed and tested in this study which are: 1) Hot Spot Analysis; 2) PS-Time; 3) Geo-PSIC. The "Hot Spot Analysis", was thought for large dataset analysis, such as for landslide mapping at regional scale. It is based on two statistical test, the Getis–Ord G_i^* statistic and the kernel density, which provide a magnitude value in a raster map that depends from the degree of clusterization of the data and their spatial distribution.

PS-Time is a statistically-based tool for time series classification. In particular, it allows classifying time series of displacement (such MT-InSAR datasets) into six distinctive targets and it differentiate stable measurement points ("uncorrelated"), from the "linear" and "bilinear" (thus showing acceleration or deceleration. The software was developed by Berti et al., (2013), and co-authored by the author of this thesis. The third tool, Geo-PSIC , implement a routine to compute the velocity components of the deformation (East-West and vertical) and it includes geomorphic criteria in the selection of the measurement points used. It has been developed in collaboration with the European Academy of Bolzano – Institute for Applied Remote Sensing – (EURAC). In order to compare the improvements introduced by Geo-PSIC, the two other methods used in literature (back-projection and resampling grid) where implemented in ArcGIS.

Chapter 4 include the application of the post-processing routines presented to landslide mapping at regional scale and slope-scale of analysis, for both Alpine and Apennine geomorphic environment. The Hot Spot Analysis was applied to identify and map potential active landslides. In the Alps, within the test areas, 34 potential active landslides were automatically mapped (20 hot spot and 14 cold spot) while in the Apennines over 25 hot spots and 30 cold spots were identified. The efficiency of the automatic mapping is discussed in this chapter, showing example of "false positive" and "true negative" spots. As a conclusion, it is recommended to analyze InSAR data by visual interpretation and possibly together with ancillary layer (such as DEM, ortho-photos, geological map and landslide inventory). The automatic The Hot Spot Analysis is suggested only for a rapid assessment of potentially active landslides.

The time series analysis with PS-Time highlighted that 60% of the measurement points in Alps are classified as “uncorrelated”, meaning that identify stable areas. Only 7% of the measurement points has shown a deformation linear in time while the remaining measurement points are characterized or by an acceleration or a deceleration (“bilinear” and “quadratic”). In the Apennine about 35% of the measurement points are classified as “uncorrelated”, about 40% are classified as linear and the remaining 35% have a change in deformation trend. For the Apennine dataset, due to the availability of additional information layer, it was carried out an additional analysis. By crossing the measurement points classified as “correlated” (with a modulus of velocity higher then 2mm/y) with the landslide inventory, it has been possible to estimate the number of landslides that need to be reclassified. Seventy-two of the active landslides should be reclassified as dormant while 49% of the dormant needs to be reclassified as “active”. However the author suggests that no-automatic classification of landslides inventory should be carried out, but field works and geomorphic analysis should be instead carried out. The precision of the SqueeSAR™ dataset was also estimated (0.5 mm/y). The different methods for the velocity components computation were first applied and then compared. As a result, it was proved that the approach used in literature to re-project the mono-dimensional velocity vector (measured along the line of sight) over the slope direction, often produce unreliable results. In the other hand has been proved that Geo-PSIC is a valid alternative to the resampling grid. Geo-PSIC has demonstrated to be particularly valuable in abrupt geomorphic conditions, such as in the Alpine environment, where even very localized deformation are enhanced. In other hand, in Apennine geomorphic conditions, Geo-PSIC and the resampling grid, can be both used achieving similar results. The

slope-scale analysis of MT-InSAR and the post-processing analysis has been focused on the time series analysis and velocity component. The angle of movement direction of the potential landslide has been evaluated for any measurement point, combining the East-West and vertical velocity component. By using the components and the angle of movement, the landslide type and the local dynamics can be defined. In the Alps has been shown that thanks to Geo-PSIC were identified roto-translational landslides. In the other hand, in Apennine the velocity component is often mainly planimetric. The time series analysis was carried out and tested at local scale and was proved that when non-linear deformation exists, PS-Time is able to highlight these areas, to evaluated the acceleration, the deceleration and the date of the change in motion. The stable area as indicated by measurement points, were also estimated using PS-Time.

Chapter 5 focus on the application of MT-InSAR and the use of the proposed routines on two different types of man-induces subsidence: 1) the longwall mining and 2) the tunneling. Post-processing InSAR application in longwall mining studies, were tested at the Metropolitan Mine (New South Wales, Australia). Two different InSAR products have been applied. The MT-InSAR, thanks to the millimeter precision, was chosen to define the limit of the zero subsidence area for any year of the mining activities. The Differential InSAR (DInSAR) was used to track the motion of the subsidence bowl center, which is related to the longwall mining. To this end, interferograms are chosen with short temporal baseline (Bt) with the aim to represents the "instantaneous" velocity in the Bt considered. It was evaluated that the subsidence bowl advances as along the layout mine, simulating a wave of deformation to the objects in surface. Both the velocity of the subsidence bowl front and

center, advance at the same velocity of the longwalls excavation (~300 m/y). By knowing the distance of the "limit of zero subsidence" from the longwall external border, it has been possible to estimate that the "angle of draw" at Metropolitan Mine has a value of 63°. The "angle of draw" is one of the key parameters in underground mining, since it directly identify which are the affected areas by the subsidence, after the extraction of a given longwall. In the Southern Coalfields of New South Wales, when no prior data are available, it is assumed that angle of draw is equal to 26.5°. It is evident that using a lower AoD value, area affected in surface can be underestimated. In order to compare the AoD evaluated in this study with InSAR (AoD_{63}), with the AoD from literature ($AoD_{26.5}$), two subsidence numerical modelling were carried out. The comparison highlighted that using the AoD_{63}, numerical modeling results are very similar to the observed values, while using the literature $AoD_{26.5}$, the affected areas are underestimated. The results have demonstrated that MT-InSAR, in addition to monitor purposes, can be used to calibrate numerical modelling, which are required in order to plan new mines layouts. The time series analysis with PS-Time has allowed linking accurately each zone of the study area to the typical phases of the subsidence curve. In addition, it has been estimated that residual subsidence over old mining areas, can last for about a decade.

The post-processing routines for tunneling applications were tested over the "Twin Tunnels of the Seymour-Capilano Water Filtration Plan". In particular, the time series analysis carried out with PS-Time allowed to identify a deformation over the urban area, in the area where the Twin Tunnels were excavated. The deformation was not evident using the mean average velocity, since in that area 81% of the measurement point's time series were non-linear. Time series have been split in "before" and

"after" the triggering event and the dates acting as "breakline" in the time series were also extracted. A statistical analysis has shown that most of dates when the motion started, was in 2006 that correspond to the working period of the Twin Tunnel. In the other hand, the spatial analysis of these dates has shown a progression parallel to the excavation direction. Thanks to the time series analysis, it has been possible to relate the deformation in the study area to the tunneling activities.

Chapter 6 discuss the main results of this study, for landslides and man-induced subsidence. This Chapter discuss also the potentiality and applicability of the proposed tools, in the different contexts. Attention to the possible limitations has been paid, providing related explanations for potential end-user. Some guidelines are also listed within this Chapter.

Chapter 7 provide a summary of the thesis while Chapter 8 list the Reference linked to this work.

As main conclusion it can be stated that the objectives of this PhD thesis were achieved. Three routines of MT-InSAR were proposed. The automated time series analysis represent a novelty, since to the author knowledge, there are no studies carried out on the classification of the type of deformation trends. Furthermore, the effectiveness introduced by Geo-PSIC with the introduction of the geomorphic criteria for velocity decomposition, was compared with the alternative approaches available in literature. It was demonstrated that in Alpine environment, Geo-PSIC highlight the local scale movement dynamics. Applicability and drawback have been provided for the Hot Spot Analysis for landslide mapping, after the testing over the Apennines and the Alps. The same procedure were tested in man-induced subsidence application and it was demonstrated that the time series with PS-Time is fundamental to

highlight the triggering phenomena (i.e. tunnel excavation) and to identify the dates of the activation of the subsidence. Also it was demonstrated that using MT-InSAR, DinDSAR and the time series analysis, it is possible to identify the longwall mining subsidence dynamics, the angle of draw and the phase of the deformation. In addition, by numerical modeling was proved that InSAR can be used to retrieve mining parameters and thus ton calibrate subsidence numerical modeling necessary for layout mine planning.

References

- Abbate, E., Bortolotti. V., Passerini, P., Sagri, M., 1970. Introduction to geology of the Northern Apennines. Sedimentary Geology 4, 207–249.

- Akliouat, H., Smara, Y., Bouchemakh, L., 2007. Synthetic Aperture Radar Image Formaton Process: Application To A Region Of North Algeria. Envisat symposium in European Space Agency - Publications- ESA.

- Allievi, J., Ambrosi, C., Ceriani, M., Crosta, G. B., Ferretti, A., Fossati, D., 2003. Monitoring slow mass movements with the Permanent Scatterers Technique. International Geosciences and Remote Sensing Symposium (IGARSS 2003). (1−3), 21–25 Jul., Toulouse, France.

- Alsdorf, D.E., Melack, J.M., Dunne, T., Mertes, L.A.K., Hess, L.L., Smith, L.C., 2000. Interferometric radar measurements of water level changes on the Amazon flood plain. Nature 404, 174–177.

- Arnaud, A., Adam, N., Hanssen, R., Inglada, J., Duro, J., Closa, J., Eineder, M., 2003. ASAR ERS Interferometric Phase Continuity, in Proceedings Geoscience and Remote Sensing Symposium 2003, IEEE International, 2:1133-1135.

- Bamler. R., Hartl, P., 1998. Synthetic aperture radar interferometry. Inverse Probl 14, 1–54.

- Berardino, P., Fornaro, G., Lanari, R., and Sansosti, E., 2002. A new algorithm for surface deformation monitoring based on small baseline

differential interferograms, IEEE Trans. Geosci. Rem. Sens., 40, 2375–2383.

- Berardino, P., Casu, F., Fornaro, G., Lanari, R., Manunta, M., Manzo, M., Pepe, A., Pepe, S., Sansosti, E., Serafino, F., Solaro, G., Tizzani, P., Zeni, G., 2007. The SBAS-DInSAR technique as a tool for the observation of active volcanic areas: Results and future perspectives. IGARSS, 10-13.

- Berti M., Corsini A., Franceschini S., Iannacone J.P., 2013. Automated classification of Persistent Scatterers Interferometry time series, Nat. Hazards Earth Syst. Sci., 13, 1945–1958.

- Bianchini, S., Cigna, F., Righini, G., Proietti, C., Casagli, N., 2012. Landslide HotSpot Mapping by means of Persistent Scatterer Interferometry. Environmental Earth Sciences, 67 (4), 1155-1172.

- Boccaletti, M., Elter, P., Guazzone, G., 1971. – Plate tectonic models for the development of the Western Alps and Northern Apennines. Nature, 234, 108-111.

- Bosellini, A., Gianolla, P., Stefani, M., 2002. The Triassic carbonate platforms of the Dolomites (northern Italy): their evolution and stratigraphic framework. Memoir Science Geology 54, 139–163.

- Brown, E.T. (Ed)., 1981. Rock characterization, testing and monitoring - ISRMsuggested methods, 171-183. Oxford, Pergamon.

- Brunori, C.A., Bignami, C., Stramondo, S., Bustos, E., 2013., 20 years of active deformation on volcano caldera: Joint analysis of InSAR and AInSAR techniques International Journal of Applied Earth Observation and Geoinformation. Vol., 23, 279–287.

REFERENCES

- Calò, F., Ardizzone, F., Castaldo, R., Lollino, P., Tizzani, P., Guzzetti, F., Lanari, R., Angeli, M., Pontoni, F., Manunta, M., 2014. Enhanced landslide investigations through advanced DInSAR techniques: the Ivancich case study, Assisi, Italy, Remote Sensing of Environment., 142, 69–82.

- Can, E., Mekik, C., Kuşcu, S., Akçın, H., 2011. Subsidence occurring in mining regions and a case study of Zonguldak-Kozlu Basin. Scientific Research and Essays 6 (6),1317–1327.

- Carmignani, L., Conti, P., Cornamusini, G., Meccheri, M., 2004. The Internal Northern Apennines, The Northern Tyrrhenian Sea and the Sardinia-Corsica Block. Special Volume of the Italian Geological Society for the IGC 32 Florence-2004.

- Carnec, C., Massonnet, D., King, C., 1996. Two examples of the application of SAR interferometry to sites of small extent. Geophysical Research Letters 23, 3579–3582.

- Carnec, C., Delacourt, C., 2000. Three years of mining subsidence monitored by SAR interferometry, near Gardanne, France. Journal of Applied Geophysics 43(1), 43–54.

- Cascini, L., Fornaro, G., Peduto, D., 2010. Advanced low- and full-resolution DInSAR map generation for slow-moving landslide analysis at different scales. Eng. Geol., 112, 29–42.

- Cascini, L., Peduto, D., Pisciotta, G., Arena, L., Ferlisi, S., Fornaro. G., 2013. The combination of DInSAR and facility damage data for the updating of slow-moving landslide inventory maps at medium scale. natural hazards and earth system sciences. Vol., 13, 1527-1549.

- Catani, F., Farina, P., Moretti, S., Nico, G., Strozzi, T., 2005. On the application of SAR interferometry to geomorphological studies: estimation of landform attributes and mass movements. Geomorphology 66, 119–131.

- Catani, F., Canuti, P., and Casagli, N., 2012. The Use of Radar Interferometry in Landslide Monitoring, paper presented at 1st Meeting of Cold Region Landslides Network and 1st Symposium on Landslides in Cold Region, Harbin, China.

- Cigna, F., Del Ventisette, C., Liguori, V., Casagli, N., 2011. Advanced radar-interpretation of InSAR time series for mapping and characterization of geological processes, Nat. Hazards Earth Syst. Sci., 11, 865–881.

- Cigna, F., Bianchini, S., and Casagli, N., 2013. How to assess landslide activity and intensity with Persistent Scatterer Interferometry (PSI): the PSI-based matrix approach, Landslides, 1–17.

- Colesanti, C., Wasowski, J., 2004. Satellite SAR Interferometry for Wide-area Slope Hazard Detection and Site-specific Monitoring of Slow Landslide. In: Lacerda, Ehrlich, Fontoura, Sayo (Eds.), Landslides: Evaluation and Stabilization. Taylor and Francis Group, London, 795–802.

- Colesanti, C., Wasowski., 2006. Investigating landslides with space-borne Synthetic Aperture Radar (SAR) interferometry. Engineering Geology. Vol. 88, Issues 3–4, 73–199.

- Corsini, A., Farina, P., Antonello, G., Barbieri, M., Casagli, N., Coren, F., Guerri, L., Ronchetti, F., Sterzai, P., Tarchi, D., 2006. Spaceborne and ground-based SAR interferometry as tools for landslide hazard management in civil protection, Int. J. Remote. Sens., 27(12), 2351–2369.

- Corsini, A., Iasio, C., Mair, V., 2012. Overview of 2001–08 GPS monitoring at the Corvara landslide and perspectives from 2010–11 use of HR X-band SAR (Dolomites, Italy). Eds. E. Eberhardt, C. Froese, A. K. Turner and S. Leroueil - Landslides and Engineered Slopes: Protecting Society through Improved Understanding - Taylor & Francis Group London. Vol.(2), 1353-1358.

- Costantini, M., Falco, S., Malvarosa, F., and Minati, F., 2008. A new method for identification and analysis of persistent scatterers in series of SAR images, paper presented at the International Geosciences Remote Sensing Symposium, Int. Geosci. Remote Sensing Symp. (IGARSS), Boston, USA.

- Crosetto, M., Gili, J.A., Monserrat, O., Cuevas-González, M., Corominas, J., Serral, D., 2013. Interferometric SAR monitoring of the Vallcebre landslide (Spain) using corner reflectors. Natural Hazards and Earth System Science, Vol., 13(4), 923-933.

- Cruden, D.M., and Varnes, D.J., 1996. Landslides Types and Processes, in: Landslides: Investigation and Mitigation, edited by: Turner, A. K. and Schuster, R. L., Washington DC, Transportation Research Board, National Academy of Sciences, Special Report 247, 36–75.

- Daniela, P., Troiani, F., Soldati, M., Notarnicola, C., Savelli, D., Schneiderbauer, S., Strada, C., 2012. Statistical analysis for assessing shallow-landslide susceptibility in South Tyrol (South-Eastern Alps, Italy). Geomorphology, 151-152, 196-206.

- Davis, J. C., 1986. Statistics and Data Analysis in Geology, John Wiley and Sons, New York, USA.

- DeBono, P., and Tarrant, G., 2011. An analysis of long term subsidence at Metropolitan colliery [online]. In: Mine Subsidence 2011: Proceedings of the Eighth Triennial Conference on Management of Subsidence, The. Pokolbin, N.S.W.: Mine Subsidence Technological Society, 81-88.

- Deck, O., Marwan, H.A., Françoise, H., 2003. Taking the soil–structure ınteraction into account in assessing the loading of a structure in a mining subsidence area. Engineering Structures 25 (4), 435–448

- Delacourt, C., Raucoules, D., Le Mouélic, S., Carnec, C., Feurer, D., Allemand, P., Cruchet, M., 2009. Observation of a Large Landslide on La Reunion Island Using Differential Sar Interferometry (JERS and Radarsat) and Correlation of Optical (Spot5 and Aerial) Images. Sensors, 9, 616-630.

- Dercourt J., Zonenshain, L.P., Ricou, L.E., Kazmin, V.G., Le Pichon, X., Knipper, A.L., Grandjacquet, C., Sbortshikov, I.M., Geyssant, J., Lepvrier, C., Pechersky, D.H., Boulin, J., Sibuet, J.C., Savostin, L.A., Sorokhtin, O., Westphal, M., Bazhenov, M.L., Lauer, J.P., Biju-Duval B., 1986. Geological evolution of the Tethys belt from the Atlantic to the Pamirs since the Lias. Tectonophysics, 123, 241-315.

- Duro, J., Inglada, J., Closa, J., Adam, N., Arnaud, A., 2003. High resolution differential interferometry using time series of ers and envisat sar data. FRINGE 2003, 1-5.

- Duro, J., 2010. Développement de Nouvelles Méthodes Utilisant les Images RSO Satellitales pour la Détection, la Mesure et le Suivi des Mouvements de Terrain. PhD thesis dissertation. Laboratoire Mathématiques et Sciences et Technologies de l'Information et de la Communication. Université Paris-Est.

- Duzgun, H.S.B., 2005. Analysis of roof fall hazards and risk assessment for Zonguldak Coal Basin underground mines. International Journal of Coal Geology 64 (1–2), 104–115.

- Emilia-Romagna SGSS (Servizio Geologico, Sismico e dei Suoli)., 2006. Geological and Soil Maps of the Emilia-Romagna Region. Historical Landslide Database. http://www.regione.emilia-romagna.it/wcm/geologia_en/Sections/Hydrogeological_risk.htm

- Farina, P., Colombo, D., Fumagalli, A., Marks, F., Moretti, S., 2006. Permanent Scatterers for landslide investigations: outcomes from the ESA-SLAM project. Engineering Geology 88, 200–217.

- Ferretti, A., Prati, C., Rocca, F., 2000. Nonlinear subsidence rate estimation using permanent scatterers in differential SAR interferometry, IEEE Trans. on Geosci. and Remote Sensing, 38 (5), 2202 – 2212.

- Ferretti, A., Prati, C., Rocca, F., 2001. Permanent scatterers in SAR interferometry, IEEE Trans. on Geosci. and Remote Sensing, 39 (1), 8 – 20.

- Ferretti, A., Fumagalli, A., Novali, F., Prati, C., Rocca, F., Rucci, A., 2011. A New Algorithm for Processing Interferometric Data-Stacks: SqueeSAR™. Geoscience and Remote Sensing, IEEE Transactions on 49 (9), 3460-3470.

- Ferretti, A., Fumagalli, A., Novali, F., Rucci, A., Prati, C., Rocca, F., 2012. DEM reconstruction with SqueeSAR™. Advances in Radar and Remote Sensing, (TyWRRS) Tyrrhenian Workshop 2012 on Advances in Radar and Remote Sensing., no., pp.198,201, 12-14 Sept., 2012. Naples, Italy.

- Franceschetti, G., Lanari, R., 1999. Synthetic Aperture Radar Processing. CRC Press, New York.

- Fruneau, B., Achache, J., Delacourt, C., 1996. Observation and modeling of the Saint-Etienne-de-Tinee landslide using SAR interferometry. Tectonophysics 265, 181–190.

- Giordan, D., Allasia, P., Manconi, A., Baldo, M., Santangelo, M., Cardinali, M., 2013. Morphological and kinematic evolution of a large earthflow: The Montaguto landslide, southern Italy. Geomorphology, 187, 61–79.

- Green, D. M., and Swets, J.A., 1966. Signal detection theory and psychophysics. New York, Wiley, 455.

- Hanssen, R., 2001. Radar Interferometry: data interpretation and error analysis. Kluwer Academic Publishers, Dordrecht, Holland, 2001.

- Henderson, F.M., Lewis, A.J. (Eds.)., 1998. Principles and Applications of Imaging Radar, 3rd edition. Vol., 2 of Manual of Remote Sensing. John Wiley & Sons, Inc., New York.

- Herrera, G., Tomás, R., Lopez-Sanchez, J.M., Delgado, J., Mallorqui, J.J., Duque, S., Mulas, J., 2007. Advanced DInSAR analysis on mining areas: La Union case study (Murcia, SE Spain). Engineering Geology 90 (3–4), 148–159.

- Herrera, G., Davalillo, J. C., Mulas, J., Cooksley, G., Monserrat, O., Pancioli, V., 2009. Mapping and monitoring geomorphological processes in mountainous areas using PSI data: Central Pyrenees case study. Natural Hazards and Earth System Science, Vol. 9, Issue 5, 2009, pp.1587-1598

- Holla, L, and Barclay, E., 2000. Mine Subsidence in the Southern Coalfield, NSW, Australia. (News South Wales Department of Mineral Resources).

- Hooper, A., 2006. Persistent Scatterer Radar Interferometry for Crustal Deformation Studies and Modeling of Volcanic Deformation. Phd dissertation. Stanford University.

- Hooper, A., Segal, P., and Zebker, H., 2007. Persistent Scatterer InSAR for Crustal Deformation Analysis, with Application to Volcán Alcedo, Galápagos, J. Geophys. Res., 112, B07407.

- Hutton, A.C., 2009. Geological Setting of Australasian Coal Deposits. In: R. Kininmonth & Baafi, E. (eds.) Australasian Coal Mining Practice. Carlton, Victoria: The Australasian Institute of Mining and Metallurgy.

- Iasio, C., Corsini, A., Mair, V., Schneiderbauer, S., Tamburini, A., 2011. Sperimentazione di corner per banda X nel monitoraggio di

colate di terra lente con COSMO SkyMed. Proc. XV Conferenza Nazionale ASITA, 15-18 Nov 2011. Reggia di Colorno, Italy.

- Jarosz, A., Karmis, M., Sroka. A., 1990. Subsidence development with time — experiences from longwall operations in the Appalachian coalfield. International Journal of Mining and Geological Engineering. Vol. 8(3), 261-273.

- Jonsson, S., Zebker, H.A., Cervelli, P., Segall, P., Carbeil, H., Mouginis-Mark, P., Rowland, S., 1999. A shallow-dipping dike fed the 1995 flank eruption at Fernandina Volcano, Galapagos: observed by satellite radar interferometry. Geophysical Research Letters 26 (8), 1077–1080.

- Jung, H-C., Kim, S-W., Jung, H-S, Min, K-D, Won, J-S 2007. Satellite observation of coal mining subsidence by persistent scatterer analysis. Engineering Geology 92, 1–13

- Karmis M., Jarosz, A., Agioutantis, Z., 1989. Predicting Subsidence with a Computer. Coal, Vol 26(12), December, 54-61.

- Karmis, M., and Agioutantis, Z., 2004. A risk analysis subsidence approach for the design of coal refuse impoundments overlying mine workings. In Proc: 8th International Symposium on Environmental Issues and Waste Management, in Energy and Mineral Production (SWEMP), May 17-20, 2004. Antalya, Turkey., 205-210.

- Kaufman, L., Rousseeuw, P.J., (eds)., 1990. Finding Groups in Data: an Introduction to Cluster Analysis. John Wiley and Sons.

- Keilich, W., Seedsman, R., Aziz, N.H., 2006. Numerical Modelling Of Mining Induced Subsidence, 2006. Iin Aziz, N (ed), Coal 2006:

Coal Operators' Conference, University of Wollongong & the Australasian Institute of Mining and Metallurgy, 313-326.

- Kimura, H., Yamaguchi, Y., 2000. Detection of landslide areas using radar interferometry. Photographic Engineering and Remote Sensing 66 (3), 337–344.

- Klebelsberg, R.V., 1935. Geologie von Tyrol, Verl. Borntraeger, Berlin.

- Kratzsch, H., 1983. Mining Subsidence Engineering. Springer Verlag, Berlin Heidelberg, New York

- Krogh, M., 2007. Management of longwall mining impacts in Sydney's southern drinking water catchments. Report by Environmental Data Analysis Pty Ltd, Jannali, NSW, 2226.

- Laubscher, H.P., 1989. The tectonics of the Southern Alps and the Austro-Alpine nappes: a comparison, Alpine Tectonics. In: Coward, M.P., Dietrich, D., Park, R.G. (Eds.), Geological Society of London, Special Publications, 45, 229–241.

- Leuratti, E., Lucente, C.C., Medda, E., Manzi, V., Corsini, A., Tosatti, G., Ronchetti, F., Guerra M., 2007. Primi interventi di consolidamento sulle frane dei Boschi di Valoria, di Tolara e Lezza Nuova (Val Dolo e Val Dragone, Appennino modenese). Giornale di Geologia. Applicata (AIGAA) 7, 17–30.

- Li, F. K., and R. M. Goldstein., 1990. Studies of multibaseline spaceborne interferometric synthetic aperture radars, IEEE Transactions on Geoscience and Remote Sensing, 28 (1), 88 – 97.

- Lloyd, P.W., Mohammad, N., Reddish, D.J., 1997. Surface subsidence prediction techniques for uk coalfields - an innovative numerical modelling approach. Proceedings of the 15th Mining Congress of Turkey.

- Lu, P., Casagli, N., Catani, F., Tofani, V., 2012. Persistent Scatterers Interferometry Hotspot and Cluster Analysis (PSI-HCA) for detection of extremely slow-moving landslides. International Journal of Remote Sensing 33 (2), 466-489.

- Lu, P., Catani, F., Tofani, V., Casagli, N., 2013. Quantitative hazard and risk assessment for slow-moving landslides from Persistent Scatterer Interferometry. Landslides, 1-12

- Luo, Y., Cheng, J-W., 2009. An influence function method based subsidence prediction program for longwall mining operations in inclined coal seams. Mining Science and Technology (China), Vol., 19(5) September 2009, 592‑598.

- Mallorquí, J.J., Mora, O., Blanco, P., Broquetas, A., 2003. Linear nad non-linear long-term terrain deformation with DInSAR (CPT): Coherent Pixels Tehcnique), Proc. of FRINGE 2003 Workshop. ESA, p., 1-8.

- Mantovani, E., Babbucci, D., Farsi, F., 1985. Tertiary evolution of the Mediterranean region: major outstanding problems. Boll. Geof. Teor. Appl., 105, 67-90.

- Mantovani, F., Soeters, R. and van Westen, C.J., 1996. Remote sensing techniques for landslide studies and hazard zonation in Europe. In: Geomorphology, 15(3), 213-225.

- Manzo, M., Berardino, P., Bonano, M., Casu, F., Manunta, M., Pepe, A., Pepe, S., Sansosti, E., Solaro, G., Tizzani, P., Zeni, G., Guglielmino, F., Puglisi, G., De Martino, P., Obrizzo, P., Tammaro, U, Lanari, R., 2012. A quantitative assessment of DInSAR Time series accuracy in volcanic areas: From the first to second generation SAR sensors. IGARSS, 911-914.

- Massonnet, D., Rossi, M., Carmona, C., Adragna, F., Peltzer, G., Fiegl, K., Rabaute, T., 1993. The displacement field of the Landers earthquake mapped by radar interferometry, Nature, 364, 138 – 142.

- Massonnet, D., Feigl, K.L., 1998. Radar Interferometry and its application to changes in the Earth's surface. Review of Geophysics 36, 441–500.

- MATTM., 2010. Piano Straordinario di Telerilevamento Ambientale (PSTA), Linee guida per l'analisi dei dati intereferometrici satellitari in aree soggette a dissesti idrogeologici. Ministero dell'Ambiente e della Tutela del Territorio e del Mare, 108pp.

- Meisina C., Zucca F., Notti . D, Colombo A., Cucchi A., Savio G., Giannico C. Bianchi M., 2008. Geological interpretation of PSInSAR data at regional scale. Sensors 2008, Volume 8(11), 7469-7492.

- Milone, G., Scepi, G., 2011. A Clustering Approach for Studying Ground Deformation Trends in Campania Region through PS-InSARTM Time Series Analysis. Journal of Applied Sciences, 11, 4, 610-620.

- Morelli, M., Piana, F., Mallen, L., Nicolò, G., Fioraso, G., 2011. Iso-Kinematic Maps from statistical analysis of PS-InSAR data of

Piemonte, NW Italy: comparison with geological kinematic trends. Remote Sensing of Environment 115, 1188–1201.

- Morgan, J., Raval, S., Macdonald, B., Falorni, G., Iannacone, J.P., 2013. Application of advanced InSAR techniques to detect vertical and horizontal displacements. In: International Symposium in Slope Stability in Open Pit Mining and Civil Engineering., 25-27 September, Brisbane, Australia.

- MSEC., 2007 .General Discussion on Systematic and Non Systematic Mine Subsidence Ground Movements

- Newman, D.A., Agioutantis, Z., Karmis, M., 2001. SDPS for Windows: An Integrated Approach to Ground Deformation Prediction. Proc. of the 20th Int. Conf. on Ground Control in Mining, 157-162.

- Ng, A.H.-M., Chang, H.C., Ge, L., Rizos, C., Omura, M., 2009. Assessment of radar interferometry performance for ground subsidence monitoring due to underground mining. Earth, Planets and Space 61 (6), 733–745.

- Ng, A.H-M., Ge, L., Yan, Y., Li, X,. Chang, H-C., Zhang, K., Rizos, C., 2010. Mapping accumulated mine subsidence using small stack of SAR differential interferograms in the Southern coalfield of New South Wales, Australia. Engineering Geology, Volume 115, (1–2) 6, 1–15.

- Notti, D., Meisina, C., Zucca, F., Colombo, A., Cucchi, A., Lanteri, L., Mallen, L., Troisi, C., 2008. Una metodologia per l'interpretazione dei dati PS-InSAR per l'individuazione e lo studio di

fenomeni geologici a scala regionale. In: 84° Congresso Nazionale Società Geologica Italiana. Rendiconti Online della Società Geologica Italiana, 15-17 Sept., 2008. Sassari, Italy.

- Notti, D., Meisina, C. Zucca F., 2010. Analysis of PSInSAR data for landslide studies from regional to local scale. In Proc. Fringe 2009 Workshop,. 30 November - 4 December 2009, Frascati, Italy.

- Notti, D., Meisina, C., Colombo, A., Lanteri, L., Zucca, F., 2013. Studying and Monitoring Large Landslides with Persistent Scatterer Data. International Conference Vajont 1963-2013. Thoughts and Analyses after 50 Years since the Catastrophic Landslide. 8-10 October 2013. Padua, Italy.

- Novali, F., Fumagalli, A., Rocca, F., Prati, C., Ferretti, A., Rucci, A., 2011. Exploitation of Temporary Coherent Scatterers in SQUEESAR™ Analysis. Fringe 2011 – Sept 19 – 123. ESA-ESRIN, Frascati, Italy.

- NSWDMR, 2003. Guideline for applications for subsidence management approvals. Tech. rep., NSW Department of Mineral Resources, Australia.

- NSWDP., 2008. Impacts of Underground Coal Mining on Natural Features in the Southern Coalfield. Strategic Review, NSW Department of Mineral Resources, Australia.

- Peltier, A., Bianchi, M., Kaminski, E., Komorowski, J., Rucci, A., 2010. PSInSAR as a new tool to monitor pre-eruptive volcano ground deformation: validation using GPS measurements on Piton de la Fournaise. Geophysical Research Letters, Vol. 37, L12301, 5.

- Perissin, D., Ferretti, D., Piantanida, R., Piccagli, D., Prati, C., Rocca, F., Rucci, A., De Zan, F., 2007. Repeat-pass SAR interferometry with partially coherent targets. In Proc. Fringe, 2007, pp., 1–7, Frascati, Italy.

- Perrone, G., Morelli, M., Piana, F., Fioraso, G., Nicolò, G., Mallen, L. Cadoppi, P., Balestro, G., Tallone, S., 2013. Current tectonic activity and differential uplift along the Cottian Alps/Po Plain boundary (NW Italy) as derived by PS-InSAR data. Journal of Geodynamics, Vol. 66, 65-78.

- Perski, Z., Jura, D., 2003. Identification and Measurement of Mining Subsidence with SAR Interferometry: Potentials and Limitations. Proceedings, 11th FIG Symposium on Deformation Measurements, , 1–7, Santorini, Greece.

- Raucoules, D., Colesanti, C., Carnec, C., 2007. Use of SAR interferometry for detecting and assessing ground subsidence. Comptes Rendus - Géoscience, Vol. 339, 5, 289-302

- Refice, A., Bovenga, F., Wasowski, J., Guerriero, L., 2000. Use of InSAR data for landslide monitoring: a case study from southern Italy. Geoscience and Remote Sensing Symposium, 2000. IGARSS 2000, Vol.6.

- Righini, G., Pancioli, V., Casagli, N., 2011. Updating landslide inventory maps using persistent scatterer interferometry (PSI). Int J Remote Sens.

- Rosen, P.A., Hensley, S., Joughin, I.R., Li, F.K., Madsen, S.N., Rodriguez, E., Goldstein, R.M., 2000. Synthetic Aperture Radar Interferometry. Proceedings of the IEEE, Vol. 88, pp. 333–376.

- Rossi, M., Witt, A., Guzzetti, F., Malamud, B.D., Peruccacci, S., 2010. Analysis of historical landslide time series in the Emilia–Romagna Region, northern Italy. Earth Surface Processes and Landforms, 35(10), 1123–1137.

- Saeidi, A., Deck, O., Verdel, T., 2009. Development of building vulnerability functions in subsidence regions from empirical methods. Engineering Structures 31 (10), 2275–2286.

- Scandone, P., 1979. Origin of the Tyrrhenian Sea and Calabrian Arc. Boll. Soc. Geol. It., 98, 27-34.

- Scanvic, J.Y., Carnec, C., Girault, F., Rouzeau, O., 1993. Evolution du potentiel des donnees SAR pour la cartographie du risque de mouvements de terrain. Proc. Int. Symp. On: From optics to radar: SPOT and ERS applications; 301-312.

- Seedsman, R., 2004. A Review of Methods to Determine Panel and Pillar Dimensions That Limit Subsidence to a Specified Impact. In Aziz, N (ed), Coal 2004: Coal Operators' Conference, University of Wollongong & the Australasian Institute of Mining and Metallurgy, 101-110.

- Silverman, B.W., 1986. Density Estimation for Statistics and Data Analysis. Chapman & Hall. London.

- Singhroy, V., Mattar, K., 2000. SAR image techniques for mapping areas of landslides. Proc. ISPRS 2000, Amsterdam, pp., 1395–1402.

- Singhroy, V., Mattar, K., Gray, L., 1998. Landslide characterization in Canada using interferometric SAR and combined SAR and TM images. Advances in Space Research 2 (3), 465–476.

- Sneed, M., Ikehara, M., Balloway, D., Amelung, F., 2001. Detection and measurement of land subsidence using global positioning system and interferometric synthetic aperture radar, Coachella Valley, California, 1996–1998. Water-Resources Investigations Report 01-4193, US Geological Survey, USA.

- Sowter, A. Bateson, L., Strange, P., Ambrose, K., Syafiudina, M.F., 2013. DInSAR estimation of land motion using intermittent coherence with application to the South Derbyshire and Leicestershire coalfields. Remote Sensing Letters. Vol. 4, (10).

- Stingl, V., Mair, V., 2005. Introduzione alla geologia dell'Alto Adige. Provincia Autonoma di Bolzano, Ufficio Geologia e Prove Materiali, Cardano, Bolzano, Italy.

- Strozzi, T., Wegmuller, U., Tosi, L., Bitelli, G., Spreckels, V., 2001. Land subsidence monitoring with differential SAR interferometry. Photogrammetric Engineering and Remote Sensing 67(11), 1261–1270.

- Strozzi, T., Farina, P., Corsini, A., Ambrosi, C., Thüring, M., Zilger, J., Wiesmann, A., Wegmüller, U., Werner, C., 2005. Survey and monitoring of landslide displacements by means of L-band satellite SAR interferometry. Landslides 2 (3), 193–201.

REFERENCES

- Suncar, O., Dueri, D., Yang, D., Buckley, S., Rathje, E., 2012 Monitoring of a Creeping Landslide in California Using Spaceborne Radar Interferometry. GeoCongress 2012, 2991-3000.

- Tantianuparp, P., Shi, X., Zhang, L., Balz, T., Liao, M., 2013. Characterization of Landslide Deformations in Three Gorges Area Using Multiple InSAR Data Stacks. Remote Sensing. 5(6), 2704-2719.

- Teatini, P., Castelletto, N., Ferronato, M., Gambolati, G., Janna, C., Cairo, E., Darzorati, D., Colombo, D., Ferretti, A., Bagliani, A., Bottazzi, F., 2011. Geomechanical response to seasonal gas storage in depleted reservoirs: A case study in the Po River basin, Italy. Journal Of Geophysical Research, Vol.116, F2.

- Tofani, V., Segoni, S., Agostini, A., Catani, F., Casagli. N., 2013. Technical Note: Use of remote sensing for landslide studies in Europe. Nat. Hazards Earth Syst. Sci., 13, 299-309.

- Ulaby, F.T, Moore R.K., Fung A.K., 1981. Microwave Remote Sensing – active and passive. Vol I. Addison-Wesley, Reading, MA, 2162p.

- Usai, S., 1997. The use of man-made features for long time scale insar. In International Geoscience and Remote Sensing Symposium, pp., 1542–1544, 3-8.

- Vladimir, G., Vlcko, J., 2012. Monitoring of post-failure landslide deformation by the PS-InSAR technique at Lubietova in Central Slovakia. Environmental Earth Sciences. Vol. 66(6), 1585.

- VPI - Virginia Polytechnic Institute and State University. Dept. of Mining and Minerals Engineering., 1987. Prediction of ground movements due to underground mining in the Eastern United States coalfields, The Department, Blacksburg, Va.

- Wegmuller, U., Strozzi, T., Werner, C., Wiesmann, A., Benecke, N., Spreckels, V., 2000. Monitoring of mining-induced surface deformation in the Ruhrgebiet (Germany) with SAR interferometry. IGARSS 2000, 24–28 July, 2771–2773. Honolulu, Hawaii, USA.

- Werner, C., Wegmuller, U., Strozzi, T., Wiesmann, A., 2003. Interferometric point target analysis for deformation mapping, presented at Geoscience and Remote Sensing Symposium, Int. Geosci. Remote Sensing Symp. (IGARSS), Toulouse, France, 2003.

- Woo, K-S., Eberhardt, E., Rabus, B., Stead, D., Vyazmensky, A., 2012. Integration of field characterisation, mine production and InSAR monitoring data to constrain and calibrate 3-D numerical modelling of block caving-induced subsidence. International Journal of Rock Mechanics & Mining Sciences 53 (2012) 166–178.

- Zebker, H.A., and Villasenor, J., 1992. Decorrelation in interferometric radar echoes, IEEE Transactions on Geoscience and Remote Sensing, 30 (5), 950 – 959.

- Zhang, L., Lu, Z., Ding, X., Jung, H-S., Feng, G., Lee, C-W., 2012. Mapping ground surface deformation using temporarily coherent point SAR interferometry: Application to Los Angeles Basin. Remote Sensing of Environment. Vol., 117, 429–439.

REFERENCES

- Zhao, C., Lu, Z., Zhang, Q., de la Fuente, J., 2012. Large-area landslides detection and monitoring with ALOS/PALSAR imagery data over Northern California and Southern Oregon, USA, Remote Sens. Environ., 124, 348–359.

- Zhao, C., Zhang, Q., Yin, Y., Lu, Z., Yang, C., Zhu, W., Li, B., 2013. Pre-, co-, and post- rockslide analysis with ALOS/PALSAR imagery: a case study of the Jiweishan rockslide, China, Nat. Hazards Earth Syst. Sci., 13, 2851-2861.

Zhu, W., Zhang, Q., Ding, X., Zhao, C., Yang, C., Qu, F., Qu, W., 2014. Landslide monitoring by combining of CR-InSAR and GPS techniques. Advances in Space Research. Vol. 53(3) 430–439.

Web references

http://ambiente.regione.emilia-romagna.it/geologia/temi/risorse-estrattive/le-risorse-estrattive

http://earth.esa.int/applications/data_util/SARDOCS/spaceborne/Radar_Courses/

http://treuropa.com/

http://tunneltalk.com/Seymour-Capilano-Apr09-Twin-tunnel-restart-comes-at-a-high-price.php

http://www.regione.emilia-romagna.it/wcm/geologia_en/Sections/Hydrogeological_risk.htm